12

SAMSO TR-77-110

ADA047736

OPTICAL ANGULAR MOTION SENSOR

PHASE TWO FINAL REPORT

31 MAY 1977

COPY AVAILABLE TO DDC DOES NOT PERMIT FULLY LEGIBLE PRODUCTION

DISTRIBUTION A - UNLIMITED

DISTRIBUTION STATEMENT A
Approved for public release;
Distribution Unlimited

DEPARTMENT OF THE AIR FORCE
HEADQUARTERS SPACE AND MISSILE SYSTEMS ORGANIZATION
LOS ANGELES, CALIFORNIA 90009

PREPARED UNDER CONTRACT NO. F04701-76-C-0044
BY CHRYSLER CORPORATION DEFENSE-SPACE DIVISION
NEW ORLEANS, LOUISIANA

AD No.____
DDC FILE COPY

DDC
DEC 13 1977
B

Best
Available
Copy

This final report was submitted by Chrysler Corporation Defense-Space Division, New Orleans, Louisiana, under contract F04701-76-C-0044 with the Space and Missile Systems Organization/YAD Los Angeles Air Force Station, P. O. Box 92960, Worldway Postal Center, Los Angeles, California 90009. Capt. George Rhue/YAD was the project officer.

This report has been reviewed by the Information Office (OI) and is releasable to the National Technical Information Service (NTIS). At NTIS, it will be available to the general public, including foreign nations.

This technical report has been reviewed and is approved for publication.

George T. Rhue
GEORGE T. RHUE, Capt., USAF
Project Officer

for LTC
ROBERT M. BOWMAN, Lt. Col., USAF
Director, Development Directorate
Deputy for Advanced Space Programs

FOR THE COMMANDER

UNCLASSIFIED

SECURITY CLASSIFICATION OF THIS PAGE (When Data Entered)

REPORT DOCUMENTATION PAGE

READ INSTRUCTIONS
BEFORE COMPLETING FORM

1 REPORT NUMBER (19)
(18) SAMSO TR-77-110

~~2 GOVT ACCESSION NO~~ (9) Final rept. 1 May 75-31 May 77

~~3 RECIPIENT'S CATALOG NUMBER~~

4 TITLE (and Subtitle)
(6) Optical Angular Motion Sensor,
Phase Two - Final Report

5 TYPE OF REPORT on Phase 2,
Technical Report
5-1-75 through 5-31-77

6 PERFORMING ORG REPORT NUMBER

(10) H. T./Braswell, S. A./Chin Bing,
J. W./Fontenot,
W. E./Miller [redacted]
N. J./Ockman

8 CONTRACT OR GRANT NUMBER(s)
(15) F04701-76-C-0044

9 PERFORMING ORGANIZATION NAME ~~AND ADDRESS~~
Chrysler Corporation Defense-Space Division
New Orleans, La. 70189

10 PROGRAM ELEMENT PROJECT TASK AREA & WORK UNIT NUMBERS
(11) 31 May 77

11 CONTROLLING OFFICE NAME AND ADDRESS
Department of the Air Force
Headquarters Space and Missile Sys. Org.
Los Angeles, California 90009

12 REPORT DATE
5-31-77

13 NUMBER OF PAGES
~~178~~ (12) 211p.

14 MONITORING AGENCY NAME & ADDRESS (if different from Controlling Office)

15 SECURITY CLASS (of this report)
Unclassified

15a DECLASSIFICATION DOWNGRADING SCHEDULE

16 DISTRIBUTION STATEMENT (of this Report)

Distribution A - Unlimited

DISTRIBUTION STATEMENT A
Approved for public release;
Distribution Unlimited

17 DISTRIBUTION STATEMENT (of the abstract entered in Block 20, if different from Report)

18 SUPPLEMENTARY NOTES

19 KEY WORDS (Continue on reverse side if necessary and identify by block number)

Triaxial Measurement	Polarization
Optical Angular Sensor	Angle Transfer
Alignment	5 Arc Seconds Accuracy

20 ABSTRACT (Continue on reverse side if necessary and identify by block number)

See Reverse Side of this Page.

DD FORM 1 JAN 73 1473 EDITION OF 1 NOV 65 IS OBSOLETE

Unclassified

SECURITY CLASSIFICATION OF THIS PAGE (When Data Entered)

083310

20. Continued.

The Optical Angular Motion Sensor (OAMS) Program, Phase II, consisted of the fabrication and testing of a prototype model to demonstrate compliance with OAMS performance requirements. The qualification model consisted of a transmitter, a receiver, and an electronics assembly. The alignment information was transmitted between the transmitter and receiver on three discrete polarized beams.

A prototype flight model was designed and the components for two (2) units plus spares have been acquired.

The primary objective of this program was to re-package the brassboard design of Phase I to reduce power, weight and size, and to improve reliability and maintainability. The performance of each of the three channels was improved by the use of higher power LEDs, more efficient collecting optics, and higher responsivity detectors.

Preferred and military standard parts were incorporated to maintain performance and ensure qualification of flight hardware.

Performance and calibration tests were performed to show compliance with the sensor requirements, and to generate system equations, i.e. curve fitting. Thermal testing was performed on the brassboard unit to demonstrate performance over a 40-100 degrees Fahrenheit temperature range. All Phase II work was performed at a separation distance of the transmitter and receiver heads of 50 feet.

ACCESSION for
NTIS Section ☑
DDC Section ☐
UNANNOUNCED ☐
JUSTIFICATION
BY
DISTRIBUTION/AVAILABILITY CODES
Dist. AVAIL. and/or SPECIAL
A

OPTICAL ANGULAR MOTION SENSOR

PHASE TWO

FINAL REPORT

CONTRACT NO. F04701-76-C-0044

PREPARED BY: H. T. BRASWELL, S. A. CHIN BING, J. W. FONTENOT,
W. E. MILLER, N. J. OCKMAN

APPROVED BY: W E Miller APPROVED BY: George Kline, Capt
DATE: 24 May 1977 DATE: 24 May 1977

DISTRIBUTION A - UNLIMITED

CHRYSLER CORPORATION DEFENSE-SPACE DIVISION
NEW ORLEANS, LOUISIANA

SUMMARY

The Optical Angular Motion Sensor (OAMS) Program, Phase II, consisted of the redesign and conversion of the Phase I OAMS Brassboard into a qualified Advanced Brassboard having a significant improvement in performance and reliability. The Phase II objective was to develop a modular OAMS design to provide the benefits of standard components and interchangeability. Component specifications were generated from the results of the Advanced Brassboard Tests and a prototype Flight Model was designed. Long lead time components for two (2) Flight Model instruments plus spares were purchased.

In Phase II modifications were made to the Phase I design which provided increased performance and allowed the range to be extended from 25 to 50 feet. The modifications included:

- The utilization of three different LED light sources which became available after the Phase I effort. These LED's were of a higher power output than those of Phase I.
- To accommodate the new LED's, a different collimating lens system was incorporated. The Phase II lens system utilized aspheric collecting optics which increased the light collection efficiency.
- The Phase I detectors were replaced by detectors having a higher responsivity.
- The electronics were replaced by preferred and military standard parts to maintain and improve performance and maintainability.

Qualification testing and evaluation was performed on all new components and a reliability program was performed in accordance with applicable parts of MIL-STD-1543 and statistical reliability studies were performed on sub-systems and systems.

Calibration curves were obtained from the Advanced Brassboard from which curve fitting polynominals were generated. In addition thermal testing over the range 40 to 100 degrees Fahrenheit was performed.

Independent tests were performed by the Guidance Test Division of Holloman Air Force Base.

The feasibility of using the polarization concepts in triaxial attitude sensing was demonstrated, and in Phase II Flight Hardware was designed and Advanced Brassboard Hardware was built

PREFACE

Chrysler Corporation Michoud Defense-Space Division submits this final report, which covers the work performed in compliance with the work statement of contract F04701-76-C-0044. This contract was issued by the Department of the Air Force, Headquarters Space and Missile Systems Organization (SAMSO), AF Unit Post Office, Los Angeles, California 90009.

The program included the redesign and modification of the Phase I Brassboard of a 3-axis Optical Angular Motion Sensor (OAMS) into an Advanced Phase II Brassboard. Qualification tests were performed on the Advanced Brassboard from which component specifications and a design for a Flight Model were generated.

The authors acknowledge many helpful discussions with Messrs. M. Arck, J. Redmann, G. Anderson, E. Farr, Dr. T. Kazangey, I. K. Egashira, J. Howell and J. Hall of Aerospace Corporation, Lt. G. Shaw and Capt. G. Rhue of SAMSO and K. Miles of Holloman A.F.B.

TABLE OF CONTENTS

Section		[illegible]
	DD FORM 1473	i
	SUMMARY	iv
	PREFACE	v
1.0	INTRODUCTION	1-1
2.0	OBJECTIVE	2-1
3.0	POLARIZATION TECHNIQUES	3-1
4.0	RECOMMENDED CONCEPT	4-1
5.0	PARAMETRIC ANALYSIS	5-1
6.0	ADVANCED BRASSBOARD DESIGN	6-1
7.0	FLIGHT MODEL DESIGN	7-1
8.0	SYSTEM TEST AND EVALUATION	8-1
9.0	CONCLUSIONS AND RECOMMENDATIONS	9-1
10.0	REFERENCES AND BIBLIOGRAPHY	10-1
Appendix A	Nuclear Survivability	

FIGURES

Number		Page
3-1	Angle Sensing Crystal	3-4
5-1	Lateral Axis Optics Schematic	5-8
5-2	Roll Axis Optics Schematic	5-13
5-3	OAMS Analysis Block Diagram	5-17
5-4	SYNC Demod Block Diagram	5-20
5-5	Advanced Brassboard Gains	5-25
5-6	OAMS Control Loop	5-34
5-7	Bode Plot	5-40
5-8	Detector/Pre-Amp Circuit	5-43
5-9	Equivalent Inverting Amplifier Circuit	5-44
5-10	Equivalent Noise Circuit	5-48
5-11	System Output Noise Measurement	5-53
6.1-1	OAMS Block Diagram	6-2
6.1-2	Pitch Yaw Channels Electrical Schematic Phase II	6-3
6.1-3	Roll Channel Electrical Schematic Phase II	6-4
6.1-4	Wiring Electronic Schematic Phase II	6-17
6.2-1a	Advanced Brassboard Transmitter - Yaw Channel	6-19
6.2-1b	Advanced Brassboard Transmitter - Pitch Channel	6-19
6.2-2	Advanced Brassboard Receiver	6-22
6.3-1	OAMS System Advanced Brassboard	6-26
6.3-2	Transmitter Base Mounted	6-27
6.3-3	Receiver Base Mounted	6-28
7.1-1	Flight Model Electronic Package	7-2
7.1-2	Flight Model Base Mounted	7-3
7.1-3	Flight Model Back Mounted	7-4
7.2-1a	Transmitter Optical Flight Model Design - Roll Channel	7-15
7.2-1b	Transmitter Optical Flight Model Design - Lateral Channel	7-15
7.2-2	Transmitter Ray Trace	7-17
7.2-3	LED Intensity Profile SLH-20	7-20
7.2-4	LED Intensity Profile SL1162-3	7-20
7.2-5	Details of Wollaston Prism	7-21
7.2-6a	Receiver Optical Flight Model Design - Roll Channel	7-24
7.2-6b	Receiver Optical Flight Model Design - Lateral Channel	7-24
7.2-7	Receiver Ray Trace	7-26
7.2-8	Detector Focal Plane	7-29
7.3-1	Transmitter Back Mounted	7-31
7.3-2	Receiver Back Mounted	7-32
8-1	Pitch Calibration Curves	8-7
8-2	Roll Calibration Curves	8-8
8-3	Yaw Calibration Curves	8-9
8-4	Pitch, Yaw and Roll Crosscoupling	8-10
8-5	Pitch and Yaw Crosscoupling	8-11

TABLES

Number		Page
5-1	Mueller Matrices	5-10
5-2	Stokes Vectors	5-11
5-3	Angular Gain Factors	5-24
5-4	Irradiance/Detector/Pre-Amp Unbalance	5-24
5-5	LED Balance Values	5-26
5-6	LED Modulation Indices	5-26
5-7	436B Divider Phase Shift	5-26
5-8	Phase Angles OAMS Advanced Brassboard	5-28
5-9	Control LED Currents	5-36
5-10	Control Loop Gains	5-41
5-11	Tabulation of Noise Data	5-54
6.1-1	OAMS Filter Characteristics	6-7
6.1-2	Electronic Units and Location Assignment	6-10
6.1-3	LED Characteristics	6-12
6.2-1	LED Relative Peak Output	6-20
6.2-2	OAMS Transmitter Optical Components Phase II	6-21
6.2-3	OAMS Receiver Optical Components Phase II	6-23
7.2-1	OAMS Flight Model Optical Components - Transmitter	7-18
7.2-2	Temperature Ranges of OAMS Optical Adhesives	7-22
7.2-3	OAMS Flight Model Optical Components - Receiver	7-27
7.3-1	Weight and Volume	7-30
8-1	LED Characteristics	8-1
8-2	LED Burn-In Test (1000 Hrs.)	8-2
8-3	OAMS System Output	8-5
8-4	Changes in Irradiance/Detector/Pre Amp Unbalance	8-6
8-5	Accuracy Advanced Brassboard	8-14

1.0 INTRODUCTION

Space missions, both present and projected, require precise alignment information of sensors with respect to the spacecraft reference axes. If the sensor is located some distance from the reference baseplate, as is often the case, structural flexure during flight can result in significant misalignment errors. As spacecraft become larger this separation distance increases to the point that no system exists which can monitor this relative alignment with the sufficient accuracy required for precision space applications. The Optical Angular Motion Sensor (OAMS) offers a solution.

Conventional methods of optical alignment are basically modifications of autocollimation techniques. These techniques involve the precise measurement of the position of the center of an image in the focal plane of an objective lens. Accuracy is improved by increasing the focal length since a given angular deviation would then produce a larger displacement of the image in the focal plane. Arc-second accuracy usually requires focal lengths of about thirty inches. The length in general creates additional problems of mounting, portability and maintaining internal alignment.

However, there are more basic limitations of autocollimation. First, with presently available image position sensing devices, accuracy is increased only by sacrificing measurement range. Beyond a certain range the device only indicates the direction of displacement and not the degree of displacement. Autocollimation devices having arc-second resolution generally have a measuring range of a few minutes of arc. (This measurement range can be increased by the use of complicated repositioning of components in the focal plane. However, the absolute accuracy suffers and the dynamic response is greatly reduced due to the moving components.) The second disadvantage of autocollimation is the requirement for high quality optics over the measurement range. For arc-second resolution diffraction limited optics is a necessity. This requirement greatly increases the cost and the complexity of the system.

OAMS replaces the long focal length by an Angle Sensing Crystal. In fact, an objective lens is not required. The only requirement is an optical system to direct the light to the detector as it emerges from the Wollaston prism. Since imaging is not required, these optics can be extremely compact and low cost. The total optical train for an arc-second resolution instrument can be made to have a total length of less than six inches as opposed to thirty inches for an autocollimator.

In addition, the measurement range of OAMS can be extended to ten degrees or more by trading absolute resolution and field of view without sacrificing dynamic response. (An autocollimator has only a very small measurement range - when this is overcome by the use of moving parts, the overall accuracy and dynamic response suffers.)

Internal alignment tolerances are virtually non-existent compared to an autocollimator. The absence of moving parts may increase reliability and resistance to vibration and shock.

OAMS is a three axis angular motion sensing device whose output signals indicate the relative angular displacement between its two main parts, transmitter and receiver. The transmitter emits three beams of polarized modulated light, one beam for each of three axes. The receiver converts the light of each beam into an electrical signal proportional to the angular displacement of its corresponding axis. Thus roll, pitch, and yaw (reference axis being the line-of-sight between transmitter and receiver) are constantly monitored.

OAMS Phase I was development of the preliminary design Phase 0. OAMS Phase 0 was a conceptual study and preliminary design. The results were used as a basis for OAMS Phase II which involved the design, development, fabrication, and testing of a brassboard demonstration model. Documentation and specifications produced and used in these three Phases were:

Final Report	SAMSO-TR-75-120
Final Report	SAMSO-TR-73-6
Performance Evaluation Test Plan	CEI No. 73-6-TP
Prime Item Development Specification	CEI No. 73-6 Rev. A
Silicon Photodetector	CEI No. 73-6-A Rev. A
Emitting Source Pitch Channel	CEI No. 73-6-B Rev. A
Emitting Source Yaw Channel	CEI No. 73-6-C Rev. A
Emitting Source Roll Channel	CEI No. 73-6-D Rev. A
Angle Sensing Crystal (ASC)	CEI No. 73-6-E Rev. A

Other potential areas in which the OAMS system may be used are:

a) Transfer reference alignment between guidance platform and tracking mounts

b) Alignment of communications satellite to earth

c) Alignment while tracking space targets

d) Angular monitoring of space objects

e) Transfer of alignment to mounts external to spacecraft

f) Transfer of alignment between tracker and pointing of high energy lasers

g) Missile aiming

h) Structure flexure monitoring

2.0 OBJECTIVE

2.1 General

The objective of Phase II was the design of a flight model of the Optical Angular Motion Sensor (OAMS) to show compliance with its performance requirements in the anticipated environments, as set forthin SAMSO Specification 73-6. The development model was bench tested at Holloman A.F.B.

2.1.1 Goals

The performance goals were a) angular deflection measurement to an accuracy of ± 2 arc second (3 axis 1 sigma), b) measurement range ± 0.25 degree about Line of Sight (LOS), and c) operation at a distance of 15.2 meters (50 feet).

2.1.2 Engineering Tasks

The following major engineering tasks were performed:

a. Data analysis and evaluation. Analyze data obtained during Phase I and obtain additional data during Phase II. Evaluate OAMS performance for short and long term stability.

b. Evaluate the demonstration model design and parametric analysis documented in Phase I Final Report.

c. Conduct design verification/development tests as specified in the approved test plan.

2.1.3 Performance Requirements

The following list defines the major performance required for an OAMS System.

a. Functional characteristics

b. Performance characteristics

   1. Measurement range; ± 900 arc sec
   2. Calibration
   3. Accuracy
   4. Output signals; 1.0 mv/arc sec
   5. Saturation characteristics
   6. Response time; 10 hz
   7. Operating distance; 15.2 meters
   8. Temperature range; 40-100°F

c. Mechanical interface

d. Functional interface

e. Optical interface

f. Volume

g. Weight

h. Structure design

i. Nuclear survivability

2.1.4 Contract Data Requirements List

Documentation required for program

2.1.5 Amendment P0001 - Increase in estimated cost and fixed fee.

2.1.6 Amendment P0002 - Contract change to redesign OAMS flight model.

2.1.7 Amendment P0003 - Increase incremental funding.

2.1.8 Amendment P0004 - Increase incremental funding.

2.1.9 Amendment P0005 - Increase incremental funding.

2.1.10 Amendment P0006 - Increase funding to cover the ordering of long lead items.

2.1.11 Amendment P0007 - Increase incremental funding to cover cost of OAMS test at Holloman AFB, New Mexico.

2.1.12 Amendment P0008 - Additional funding.

2.1.13 Amendment P0009 - Realign the work effort in accordance with new schedule.

A summary of the results for each listed item follows:

Item 2.1.1: Performance goals a,b and c met under all test conditions.

Item 2.1.2: Engineering tasks completed:

a. Data analysis and evaluation

b. Model design evaluated; parametric analysis documentated.

c. Design verification/development tests conducted.

Item 2.1.3: Performance Requirements

a. Functional characteristics of the system met the general requirements of the OAMS system

b. Performance characteristics met pitch, roll and yaw requirements.

The following primary requirements were:

1. Measurement range - The angular range met the goals of 900 arc seconds in each axis.
2. Calibration - Calibration curves are generally a sine curve and can be defined by a low order polynomial of less than six terms.
3. Accuracy - Systematic errors generally met the requirements of less than ± 5 arc seconds for rotations about any single axis at the 900 arc seconds range.
4. Ouput signals of the brassboard are adjustable to 1 mv per arc second.
5. Response time - 10 Hertz requirement was met.
6. Operating distance - required distance of 50 feet was met.
7. Temperature range - determination of performance throughout the range 40° - 100° needs further effort.
8. Mechanical interface - to be determined.
9. Functional interface - to be determined.
10. Optical interface - requirements met.
11. Volume - transmitter and receiver met volume requirements.
12. Weight - transmitter and receiver met weight requirements.
13. Multiple targets - not applicable to Phase II.
14. Structure design - mechanical and thermal requirements met.
15. Nuclear survivability - Study only. (Appendix A)

Item 2.1.4: CDRL - All documents submitted.

The reports that were produced during the Phase I contract were:

General Test Plan (OAMS Brassboard) - CEI No. 73-6-TP, Rev A

Critical Component Test Plans - CEI No. 73-6-CCTP

Configuration Prime Item Development Specification - CEI No. 73-6, Rev A

Configuration Item Critical Components Specifications:

Silicon Photodetector - CEI No. 73-6-A, Rev A

Emitting Source - Pitch Channel - CEI No. 73-6-B, Rev A

Emitting Source - Yaw Channel - CEI No. 73-6-B, Rev A

Emitting Source - Roll Channel - CEI No. 73-6-D, Rev A

Angle Sensing Crystal - CEI No. 73-6-E, Rev A

Final Technical Report - SAMSO TR-75-120

The reports that were produced during the Phase II contract were:

Optical Angular Motion Sensor Phase II - Final Report, May 1977.

Critical Design Review April 1977.

OAMS Evaluation After Temperature Testing, November 1976.

Preliminary Design Review, March 1976.

Item 2.1.5: Amendment P0001 - Modified the contract to cover ordering the necessary long lead items for redesign and rebuild of the brassboard electronics.

Item 2.1.6: Amendment P0002 - Modified contract to cover effort to be performed in the design of the OAMS flight model up to the completion of Critical Design Review (CDR).

Item 2.1.7: Amendment P0003 - Increased the incremental funding.

Item 2.1.8: Amendment P0004 - Increased incremental funding to cover period through 15 August 1976.

Item 2.1.9: Amendment P0005 - Increased incremental funding to cover period through 30 September 1976.

Item 2.1.10: Amendment P0006 - Modified contract to cover the ordering of long lead time items required for fabrication of the qualification and flight model; increased funding to cover this additional procurement.

Item 2.1.11: Amendment P0007 - Covered cost of participating in testing the OAMS System at the Central Inertial Guidance Test Facility, Holloman AFB, New Mexico. Increased allotted incremental funding to cover estimated period through 15 March 1977.

Item 2.1.12: Amendment P0008 - Provided additional funding for estimated coverage through 30 November 1976.

Item 2.1.13: Amendment P0009 - Work effort realigned in accordance with new schedule; Final Report delivery date: 31 May 1977.

2.2 Design

The design areas covered in Phase II were twofold: 1) a redesign of the Phase I Brassboard into a Phase II Advanced Brassboard suitable for qualification testing, and 2) the design of a prototype Flight Model.

2.2.1 Advanced Brassboard Design

The Advanced Brassboard was a modification of the Phase I Brassboard. The areas of major redesign consisted of the following:

Transmitter

- LED's - the Phase I LED's were replaced by LED's having a higher light output.
- Collimating Lenses - the collimating lenses were changed to accommodate the new LED's and to provide the required field of view for Phase II. (This change was made only in the pitch channel for comparison purposes).
- Mechanical - mechanical changes were made in component mounting hardware to accommodate the new LED's and Lenses.

Receiver

- Detectors - the Phase I detectors were replaced by detectors having a higher effective responsivity.
- Objective Lenses - new objective lenses were incorporated in the receiver to accommodate the detectors and the required field of view.
- Mechanical - mechanical changes were made in the detector and less mounting hardware to accommodate the new components.

Electronics

- Standard Parts - where possible preferred and military standard parts were used.
- Power Consumption - reduced power consumption was achieved by redesign of the power supply and LED drivers. The power consumption was reduced from 150 to 20 watts.

- Operational Amplifiers - the operational amplifiers were replaced by units having low noise, low output offset, and low output offset drift with temperature.

- Packaging - The electronics were repackaged into a smaller volume and weight configuration. Modular design was incorporated to improve maintainability.

2.2.2 Flight Model

The Advanced Brassboard was tested. From the results of the testing and from additional analysis a design and component specifications were generated for a prototype flight model. In addition to the testing of the Advanced Brassboard the following design and/or analysis was performed.

Transmitter

- Angle Sensing Crystal - The Angle Sensing Cristal thickness was changed from 2.0 to 3.0 mm to accommodate the required field of view of the flight model.

- Mechanical - mechanical redesign was performed to provide for new components and flight model configuration.

- Optical Ray Trace - an optical ray trace was performed on the transmitter optical design.

Receiver

- Angle Sensing Crystal - the thickness was changed from 2.0 to 3.0 mm to provide for the required field of view.

- Filters - the roll channel filter was changed from 930 mm to 935 mm to accommodate for a slightly different LED peak wavelength from the Phase I design.

- Mechanical - mechanical redesign was performed to provide for new components and flight model configuration.

- Optical Ray Trace - an optical ray trace was performed on the receiver optical design.

Electronics

- Reliability - "S" level failure rate components were chosen if available from manufacturers. Non "s" level components were selected for the lowest failure rate manufactured.

- Packaging - the electronics were repackaged to meet the size and maintainability requirements in Prime Item Spec. CEI No. 73-6, Rev. A.

- Power Supply - the power supply was optimized for system efficiency.

2.3 Summary of Results

2.3.1 Summary of Phase O

In the initial phase of the OAMS Program, concepts that could be used for angular measurement were identified and evaluated. A concept making use of the polarized nature of radiation and the interaction of polarized radiation in optical crystals was selected as the OAMS concept. The feasibility of the concept was proven analytically and demonstrated experimentally in the laboratory. A preliminary design of an angular measurement system based upon the polarization concept was accomplished. The preliminary design included the generation of optical, mechanical and electrical drawings.

2.3.2 Summary of Phase I

A brassboard OAMS system was fabricated and tested to evaluate the capability of achieving the required goals. The feasibility of using polarization and birefringent crystals for precision angular measurement was demonstrated. The brassboard demonstrated that relative angular motion in roll, pitch and yaw could be measured to an accuracy of better than five arc seconds.

The test results of the brassboard were generally within the prototype requirements. Translation errors were greater than expected. An analysis of this problem resulted in a redesign of the LED control loop to compensate for the variations in the energy profile of the LEDs while moving across the field of view. The new LED control loop was installed in the brassboard.

The signal to noise ratio of the roll channel was higher than expected due to decreased light levels. At 25 feet the resolution was below requirements but at 10 feet they were satisfactory. The internal optical system was degraded due to components variation from specifications. This situation was corrected during the program extension.

The Light Emitting Diodes in the pitch and yaw channels degraded during tests and in the brassboard tests. They were unsatisfactory for flight hardware and were replaced by another type of LED.

2.3.3 Summary of Phase II

All the components that will be used in the flight model were purchased and assembled into an advanced brassboard model (only the reliability level will be better for the flight models, cost and delivery time were the reason for this level of components in the advanced brassboard model).

The transmitter head in an advanced brassboard configuration is complete. This includes components that will be used in the flight model. Due to funding and time limitations only the pitch channel in the advanced brassboard transmitter head was completely changed to the flight model design. Assembly and detail drawings are available for this configuration. The flight model design is a particular back mounting configuration and is shown in general assembly drawings.

The receiver head in an advanced brassboard configuration is complete. This includes components that will be used in the flight model. Assembly and detail drawings are available for this configuration. The flight model design is a particular back mounting configuration and is shown in general assembly drawings.

The electronics unit in an advanced brassboard configuration is complete. This includes components that will be used in the flight model. Assembly and detail drawings are available for this configuration. This configuration uses all the electronics components that will be used in the flight model but no flight model packaging was considered in the advanced brassboard design; also, a test panel unit is incorporated in this unit. Schematic, circuit and wiring diagrams are available and included on these are general circuit board layouts. The flight model design is a particular mounting configuration and is shown in general assembly drawings showing printed circuit board positions and board component sensity layouts. Schematic circuit and wiring diagrams are drawn for the flight model design, this also includes a test panel unit.

2.4.1 Applicable Documents

The following documents were applicable to the OAMS Phase II program to the extent specified in the column entitled "Tailored Application".

Document No.	Title	Tailored Application
MIL-STD-1543	Reliability Program Requirements for Space and Missile Systems	Para 4.0, 4.1, 4.3 4.5, 4.5.1, 4.5.2, 4.6, 5.1, 5.2.1, 5.2.3, 5.3, 5.4.1, and 5.4.2
MIL-STD-1521	Technical Reviews and Audits for Systems Equipment and Computer Programs	Appen C, 30.2, 30.3, 30.4, 30.8, 30.9, 30.12, 30.18
MIL-I-45208A 16 Sep 63	Inspection System Requirements	ALL
SAMSO Specification No. 73-6 31 Dec 72	Prime Item Development Specification for an Optical Angular Motion CEI Part I	ALL
SAMSO Specification No. 73-6 30 June 75	Specification for an Optical Angular Motion CEI Part I	ALL
SAMSO STD 73-2C 2 Sept 1975	SAMSO Electronic Parts Standard	To suit OAMS requirements per modification P00006 to contract.

2.4.2 Reference Documents for OAMS Phase II

Document No.	Date	
MIL-E-8983A	30 Nov. 71	Electronic Equipment Aerospace Extended Space Environment, General Specification for
MIL-Q-9858A	16 Nov. 63	Quality Program Requirements
USAF Specification Bulletin 515	3 Nov. 59	Control of Non-conforming Supplies
SAMSO CEI Spec. 73-6	31 Dec. 72	Prime Item Development Specification for an Optical Angular Motion Sensor
MIL-STD-891A	1 June 72	Contractor Part Control and Standardization Program
MIL-STD-1515	2 Oct. 72	Fasteners Used in the Design and Construction of Aerospace Mechanical Systems
SYGS Exhibit 10002 Revision 1	15 June 70	Nuclear Survivability
SAMSO-TR-73-6	31 Dec. 72	Optical Angular Motion Sensor Concept Definition and Preliminary Design Phase
Test Plan No. 73-6-TP	31 Dec. 72	Performance Evaluation Test Plan for the Engineering Prototype of an Optical Angular Motion Sensor
Test Plan No. 73-6-TP Revision A	15 Mar. 76	General Test Plan for the Engineering Prototype of an Optical Angular Motion Sensor.
SAMSO-TR-75-120	30 Apr. 75	Optical Angular Motion Sensor Phase I Final Report
Test Plan No. EO-76, TR-1	15 Sep. 76	Performance Evaluation Test Plan for the Brassboard of an Optical Angular Motion Sensor
Test Plan No EO-76 TP-2	15 Nov. 76	Optical Component Performance Evaluation Test Plan for a Brassboard of an Optical Angular Motion Sensor

3.0 POLARIZATION TECHNIQUES

3.1 Polarization

Polarization is a property which defines the transverse nature of light electric waves. Fully polarized light is characterized by orientation of all the electric wave transverse planes in one direction. Unpolarized light is characterized by the transverse plane orientation being equally distributed in all directions. Partially polarized light is a combination of the two conditions.

Light or radiation is not fully defined until its Stokes parameters are known. In 1852 G. G. Stokes defined four unique characteristics of light which fully describe its intensity and polarization components. The parameters are generally illustrated by the following vector referred to as the Stokes Vector.

$$\begin{bmatrix} S_0 \\ S_1 \\ S_2 \\ S_3 \end{bmatrix}$$

where S_0 - intensity of light (polarized and unpolarized)

S_1 - horizontal/(vertical) plane preference

S_2 - 45 degree/(-45 degree) plane preference

S_3 - right/(left) hand circular preference

These are the unique characteristics of polarized light that can be separated, identified and measured.

Each Stokes parameter has the dimension of intensity and applies to polarized light when treated as a quasi-monochromatic wave. Super position techniques are used for wide optical bands not meeting the quasi-monochromatic condition by dividing it into a number of quasi-monochromatic wavelength bands. The parameter S_0 represents the total intensity. The parameter S_1 is equal to the excess in intensity of light transmitted by a polarizer that accepts linear polarization in the azimuth $\theta = 0$ degrees over the light transmitted by a polarizer that accepts linear polarization in the azimuth $\theta = 90$ degrees.

The parameter S_2 has a similar interpretation with respect to the azimuths $\theta = 45$ degrees and $\theta = 135$ degrees. Finally, the parameter S_3 is equal to the excess in intensity of light transmitted by a device that accepts right-handed circular polarization over the light transmitted by a device that accepts left-handed circular polarization. A positive

Stokes parameter value indicates a horizontal, 45 degree, or right circular preference, whereas a negative value indicates its orthogonal component; that is, vertical, -45 degrees, or left circular preference.

The Stokes vector, in addition to defining polarized light characteristics also provides a useful tool for systematic analysis of polarized light. Through the use of Mueller matrices for polarized optical elements such as quarter-wave plates, polarizers, modulators, Wollastons and analogous components it is possible to predict the resultant polarized light characteristics after passing through a series of these elements. Reference 2.

Techniques

Numerous polarization systems have been designed and built for measuring angles by means of measuring changing polarization parameters such as phase relationship.

The first phase of this study was the review of known polarization systems for adaptability to spacecraft requirements as outlined in the OAMS technical requirements for performance and design.

Earlier programs had utilized several modulation techniques which included rotating polarizers, oscillating crystals, Kerr cells, light choppers, electro-optical light modulators (EOLM), scanners, and source modulation.

Of this group, both the EOLM and source modulation have several advantages for use in OAMS system as such devices are static (non-moving). The polarization modulation technique can be demodulated with synchronous detection techniques offering excellent, narrow band, signal-to-noise characteristics. A disadvantage associated with the EOLM concept is the high operating voltage of the device. Modulation of the source with either continuous wave (CW) or pulses offers a low voltage system but results in more complex data handling subsystems.

A new system was developed which combines 2 LED sources multiplexed into a single modulated polarized light beam. This accomplished the advantages of the EOLM and low voltage modulation requirements of a spacecraft.

The next requirement was the projection of a polarized light beam from the transmitter with a defined polarization signature which will not change unless birefringence is introduced. This was accomplished by the use of birefringent crystals which establish and maintain the polarization characteristics as a function of the angular relationship of the light to the crystals.

3.2 Roll Axis

In the case of roll measurement about the LOS, the transmitter Wollaston prism passes two orthogonal plane-polarized beams of light (one plane assocated with each LED) which are oriented in a fixed manner to the transmitter body. The receiver Wollaston prism (which is rotated about its axis 45 degrees to the transmitter prism) splits each polarized LED beams into two orthogonal components that fall onto two separate detectors. At zero roll angle, both components of each LED are equal and the difference in the output of the two detectors is zero. For non-zero roll angle, the light from each LED is not equally distributed to the detectors and the difference is a measure of the roll angle.

A translation of the receiver across the transmitter beam should not be sensed, since the orientation of the polarization from each LED is uniform across the beam, and is not affected by translation. Separation of the signals in the three channels is achieved by using LEDs of three different output wavelengths (permitting use of optical bandpass filters) and by using three electrical modulation frequencies (one per channel) to drive the LEDs, permitting electrical filtering. The Roll channel LED wavelength is 935 nm and its modulation frequency is 925 hz.

3.3 Lateral Axis

In the case of pitch and yaw axis sensing, polarization angle measuring techniques have been developed by Chrysler. Each axis is sensed in an identical manner, thus the description to follow applies to both. The primary optics of the transmitter consist of a Wollaston prism, quarter-wave plate and an ASC. The receiver optics consist of a matching ASC, Wollaston prism and filter. The ASC was developed to introduce optical (polarization) phase shift between the ordinary and extraordinary rays as a function of the entrance of light. The ASC is composed of two identical birefringent crystals with the optical axis oriented at 45° to the surface of the crystal. The two crystals are turned at 90° to each other so that the extraordinary and ordinary rays of the polarized light passing through the first crystal are transposed in the second crystal as shown in Figure 3-1.

A zero optical phase shift between the e- and o-rays will occur for light perpendicular to the surface of the crystal. But for light not perpendicular, the phase retardation of the polarized light leaving the crystal will change as a function of the entrance angle. The crystals have one sensitive axis and one insensitive axis. The sensitivity of the angle sensing crystal is a function of the crystal line material and its thickness (see Ref. 3).

The quarter-wave plate positioned between the transmitter Wollaston and ASC converts the diverging orthogonally polarized beams from the two LEDs to circularly polarized beams, one left-handed and one right-handed. As the diverging beams traverse the transmitter ASC, the circularly

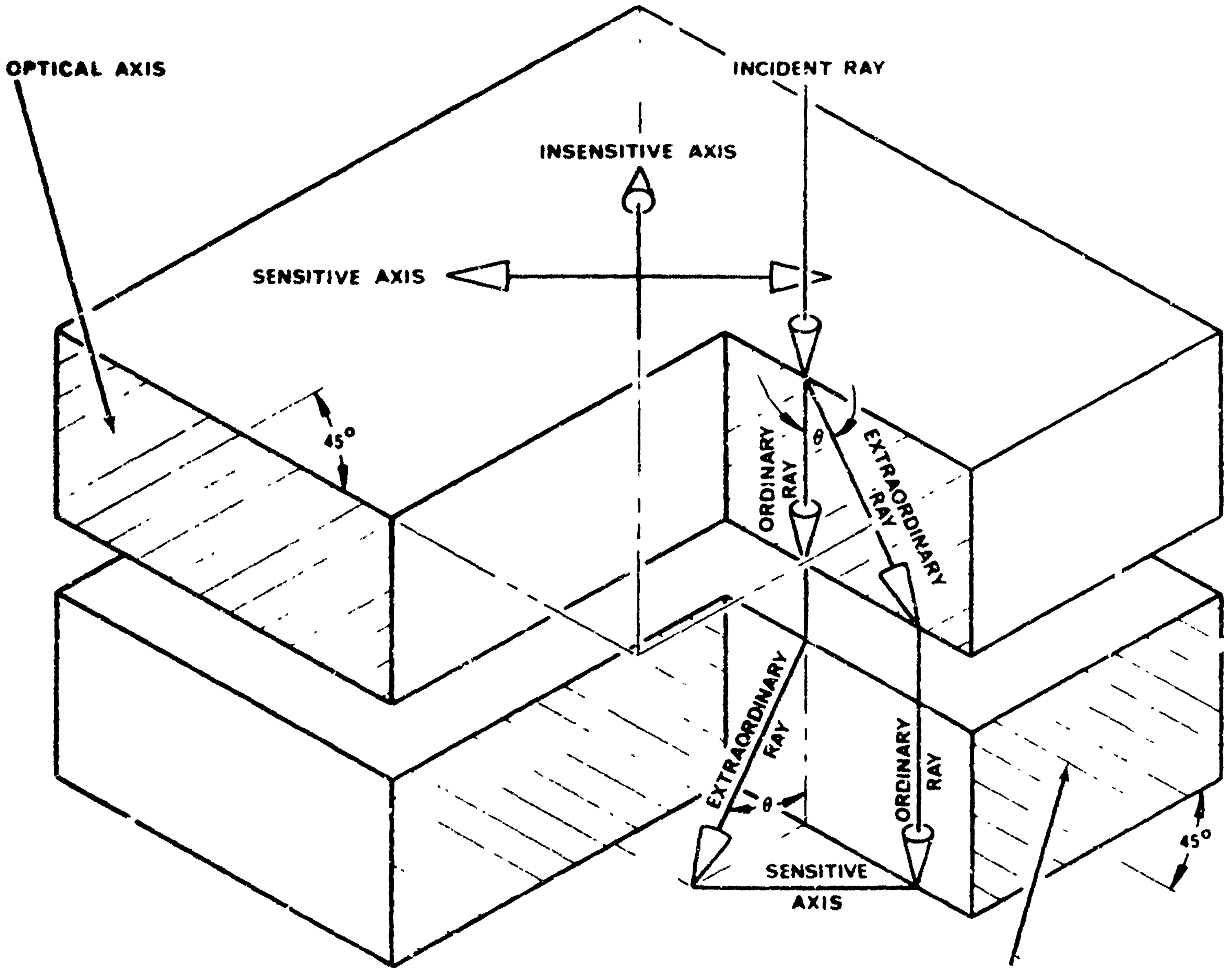
OPTICAL AXIS
INCIDENT RAY
INSENSITIVE AXIS
SENSITIVE AXIS
45°
θ
ORDINARY RAY
EXTRAORDINARY RAY
EXTRAORDINARY RAY
θ
ORDINARY RAY
SENSITIVE AXIS
45°
OPTICAL AXIS

Figure 3-1. Angle Sensing Crystal

polarized beams become elliptically polarized, the degree of ellipticity being a function of the angle of the beam with the ASC surface. The ASC in the receiver is reversed in orientation (i.e. backwards) to that in the transmitter, and as long as the two ASCs are parallel, the ellipticity introduced by the transmitter ASC is cancelled by the receiver ASC, resulting in circularly polarized beams. This feature permits lateral translation without affecting pitch or yaw measurements. When the circularly polarized beams are split by the Wollaston prism, the two detectors receive equal irradiance from each LED and the difference is zero, indicating zero pitch (or yaw) angle. When the face of the receiver ASC is not parallel to the face of the transmitter ASC, the resulting beams on the receiver Wollaston prism are elliptically polarized (rather than circular) and the two detectors are given unequal amounts of irradiance from each LED, with the difference being indicative of the pitch (or yaw) angle. The pitch and yaw channel sensitive axes are orthogonal and signal separation is accomplished by light sources of different wavelengths (810 nm - pitch and 850 nm - yaw). This separation is enhanced by the use of optical filtering and by driving the light source at different frequencies (one octave separation).

4.0 RECOMMENDED CONCEPT

The present Advanced Brassboard design and subsequent recommended flight model are a derivative of three stages of study/work effort. The first stage called OAMS Phase 0 investigated various concepts for OAMS applications that would meet the program requirements. This investigation considered the latest state-of-the-art components in the evaluation effort to determine their feasibility in OAMS use. During the latter portion of this effort, a single channel breadboard of the recommended concept was assembled to demonstrate its feasibility.

The recommended concept from Phase 0 consisted of three channels used in measuring angular movements in pitch, roll and yaw. Basic to the system is the generation of plane polarized light and to operate optically and electronically on this light to extract the desired angular information. Physically the OAMS is made up of three units, namely a transmitter, receiver and the electronics for processing purposes. Each channel, at the transmitter, uses two LEDs that are electrically driven in a manner where the emitted light is amplitude modulated at a frequency with one octave separation between channels. In addition, each LED pair is chosen to emit light at a distinct wavelength. With frequency and wavelength separation, plus the use of a narrow bandwidth optical filter (selected for each channel) at the receiver, cross axis interference from the signal sources is negligible.

Common to all channels at the transmitter is the focusing lens and a Wollaston prism. This configuration describes the roll transmitter channel. A quarter-wave plate and an ASC are the additional optics required for each of the pitch and yaw channels.

The receiver unit is within the cone of light projected by each channel. The unit contains three distinct polarization sensing assemblies. The pitch and yaw channel assemblies are each composed of an ASC (matched to the transmitter ASC), a Wollaston prism, optical filter, focusing lens and two detectors. The roll assembly is similar but does not contain the ASC.

The electronic unit takes the difference of the a.c. signal from the detector pair and in conjunction with the d.c. sum signal operator on the differential signal as an Automatic Gain Control (AGC). The AGC adjusts the differential signal to compensate for varying light level changes. A LED control loop is employed to balance the light output of the two LEDs.

OAMS Phase I implemented the concept described in "Phase 0" with a brassboard design. As a result of tests on this design, several improvements were recommended towards the latter portion of this phase. These improvements consist of 1) high light output and longer life LEDs,

2) improved LED control loop, 3) larger active area and higher responsivity detectors, and 4) improved circuit design. In Phase II, the recommended design changes of Phase I were incorporated in a new advanced brassboard design. Tests made on this latest design indicated areas of additional design improvements and optical adjustment methodology for the present recommended flight model design.

PARAMETRIC ANALYSIS NOMENCLATURE

A_o	Op amp open loop gain; volt/volt
A_{gc}	Transconductance of CONT LED drive amp; mhos
A_n	n^{th} signal peak amplitude; mv
A_{rh}	Horizontal detector/pre-amp transresistance; ohms
A_{rc}	Transresistance of CONT LED light path; ohms
A_{rr}	Transresistance of REF LED light path; ohms
A_{rv}	Vertical detector/pre-amp transresistance; ohms
ASC_R	RCVR Angle sensing crystal operator
ASC_T	XMTR angle sensing crystal operator
A_{vc}	Voltage gain of detector/pre-amp circuit; volt/volt
A_{vn}	Noise voltage gain of detector/pre-amp circuit; volt/volt
$1/a$	Lead/lag network attenuation factor
B_n	n^{th} signal peak amplitude (mv); Noise bandwidth (hz)
b_c, b_r	Factor used to account for LED inefficiency and light attenuation
C	Abbreviation for cosine term
C_j	Detector junction capacitance; pf
C_p	Bypass capacitance; μf
e_c	Control signal time-varying voltage; mv
e_d	Differential time-varying voltage; mv
e_H	Detector/pre-amp instantaneous voltage; mv
e_n	Op amp thermal spot voltage noise; nv/(hz)$^{\frac{1}{2}}$
e_{nf}	Feedback resistor thermal voltage noise; μv/(hz)$^{\frac{1}{2}}$

$e_{n\omega}$	Detector/pre amp thermal voltage noise; $\mu v/(hz)^{\frac{1}{2}}$
e_{oc}	Oscillator time-varying voltage; volts
e_{nos}	System output thermal voltage noise; mv rms
e_o	Processing branch time-varying voltage; mv
e_o'	Processing branch time-varying full-wave voltage; mv
e_S	Sum instantaneous voltage (mv);
	Square wave time-varying voltage (volts)
e_V	Detector/pre amp instantaneous voltage; mv
f_i	i^{th} frequency; hz
f_n	10 hz filter corner frequency; hz
f_o	Op amp 1st break frequency; hz
$G(s)$	Forward loop gain; volt/volt
G_c	CONT amp gain; volt/volt
G_d	Differential gain; volt/volt
G_f	AGC 10 hz filter gain; volt/volt
G_m	CONT loop SYNCH DEMOD gain; volt/volt
G_s	Sum gain; volt/volt
G_x	AGC divider gain; volt/volt
$H(s)$	Feedback loop gain; volt/volt
I_b	Background light dc current component; ma
I_c	CONT LED dc current; ma
I_r	REF LED dc current; ma
i_C	CONT LED instantaneous current; ma
i_c	CONT LED time-varying current; ma
i_{dh}	Horizontal detector instantaneous current; μa
i_{dv}	Vertical detector instantaneous current; μa

i_n	Op amp thermal spot current noise; pa/(hz)$^{1/2}$
i_{nh}	Horizontal detector thermal spot current noise; pa/(hz)$^{1/2}$
i_R	REF LED instantaneous current; ma
i_r	REF LED time-varying current; ma
J_C	CONT LED irradiance; w/cm^2
J_d	Irradiance at RCVR, w/cm^2
J_{dh}	Irradiance at horizontal detector; w/cm^2
J_{dv}	Irradiance at vertical detector; w/cm^2
J_R	REF LED irradiance; w/cm^2
J_t	Irradiance at XMTR; w/cm^2
K	Angular multiplying factor (arc sec./rad); Total loop gain (volt/volt) Degrees Kelvin
k	Optical angular gain; Boltzmann's constant = 1.374×10^{-23} joules/^{o}K
m_c	CONT LED Modulation index
m_r	REF LED Modulation index
$P(\xi)$	General linear polarizer operator
p	Lead/lag pole radian frequency; rad/sec
Q	Quarter-wave plate operator
R_d	Damping resistor; ohms
R_f	Feedback resistor; ohms
R_i	i^{th} resistor; ohms
R_j	Detector junction resistance; ohms
R_p	Op amp circuit input bias resistor; ohms
R_s	Detector series resistance; ohms
R_{sh}	Responsivity of horizontal detector; amp/w

R_{sv}	Responsivity of vertical detector; amp/w
S	Abbreviation for sine terms
s	Laplace operator
$\bar{S}_i$	Stokes vector unpolarized light (REF or CONT) operator
$\bar{S}$	Stokes vector operator
T	Temperature, ^{o}K
$T(\theta_r)$	Roll matrix operator
t	Time
u	Relative ratio of CONT to REF LED a.c. light signal
V_c	Control voltage;
	Divider denominator dc input voltage; volts
V_{cos}	Control dc voltage offset; volts
V_o	System output voltage; mv
V_s	Sum dc voltage; volts
V_{xos}	DC voltage offset at AGC divider denominator; mv
V_x	Divider denominator dc voltage; volts
V_y	CONT divider or AGC divider instantaneous output voltage; volts
V_z	CONT divider or AGC divider instantaneous numerator input voltage; volts
W_R	RCVR Wollaston prism operator
W_T	XMTR Wollaston prism operator
$\bar{X}$	Mean of noise data; mv
x_i	i^{th} noise data; mv
z	Lead/lag network zero; rad/sec
α	ASC_T incident angle; arc sec.
	Roll Channel nonorthogonality angular displacement; deg.

α_c	Phase shift in CONT LED driver circuit; deg.
α_h	Damping factor of horizontal detector/pre amp
α_n	Damping factor of 10 hz filter
α_r	Phase shift in REF LED driver circuit
α_v	Damping factor of vertical detector/pre amp
β	ASC_R incident angle (deg.)
	Voltage feedback ratio of op amp circuit (volt/volt)
ΔJ	Irradiance difference of CONT and REF LED; w/cm^2
δ_n	Damping ratio of 10 hz filter
δ_h	Damping ratio of detector/pre amp circuit
ϵ	Detector/pre amp phase shift; deg.
θ	Generalized rotational angle; arc sec.
θ_c	Total phase shift at CONT loop SYNCH DEMOD; deg.
θ_p	Total phase shift at processing SYNCH DEMOD; deg.
θ_r	Roll angular movement; arc sec.
ΛJ	ΔJ multiplied by $\sin\xi_r$ or $\cos\xi_r$; w/cm^2
ξ_c	W_T polarization plane angle assigned to CONT LED; deg.
ξ_h	W_R polarization plane angle assigned to horizontal detector; deg.
ξ_r	W_T polarization plane angle assigned to REF LED; deg.
ξ_v	W_R polarization plane angle assigned to vertical detector; deg.
Σ	Sum
ΣJ	Irradiance sum of CONT and REF LED; w/cm^2
σ_n	System noise standard deviation; mv rms
ϕ	Control loop phase shift; deg.
ϕ^+	Phase angle due to CONT and REF LED driver circuit reflected in processing path; deg.

ϕ^-	Phase angle due to CONT and REF LED driver circuit reflected in control loop; deg.
ϕ_a	Op amp phase shift; deg.
$\phi_{a\Delta}$	Differential circuit phase shift; deg.
$\phi_{a\Sigma}$	Sum circuit phase shift; deg.
ϕ_1	Difference of ξ_r and ξ_h; deg.
ϕ_2	Sum of ξ_r and ξ_h; deg.
ψ	Generalized phase shift; deg.
ω	Generalized radian frequency; rad/sec.
ω_n	Horizontal detector/pre-amp natural radian frequency; rad/sec
ω_o	Op amp 1st break radian frequency; rad/sec
ω_n	Control loop 10 hz filter natural radian frequency; rad/sec
$_v$	Vertical detector/pre-amp natural radian frequency; rad/sec

5.0 PARAMETRIC ANALYSIS

This section summarizes pertinent findings where some are salient and others not so obvious without some detail analysis. The usual pattern followed here is to present the analysis along with assumptions and rationale and then confirm the results by actual laboratory measurements or comments on our experience while working with OAMS. The subjects discussed are: 1) the optical model development for the lateral and roll channels along with analysis of the effect of Wollaston nonorthogonality, 2) the control loop analysis and 3) the detector/pre amp circuit analysis and special requirements necessary to maintain system electrical noise to a minimum.

5.1 System Equations

The system equations presented here are an outgrowth of the analysis described in the OAMS Phase I report. Modifications are made to reflect our deeper understanding, based upon many hours of experimentation with OAMS, of the system operation and peculiarities. The intent is not to replace previous derivations, but to update the models, where required, in order to bring to light a fuller understanding of the operating features of OAMS.

The optical model development starts with the application of the Mueller matrices that describe the behavior of polarized and unpolarized light irradiance through various optical elements used in OAMS. Of course the OAMS concept is keyed upon the premise of optical paraxial characteristics, a key requirement in OAMS applications. Using a similar approach, but under a separate subsection, equations relating the effects of Wollaston prixm nonorthogonality are developed.

Following the optical model development, the rationale and required algebra are developed to interlink the electrical signal equations with that of the optics to form one composite mathematical model. Interpretation of the system equations is presented for each case. The model is not general since to incorporate every feature greatly increases the complexity of an already complex model and muddles our perception of the importance of that one key parameter that governs a particular aspect of OAMS operation.

5.1.1 Optical/Electrical Model Development

The objective of OAMS is to accurately measure (within 9 arc seconds) the relative angular movements in pitch, roll and yaw, over a ± 15 arc minute range, between a transmitter (XMTR) and a receiver (RCVR) separated by a distance of 15.2 m. Signal separation enhancement for each channel is attained by assigning each channel a particular spectral wave length and electrical frequency. The unpolarized light source for each channel is derived from two light-emitting-diodes (LEDs); one called Reference (REF LED) and the other Control (CONT LED). The LEDs are chosen to emit light about a center spectral wavelength of about 810 nm for pitch, 935 nm for roll and 850 nm for yaw. The optical bandwidth (BW) for each channel is further modified by an optical filter located in the RCVR. The a.c. light intensity for each channel is electrically modulated at 925 hz for roll, 1850 hz for yaw and 3700 hz for pitch.

The equations, describing the irradiance at the two detector surfaces for the lateral channels (pitch and yaw) will be derived first. Following the derivation of the roll irradiance equations, the technique for coupling the optical and electronics into one composite system equation will be presented along with our interpretations.

5.1.1.1 Lateral Channels

OAMS lateral channel optics for analysis purposes (Figure 5-1) is divided into two sections, namely, the transmitter and receiver optics. The transmitter optics consist of two LEDs, Wollaston prism (W), quarter-wave plate (Q), and angle sensing crystal (ASC_T). Each LED is electrically driven by a d.c. and a.c. component. The composite is an amplitude modulated light signal with the REF LED a.c. term driven 180° out-of-phase from that of the CONT LED. The resulting unpolarized light, from each LED, is fed thru an objejtive lens (not shown) for collimation purposes. The transmitter Wollaston prism (W_T) is reversed fed whereby the constituent LED light is imparted along the prism's e-ray or o-ray path. Wollaston deviation angle between the two beams is determined by the prism's wedge angle. (Note that REF or CONT LED position with respect to e- or o-ray path is of no concern since the OAMS angular polarity is controlled electronically by the synchronous demodulator (SYNCH DEMOD) circuitry).

Light output from W_T consists of a usable beam with one-half of the total LED irradiance, and the rejected beam with the other one-half is deviated away from the system's central axis. The quarter-wave plate converts the usable beam into a right- or left-handed circular beam. It should be noted, at this point, that the beam entering Q consists of two components - one vertical (CONT LED) and the other horizontal (REF LED). Assignment of the CONT and REF LEDs to these planes for analysis purposes is arbitrary and will only involve a polarity change should our assumption be incorrect. As the diverging beams traverse ASC_T, the circularly polarized beams become elliptically polarized, the degree of ellipticity being

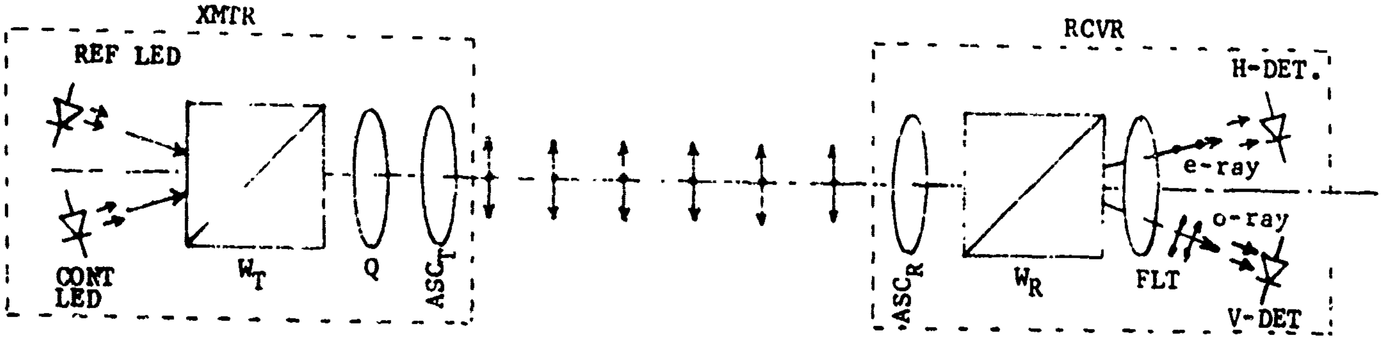

Figure 5-1. Lateral Axis Optics Schematic

a function of the angle of the beam with the surface of ASC_T. ASC_R is reversed in orientation (i.e. backwards) to ASC_T and as long as the two ASCs are parallel, the ellipticity introduced by ASC_T is cancelled by ASC_R, resulting in circularly polarized beams. This feature permits lateral translation without affecting pitch or yaw measurements. The beam enters W_R in the forward direction and the resulting output consists of two beams, one horizontal and the other vertical, that are sensed by the horizontal and vertical detectors. Following W_R an optical filter is used to narrow the BW to 32 nm for pitch and 30 nm for yaw. Also, not shown on the diagram is the plano-convex lens that focuses the beam to the detectors.

Analysis of the pitch and yaw channels is identical with the exception that their sensitive axes are orthogonal. The sensitive axis for pitch at the XMTR is vertical while for yaw it is (orthogonal to that of pitch) horizontal. Employing the Muller matrices listed in Table 5-1 and the Stokes vectors of Table 5-2, the irradiance at the transmitter aperture and at the detectors is shown in operator form by Eq. (5-1) and (5-2).

$$J_t = ASC_T(\alpha,0^\circ)\ Q(45^\circ)\ \bar{S}(0^\circ,90^\circ) \qquad (5\text{-}1)$$

$$J_d = W_R(0^\circ,90^\circ)\ ASC_R(\beta,180^\circ)\ T(\theta_r)\ J_t \qquad (5\text{-}2)$$

$$= W_R(0^\circ,90^\circ)\ ASC_R(\beta,180^\circ)\ T(\theta_r)\ ASC_T(\alpha,0^\circ)\ Q(45\ )\ \bar{S}(0^\circ,90^\circ)$$

Equation (5-2) is an exceedingly compact description of incident irradiance at the detector surfaces and a few clarifying words are in order. When expanding this equation, it must be remembered that matrices do not commute; therefore they must be applied in the proper order. Other keypoints about the equation and the matrix/vector elements are:

a. Stoke vector, $\bar{S}(0^\circ,90^\circ)$ says the irradiance output from W_T is composed of two orthogonal beams, one at zero degrees and the other at 90 degrees (see ref. 1 and 2). In all cases the beams are referenced to W_T and are always orthogonal (in the ideal case).

b. The quarter-wave plate's fast axis (FA) was positioned at + 45° rather than - 45° from the zero reference axis. This is an arbitrary choice for OAMS and could have been just as well positioned at -45° without any degradation of system output.

c. ASC_T and ASC_R must be positioned in a complementary mode in order for the incident angles to subtract.

d. The operator $T(\theta_r)$ represents the roll geometrical relationship between the Poincare' sphere (see ref. 2) and the Stokes vector. It represents the effect of the system roll on the polarization state of the beam and can be represented by a matrix very much like those used in the rotation of coordinate systems (right-handedness for this case) in cartesian geometry.

Table 5-1. Mueller Matrices

Linear Optical Elements and Operator Notations	Mueller Matrices
Wollaston prism $W_R(0^\circ, 90^\circ)$ ↕ $(+ \longrightarrow 0^\circ)$ $(- \longrightarrow 90^\circ)$	$1/2 \cdot \begin{bmatrix} 1 & \pm 1 & 0 & 0 \\ \pm 1 & 1 & 0 & 0 \\ 0 & 0 & 0 & 0 \\ 0 & 0 & 0 & 0 \end{bmatrix}$
Angle Sensing Crystal $ASC_R(\beta, 180^\circ)$	$\begin{bmatrix} 1 & 0 & 0 & 0 \\ 0 & C_{k\beta} & 0 & S_{k\beta} \\ 0 & 0 & 1 & 0 \\ 0 & -S_{k\beta} & 0 & C_{k\beta} \end{bmatrix}$
$ASC_T(\alpha, 0^\circ)$	$\begin{bmatrix} 1 & 0 & 0 & 0 \\ 0 & C_{k\alpha} & 0 & -S_{k\alpha} \\ 0 & 0 & 1 & 0 \\ 0 & S_{k\alpha} & 0 & C_{k\alpha} \end{bmatrix}$
Quarter-wave plate $Q(45^\circ)$ ⤢	$\begin{bmatrix} 1 & 0 & 0 & 0 \\ 0 & 0 & 0 & -1 \\ 0 & 0 & 1 & 0 \\ 0 & 1 & 0 & 0 \end{bmatrix}$
$Q(-45^\circ)$ ⤡	$\begin{bmatrix} 1 & 0 & 0 & 0 \\ 0 & 0 & 0 & 1 \\ 0 & 0 & 1 & 0 \\ 0 & -1 & 0 & 0 \end{bmatrix}$
Roll rotation transformation $T(\theta_r)$	$\begin{bmatrix} 1 & 0 & 0 & 0 \\ 0 & C_{2\theta_r} & -S_{2\theta_r} & 0 \\ 0 & S_{2\theta_r} & C_{2\theta_r} & 0 \\ 0 & 0 & 0 & 1 \end{bmatrix}$
General linear polarizer $P(\xi)$	$1/2 \cdot \begin{bmatrix} 1 & C_{2\xi} & S_{2\xi} & 0 \\ C_{2\xi} & C_{2\xi}^2 & C_{2\xi}S_{2\xi} & 0 \\ S_{2\xi} & C_{2\xi}S_{2\xi} & S_{2\xi}^2 & 0 \\ 0 & 0 & 0 & 0 \end{bmatrix}$

Table 5-2. Stokes Vectors

POLARIZATION STATE	VECTORS
Lateral axes W_T output $\bar{S}(0^\circ, 90^\circ)$	$\frac{1}{2}\begin{bmatrix} \Sigma J \\ \Delta J \\ 0 \\ 0 \end{bmatrix}$
Roll axes W_T output $\bar{S}(\pm 45^\circ)$	$\frac{1}{2}\begin{bmatrix} \Sigma J \\ 0 \\ \Delta J \\ 0 \end{bmatrix}$
LED unpolarized light (i = r or c) $\bar{S}_i$	$\begin{bmatrix} J_i \\ 0 \\ 0 \\ 0 \end{bmatrix}$
Generalized for lateral channel W_T output $\bar{S}(\xi_r, \xi_c)$	$\frac{1}{2}\begin{bmatrix} \Sigma J \\ \Delta J \\ \Lambda J \\ 0 \end{bmatrix}$
Generalized for roll channel W_T output $\bar{S}(\xi_r, \xi_c)$	$\frac{1}{2}\begin{bmatrix} \Sigma J \\ \Lambda J \\ \Delta J \\ 0 \end{bmatrix}$

c. Since $\overline{S}(0^\circ, 90^\circ)$ is a column vector the resulting composition of J_d is also a column vector. The first term (first row) of the resulting column vector is the incident irradiance and the other terms describe the polarization state of the beam.

Substitution of the appropriate matrices for the operators shown in Eq. (5-2) and performing the indicated multiplication, the following irradiance equation is derived:

$$J_d = \tfrac{1}{2}\{ \Sigma J + (\pm) \Delta J(C_{k\alpha} S_{k\beta} - C_{2\theta_r} S_{k\alpha} C_{k\beta}) \} \qquad (5\text{-}3a)$$

Please note that the terms C and S are short hand notation for cosine and sine, respectively. Substitution of the trigonometric identity

$$S_{k(\alpha-\beta)} = S_{k\alpha} C_{k\beta} - C_{k\alpha} S_{k\beta}$$

into Eq. (5-3a) yields,

$$J_d = \tfrac{1}{2}(\Sigma J - (\pm) \Delta J(S_{k(\alpha-\beta)} - S_{k\alpha} C_{k\beta} (1 - C_{2\theta_r}))\} \qquad (5\text{-}3b)$$

Assumption No. 1 -

The third term in Eq. (5-3b) is much smaller than the second term. This is particularly true for θ_r's of 1800 arc second or less, plus the product of $S_{k\alpha}C_{k\beta}$ will further diminish the third term.

Therefore, the irradiance at the horizontal and vertical detector surfaces is:

$$J_{dh} = \tfrac{1}{2}(\Sigma J - \Delta J S_{k(\alpha-\beta)}) \qquad (5\text{-}4a)$$

$$J_{dv} = \tfrac{1}{2}(\Sigma J + \Delta J S_{k(\alpha-\beta)}) \qquad (5\text{-}4b)$$

Assumption No. 2 -

Lateral and roll channel optics are assumed ideal; detectors are aligned properly.

5.1.1.2 Roll Channel

OAMS roll channel optics for analysis purposes is shown in Figure 5-2. In a similar way as that of the lateral channels, the objective lens at the XMTR and RCVR focusing lens are not shown.

Unlike the lateral channels the Wollaston prism W_T is rotated + 45° and the polarization planes are thus positioned as illustrated. The Stokes vector representation for two planes is defined in Table 5-2.

The irradiance at the detector surface is shown in operator form by Eq. (5-5). Substituting the appropriate matrices in Eq. (5-5) and performing the indicated multiplication yields Eq. (5-6).

$$J_d = W_R(0,90^o)T(\theta_r)\overline{S}(\pm 45^o) \qquad (5\text{-}5)$$

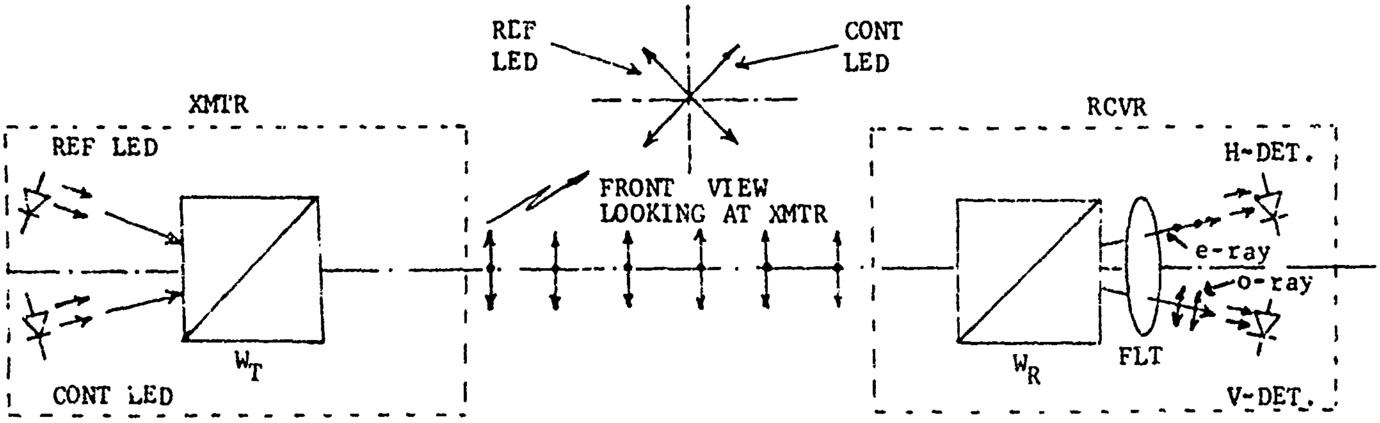

Figure 5-2. Roll Axis Optics Schematic

$$J_d = \tfrac{1}{2}(\Sigma J - (\pm)\ \Delta J S_{2\theta_r}) \qquad (5\text{-}6)$$

The resulting irradiance at the horizontal and vertical detector surfaces are:

$$J_{dh} = \tfrac{1}{2}(\Sigma J - \Delta J\ S_{2\theta_r}) \qquad (5\text{-}7a)$$

$$J_{dv} = \tfrac{1}{2}(\Sigma J + \Delta J\ S_{2\theta_r}) \qquad (5\text{-}7b)$$

Equations (5-4) and (5-7) are similar with the exception of the rotational angles. If we substitute θ for (α-β) and θ_r and letting k = 2 in the roll equations, a standard irradiance equation for the lateral and roll channels is established. Therefore, succeeding analysis can be performed with this generalization in mind.

5.1.1.3 Coupling of Optics and Electronics

With the development of the irradiance equations we can now commence with the detailed portion of the analysis. The next step is to expand SUM J and DELTA J terms of the Stokes vector, which are functions of LED intensities, in a manner that will include all pertinent electrical parameters. Once this is accomplished, these terms are substituted into the horizontal and vertical detector irradiance equations where grouping of the a.c. and d.c. components occur. The irradiance terms are then converted to electrical terminology whereby the OAMS electronic processing techniques are introduced and a composite set of system equations emerges.

$$J = J_C + J_R \qquad (5\text{-}8)$$

$$J = J_R - J_C \qquad (5\text{-}9)$$

Note that Eq. (5-9) implies the LED preferential plane, that is, vertical and horizontal for the lateral channels or ± 45° for the roll channel.

REF and CONT LED electrical drive signals are defined as:

$$i_R = I_r - i_r S(\omega t - \alpha_r) \qquad (5\text{-}10)$$

$$i_C = I_c + i_c S(\omega t - \alpha_c) \qquad (5\text{-}11)$$

To convert these current terms to irradiance requires our multiplying Eq. (5-10) and (5-11) by a suitable nonlinear conversion factor. A linear approximation will be used to account for LED efficiency and intensity loss of the beam during transit through the various optical elements and space. Therefore, J_C and J_R will be approximated by

$$J_C = b_c(I_c + i_c\, S(\omega t - \alpha_c)) \qquad (5\text{-}12)$$

$$J_R = b_r(I_r - i_r\, S(\omega t - \alpha_r)) \qquad (5\text{-}13)$$

The current-to-optical intensity characteristic of the LED is nonlinear and due to the nonlinearity harmonic terms are present in the OAMS processing circuitry. Spectral measurements were recorded in the pitch channel (Brassboard No. 2) and the data indicated the presence of both higher and lower harmonic terms. The even harmonic terms are filtered out by the SYNC DEMOD circuit while a small d.c. signal proportional to the odd harmonic terms are allowed through, but their magnitudes were measured to be constant over the ambient to 37.8°C (100°F) temperature. The d.c. intensity terms due to these frequencies cannot be removed and are an integral part of the total d.c. light level intensities. We do know that the composite d.c. term constitutes a small per cent of the total light intensity and since it is relatively constant, its effect on OAMS is minimal. This rationale will be made clearer later in the analysis. Also, laboratory tests indicate that normal room lighting (flourescent derivative) has no noticeable effect on OAMS system output. However, an incandescent light will have an effect since a certain proportion of this light has spectral wavelength within that of an OAMS filter bandwidth. This form of background lighting would introduce a d.c. term in the processing circuitry and thus cause scaling errors in the angular measurement. OAMS operation in such an environment would of course require some form of shading and baffle apparatus to prevent direct lighting of the RCVR apertures. In the interest of simplification in the derivation we shall ignore this d.c. term and in the final equation introduce a term at the appropriate point that will account for its effect.

Assumption No. 3 -

Even harmonic terms are eliminated by the SYNC DEMOD circuitry.

Substitution of Eqs. (5-12) and (5-13) into (5-8) and (5-9) yields,

$$\Sigma J = b_c I_c + b_r I_r + b_c i_c S_{(\omega t-\alpha_c)} - b_r i_r S_{(\omega t-\alpha_r)} \qquad (5\text{-}14)$$

$$\Delta J = b_r I_r - b_c I_c - (b_r i_r S_{(\omega t-\alpha_r)} + b_c i_c S_{(\omega t-\alpha_c)}) \qquad (5\text{-}15)$$

Plugging in Eqs. (5-14) and (5-15) into the horizontal and vertical detector irradiance equation and letting kθ be the angle of the sine term the following set of irradiance equations are derived:

$$J_{dh} = \tfrac{1}{4}(A^+ - A^- - a^- + a^+ S_{k\theta}) \qquad (5\text{-}16)$$

$$J_{dv} = \tfrac{1}{4}(A^+ + A^- - a^- - a^+ S_{k\theta}) \qquad (5\text{-}17)$$

where

$$A^+ = b_r I_r \left(1 + \frac{b_c I_c}{b_r I_r}\right)$$

$$A^- = b_r I_r \left(1 - \frac{b_c I_c}{b_r I_r}\right) S_{k\theta}$$

$$a^+ = b_r i_r \left(S_{(\omega t-\alpha_r)} + \frac{b_c i_c}{b_r i_r} S_{(\omega t-\alpha_c)}\right)$$

$$a^- = b_r i_r \left(S_{(\omega t-\alpha_r)} - \frac{b_c i_c}{b_r i_r} S_{(\omega t-\alpha_c)}\right).$$

Please note that the "A" terms correspond to d.c. intensity while "a" terms are for a.c. intensity. A key point to notice here (not obvious until the later stages of OAMS development) is that both REF and CONT LED drive signals are phase shifted and that the terms a^+ and a^- are the result of a linear superposition of two waves of somewhat different amplitudes. To expand the sine terms by an

identity without regrouping terms would introduce cosine terms that would later muddle our interpretation. Instead we shall reformulate a^+ and a^- into a composite wave of the same frequency as the constituents although its amplitude and phase are different. Using the required trigonometric identities in a^+ and a^-, grouping sine and cosine terms, and then finding the resultant and total phase, the following equations were derived:

$$a^+ = b_r i_r a_0 \sin(\omega t + \phi^+) \qquad (5\text{-}18a)$$

$$a_0 = (1 + u^2 + 2u \cos(\alpha_c - \alpha_r))^{\frac{1}{2}} \qquad (5\text{-}18b)$$

$$\phi^+ = \tan^{-1}\left(-\frac{u \sin\alpha_c + \sin\alpha_r}{u \cos\alpha_c + \cos\alpha_r} \right) \qquad (5\text{-}18c)$$

$$a^- = b_r i_r a_1 \sin(\omega t + \phi^-) \qquad (5\text{-}19a)$$

$$a_1 = (1 + u^2 - 2u \cos(\alpha_c - \alpha_r))^{\frac{1}{2}} \qquad (5\text{-}19b)$$

$$\phi^- = \tan^{-1}\left(-\frac{u \sin\alpha_c - \sin\alpha_r}{u \cos\alpha_c - \cos\alpha_r} \right) \qquad (5\text{-}19c)$$

where $u = b_c i_c / b_r i_r > 1$.

It is important at this point to observe that u is the ratio of the CONT LED intensity (as seen by the detector) relative to that of the REF LED. These intensities are not exactly equal (reason for this will be explained later) thus ϕ^+ and ϕ^- are not only functions of phase shifts but are also functions of LED intensities. In addition, we know from measurements made on OAMS and on specific electrical components that neither α_c nor α_r are zero and that $\alpha_c > \alpha_r$. That $\alpha_c > \alpha_r$ is generally true, but cannot be assured in all cases. It will be shown later that the terms of Eq. (5-18) are associated with the forward path of the processing branch while the terms of Eq. (5-19) are associated with the LED control loop. Of particular interest here is a_1 which is the term used to describe LED balancing and ϕ^- the phase angle associated with the control loop. Examination of ϕ^- indicates that it is very sensitive to changes in u, α_c and α_r. Also, with $u > \cos\alpha_r / \cos\alpha_c$ a phase lag condition will be maintained by ϕ^- (more on this subject later).

With the irradiance equation in the format described we can now multiply each equation by a responsivity term to convert irradiance to electrical current as shown in the generalized block diagram of Fig. (5-3).

$$i_{dh} = \frac{R_{sh}}{4} J_{dh}$$

$$= \frac{R_{sh}}{4} (A^+ - A^- - a^- + a^+ S_{k\theta}) \qquad (5\text{-}20)$$

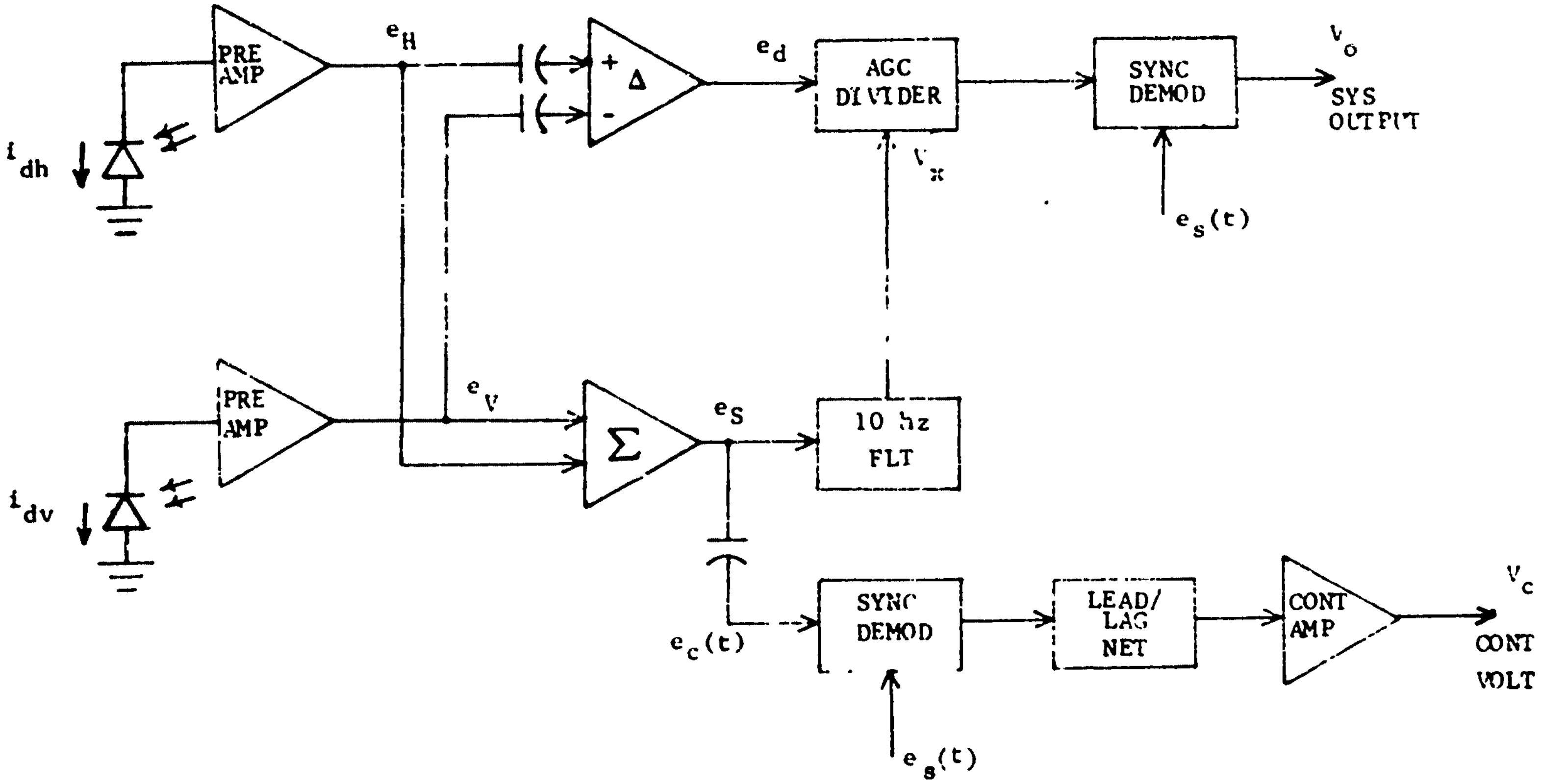
PRE AMP
PRE AMP
i_{dh}
i_{dv}
e_H
e_V
+
-
Δ
Σ
e_d
e_S
AGC DIVIDER
V_x
10 hz FLT
SYNC DEMOD
$e_s(t)$
V_o
SYS OUTPUT
$e_c(t)$
SYNC DEMOD
$e_s(t)$
LEAD/ LAG NET
CONT AMP
V_c
CONT VOLT

Figure 5-3. OAMS Analysis Block Diagram

$$i_{dv} = \frac{R_{sv}}{4} J_{dv}$$

$$= \frac{R_{sv}}{4} (A^{+} + A^{-} - a^{-} - a^{+} S_{k\theta}) \qquad (5\text{-}21)$$

The differential output can be obtained by performing the indicated operation according to Fig. (5-3).

$$e_d = G_d (e_H - e_V)$$

$$e_H = A_{rh} i_{dh}$$

$$e_V = A_{rv} i_{dv}$$

$$e_d = G_d (A_{rh} i_{dh} - A_{rv} i_{dv}) \qquad (5\text{-}22)$$

Substituting i_{dh} and i_{dv} into Eq. (5-22) and dropping the d.c. terms, since they are blocked by the capacitors, the following expression for the differential output results.

$$e_d \cong \frac{G_d A_{rh} R_{sh}}{4} \left\{ \left(\frac{A_{rv} R_{sv}}{A_{rh} R_{sh}} - 1 \right) a^{-} + \left(\frac{A_{rv} R_{sv}}{A_{rh} R_{sh}} + 1 \right) a^{+} \; S_{k\theta} \right\} \qquad (5\text{-}23)$$

Using a similar rationale for derivation of the sum expression the following group of equations result.

$$e_S = G_s (e_H + e_V)$$

$$e_S = G_s (A_{rh} i_{dh} + A_{rv} i_{dv}) \cong V_s + e_c$$

$$V_s = \frac{G_s A_{rh} R_{sh}}{4} \left\{ \left(\frac{A_{rv} R_{sv}}{A_{rh} R_{sh}} - 1 \right) A^{-} + \left(\frac{A_{rv} R_{sv}}{A_{rh} R_{sh}} + 1 \right) A^{+} \right\}$$

$$e_c = - \frac{G_s A_{rh} R_{sh}}{4} \left\{ \left(\frac{A_{rv} R_{sv}}{A_{rh} R_{sh}} - 1 \right) a^{+} \; S_{k\theta} + \left(\frac{A_{rv} R_{sv}}{A_{rh} R_{sh}} + 1 \right) a^{-} \right\}$$

The first term in V_s is much smaller than the second term since the result involves the product of the difference of two terms. The $S_{k\theta}$ in A^{-} further diminishes this product for small angles. A similar rationale applies for the first term in e . Therefore, these two equations simplify to the approximations listed here.

$$V_S \cong \frac{G_s A_{rh} R_{sh}}{4} \left(\frac{A_{rv} R_{sv}}{A_{rh} R_{sh}} + 1 \right) A^{+}$$

$$e_c \cong - \frac{G_s A_{rh} R_{sh}}{4} \left(\frac{A_{rv} R_{sv}}{A_{rh} R_{sh}} + 1 \right) a^-$$

Assumption No. 4 -

Phase angle shifts by the horizontal and vertical detector pre-amp circuitry are approximately the same. Proof verified later.

Modifying a^- to account for the detector/pre-amp circuit phase shift and substituting into e_c yields the following:

$$e_c \cong - \frac{G_s A_{rh} R_{sh}}{4} \left(\frac{A_{rv} R_{sv}}{A_{rh} R_{sh}} + 1 \right) b_r \, i_r \, a_1 \sin(\omega t + \theta_c) \qquad (5\text{-}24)$$

where

$$\theta_c = \phi^- - \varepsilon .$$

Returning to Fig. (5-3) we can now calculate

$$e_o = G_x \frac{e_d}{V_x}$$

$$e_o \cong \frac{G_d G_x}{G_s G_f} \left\{ \frac{\left(\frac{A_{rv} R_{sv}}{A_{rh} R_{sh}} - 1 \right) a^-}{\left(\frac{A_{rv} R_{sv}}{A_{rh} R_{sh}} + 1 \right) A^+} + \frac{a^+}{A^+} \quad S_{\psi} \right\}$$

$$e_o = K m_r \left\{ \frac{\left(\frac{A_{rv} R_{sv}}{A_{rh} R_{sh}} - 1 \right) a_1 S(\omega t + \theta_c)}{\left(\frac{A_{rv} R_{sv}}{A_{rh} R_{sh}} + 1 \right) \left(1 + \frac{b_c I_c}{b_r I_r} \right)} + \frac{a_o S_{k\theta} S(\omega t + \theta_p)}{\left(1 + \frac{b_c I_c}{b_r I_r} \right)} \right\} \qquad (5\text{-}25)$$

where

$$m_r = \frac{i_r}{I_r}$$ (REF LED modulation index)

$$\theta_p = \phi^+ - \varepsilon$$

and $K = \dfrac{G_d G_x}{G_s G_f}$ (To be used only if the coefficient of $S_{(\omega t + \theta_p)}$ at detector output is measured in volts).

Note that θ_c and θ_p are the amount of lagging phase shift required to properly synchronize the demodulator circuit. In order to account for background lighting and harmonic components in the d.c. sum, Eq. (5-25) can be modified to yield the more general form shown in Eq. (5-26) and (5-27).

$$e_o \cong \frac{K\, m_r}{\left(1+\frac{b_c I_c}{b_r I_r}+\frac{I_b}{b_r I_r}\right)}\left\{\frac{\left(\frac{A_{rv}R_{sv}}{A_{rh}R_{sh}}-1\right)a_1 S(\omega t+\theta_c)}{\left(\frac{A_{rv}R_{sv}}{A_{rn}R_{sn}}+1\right)}+a_o S_{k\theta}S(\omega t+\theta_p)\right\} \qquad (5\text{-}26)$$

$$V_s \cong \frac{G_s A_{rh}R_{sh}}{4}\left(\frac{A_{rv}R_{sv}}{A_{rh}R_{sh}}+1\right)\left(1+\frac{b_c I_c}{b_r I_r}+\frac{I_b}{b_r I_r}\right) b_r I_r \qquad (5\text{-}27)$$

Eqs. (5-24), (5-26) and (5-27) are the basic equations describing the OAMS system with both the CONT and REF LED on. With the REF LED on and CONT LED off Eqs. (5-28, (5-29) and (5-30) describe the system equations.

$$e_o \cong \frac{K\, m_r}{\left(1+\frac{I_b}{b_r I_r}\right)}\left\{\frac{\frac{A_{rv}R_{sv}}{A_{rh}R_{sh}}-1}{\frac{A_{rh}R_{sh}}{A_{rh}R_{sh}}+1}+\sin k\theta\right\}\sin(\omega t-\alpha_r-\varepsilon) \qquad (5\text{-}28)$$

$$V_s \cong \frac{G_s A_{rh}R_{sh}}{4}\left(\frac{A_{rv}R_{sv}}{A_{rh}R_{sh}}+1\right)\left(1+\frac{I_b}{b_r I_r}\right) b_r I_r \qquad (5\text{-}29)$$

$$e_c = -\frac{G_s A_{rh}R_{sh}}{4}\left(\frac{A_{rv}R_{sv}}{A_{rh}R_{sh}}+1\right) b_r i_r \sin(\omega t-\alpha_r-\varepsilon) \qquad (5\text{-}30)$$

System equation description is incomplete without some mathematical description of the SYNC DEMOD function. Briefly, the SYNC DEMOD consist of a gating circuit, a differential amplifier circuit and a 10 hz filter (see Fig. (5-4)). The signal

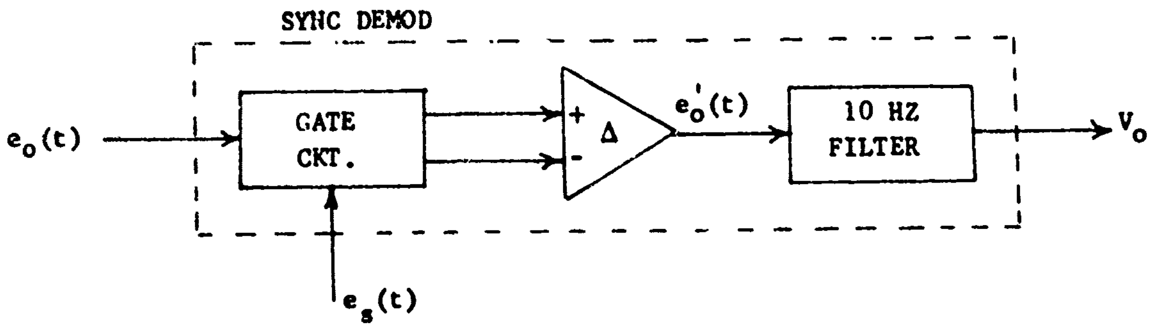

Figure 5-4. SYNC DEMOD Block Diagram

$e_s(t)$ is a periodic square wave synchronized with the channel frequency and phase shifted by θ_c or θ_p. Once the phase of $e_s(t)$ is synchronized with $e_o(t)$ the SYNC DEMOD output, V_o is proportional to the reference frequency amplitude and almost completely insensitive to its harmonics. What we want to explore here are the conditions where errors can be introduced due to harmonics and subsequent phase shift changes in $e_o(t)$ or $e_c(t)$. The output gating process along with the differential action is equivalent to multiplying the signal $e_o(t)$ or $e_c(t)$ by a square wave whose amplitude varies between +1 and -1, respectively. To hat end we can represent $e_s(t)$ by the Fourier series shown in Eq. (5-31) and $e_o(t)$ by Eq. (5-32). In Eq. (5-32) we are assuming that the first term in Eq. (5-26) is negligible (this reasoning will be discussed later).

$$e_s(t) = \frac{4}{\pi} \left(\sin \omega t + \frac{\sin 3\omega t}{3} + \frac{\sin 5\omega t}{5} + \ldots\right) \qquad (5\text{-}31)$$

$$e_o(t) = \sum_{n=1}^{\infty} A_n \sin n\omega t \qquad (5\text{-}32)$$

Multiplying Eqs. (5-31) and (5-32) and performing the required trigonometric functions, the following result is obtained:

$$e_o'(t) = e_o(t)\, e_s(t) \qquad (5\text{-}33)$$

$$= \frac{4}{\pi}\left\{ \sum_{n=1}^{\infty} \frac{A_n}{2} (\cos(n-1)\omega t - \cos(n+1)\omega t + \frac{1}{3}(\cos(n-3)\omega t - \cos(n+3)\omega t) + \frac{1}{5}(\cos(n-5)\omega t - \cos(n+5)\omega t) + \ldots)\right\} .$$

The 10 hz filter attenuates all frequency components in Eq. (5-33) according to the formula shown in Eq. (5-34).

$$At_n = (12\ ^{db}/_{oct}) \left(\frac{\log_{10} {}^{fi}/_{fo}}{\log_{10} 2} \right) \qquad (5\text{-}34)$$

Expansion of Eq. (5-33) and applying the condition described by (5-34) will result in the following output for V_o.

$$V_o = \frac{2}{\pi} \left(A_1 + \frac{A_3}{3} + \frac{A_5}{5} + \ldots\right) \qquad (5\text{-}35)$$

If $e_o(t)$ was phase shifted by an angle ψ as shown in Eq. (5-36) and following the same procedure described in deriving Eq. (5-33) the errors introduced are shown in Eq. (5-37).

$$e_o(t) = \sum_{n=1}^{\infty} A_n \sin(n\omega t - \psi) \qquad (5\text{-}36)$$

$$V_o = \frac{2}{\pi} \left(A_1 + \frac{A_3}{3} + \frac{A_5}{5} + \ldots\right) \cos \psi \qquad (5\text{-}37)$$

If $e_o(t)$ contains cosine terms their contributions to V_o are zero. If the cosine terms are phase shifted by ψ, V_o output will contain the terms shown in Eq. (5-38).

$$e_o(t) = \sum_{n=1}^{\infty} B_n \cos(nwt - \psi)$$

$$V_o = \frac{2}{\pi} \left(B_1 + \frac{B_3}{3} + \frac{B_5}{5} + \ldots\right) \sin \psi \qquad (5\text{-}38)$$

5.1.1.4 Equation Interpretations

Now that the OAMS system equations are derived, our task now is to interpret the meaning of the coefficients as applied to OAMS applications. Beginning with the system output Eq. (5-26), the first term represents an offset error that is a function of LED intensity balance factor and irradiance/detector/pre-amp balance factor. Note that per unit method of expressing one element function relative to another was used since it is easier to make comparisons on a percentage basis. LED balance is achieved by the CONT LED control loop (see Subsection 5.2) whose purpose is to maintain LED intensities in balance such that a_1 (Eq. 5-19b) approaches zero under ideal conditions. Because of the technique required to drive the CONT LED this error can only be maintained to within one per cent. The offset term is further diminished by the irradiance/detector/pre-amp factor, $\left(\frac{A_{rv}R_{sv}}{A_{rh}R_{sh}} - 1\right)$. By careful selection or pairing of the RCA-C30852 detectors, detectors with responsivity (R_{sv} and R_{sh}) differences of two per cent or less can be obtained. However, to account for pre amp circuit difference and irradiance difference at the detector surfaces the close-loop transresistance of one pre amp circuit is varied. Transresistance adjustment technique can best be understood if we momentarily refer to Eq. (5-28). With $\sin k\theta$ equal zero the offset term is the only remaining term, thus one can adjust the transresistance until system output approaches a small value. Once this balance is accomplished, the offset term of Eq. (5-26) is greatly diminished by the product of a_1 and the irradiance/detector/pre-amp factor. However, balancing error due to phase differences as that described by Eq. (5-37) may exist since $\theta_p \neq \alpha_r + \varepsilon$. These errors are kept small since the relative difference between the angles is small.

The second term in Eq. (5-26) is of course the one that yields the angular information desired from OAMS. For small angles the $\sin k\theta \approx k\theta$

radians and is scale factor modified by a_o divided by the denominator of the equation. Under ideal conditions the cosine term in Eq. (5-18b) is equal to two. Since phase angles exist the scale factor is a function of the difference between α_c and α_r. The requirements stipulated by a_o dictates that phase angle changes must be small in order to prevent scale factor changes over the required angular range. (This problem was very real at one stage of OAMS Brassboard No. 1 design). As shown in Eq. (5-18c) $\emptyset^+$ is not sensitive to reasonable changes in α_c, α_r and u, thus scale factor errors of the form described by Eq. (5-36) and (5-38) are minimized. SYNC DEMOD phase adjustments should be performed with both LED at several angular positions beginning with large angles down to small angles while simultaneously monitoring phase shifts. The term I_b found in the system and sum equations was included to account for the d.c. light introduced by harmonics and background illuminations. The harmonic terms are an integral portion of the sum voltage and will contribute to scale factor changes. Fortunately, the a.c. harmonics were measured and they are relatively constant with respect to time, therefore one could safely assume that the d.c. terms constitute a steady state condition and their effects cancelled out when the system is scale factor adjusted.

The control LED signal, Eq. (5-24), shows that the controlling factor is a_1. In a_1 the term 2u is diminished by the cosine term and thus indicates that the balancing effort must accommodate for phase angle difference between the phases generated in the CONT LED and REF LED drive circuits. Also, since $\emptyset^-$ is sensitive to α_c, α_r and u synchronization of $e_c(t)$ with the SYNC DEMOD periodic square wave must be made with both LED (compare phases shown in Eq. (5-24) and (5-30)). Any change in phase after SYNC DEMOD adjustment will affect the signal according to Eq. (5-37) and will therefore increase the LED balance errors. This phase shift along with the odd harmonics (Eq. 5-37) will hinder LED balance since the control voltage magnitude must account for these errors.

Irradiance/detector/pre-amp balance can be calculated by setting θ to zero and solving for the ratio $A_{rv}R_{sv}/A_{rh}R_{sh}$. Eq. (5-39) enables this calculation (note that V_o is expressed in mv).

$$\frac{A_{rv}R_{sv}}{A_{rh}R_{sh}} = \left| \frac{V_o\left(1 + \frac{I_b}{b_r I_r}\right) + Km_r}{V_o\left(1 + \frac{I_b}{b_r I_r}\right) - Km_r} \right| \tag{5-39}$$

In order to compute the multiplying factor K, the angular gain factor k for the pitch and yaw channels must be found using Eq. (5-40) (see Ref. 3, p. 484).

$$k = 180^o\ g/\lambda \tag{5-40}$$

where $g = 0.0084t$ for a quartz ASC(t equals crystal thickness).

The multiplying factor K is computed according to Eq. (5-41). See Table 5-3 for values of k and K. Note that the effects of sin $k\theta$ can be linearized by multiplying K by (kθ rad)/sin kθ. For example at 900 arc. sec. the sinkθ introduces a scale factor error of 1.2 per cent. Table 5-4 lists irradiance/detector/pre-amp unbalance on a percentage basis for system outputs of 100 and 1000 mv/arc sec. Background illumination and harmonic contents were assumed to be 5 per cent in calculation of these percentages.

$$K = \left(\frac{180^\circ}{\pi\ \text{rad}}\right)\left(\frac{3600\ \text{arc sec}}{1.0\ \text{deg}}\right)\left(\frac{1}{k}\right) \tag{5-41}$$

Table 5-3. Angular Gain Factors

Channel	k	K
Pitch	65.2	3165.6 $\frac{\text{arc sec}}{\text{rad}}$
Yaw	62.1	3321.5 $\frac{\text{arc sec}}{\text{rad}}$
Roll	2	103,132.4 $\frac{\text{arc sec}}{\text{rad}}$

Table 5-4. Irradiance/Detector/Pre-Amp Unbalance

Channels	V = 100 mv/arc sec	V = 1000 mv/arc sec
Pitch	8.0%	125.6%
Yaw	7.6%	116.3%
Roll	0.24%	12.1%

Note that the roll channel system output voltage is about 30 times more sensitive to unbalance changes. Physically this means that a higher differential gain G_d (see Fig. 5-5) is required and this naturally amplifies any electrical noise generated in the detector/pre-amp circuit. Also, according to RCA, the detector (hermetically sealed unit) relative responsivity changes will be less than 0.25 per cent over ambient to 37.8°C temperature range. Therefore, any unbalance in the order of 1000 mv/arc sec are not detector derivative.

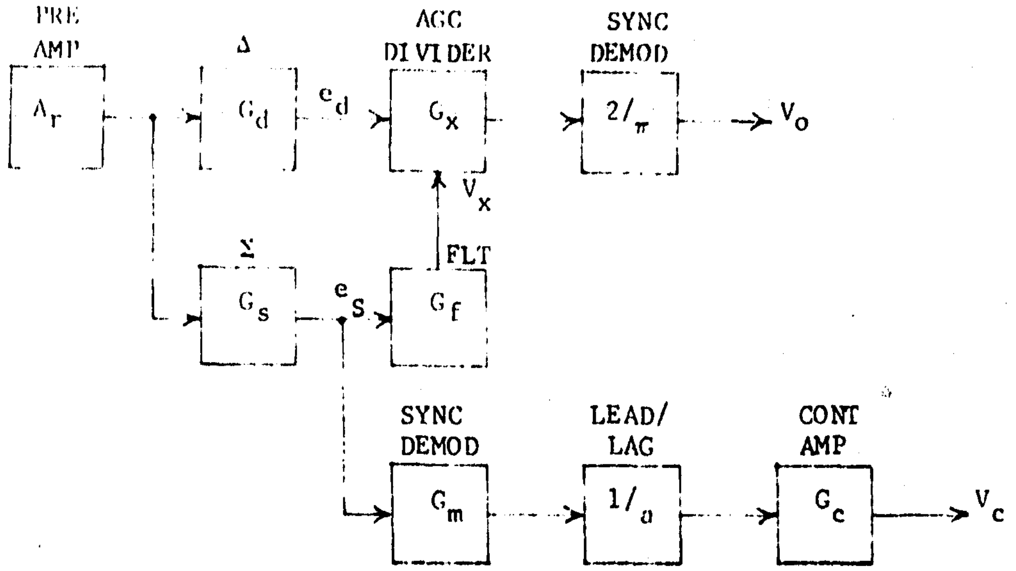
PRE AMP
A_r
Δ
G_d
e_d
AGC DIVIDER
G_x
SYNC DEMOD
$2/\pi$
V_o
V_x
FLT
Σ
G_s
e_S
G_f
SYNC DEMOD
G_m
LEAD/ LAG
$1/a$
CONT AMP
G_c
V_c

Channel	Gain Values						
	G_d	G_s	G_x	G_f	G_m	1/a	G_c
Pitch	16.8	2.12	2.0	21.0	6.37	0.125	3600.0
Yaw	11.3	1.91	2.0	10.1	6.37	0.125	3600.0
Roll	122.1	1.97	2.0	4.4	6.37	0.125	843.9

Figure 5-5. Brassboard No. 2 Gains

The ratio u, which expresses the amount of a.c. LED unbalance, is computed by Eq. (5-42).

$$u = 1 + \left(\frac{a(V_c \pm V_{cos})}{G_c G_m}\right) \div \left(\frac{(V_x \pm V_{xos})m_r}{2\ G_f}\right) \qquad (5\text{-}42)$$

Typical values for u, along with parameters required to calculate, are shown in Table 5-5 and 5-6. The modulation indices were chosen to avoid driving the LED current below 10 ma where the nonlinear characteristics are worst.

Table 5-5. LED Balance Values

Parameters	Pitch	Yaw	Roll
V_c	5.889 V	7.509 V	6.715 V
V_{cos}	2.3 V	0.4 V	2.2 V
* V_x	4.712 V	5.24 V	5.089 V
* V_{xos}	-59.4 MV	-41.9 MV	-54.0 MV
u	1.0129	1.0111	1.0129

$*V_x = G_f V_s$

Table 5-6. LED Modulation Indices

Channel	m_r	m_c
Pitch	0.856	0.863
Yaw	0.857	0.877
Roll	0.878	0.886

The phase angles θ_p and θ_c can be approximately calculated by the use of Eq. (5-43), which relates the phase angles in each op-amp circuit (except for the detector/pre amp (see Subsection 5.3)), and a 436B divider phase shift tabulation shown in Table 5-7. The phase angles in Table 5-7 were measured and are essentially constant from ambient to 37.8°C.

Table 5-7. 436 B Divider Phase Shift

V_x	925 hz	1850 hz	3700 hz
10	0°	-0.1°	-1.3°
9	0°	-0.2°	-1.4°
8	0°	-0.3°	-1.6°
7	-0.1°	-0.3°	-1.7°
6	-0.1°	-0.6°	-1.8°
5	-0.2°	-0.6°	-1.9°
4	-0.3°	-0.6°	-2.1°
3	-0.3°	-0.7°	-2.3°

$$\phi_a = \arctan\,(-f/f_o A_o \beta) \qquad (5\text{-}43)$$

The divider operation is described by the ideal equation where

$$V_y = 10\ V_z/V_x = G_x V_z$$

It was found during laboratory testing of OAMS, that the 436 dividers supply voltage must be 15 VDC since higher voltages, say 16 VDC, will cause errors in the modulation indices.

With the results of Table 5-5 and 5-7, plus the sum of all the appropriate ϕ_a's, ϕ^-, ϕ^+ and ε (see Subsection 5.3), the resulting calculations of phase angles are shown in Table 5-8. The phase angle calculations were based upon typical component characteristics. Very little correlation can be made between the calculated and actual values (determined by use of the phase shift network values found on Board No. 5). Because θ_c contains ϕ^- it is easy to see where the differences exist since ϕ^- is very sensitive to α_r and α_c magnitudes as demons rated in the pitch channel case. The cause of the θ_p difference from actual is not obvious, especially in the roll channel, and suggest an atypical phase shift of a component may be the cause.

5.1.2 Wollaston Prism Nonorthogonality

In the course of OAMS Brassboard No. 1 development/modifications many hours were spent discussing and studying Wollaston prism nonorthogonality. Laboratory measurements and observations were made to confirm that it existed and its effect on OAMS system output. The resulting outcome of this effort is: 1) Wollaston prism polarization planes for roll Brassboard No. 1 are nonorthogonal by about ± 1°, 2) the manufacturer cannot guarantee Wollaston prisms with better plane accuracy, 3) the effects are noticeable only in the roll channel and 4) the effect on roll can be minimized by careful pairing of the prism or in some cases rotation of the prism by 90°. Lack of a uniform image pattern of the light seen by the detector and the questionable techniques used in differentiating the effects on OAMS necessitate that an analysis be performed in order to gain some perception into the problem. The approach taken here will be similar to that of Subsection 5.1.1 where the lateral channels will be considered first followed by roll. The objective will be to derive irradiance expressions similar to that of Eq. (5-4) and take advantage of previous development, were applicable, in reaching a conclusion.

5.1.2.1 Lateral Channels Nonorthogonality

The output of a nonorthogonal Wollaston prism, say W_T, being reversed fed by the REF and CONT LED, can be derived with the use of the Mueller matrix $P(\xi)$ and Stokes vectors $\overline{S}_i$ and $\overline{S}(\zeta_r,\zeta_c)$ shown in Tables 5-1 and 5-2. Each polarization plane of the Wollaston prism is analogous to a general linear polarizer. The development of the Stokes vector $\overline{S}(\zeta_r,\zeta_c)$, using operator notation, begins with Eq. (5-44).

Table 5-8. Phase Angles OAMS Advanced Brassboard

Channel	Calculated									Actual	
	$*\alpha_r$	$*\alpha_c$	ϕ^+	ϕ^-	$*\epsilon$	$\phi_{a\Delta}$	$\phi_{a\Sigma}$	θ_p	θ_c	θ_p	θ_c
Pitch	-1.49°	-2.1°	-1.8°	-41.5°	-18.4°	-6.3°	-0.5°	-26.5°	-50.4°	-42.1°	-30°
Yaw	-0.74°	0.77°	-0.76°	- 3.5°	- 9.1°	-2.1°	-0.25°	-12.0°	-12.9°	- 5.9°	-42.6°
Roll	-0.37°	0.34°	-0.36°	2.0°	- 4.5°	-1.6°	-0.12°	- 6.6°	- 2.6°	-18.8°	-34.5°

* Use absolute values when substituting in equations.

$$\overline{S}(\xi_r,\xi_c) = P(\xi_r)\,\overline{S}_r + P(\xi_c)\,\overline{S}_c \tag{5-44}$$

where

$$\Sigma J = J_C + J_R$$

$$\Delta J = J_R C_{2\xi_r} + J_C C_{2\xi_c}$$

$$\Lambda J = J_R S_{2\xi_r} + J_C S_{2\xi_c}$$

Ideally $\xi_r = 0^\circ$ and $\xi_c = 90^\circ$; however, for the nonideal case we can let $\xi_c = 90^\circ - \xi_r$. In this case ξ_r is a small angle causing the nonorthogonality. Substituting this identity into ΔJ and ΛJ will convert these intensities as a function of angle ξ_r where,

$$\Delta J = (J_R - J_C)\,C_{2\xi_r}$$

$$\Lambda J = (J_R - J_C)\,S_{2\xi_r}$$

Correctness of this derivation can be quickly verified by letting $\xi_r = 0^\circ$ and the Stokes vector is similar to $\overline{S}\,(0^\circ,\ 90^\circ)$. The irradiance at the XMTR aperture and at the detector surfaces is defined in operator form by Eqs. (5-45), (5-46) and (5-47).

$$J_t = ASC_T(\alpha,0^\circ)Q(45^\circ)\,\overline{S}(\xi_r,\ \xi_c) \tag{5-45}$$

$$J_{dh} = P(\xi_h)ASC_R(\beta,180^\circ)T(\theta_r)\ J_t \tag{5-46}$$

$$J_{dv} = P(\xi_v)ASC_R)(\beta,180^\circ)T(\theta_r)\ J_t \tag{5-47}$$

Substituting the appropriate matrices in J_t, J_{dh} and J_{dv} and performing the required matrix multiplication gives us the general irradiance at the detector surfaces.

$$J_{dh} = \tfrac{1}{2}\Big\{ \Sigma J - \Delta J((S_{k(\alpha-\beta)} - S_{k\alpha}C_{k\beta}(1 - C_{2\theta_r}))C_{2\xi_h}$$

$$+ S_{k\alpha}S_{2\theta_r}S_{2\xi_h}) + \Lambda J(C_{2\theta_r}S_{2\xi_h} - S_{2\theta_r}C_{k\beta}C_{2\xi_h})\Big\}$$

$$J_{dv} = \tfrac{1}{2}\Big\{ \Sigma J + \Delta J((S_{k(\alpha-\beta)} - S_{k\alpha}C_{k\beta}(1-C_{2\theta_r}))\,C_{2\xi_h}$$

$$- S_{k\alpha}S_{2\theta_r}S_{2\xi_h}) + \Lambda J(C_{2\theta_r}S_{2\xi_h} + S_{2\theta_r}C_{k\beta}C_{2\xi_h})\Big\}$$

The trigonometric identities

$$S_{k(\alpha-\beta)} = S_{k\alpha}C_{k\beta} - C_{k\alpha}S_{k\beta}$$

and $$\xi_V = 90^o - \xi_h$$

were used in the expansion of these equations. Applying Assumptions No. 1 and 5, plus noting that ΛJ is a function of sin $2\xi_r$, the

> Assumption No. 5 -
>
> The deviation from orthogonality is no greater than one degree; therefore, the worst case angle for ξ_r and ξ_h is one degree.

irradiance equations simplify to the form shown in Eq. (5-48).

$$J_{dh} = \tfrac{1}{2} \left\{ \Sigma J - \Delta J \; S_{k\theta} \; C_{2\xi_h} \right\} \qquad (5\text{-}48a)$$

$$J_{dv} = \tfrac{1}{2} \left\{ \Sigma J + \Delta J \; S_{k\theta} \; C_{2\xi_h} \right\} \qquad (5\text{-}48b)$$

Equation (5-48) is similar to that of Eq. (5-4) except that the second term contains cos $2\xi_h$. Therefore, the second term of the system output, Eq. (5-26), is modified by the product of cos $2\xi_h$. Thus, the lateral channel output is only sensitive to the nonorthogonality of the RCVR Wollaston prism and its effect would be a small constant-scale-factor error that is compensated by differential gain G_d.

5.1.2.2 Roll Channel Nonorthogonality

Analytical approach for the roll channel will be somewhat similar to that taken for the lateral channels. The terms ΛJ and ΔJ of $\overline{S}(\xi_r, \xi_c)$ will be different and their location in the Stokes vector are interchanged (see Table 5-2).

$$\Delta J = (J_R - J_C) \; S_{2\xi_r}$$

$$\Lambda J = (J_R - J_C) \; C_{2\xi_r}$$

$$\xi_c = \xi_r - 90^o$$

Application of Assumption No. 5 will thus define $\xi_r = 45^o \pm 1^o$. Letting $\xi_r = 45^o$ would yield $\overline{S}(\pm 45^o)$ listed in Table 5-2. The irradiance at the detector surface in operator notation is defined by Eq. (5-49).

$$J_{dh} = P(\xi_h) \; T(\theta_r) \; \overline{S}(\xi_r, \xi_c) \qquad (5\text{-}49a)$$

$$J_{dv} = P(\xi_v) \; T(\theta_r) \; \overline{S}(\xi_r, \xi_c) \qquad (5\text{-}49b)$$

where $\xi_V = 90^\circ - \xi_h$.

Substitution of the required matrices in Eq. (5-49), performing the specified expansion, and grouping of terms yield the following irradiance equations.

$$J_{dh} = \tfrac{1}{2}\left(\Sigma J + \Delta J\, S_{2(\xi_h - \theta_r)} + \Lambda J C_{2(\xi_h - \theta_r)} \right) \qquad (5\text{-}50a)$$

$$J_{dv} = \tfrac{1}{2}\left(\Sigma J + \Delta J\, S_{2(\theta_r + \xi_h)} - \Lambda J C_{2(\theta_r + \xi_h)} \right) \qquad (5\text{-}50b)$$

and the trigonometric identities

$$S_{2(\xi_r \pm \theta_r)} = S_{2\xi_r} C_{2\theta_r} \pm C_{2\xi_r} S_{2\theta_r}$$

$$C_{2(\xi_r \pm \theta_r)} = C_{2\xi_r} C_{2\theta_r} \pm S_{2\xi_r} S_{2\theta_r}$$

where used.

Inserting the ΔJ and ΛJ into J_{dh} and J_{dv} yields Eq. (5-51).

$$J_{dh} = \tfrac{1}{2}\left(\Sigma J + \Delta J\, C_{2(\theta_r + \phi_1)} \right) \qquad (5\text{-}51a)$$

$$J_{dv} = \tfrac{1}{2}\left(\Sigma J - \Delta J\, C_{2(\theta_r + \phi_2)} \right) \qquad (5\text{-}51b)$$

where

$$\phi_1 = \xi_r - \xi_h$$

$$\phi_2 = \xi_r + \xi_h$$

Using Eqs. (5-14) and (5-15), J_{dh} and J_{dv} can be written as follows:

$$J_{dh} = \tfrac{1}{2}\left(A^+ - A^- - a^- + a^+ C_{2(\theta_r + \phi_1)} \right) \qquad (5\text{-}52a)$$

$$J_{dv} = \tfrac{1}{2}\left(A^+ + A^- - a^- - a^+ C_{2(\theta_r + \phi_2)} \right) \qquad (5\text{-}52b)$$

Employing the relationships expressed by Eqs. (5-20) and (5-21) and substituting the a.c. terms of J_{dh} and J_{dv} into Eq. (5-22) yields,

$$e_d = \frac{G_d A_{rh} R_{sh}}{4} \left\{ \left(\frac{A_{rv} R_{sv}}{A_{rh} R_{sh}} - 1 \right) a^- + \left(C_{2(\theta_r + \phi_1)} + \frac{A_{rv} R_{rv}}{A_{rh} R_{sh}} C_{2(\theta_r + \phi_2)} \right) a^+ \right\} \qquad (5\text{-}53)$$

The basic difference between Eq. (5-53) and (5-23) is in the second term where the desired angular rotation θ_r is contained. Our goal now is to expand the second term in a form which will facilitate our interpretation. Let,

$$y = \cos 2(\theta_r+\phi_1) + x \cos 2(\theta_r+\phi_2)$$

where y is the coefficient of a^+ and, $x = A_{rv}R_{rx}/A_{rh}R_{sh}$.

$$y = -(\sin 2\phi_1 + x \sin 2\phi_2) \sin 2\phi_r$$

$$+(\cos 2\phi_1 + x \cos 2\phi_2) \cos 2\phi_r$$

which is equivalent to

$$y = z \sin 2(\theta_r + \frac{\alpha}{2}) \quad (5\text{-}54a)$$

$$z = (1 + x^2 + 2 x \cos 2(\phi_1 - \phi_2))^{\frac{1}{2}} \quad (5\text{-}54b)$$

$$\alpha = \tan^{-1}\left(-\frac{\cos 2\phi_1 + x \cos 2\phi_2}{\sin 2\phi_1 + x \sin 2\phi_2}\right) \quad (5\text{-}54c)$$

(Note that in z, $\phi_1 - \phi_2 = -2\xi_h$).

The validity of Eq. (5-54) can be easily verified by letting $\xi_r = 45^o$ and $\xi_h = 0^o$ and Eq. (5-55) should be identical to Eq. (5-23) when $k = 2$.

$$e_d \cong \frac{G_d A_{rh} R_{sh}}{4} \left\{ \left(\frac{A_{rv}R_{sv}}{A_{rh}R_{sh}} - 1 \right) a^- + z\, a^+ \sin 2(\theta_r + \frac{\alpha}{2}) \right. \quad (5\text{-}55)$$

If we use the same rationale as that previously used in deriving e_c and V_s, it will be clear that nonorthogonal planes will have neglibible effects on these terms. Therefore, for our purpose the system output equation after substitution for a^- and a^+ can be written as shown in Eq. (5-56).

$$e_o \cong \frac{K\, m_r}{\left(1 + \frac{b_c I_c}{b_r I_r} + \frac{I_b}{b_r I_r}\right)} \left\{ \frac{\left(\frac{A_{rv}R_{sv}}{A_{rh}R_{sh}} - 1\right) a_1}{\left(\frac{A_{rv}R_{sv}}{A_{rh}R_{sh}} + 1\right)} S_{(\omega t+\theta_c)} + a_o z S_{2(\theta_r+\frac{\alpha}{2})} S_{(\omega t+\theta_p)} \right\} \quad (5\text{-}56)$$

Examination of the second term in Eq. (5-56), we can see that z will alter the scale factor, if $\xi_h \neq 0$, and a displacement from true zero by an angle $\frac{\alpha}{2}$ will exist. Therefore, in order to compensate for $\alpha/2$ either W_T or W_R or both must be rotated counter-clockwise or clockwise from their desired position. However, this will then result in cross coupling angular errors when the lateral channels are rotated. In order for us to get a feel of what magnitude of error this will yield, let's assume that the following conditions exist:

a) Irradiance/detector/pre-amp is unbalanced by 0.24%

b) $\xi_r = 46^o$

and c) $-1^o \leq \xi_h \leq 1^o$

where values of ξ_r and ξ_h are assumed to be the worst case conditions. With the aid of Eq. (5-54) the following values are computed:

$x = 1.0024$, $z = 2.001$ (ideal $z = 2.0$)

$\alpha = 2.002^o$; $\frac{\alpha}{2} = 1.001^o \approx 3603.6$ arc secs.

These calculations indicate that the scale factor error is negligible, but the one degree angular error must be compensated by rotation of the Wollastons until the system output is zero. The expense paid in doing this (unavoidable) is to increase the likelihood of cross coupling in the roll channel when pitching and yawing occur. Perturbation of ξ_r and ξ_h within the $\pm 1^o$ limit specified indicates that the magnitude of α is controlled only by the XMTR Wollaston's deviation from orthogonality. Thus, if $\xi_r = 45$ and ξ_h is allowed to vary $\pm 1^o$ it will be found, for all practical purposes, that $\alpha = 0^o$. Therefore, when selecting XMTR Wollaston prisms, the prism with the best orthogonal fit should be used in the roll channel.

5.2 Led Control Loop

The function of the LED control loop is to assure a.c. and d.c. intensity balance, as seen by the horizontal and vertical detectors, of the CONT LED relative to the REF LED. The purpose of balancing action is to maintain the term a_1, found in Eq.(5-26), as near zero as possible in order that its product with the irradiance/detector/pre-amp balance term will drive the offset described in Eq.(5-26) to a minima. In addition the LED balance scheme will provide the same modulation index for the CONT LED drive signal as that of the REF LED, thus $m_c \approx m_r$. This will assure that the ratio b_cI_c/b_rI_r found in Eq. (5-26) is near unity under varying light intensities.

5.2.1 Block Diagram Description

The OAMS control loop model along with the identification of its constituent mathematical blocks are shown in Figure 5-6. A unique feature of this loop is the need for a divider which maintains the CONT LED modulation index m_c equal to that of the REF LED drive signal. A constant signal, with the required modulations index, is fed in the numerator and the output V_y is amplitude scaled by the denominator V_c. Since V_c must be greater than zero (lower limit set to be $V_c \geq +3.1$ VDC) this requires that the LED intensities be unbalanced by a certain percentage in order to maintain this voltage at a prescribed level. In order to accomplish this and at the same time maintain a LED balance between 1.0 to 2.0 per cent, a large voltage gain must be developed between the control signal e_c and the control voltage V_c (also referred to as error voltage). Of course it would be most desirable to maintain LED balance to a smaller percentage, thus putting less reliance on the irradiance/detector/pre-amp balance (see Eq.(5-26)), but a compromise must be attained between LED balance and control loop phase and gain margins.

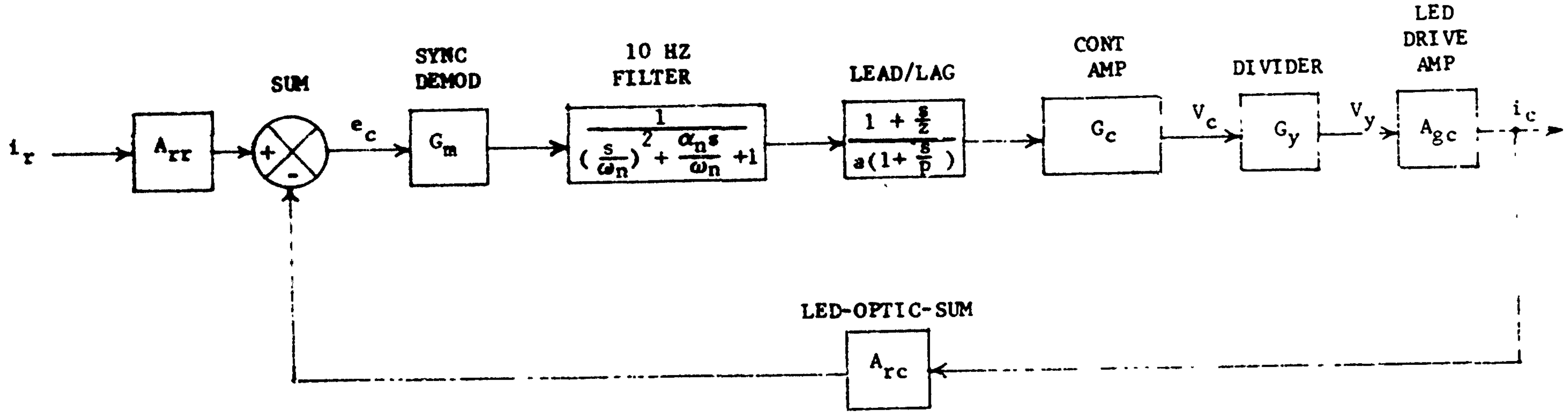
i_r
A_{rr}
SUM
+
-
e_c
SYNC DEMOD
G_m
10 HZ FILTER
$\frac{1}{(\frac{s}{\omega_n})^2 + \frac{\alpha_n s}{\omega_n} + 1}$
LEAD/LAG
$\frac{1 + \frac{s}{z}}{a(1 + \frac{s}{p})}$
CONT AMP
G_c
V_c
DIVIDER
G_y
V_y
LED DRIVE AMP
A_{gc}
i_c
LED-OPTIC-SUM
A_{rc}

Figure 5-6. GAMS Control Loop

It should also be emphasized at this point that the control loop LED balance effects on the system output V_0 are somewhat diminished by the AGC divider and the irradiance/detector/pre-amp balance. If the pre-amp balance were zero or very small at all times larger unbalances could be tolerated. A lower limit for the divider denominator must be establish to prevent operation at close to zero voltage where oscillation and/or indeterminate operation results. In addition divider phase shifts are pronounced as V_c approaches small values.

Determination of the divider gain G_y, LED drive amp transconductance A_{gc}, LED-Optics-Sum transresistance A_{rc}, and the corresponding rationale will be presented here. The control loop is basically nonlinear because of the divider characteristics and to that end we shall circumvent this problem by Assumption No. 6.

Assumption No. 6 -

> The largest divider gain value is at V_c = + 3.1 VDC. Increasing values of V_c will increase the relative stability of the control loop.

In addition we will work with d.c. values in the determination of these gains. For an oscillator signal of 1.0 V RMS, a voltage divider network composed of R_1 and R_9 (see Board No. B1, Pg. 6-4), and a modulation index of about 0.86, the following d.c. numerator term results:

$$V_z = \frac{(2)^{1/2} e_{oc} R_9}{m_c \; (R_1 + R_9)}$$

Substitution of V_z into the divider ideal equation yields,

$$V_y = \frac{10(2)^{1/2}}{V_c} \left(\frac{e_{oc} R_9}{m_c (R_1 + R_9)} \right) \qquad (5\text{-}57)$$

where $V_x = V_c$. Dividing both sides of Eq. (5-57) by V_c gives,

$$G_y = \frac{V_y}{V_c} = \frac{10(2)^{1/2} \; e_{oc} R_9}{V_c^2 \; m_c \; (R1 + R9)} \qquad (5\text{-}58)$$

For values of

R_1 = 100 kΩ
R_9 = 17.2 kΩ
V_c = 3.1 VDC

$$G_y = \frac{10(2)^{1/2} \; (1.0) \; 17.2}{(3.1)^2 (0.86)(117.2)} = 0.251 \text{ v/v}.$$

The transconductance of the inverting amplifier circuit (consisting of A_6 and the Darlington transistor pair) is defined by Eq. (5-59).

$$A_{gc} = \left| I_c / V_y \right| = R_3 / R_1 R_{16} \qquad (5\text{-}59)$$

For values of,

$R_3 = 25.8\ \text{k}\Omega$, Roll

$R_3 = 27.6\ \text{k}\Omega$, Pitch and Yaw

$R_1 = 10\Omega$

$R_{16} = 10\ \text{k}\Omega$,

then $A_{gc} = 0.258$ mhos for Roll and $A_{gc} = 0.276$ mhos for Pitch and Yaw.

Control LED current I_c, for varying values of V_c, are listed in Table 5-9.

Table 5-9. Control LED Currents

V_c (VDC)	V_y (VDC)	I_c (Roll) (ma)	I_c (Pitch and Yaw) (ma)
10	0.241	62.2	66.5
9	0.268	69.1	74.0
8	0.302	77.9	83.4
7	0.347	89.5	95.8
6	0.402	103.7	111.0
5	0.483	124.6	133.3
4	0.603	155.6	166.4
3.1	0.779	201.0	215.0

Before determining the LED-Optic-Sum transresistance A_{rc}, a rationale must be developed which defines the signals being summed. Recall that

$$e_S = G_s\ (e_H + e_V).$$

Now if we make use of Assumption No. 7 our computation will be simplified without too great a sacrifice in accuracy. In addition we will

Assumption No. 7 -

The irradiance for the horizontal and vertical paths to both detectors are exactly equal.

limit the analysis to a.c. components, therefore, after substitution of the appropriate values,

$$e_s = e_c = 2G_s\, A_{rh}\, i_{dh}.$$

Substitution of Eq. (5-20) for i_{dh} and remembering that the a^- term is the controlling term,

$$e_c = -\, G_s\, A_{rh} R_{sh} a^-/2$$

where

$$a^- = b_r i_r (1 + u^2 - 2u \cos\, (\alpha_c - \alpha_r))^{\frac{1}{2}}$$

If $\alpha_c - \alpha_r \approx 0$, a^- can be written as

$$a^- = b_r i_r (1 + u^2 - 2u)^{\frac{1}{2}}$$

$$a^- = b_r i_r (1 - u)$$

or $$a^- = b_r i_r - b_c i_c.$$

Inserting a^- into e_c yields,

$$e_c = \frac{G_s A_{rh} R_{sh}}{2}\, (b_c i_c - b_r i_r) \qquad (5\text{-}60)$$

Letting,

$$A_{rr} = G_s A_{rh} R_{sh} b_r/2$$

and

$$A_{rc} = G_s A_{rh} R_{sh} b_c/2.$$

then,

$$e_c = A_{rc} i_c - A_{rr} i_r \qquad (5\text{-}61)$$

Eq. (5-61) is the basic equation used in the development of the OAMS control loop block diagram. If we know the sum voltage V_s for a particular I_c, an equivalent value for A_{rc} can be calculated. Assuming that exactly half of V_s is contributed by the CONT LED, the peak magnitude for e_c, due to the CONT LED, can be computed per Eq. (5-62).

$$e_{cp} = 1.71\, V_s/2\, G_f, \text{ Pitch} \qquad (5\text{-}62a)$$

$$e_{cp} = 1.42\ V_s/2\ G_f,\ \text{Yaw} \tag{5-62b}$$

$$e_{cp} = 1.27\ V_s/2\ G_f,\ \text{Roll} \tag{5-62c}$$

The numerical factors in Eq. (5-62) compensate for the increased LED efficienty at 4.44°C (40°F) as determined in laboratory measurements made on July 22, 1976. Note that at 4.44°C the loop gain increases, thus driving the control loop closer to instability. The ratio of $e_{cp}/I_c = A_{rc}$ and from the results of Fig. 5-5 and Table 5-5 and 5-9.

$$A_{rc} = \frac{1.71(4.77)}{2(21)(111 \times 10^{-3})} = 1.75,\ \text{Pitch}$$

$$A_{rc} = \frac{1.42(5.28)}{2(10.1)(88.7 \times 10^{-3})} = 4.18,\ \text{Yaw}$$

$$A_{rc} = \frac{1.27(5.14)}{2(4.4)(92.73 \times 10^{-3})} = 8.0\ ,\ \text{Roll}$$

Please note that the values of A_{rc} are proportional to the separation distance between the XMTR and RCVR. For a reduction in range a new setting for the CONT AMP gain must be made to maintain the prescribed gain and phase margins defined in the stability analysis subsection. The same applies for the case when significantly hotter LED or improved optics are introduced with a resulting increase in light intensity.

5.2.2 Control Loop Stability Analysis

A Bode analysis of the loop transfer function must now be performed in order to select an appropriate CONT AMP gain $1/\beta$ that will maintain loop stability. Using control analysis notation, the loop transfer function can be written as

$$G(s)H(s) = \frac{K(1 + s/z)}{\left(\frac{s^2}{\omega_n^2} + \frac{\alpha_n s}{\omega_n} + 1\right)(1 + s/p)} \tag{5-63}$$

z = 387.7 rad./sec

p = 3090.0 rad./sec

ω_n = 62.84 rad./sec

α_n = 1.414

$K = G_c G_m G_y A_{gc} A_{rc}/a$

If we let s = jω and normalize the lead-lag transfer function terms, the gain equation becomes

$$\frac{G(j\omega)H(j\omega)}{K} = \frac{1 + j\frac{\omega}{\omega_n N_z}}{\left(1 - \left(\frac{\omega}{\omega_n}\right)^2 + j\frac{\alpha_n\omega}{\omega_n}\right)\left(1 + j\frac{\omega}{\omega_n N_p}\right)} . \qquad (5\text{-}64)$$

The magnitude of G(jω)H(jω)/K in decibels is,

$$20 \log_{10} \left| \frac{G(j\omega)\,H(j\omega)}{K} \right| = \qquad (5\text{-}65)$$

$$20 \log_{10}\left(1 + \left(\frac{\omega}{\omega_n N_z}\right)^2\right)^{\frac{1}{2}} - 20 \log_{10}\left(1 + \left(\frac{\omega}{\omega_n N_p}\right)^2\right)^{\frac{1}{2}}$$

$$- 20 \log_{10}\left(\left(1 - \frac{\omega}{\omega_n}\right)^2\right)^2 + \left(\frac{\alpha_n\omega}{\omega_n}\right)^2\Bigg)^{\frac{1}{2}}$$

where

$$N_z = \frac{z}{\omega_n} \text{ and } N_p = \frac{p}{\omega_n}$$

The phase shift $\emptyset$ is,

$$\emptyset = \mathrm{Arg}(G(j\omega)H(j\omega) = \qquad (5\text{-}66)$$

$$\tan^{-1}\left(\frac{\omega}{\omega_n N_z}\right) - \tan^{-1}\left(\frac{\omega}{\omega_n N_p}\right) - \tan^{-1}\left(\frac{\frac{\alpha_n\omega}{\omega_n}}{1-\left(\frac{\omega}{\omega_n}\right)^2}\right)$$

Figure 5-7 is a plot of the magnitude and phase versus the normalized frequency ω/ω_n. Selecting a phase margin (PM) of 31.2° gives us a gain of 57.4 db. or K = 741.3v/v at ω/ω_n = 70.0. With K known we can now write the following relationship,

$$G_c = K\, a /\, G_m G_y A_{gc} A_{rc} . \qquad (5\text{-}67)$$

Substituting the appropriate values in Eq. (5-67) yields,

G_c = 7661, Pitch

G_c = 3207, Yaw

G_c = 1793, Roll

Table 5-10 summarizes the loop gains for the three channels and the conditions used to calculate.

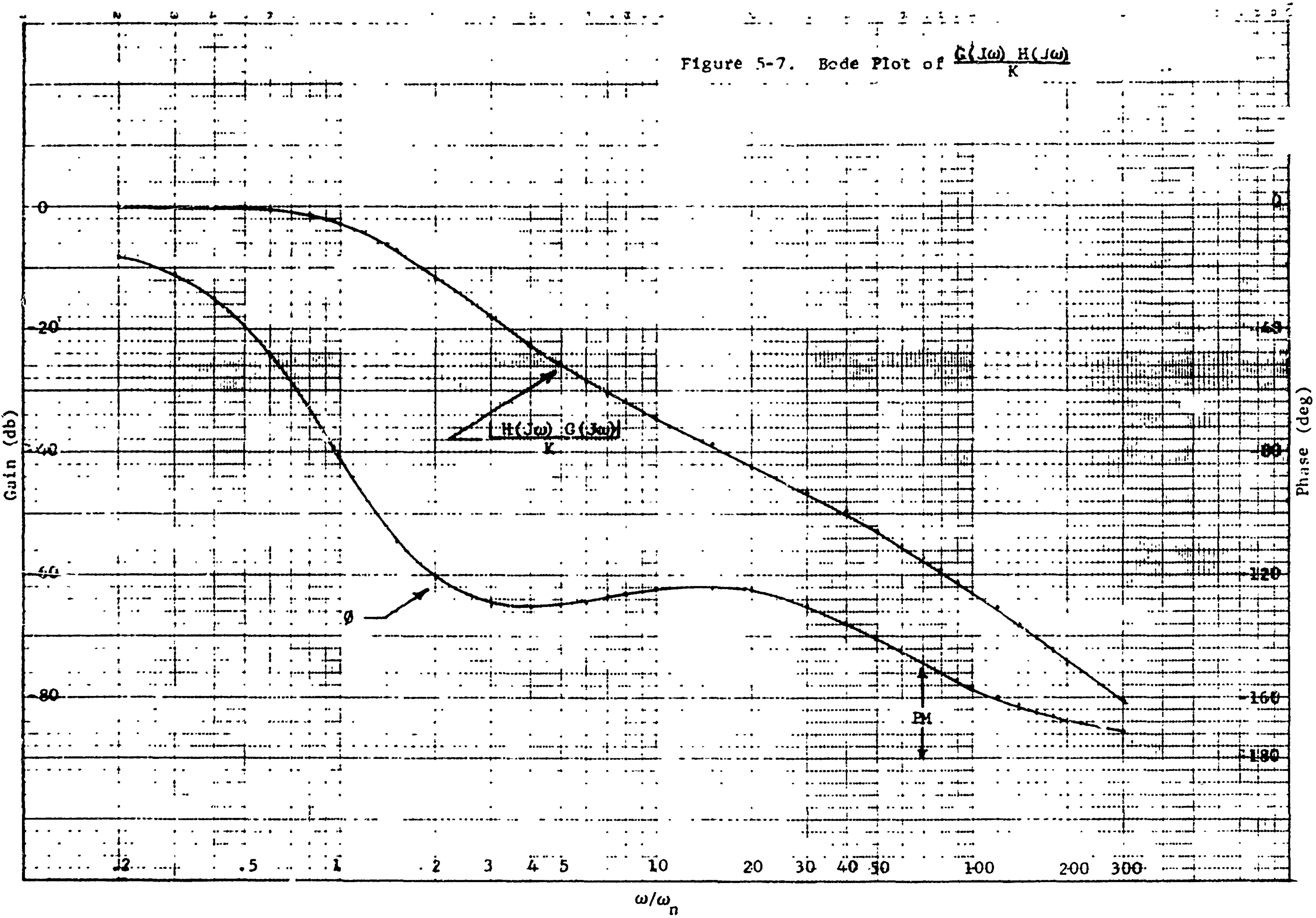

Figure 5-7. Bode Plot of $\frac{G(J\omega)\ H(J\omega)}{K}$

Table 5-10. Control Loop Gains

Channel	G_m	a	G_y	A_{gc}	A_{rc}	G_c	PM
Pitch	6.37	7.981	0.251	0.276	1.75	7661.0 * 3600.0	31.2° * 44.0°
Yaw	6.37	7.981	0.251	0.276	4.18	3207.0 * 3600.0	31.2° * 30.0°
Roll	6.37	7.981	0.251	0.258	8.0	1793.0 * 843.9	31.2° * 42.0°

* Actual values on Brassboard No. 2

Conditions:

1. I_c = 201.0 ma, Roll
   I_c = 215.0 ma, Pitch and Yaw
2. Temp. = 4.44°C
3. Range = 15.2 m.
4. $V_o \leq 100$ arc sec/REF LED on
   $V_o \leq 1.0$ arc sec/Both LED on

An important and subtle point to note is that a relatively large op amp circuit close loop gain is required for G_c. This gain will naturally cause the op amp circuit to produce a phase lag according to Eq. (5-68).

$$\phi_a = - \tan^{-1}(\omega/\omega_n N) \tag{5-68}$$

where

$$N = 2\pi f_o A_o/G_c \omega_n$$

For example, consider the case where op-amp (Mono OP-07) is used.

$A_o = 110$ db $= 316,227.8$ v/v

$f_o = 2.7$ hz

$\omega_n = 62.84$ rad/sec

$N = 23.71$

$G_c = 3600.0$

$\omega/\omega_n = 70$

$\phi_a = -71.3^o$.

Obviously, the introduction of a -71.3^o phase shift by the CONT AMP will cause instability in the control loop. This necessitates either our using a wider bandwidth op amp or splitting the op amp circuit into several stages whose product equals the desired G_c. We have chosen the latter where two cascade stages, each with a gain of 60 (lateral channels) and a corresponding phase lag of 2.82^o, are used to generate G_c. This application yields a considerably smaller phase lag with minimal effect on the control loop phase.

5.3 Detector Pre Amp Analysis

The OAMS system requires, per channel, a pair of detector/pre amplifier circuit, one called the horizontal and the other vertical, as described in the system equation analysis. It is clear from the connotation that a detector and pre-amp circuit are the two main components making up the whole circuit. What is not so obvious is that special care must be taken in the application that requires joining the two to form a composite circuit. The circuit analysis to follow will address itself towards the derivation of equations describing the signal and noise components. The proper choice of components in this circuit is key towards proper operation of the OAMS system. Following equation derivations, noise calculations based upon op amp data and circuit gains will be compared with actual measurements made on OAMS.

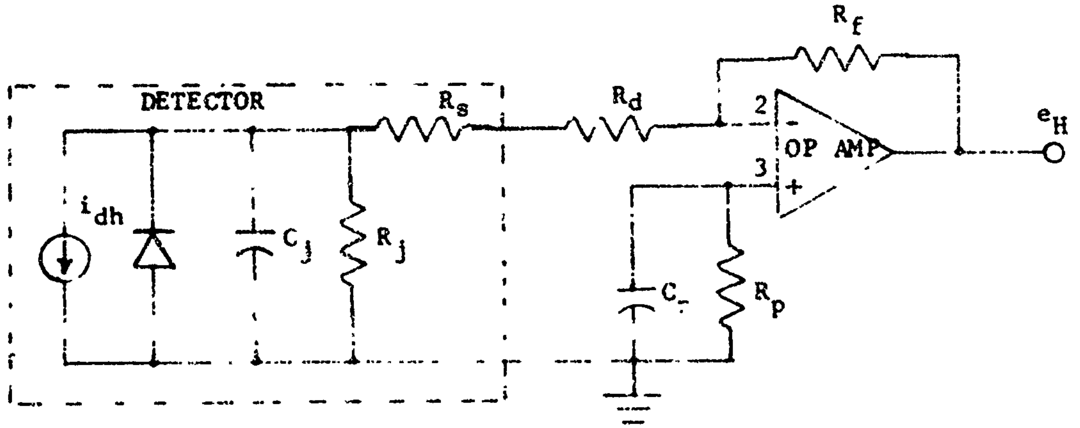
DETECTOR
i_{dh}
C_j
R_j
R_s
R_d
R_f
2
3
-
+
OP AMP
e_H
C_T
R_p

Figure 5-8. Detector/Pre-Amp Circuit

5.3.1 Signal Output Model

Figure 5-8 depicts the basic current-to-voltage converter circuit with an equivalent circuit of the detector. The objective here is to derive an output equation for the horizontal detector/pre-amp circuit as a function of the various parameters after making suitable simplifying assumptions. The horizontal detector/pre-amp notations shall be used throughout this derivation and the results are the same for the vertical detector/pre-amp circuit.

Assumption No. 8 -

> Op amp input terminals draw virtually no current because of the large differential input resistance, R_{id}.

Assumption No. 9 -

> Voltage across input terminals is zero since the positive input terminal is at ground potential (no current flow); the negative input terminals must be at zero voltage also.

Assumption No. 10 -

> The series resistance R_s is approximately 30 ohms and is much smaller than the damping resistance R_d.

R_p is added to prevent input bias current I_b from producing a d.c. offset at the op amp output. Capacitor C_p is required to bypass the thermal noise of R_p to ground.

Applying Thévenin's theorem and Assumption No. 8, 9 and 10, the circuit of Figure 5-8, for analysis purposes, can be simplified to that shown in Figure 5-9. The voltage gain equation for the circuit is,

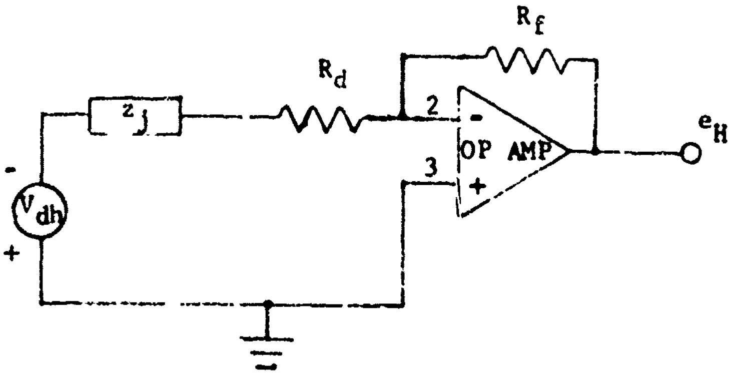

Figure 5-9. Equivalent Inverting Amplifier Circuit

$$A_{vc} = e_H/V_{dh} = (1-1/\beta)(1 + 1/A_v\beta) \qquad (5\text{-}69)$$

where

$$\beta = Z1/(Z1 + R_f)$$

$$Z_1 = Z_j + R_d$$

$$A_v = A_o/(1 + \tau_o s) \approx \frac{A_o}{\tau_o s}$$

$$Z_j = R_j/(1 + R_jC_js).$$

Expansion of the numerator and denominator of Eq. (5-69) gives,

$$1 - 1/\beta = -R_f(1 + R_jC_js)/R_j(1 + R_dC_js)$$

$$1 + 1/A_v\beta = \frac{\frac{\tau_o\ C_j\ R_f s^2}{A_o} + \left(R_dC_j + \frac{\tau_o}{A_o}\left(1 + \frac{R_f}{R_j}\right)\right) s + 1}{1 + R_dC_js}$$

with $R_j \gg R_d$ and $R_f \gg R_d$.

$$A_{vc} = \frac{-\ R_f\ (1 + R_jC_js)}{R_j\left(\frac{\tau_oC_jR_fs^2}{A_o} + \left(R_dC_j + \frac{\tau_o}{A_o}\left(1 + \frac{R_f}{R_j}\right)\right) s + 1\right)} \cdot$$

From Eq. (5-69),

$$e_H = A_{vc}\ V_{dh}$$

and $V_{dh} = -\ i_{dh}\ Z_j = -\ R_ji_{dh}/(1 + R_jC_js)$.

Therefore,

$$e_H = \frac{R_f\ i_{dh}}{\frac{\tau_o\ C_j\ R_fs^2}{A_o} + \left(R_dC_j + \frac{\tau_o}{A_o}\left(1 + \frac{R_f}{R_j}\right)\right) s + 1} \qquad (5\text{-}70)$$

Eq. (5-70) can be written in a more familiar form as shown in Eq. (5-71).

$$e_H = \frac{R_fi_{dh}}{\left(\frac{s}{\omega_h}\right)^2 + \frac{\alpha_hs}{\omega_h} + 1} \qquad (5\text{-}71)$$

where,

$$\omega_h = (2\pi f_o A_o / C_j R_f)^{\frac{1}{2}}$$

and

$$\alpha_h = \omega_h (R_d C_j + (1 + R_f/R_j)/2\pi f_o A_o)$$

The transresistance A_{rh} can now be written as

$$A_{rh}(s) = \frac{e_H}{i_{dh}}(s) = \frac{R_f}{(\frac{s}{\omega_h})^2 + \frac{\alpha_h s}{\omega_h} + 1} . \qquad (5\text{-}72)$$

If we let $s = j\omega$, the last equation becomes

$$A_{rh}(j\omega) = \frac{R_f}{1 - (\frac{\omega}{\omega_h})^2 + j\frac{\alpha_h \omega}{\omega_h}}$$

and the phase shift is

$$\epsilon_h = - \tan^{-1} \left(\frac{\alpha_h \ \omega/\omega_h}{1 - (\frac{\omega}{\omega_h})^2} \right) \qquad (5\text{-}73)$$

For detectors with equal R_j and C_j it can be proven that to have the same phase shift for each detector/pre-amp leg that $R_{dh} = R_{dv}$. The proof is as follows:

$$\epsilon_h = \epsilon_v$$

$$\frac{\alpha_h \ \omega/\omega_h}{1 - (\frac{\omega}{\omega_h})^2} = \frac{\alpha_v \ \omega/\omega_v}{1 - (\frac{\omega}{\omega_v})^2}$$

or

$$\alpha_h \omega_h = \left(\frac{\omega_h^2 - \omega^2}{\omega_v^2 - \omega^2} \right) \omega_v \alpha_v$$

If $\omega^2_h \gg \omega^2$ and $\omega^2_v \gg \omega^2$, then

$$\alpha_h/\omega_h = \alpha_v/\omega_v$$

Substitution of the appropriate terms for α_h/ω_h and α_v/ω_v and solving for R_{dh} results in Eq. (5-74).

$$R_{dh} = R_{dv} + (R_{fv}-R_{fh})/2\pi f_o A_o C_j R_j \qquad (5\text{-}74)$$

Since R_{fv} and R_{fh} are generally less than 100k ohms difference, Eq. (5-74) reduces to the form where $R_{dh} \cong R_{dv}$.

At this point an analysis, using actual component values, is desirable. From the date of the RCA C30852 photovoltaic photodiode,

$C_j = 250$ pf

$R_j = 10 \times 10^6$ ohms

$R_s = 30$ ohms (calculated from EG & G data sheet D3002A-1).

The pre amp circuit values are:

$R_f = 2 \times 10^6$ ohms

$R_d = 53.6 \times 10^3$ ohms

$A_o = 110$ db $= 316,227.8$ v/v

$f_o = 2.7$ hz

Substituting these component values into the equations for ω_h, α_h, A_{rh} and ϵ_h yields,

$\omega_h = 103,582.6$ rad/sec

$\alpha_h = 1.41$

$\delta_h = 0.706$

$$\left.\begin{aligned}\epsilon_h &= 18.4^\circ\\ \omega &= 23,247.8 \text{ rad/sec}\\ A_{rh} &= 1,998,065 \text{ ohms}\end{aligned}\right\}\quad \text{Pitch}$$

$$\left.\begin{aligned}\epsilon_h &= 9.2^\circ\\ \omega &= 11,623.9 \text{ rad/sec}\\ A_{rh} &= 1,999,991 \text{ ohms}\end{aligned}\right\}\quad \text{Yaw}$$

$$\left.\begin{aligned}\epsilon_h &= 4.54^\circ\\ \omega &= 5811.9 \text{ rad/sec}\\ A_{rh} &= 2,000,028 \text{ ohms}\end{aligned}\right\}\quad \text{Roll}$$

If R_d where zero the α_h equation would then take the form

$$\alpha_h = \omega_h\ (R_s C_j + (1 + R_f/R_j)/2\pi\, f_o A_o).$$

With R_s = 30 ohms
α_h = 0.0239

and $A_{rh}(j\omega)$ is very much underdamped. In such a case the response of e_H to changes in light intensities will die out slowly. Small damping constants, such as this, will also amplify the voltage noise of the op amp as shown in following section. In the previous calculation we have selected R_d (using Eq. (5-75)) for a damping ratio of 0.706.

$$R_d = \left(\frac{\alpha_h}{\omega_h} - (1 + R_f/R_j)/2\pi\, f_o A_o\right)/C_j \qquad (5\text{-}75)$$

5.3.2 Electrical Noise Model

The detector/pre-amp circuit has basically four thermal noise sources, i.e. op amp voltage e_n, feedback resistor voltage e_{nf}, op amp current i_n and the detector i_{nh}. We shall direct our effort towards derivation of an expression relating the voltage noise output of the circuit since the magnitude is related to our choice of damping constant. The current noise circuit output is easily related by the product of the constituent current by the transresistance. Figure 5-10 is an equivalent circuit that will be used in this analysis. The voltage noise gain equation for the noninverting configuration is

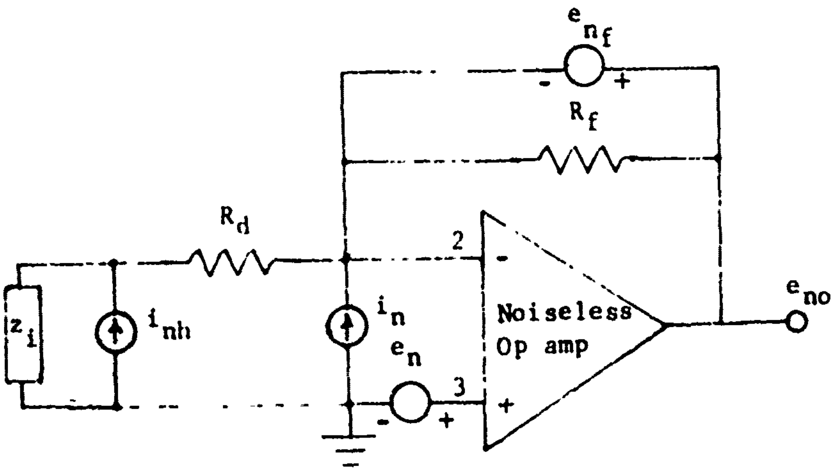

Figure 5-10. Equivalent Noise Circuit

$$A_{vn} = e_{no}/e_n = \frac{1/\beta}{1 + 1/A_v\beta} \qquad (5\text{-}76)$$

Expansion of $1/\beta$ and incorporating the conditions where $R_j \gg R_d$ and $R_f \gg R_d$, $1/\beta$ becomes,

$$1/\beta = \frac{(R_j + R_f)(1 + R_f R_j C_j s/(R_j + R_f))}{R_j\ (1 + C_j R_d s)}$$

Substitution of $1/\beta$ and $1 + 1/A_v\beta$ (from the previous section) into Eq. (5-76) yields,

$$A_{vn} = \frac{(1 + \frac{R_f}{R_j})(1 + R_f R_j C_j s/(R_j + R_f))}{(\frac{\tau_o\ C_j R_f}{A_o}\ s^2 + (R_d C_j + \frac{\tau_o}{A_o}\ (1 + \frac{R_f}{R_j}))s + 1} \qquad (5\text{-}77)$$

Eq. (5-77) can be written in a conventional form as shown in Eq. (5-78).

$$A_{vn} = \frac{\left(1 + \frac{R_f}{R_j}\right)(1 + \tau_j s)}{\left(\frac{s}{\omega_h}\right)^2 + \frac{\alpha_h s}{\omega_h} + 1} \qquad (5\text{-}78)$$

where,

$$\tau_j = R_f R_j C_j/(R_j + R_f) = 4.17 \times 10^{-4}\ \text{sec.}$$

ω_h and α_h are defined in Eq. (5-71). Because of the similarity of Eq. (5-78) and (5-71) it is apparent that the damping constant α_h will affect the noise voltage e_{no} in a similar manner as that for e_H. The magnitude of $A_{vn}(j\omega)$ is

$$\left|A_{vn}(j\omega)\right| = \frac{(1 + R_f/R_j)(1 + (\tau_j\omega)^2)^{\frac{1}{2}}}{(1 - (\frac{\omega}{\omega_h})^2)^2 + (\frac{\alpha_H\omega}{\omega_h})^2)^{\frac{1}{2}}} \qquad (5\text{-}79)$$

A careful study of either Eq. (5-78) or (5-79) plus knowledge of system requirements indicate that:

a. The zero will cause the noise magnitude to increase, undiminished by the second order pole, until the radian frequency reaches about $\omega_h/10$.

b. The magnitude of $|A_{vn}(j\omega)|$, for all practical purposes, is equal to $1 + R_f/R_j$ for frequencies less than 100 hz.

c. Without R_d the damping constant (as explained before) would be small; therefore high and low frequency noise components would have a tendency to modulate the signal e_H.

d. Sync. Demod. action will attenuate noise frequencies according to Eq. (5-36) and (5-38). Whatever component gets through will be further attenuated by the 10 hz filter according to Eq. (5-34). Therefore, the system noise output will consist, mainly, of low frequency noise of 100 hz or less with the dominate components in the 10 hz bandwidth region.

With R_d selected to yield a damping ratio of 0.706 and the rationale listed, A_{vn} reduces to,

$$A_{vn} = \frac{e_{no}}{e_n} = 1 + \frac{R_f}{R_j} \qquad (5\text{-}80a)$$

$$\text{or} \quad e_{no} = e_n\,(1 + R_f/R_j) \qquad (5\text{-}80b)$$

Of course e_{no} must be modified to account for the voltage noise of R_f and the current noise of the op amp and detector as shown in Eq. (5-81).

$$e_{no}(10\text{ hz}) = (e_n^2\,(1 + R_f/R_j)^2 + e^2{}_{nf} + R_f{}^2(i_n{}^2 + i_{nh}^2))^{\frac{1}{2}}(B_n)^{\frac{1}{2}} \qquad (5\text{-}81)$$

Since RCA does not list the current spot noise for 10 hz, we must accept the 1000 hz value given with the assumption that the magnitude is within the same range. Using the following op amp and detector noise data, the total voltage noise from one detector/pre-amp leg is calculated.

$e_{nf} = (4kTR_f)^{\frac{1}{2}} = 0.182\ \mu v/(hz)^{\frac{1}{2}}$ at 25°C
$e_n = 10.3\ nv/(hz)^{\frac{1}{2}}$
$i_n = 0.32\ pa/(hz)^{\frac{1}{2}}$
$i_{nh} = 0.08\ pa/(hz)^{\frac{1}{2}}$

and

$$e_{no}(10\text{ hz}) = 0.68\ \mu v\ (B_n)^{\frac{1}{2}}$$

Note that the op amp current noise contributed significantly to e_{no}(10 hz) and almost swamps out the effect of the other noise source. The voltage noises for the differential amp are negligible compared to those contributed by the detector/pre-amp. The output voltage noise due to both detector/pre-amp paths following the differential amplifier is

$$e_{nos} = G_n(e_{noh}^2 + e_{nov}^2)^{\frac{1}{2}} (B_n)^{\frac{1}{2}} \qquad (5\text{-}82)$$

where

$$G_n = \frac{2}{\pi} G_d \, G_x$$

Multiplying each of the voltage noise values by the corresponding gains outlined in Figure 5-5 yields,

$$e_{nos} = 21.8 \ \mu v \ (B_n)^{\frac{1}{2}}, \text{ pitch}$$

$$e_{nos} = 13.2 \ \mu v \ (B_n)^{\frac{1}{2}}, \text{ yaw}$$

$$e_{nos} = 0.147 \text{ mv } (B_n)^{\frac{1}{2}}, \text{ roll}$$

The noise bandwidth of the system is determined by the poles of the second order 10 hz filter and is expressed by the following:

$$B_n = \frac{\int_0^{\infty} |H_i \ (j\omega)|^2 d\omega}{|H_i(j\omega)|^2} \qquad (5\text{-}83)$$

where,

$$H(s) = \frac{\omega_n^2}{(s - m_1)(s - m_2)} \qquad (5\text{-}84)$$

and $i = 1$ or 2.

Letting $s = j\omega$,

$$H(j\omega) = H_1(j\omega) \ H_2(j\omega)$$

and

$$H_1(j\omega) = \frac{\omega_n}{j\omega - m_1}$$

$$H_2(j\omega) = \frac{\omega_n}{j\omega - m_2}$$

where $m_1, m_2 = \omega_n(-\delta_n \pm j \ (1 - \delta_n^2)^{\frac{1}{2}})$

and $\delta_n < 1.0$

Substituting $H_1(j\omega)$ and $H_2(j\omega)$, one at a time, into Eq. (5-83) and performing the required integration yields,

$$B_n = \frac{2\,\omega_n}{\delta_n}\left(\frac{\pi}{2} - \tan^{-1}\left(\pm\, 2\left(\frac{1}{\delta_n^2} - 1\right)^{\frac{1}{2}}\right)\right)$$

For $\delta_n = 0.707$

$$B_n = \frac{2\omega_n}{0.707}\left(\frac{\pi}{2} - (\pm)\ 1.107 \text{ rad.}\right)$$

$$B_n = 1.312\ \omega_n \text{ or } 7.58\ \omega_n$$

Since the pole with the narrowest B_n will govern and B_n is to be expressed in hz,

$$B_n = 1.312\ \omega_n/2\pi$$

or $\quad B_n = 1.312\ f_n$

With $f_n = 10$ hz we can now calculate e_{nos} with the results as shown below.

$e_{nos} = 0.079$ mv rms, pitch

$e_{nos} = 0.048$ mv rms, yaw

$e_{nos} = 0.532$ mv rms, roll

These are the ideal thermal noise values calculated from typical op amp data.

System output noise measurements were made with an H.P. 135 X-Y recorder whose maximum pen speed is 20 inches/sec. The noise output is shown in Figure 5-11. With these graphs 50 voltage points were taken at 100 ms intervals and are tabulated in Table 5-11. The sampling interval of 100 ms was chosen to ensure independent measurements (see ref. 4, Pg. 375 and 392) and with 50 sample points a good approximation to a, gaussian-shaped, probability-density curve can be obtained. With this noise data the standard deviation was calculated for each channel by Eq. (5-87).

$$\sigma_n = \left(\frac{1}{n-1}\sum_{i=1}^{n} X_i^2 - \frac{n}{n-1}\,\overline{X}^2\right)^{\frac{1}{2}} \qquad (5\text{-}87)$$

$$\left.\begin{aligned} \sigma_n &= 0.604 \text{ mv rms, pitch} \\ \sigma_n &= 0.437 \text{ mv rms, yaw} \\ \sigma_n &= 1.504 \text{ mv rms, roll} \end{aligned}\right\} \quad 10 \text{ hz filter}$$

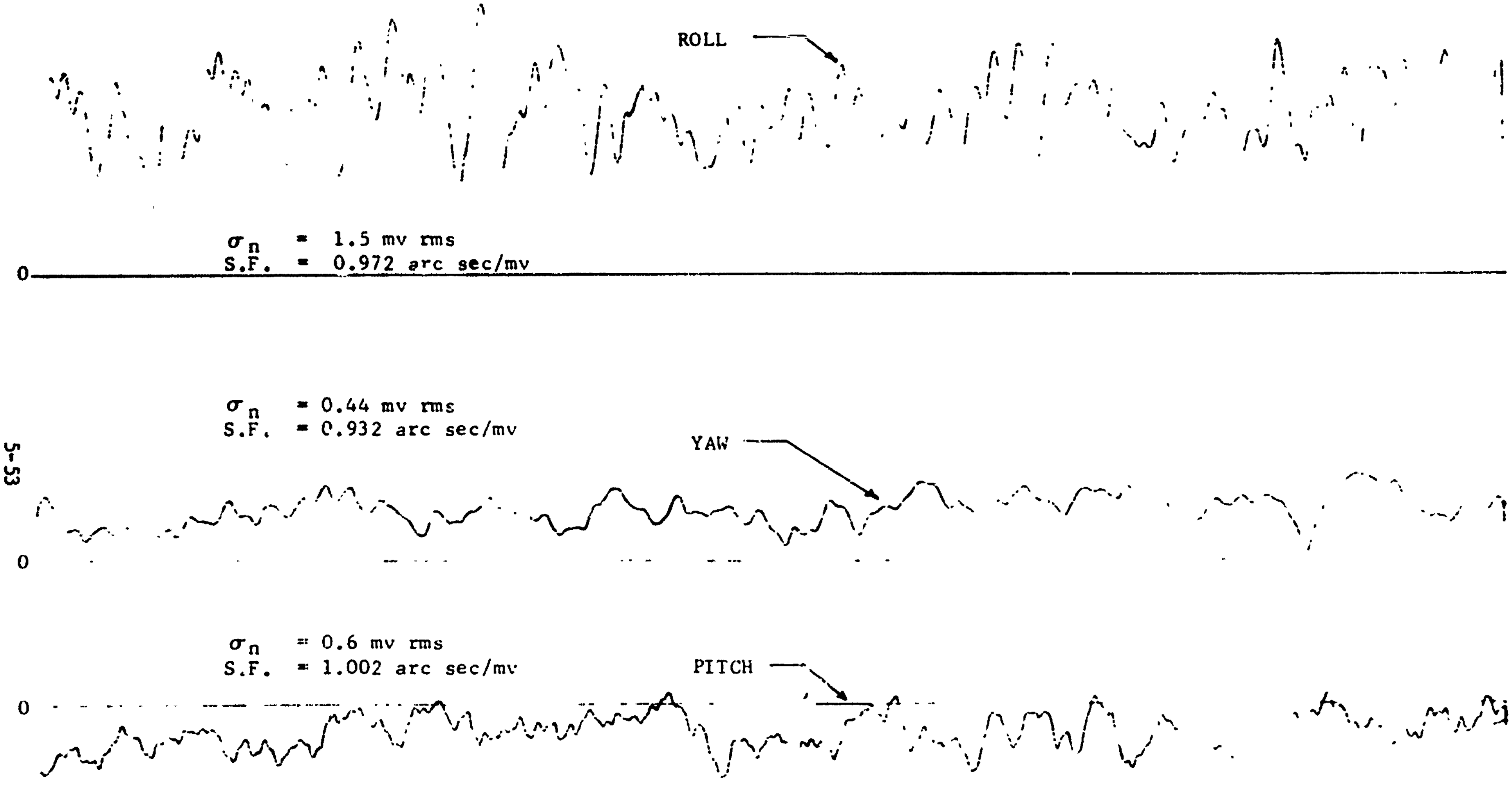

Figure 5-11. System Output Noise Measurement

1-12-77 1:00 PM

Table 5-11. Tabulation of Noise Data

Sample	Pitch (mv)	Yaw (mv)	Roll (mv)
1	-2.2	2.2	6.8
2	-1.7	1.2	6.5
3	-1.5	1.1	5.2
4	-1.9	1.0	5.0
5	-1.6	1.1	4.5
6	-0.7	1.1	6.6
7	-1.1	1.1	4.1
8	-1.8	1.1	2.5
9	-1.2	1.0	5.0
10	-1.2	0.9	4.5
11	-0.9	1.4	5.1
12	-0.8	1.2	7.1
13	-1.7	1.7	7.6
14	-1.5	1.5	7.1
15	-1.7	1.4	6.5
16	-1.5	2.0	6.0
17	-1.8	1.6	3.2
18	-1.7	2.0	6.4
19	-1.8	2.1	6.2
20	-0.6	2.6	7.0
21	-0.5	2.3	3.5
22	-0.2	2.3	7.5
23	-0.8	2.1	6.5
24	-0.9	2.0	6.5
25	-1.4	1.6	8.5
26	0.1	1.1	7.0
27	-0.1	1.3	8.5
28	-0.3	1.5	6.5
29	-0.5	1.4	3.0
30	-1.1	1.7	6.5
31	-1.2	2.2	8.0
32	-0.8	1.8	3.5
33	-0.7	1.6	5.5
34	-1.1	1.4	6.7
35	-0.8	1.5	5.6
36	-1.2	1.0	.9
37	-1.0	1.1	6
38	-0.3	1.6	4.5
39	-0.7	2.1	6.8
40	-0.5	2.5	4.5
41	-0.5	1.8	6.0
42	0	1.5	6.0
43	0.2	1.5	5.5
44	-0.1	2.2	4.5
45	-0.7	1.6	4.5
46	-1.8	1.5	3.7
47	-2.1	1.8	4.9
48	-1.3	1.5	6.5
49	-1.5	1.5	3.7
50	-1.1	1.2	5.0

However, one must also realize that the calculated data can not account for other types of noise disturbance such as 1/f noise, shot noise, and perhaps most importantly variations in the irradiance light source from LED emission to detection at the detector surfaces. Noise in the roll channel is larger because of the increased gain required in scaling of the output as indicated in Section 5.1.1.4. In addition higher power LEDs would cause a reduction in gain and thus reduced noise amplification in the system's processing path.

The 10 hz filter restricts the OAMS Brassboard No. 2 system to a 10 hz dynamic response. However, it was mentioned lately that a 40 hz dynamic response is more representative of future applications. An estimate of the OAMS noise output with a 40 hz low pass filter can be calculated by multiplying the results of Eq. (5-87) by 2.0. The standard noise deviation is then 1.208, 0.874 and 3.008 mv rms for pitch, yaw and roll, respectively.

Finally the selection of the RCA C30852 photovoltaic photodiode was based upon a higher responsivity and a lower junction capacitor, for a given surface area, which in turn yields a higher natural frequency ω_h. Note that large values of ω_h produce smaller phase shifts in each detector/pre amp path as shown by (Eq. (5-73). These detectors are not amphoterically built; therefore, protection against radiation is less stringent.

5.4 Conclusion

It was proven by an analytical model of the lateral and roll channels that, with proper LED and irradiance/detector/pre-amp balance, offsets in system output can be held to about one arc second. Changes in phase shift, once the SYNC DEMOD is synchronized, would generally occur when the relative intensities between the REF and CONT LED are changing. These intensity changes may be due to uneven relative degradation in light output with passage of time or uneven light pattern of either LED as the RCVR and XMTR are rotated about their axes. Phase shift changes would manifest themselves in larger LED unbalance and offset minimization would rely more on the irradiance/detector/pre-amp balance. Background illumination within the optical filter BW will introduce a d.c. quantity that causes a shift in system scale factor. Therefore, if OAMS application dictates operation in an environment where the background lighting has spectral range overlapping that of OAMS, light shades with baffles about the RCVR aperture are required to prevent direct lighting of the detectors.

Wollaston prism nonorthogonality will introduce a small constant scale factor error in the lateral channels. This error is compensated by an increased gain when initial scale factor adjustments are made.

In the roll channel nonorthogonality will introduce scale factor and cross coupling errors. The scale factor error is compensated in a similar manner to that of the lateral channel by increased gain in the processing branch. The cross coupling error cannot be compensated out except that it is constant over the angular range. The analysis indicates that this error in roll can be reduced significantly by proper selection of XMTR Wollaston prisms with the one having the least nonorthogonality between the polarization planes used in the roll channel.

The CONT LED control loop is nonlinear because of the application of the divider which regulates the modulation index and CONT LED intensity. The control voltage is used to regulate the LED signal and is applied to the denominator of the divider. Control loop gain values were selected for the worst case condition, that is, when the XMTR is at 4.44°C and the CONT LED intensity has degradated to the point where the extreme lower limit in the divider denominator calls for a maximum LED a.c. current of approximately 208 ma. The analysis indicates that the loop gain must be tailored for each individual OAMS application since loop gain is dependent upon range and intensity of the LED. For a given loop gain, as the range decreases, the phase margin decreases until loop instability sets in while an increase in range would increase the phase margin and increase loop stability. Loop gain values selected will maintain, assuming that the signal phase shift are kept within some reasonable bound, LED balance at about one per cent.

Detector/pre amp circuit analysis indicates the need of a damping resistor to set the circuit damping ratio to an established value of about 0.707. Without a damping resistor the circuit is highly underdamped and the signal is prone to modulation and perturbation by electrical noise or variations in light intensities. It was also proven that the signal phase shift in each detector/pre amp leg is constant and is of the same magnitude. The measured electrical noise values were 0.604, 0.437 and 1.504 mv rms for pitch, yaw and roll, respectively.

6.0 ADVANCED BRASSBOARD DESIGN

6.1 ELECTRONIC DESIGN

The Optical Angular Motion Sensor Electronic Subsystem consists of three channels operated on an analog basis with three distinct frequencies of 925, 1850 and 3700 hertz for roll, yaw and pitch, respectively. Each channel is integrated with three independent optical subsystems for the purpose of measuring relative angular displacement between two points in a three-axis coordinate system. The composite system is a precision measurement device that converts small angular deflections (arc seconds) in roll, yaw and pitch between a reference point and a remote point into an electronic output. The assembly is shown in Figure 6.3-1.

Basically, the electronic circuits for each channel perform two functions. That is, 1) an input to the system is provided in the form of an intensity modulated light source about a quiescent level and 2) this polarized light source as a function of angular displacement and range is detected. The resulting signal is processed to yield an electrical output proportional to angular rotation.

With the aid of the block diagram shown in Figure 6.1-1 and schematic drawings (Figures 6.1-2 and 6.1-3) a comprehensive description of the functional operation of the OAMS electronic circuits is presented. The electronic subsystem description will be subdivided into the following three subgroups: 1) LED drive, 2) Signal Processing Electronics and 3) LED Control Loop. These three subgroups will be identified and their functional operation and relationship upon each other described. Since all three channels are essentially the same with exceptions for amplifier gain values and operating frequencies, this section will, where practical, address itself to a common description as indicated by the block diagram. Each block is assigned a number for identification within the test. Following these three subsections an electronic network/component description in subsection 6.1.4 will describe the individual networks and components and their application for the OAMS electronic circuits.

6.1.1 LED Drive

Two light emitting diodes (LEDs) located in the transmitter provide the input light source for each channel. Each LED pair is selected to emit energy in one of the three spectral regions to prevent cross coupling the light between channels. In both the transmitter and receiver the principle of duality was employed to increase system reliability and signal-to-noise ratio (SNR). The modulation frequencies of operation for the channels are one octave apart. This provides additional immunity to channel cross talk since even harmonics are averaged to zero with the aid of the synchronous demodulator/low pass filter (5). Odd harmonics from a channel may enter other channels but are significantly attenuated by the optical filters and the action of the synchronous demodulator/low pass filters.

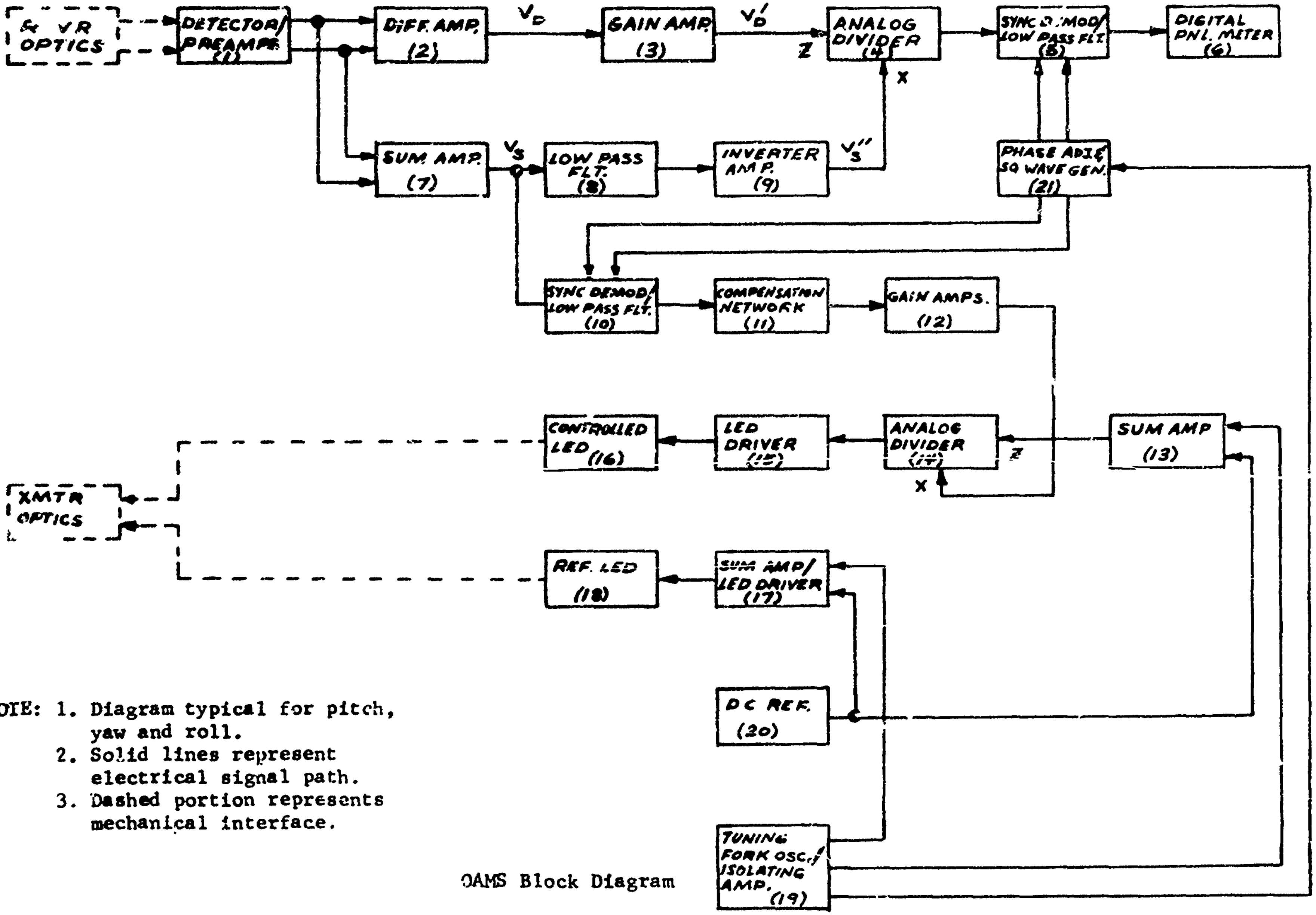
RCVR OPTICS
DETECTOR/PREAMPS (1)
DIFF. AMP. (2)
V_D
GAIN AMP. (3)
V_D'
Z
ANALOG DIVIDER (4)
X
SYNC DEMOD/LOW PASS FLT. (5)
DIGITAL PNL. METER (6)
SUM AMP. (7)
V_S
LOW PASS FLT. (8)
INVERTER AMP. (9)
V_S''
PHASE ADJ & SQ WAVE GEN. (21)
SYNC DEMOD/LOW PASS FLT. (10)
COMPENSATION NETWORK (11)
GAIN AMPS. (12)
CONTROLLED LED (16)
LED DRIVER (15)
ANALOG DIVIDER (14)
Z
X
SUM AMP (13)
XMTR OPTICS
REF. LED (18)
SUM AMP/LED DRIVER (17)
DC REF. (20)
TUNING FORK OSC./ISOLATING AMP. (19)

NOTE: 1. Diagram typical for pitch, yaw and roll.
2. Solid lines represent electrical signal path.
3. Dashed portion represents mechanical interface.

OAMS Block Diagram

Figure 6.1-1

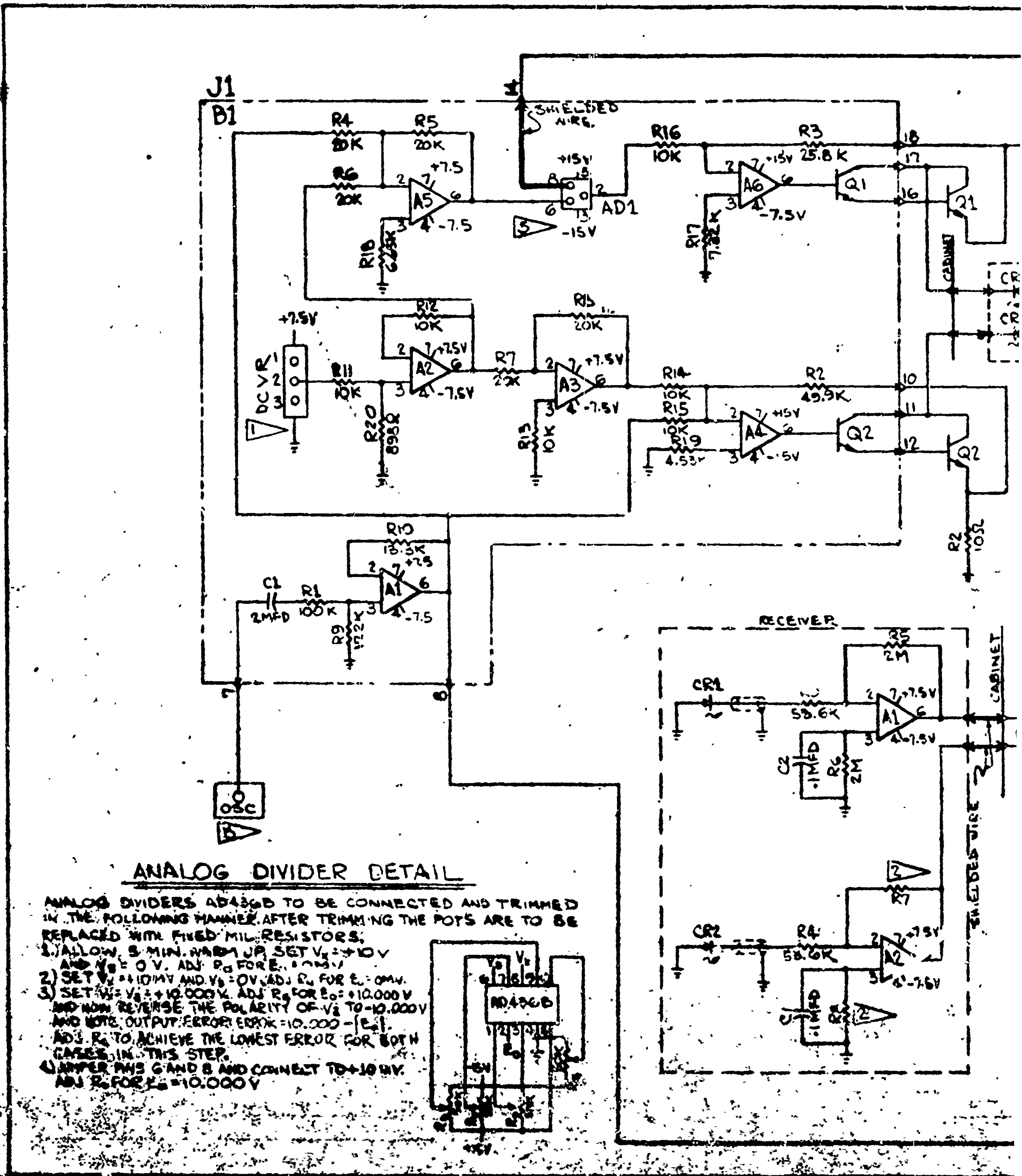
J1
B1
R4 20K
R5 20K
R6 20K
A5
+7.5
-7.5
R18 6.25K
SHIELDED WIRE
+15V
AD1
-15V
R16 10K
R3 25.8K
A6
+15V
-7.5V
R17 7.32K
Q1
Q1
18
17
16
CABINET
CR
R12 10K
R13 20K
+7.5V
DCVR
R11 10K
A2
-7.5V
R7 20K
A3
R13 10K
R20 898Ω
R14 10K
R15 10K
R19 4.53K
A4
+15V
-15V
R2 49.9K
10
11
12
Q2
Q2
R2 10Ω
R10 13.3K
A1
+7.5
-7.5
C1 2MFD
R1 100K
R9 1.21K
OSC
RECEIVER
R5 2M
CR1
58.6K
A1
+7.5V
-7.5V
C2 1MFD
R6 2M
CABINET
SHIELDED WIRE
CR2
R4 58.6K
R7
A2
+7.5V
-7.5V
AD436B
-15V
+15V

ANALOG DIVIDER DETAIL

ANALOG DIVIDERS AD436B TO BE CONNECTED AND TRIMMED IN THE FOLLOWING MANNER. AFTER TRIMMING THE POTS ARE TO BE REPLACED WITH FIXED MIL RESISTORS.

1.) ALLOW 5 MIN. WARM UP, SET V_x = +10 V AND V_z = 0 V. ADJ R_o FOR E_o = 0 mV
2) SET V_x = +10 mV AND V_z = 0 V, ADJ R_x FOR E_o = 0 mV.
3) SET V_x = V_z = +10.000 V. ADJ R_s FOR E_o = +10.000 V AND NOW REVERSE THE POLARITY OF V_z TO -10.000 V AND NOTE OUTPUT ERROR: ERROR = 10.000 - $|E_o|$. ADJ R_z TO ACHIEVE THE LOWEST ERROR FOR BOTH CASES IN THIS STEP.
4) JUMPER PINS 6 AND 8 AND CONNECT TO +10 mV. ADJ R_o FOR E_o = 10.000 V

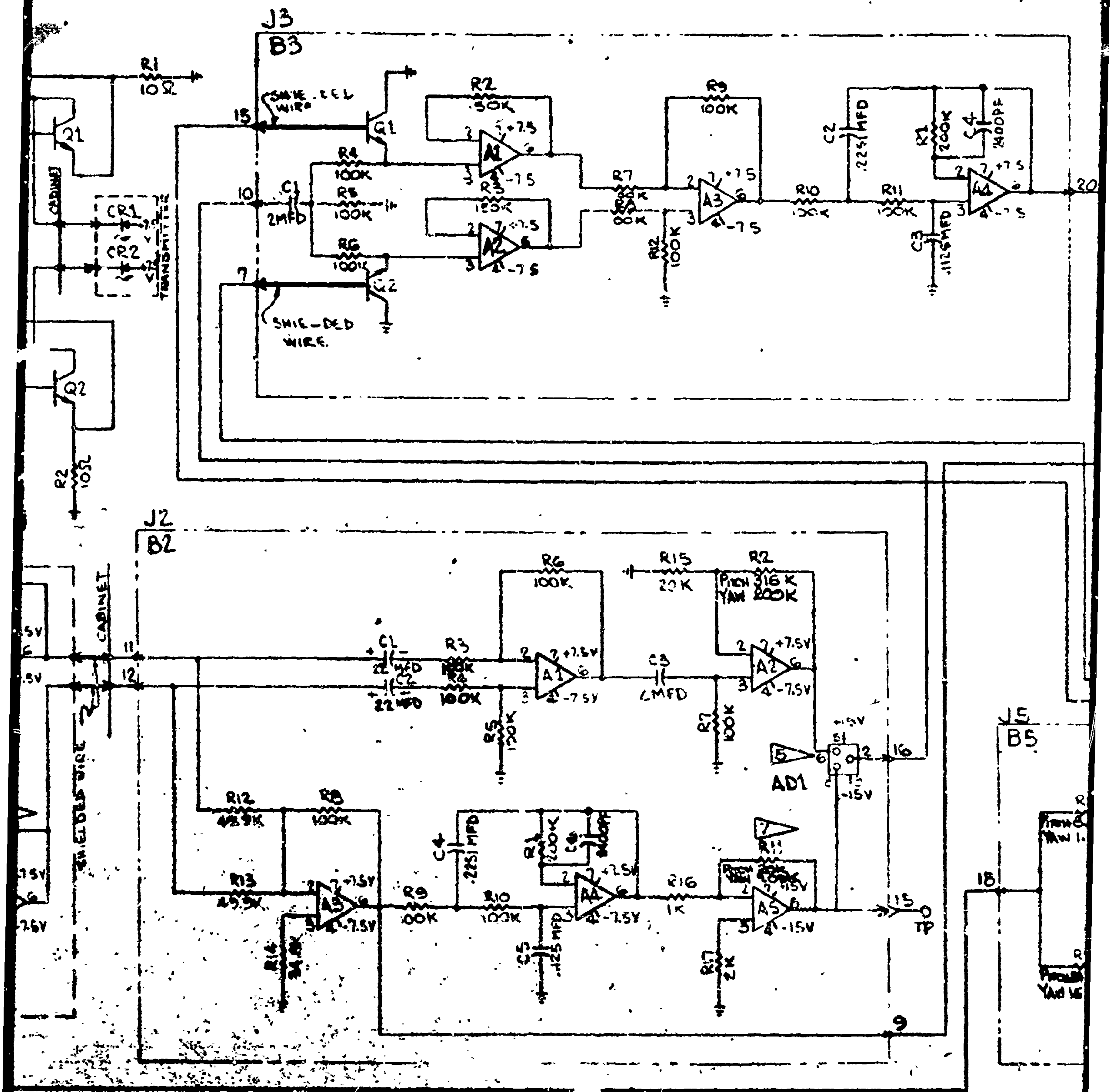
J3
B3
R1
10Ω
Q1
Q2
CABINET
CR1
CR2
TRANSMITTER
R2
10Ω
15
SHIELDED WIRE
10
C1
2MFD
7
R4
100K
R5
100K
R6
100K
R2
50K
R3
125K
A1
A2
+7.5
-7.5
R7
50K
R8
100K
R9
100K
A3
R12
100K
R10
100K
R11
100K
C2
.225 MFD
C3
.1125 MFD
R1
200K
C4
1400PF
A4
20
J2
B2
CABINET
SHIELDED WIRE
11
12
+7.5V
-7.5V
C1
22 MFD
C2
22 MFD
R3
100K
R4
100K
R5
120K
R6
100K
A1
C3
2MFD
R15
20K
R2
PITCH 316K
YAW 200K
R7
100K
A2
+15V
-15V
5
AD1
S1
16
J5
B5
R12
49.9K
R8
100K
R13
49.9K
R14
24.9K
A3
R9
100K
C4
.225 MFD
R1
200K
R10
100K
C5
.1125 MFD
A4
R16
1K
7
R11
PITCH 20K
YAW 100K
A5
R17
2K
15
TP
9
18
PITCH
YAW

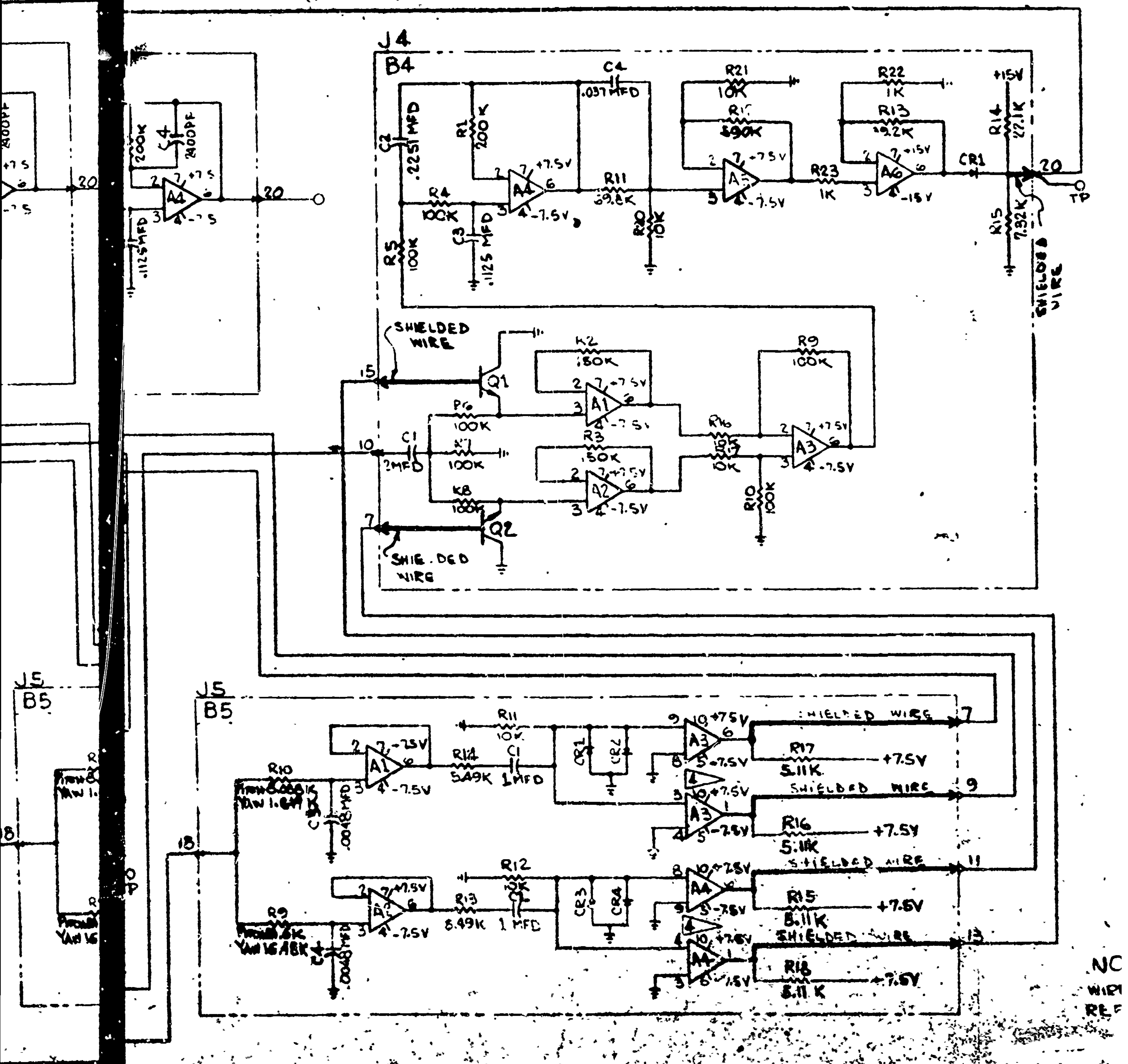
J4
B4
C4
.037 MFD
C2
.2251 MFD
R1
200 K
R4
100K
R5
100K
C3
.1125 MFD
A4
+7.5V
-7.5V
R11
69.8K
R10
10K
R21
10K
R19
390K
A5
-7.5V
R23
1K
R22
1K
R13
19.2K
A6
+15V
-15V
CR1
R14
27.1K
R15
7.32K
20
TP
SHIELDED WIRE
15
Q1
R2
150K
A1
R6
100K
10
C1
2MFD
R7
100K
R3
150K
A2
R8
100K
7
Q2
R16
10K
R9
100K
A3
R10
100K
J5
B5
R10
PITCH 6.65K
YAW 1.64K
C3
.0048 MFD
A1
-7.5V
R14
5.49K
C1
1MFD
R11
10K
CR1
CR2
A3
+7.5V
R17
5.11K
9
R16
5.11K
11
18
R9
PITCH 6.65K
YAW 16.48K
C4
.0048 MFD
A2
R13
5.49K
R12
10K
C2
1 MFD
CR3
CR4
A4
R15
5.11K
13
R18
5.11 K
2800PF
200K
.1125 MFD
NO
WIR
REF

3

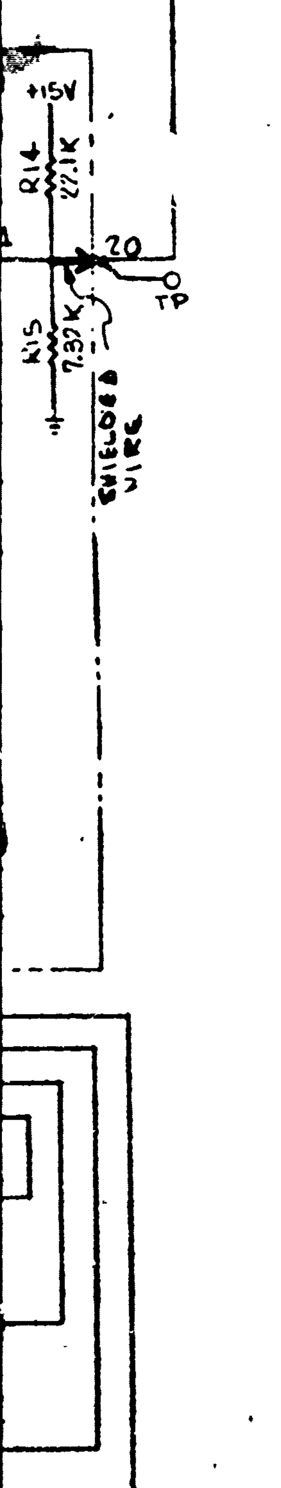

NOTES

1 > VOLTAGE REF TO BE 728 FAIRCHILD WHEN AVALABLE, AD580 SHOWN.

2 > RESISTOR VALUES TO BE SELECTED AS REQD FOR DETECTOR & PRE-AMP BALANCE

3 ALL RESISTORS ARE TO MEET MIL-R-55182E WITH CHARACTERISTICS EXCLUDING RESISTANCE VALUES AS FOLLOWS: RNR65E $\boxed{\text{VALUE}}$ B1.S.

4 > PINS 2 AND 7 TO BE CONNECTED TO -15V

5 > SEE ANALOG DIVIDER DETAIL

6 > NOMINAL RESISTANCE VALUES SHOWN. SELECT FOR CORRECT PHASE BETWEEN SIGNAL AND REFERENCE IN DEMODS.

7 > AFTER WARM-UP THE CONTROL VOLTAGE AT PIN 8 OF THE AGC ANALOG DIVIDER SHOULD BE APPROX +9.5 VDC WITH MAX. OPERATING LIGHT (FUNCTION OF DISTANCE/ANGLE ETC.) ON THE DETECTORS. TRIM THIS 67.3K RESISTANCE IF REQD TO MAKE THIS VOLTAGE APPROX +9.5VDC

8 > A.C. OSC VOLTAGE REQD FOR THIS DESIGN IS 1 V RMS.

9. ALL BOARDS CONTAIN .10MFD CERAMIC CAPACITORS FOR POWER SUPPLY DECOUPLING. CARDS B2&B3 ALSO HAVE 10MFD CAPACITORS FOR THE SAME PURPOSE.

	CR1,CR2	SLH19	2	DETECTOR (TI) RECEIVER	PITCH	
	CR1,CR2	C30852	2	DETECTOR (RCA) RECEIVER	YAW	
RECEIVER BOARD	C1 C2	1 MFD	2	CAPACITOR RECEIVER		
	R7 R8	2 >	2	RESISTOR RECEIVER		
	R5 R6	2M	2	RESISTOR RECEIVER		
	R3 R4	53.6K	2	RESISTOR RECEIVER		
	R1 & R2	10Ω	2	RESISTOR CABINET		
	Q1 & Q2	2N3766	2	TRANSISTOR CABINET		
	CR1 & CR2	SL1162-3	2	L.E.D. (T.I.) TRANSMITTER		
	R10	1.849K	1	RESISTOR (YAW CHANNEL ONLY)		
	A3 & A4	LM119H	2	COMPARATORS		
	A1 & A2	OP07AJ	2	AMPLIFIER		
	CR1 THRU CR4	1N4154	4	DIODE		
	C3 & C4	.0048 MFD	2	CAPACITOR		
B5	C1 C2	1 MFD	2	CAPACITOR		
	R15 THRU R18	5.11K	4	RESISTOR		
	R13 R14	5.49K	2	↕		
	R11 R12	10K	2	↕		
	R9	24.6K	1	RESISTOR PITCH CHANNEL ONLY		
	R9	16.48K	1	YAW " "		
	R10	6.008K	1	RESISTOR PITCH " "		
	R15	7.32	1	RESISTOR		
	CR1	1N4153	1	DIODE		
	Q1,Q2	2N2432	2	TRANZISTOR		
	A5,A6	HA2-2620-2	2	AMPLIFIER		
	~~A1 THRU A4~~	~~OP-07AJ~~	~~4~~	AMPLIFIER		
B4	C3	.1125MFD	1	CAPACITOR		
	C2	.2251-MFD	1	CAPACITOR		
	C1	2MFD	1	CAPACITOR		
	R21 R22 R23	1K	3	RESISTOR		
	R16,R17,R20	10K	3	RESISTOR		
	R14	22.1K	1	RESISTOR		
BOARD NO	SHORT SIGN	PART NO.	NO. REQD	DESCRIPTION	MATERIAL	

	R12	590K	1
	R13	39.2K	2
B4	R11	69.8K	1
	R4 THRU R10	100K	7
	R2 R3	150K	2
	R1	200K	1
	Q1-Q2	2N2432A	2
	A1 THRU A4	OP-07AJ	4
	C3	.1125 MFD	1
B3	C2	.2251 MFD	1
	C1	2MFD	1
	R1	200K	1
	R4 THRU R12	100K	9
	R2, R3	150K	2
	R11	20K	1
	R11	9.09K	1
	AD1	AD436B	1
	A1 THRU A5	OP-07AJ	5
	C5	.1125 MFD	1
	C4	.2251 MFD	1
	C3	2MFD	1
	C1, C2	22 MFD	2
B2	R17 R16	3K 1K	2
	R15	20K	1
	R14	34.8K	1
	R12, R13	49.9K	2
	R2	200K	1
	R3 THRU R10	100K	8
	R2	316K	1
	R1	200K	1
	C6	2400 PF	1
	AD1	AD436B	1
	C1	2MFD	1
	DCVR	728	1
	Q1 Q2	2N2192A	2
	A1 THRU A6	OP07AJ	6
	R20	398 Ω	1
	R19	4.53K	1
B1	R18	6.65K	1
	R17	7.32K	1
	R11 THRU R16	10K	6
	R10	13.3K	1
	R9	17.2K	1
	R4 THRU R8	20K	5
	R3	25.8K	1
	R2	49.9K	1
	R1	100K	1
BOARD NO.	SHORT SIGN	PART NO.	NO. REQD

BILL OF MATERIAL

REV. 12-27-76

NOTE:
WIREING NOT SHOWN ON BOARDS
REF ONLY SEE OM1606

SEE ENGINEERING RECORDS

NEXT ASSY | USED ON

APPLICATION

UNLESS OTHERWISE SPECIFIED
DIMENSIONS ARE IN INCHES
TOLERANCES ON
FRACTIONS DECIMALS ANGLES

MATERIAL

HEAT TREATMENT

FINAL PROTECTIVE FINISH

ORIGINAL DATE OF DRAWING DEC. 7

4

FAIRCHILD WHEN AVALABLE, AD580 SHOWN.
ELECTED AS REQD FOR DETECTOR PRE-AMP BALANCE
MIL-R-55182E WITH CHARACTERISTICS EXCLUDING
IONS: RNR65E [VALUE] B1.S.
NNECTED TO -15V
TAIL
SHOWN. SELECT FOR CORRECT PHASE
FFERENCE IN DEMODS.
L VOLTAGE AT PIN 8 OF THE AGC ANALOG DIVIDER
VDC WITH MAX. OPERATING LIGHT FUNCTION
ON THE DETECTORS. TRIM THIS 57.3K
O MAKE THIS VOLTAGE APPROX +9.5VDC
D FOR THIS DESIGN IS 1 VRMS.

10MFD CERAMIC CAPACITORS FOR POWER
B2&B3 ALSO HAVE 10MFD CAPACITORS FOR THE

TECTOR (T.I.) RECEIVER	PITCH	
TECTOR (RCA) RECEIVER	YAW	
PACITOR RECEIVER		
SISTOR RECEIVER		
SISTOR RECEIVER		
SISTOR RECEIVER		
SISTOR CABINET		
ANSISTOR CABINET		
D. (T.I.) TRANSMITTER		
SISTOR (YAW CHANNEL ONLY)		
OMPARATORS		
MPLIFIER		
ODE		
PACITOR		
PACITOR		
SISTOR		
SISTOR PITCH CHANNEL ONLY		
YAW " "		
ESISTOR PITCH " "		
ESISTOR		
ODE		
ANZISTOR		
MPLIFIER		
MPLIFIER		
APACITOR		
APACITOR		
APACITOR		
ESISTOR		
ESISTOR		
ESISTOR		
DESCRIPTION	MATERIAL	

BILL OF MATERIAL

B4	R12	590K	1	RESISTOR		
	R13	39.2K	2	RESISTOR		
	R11	69.8K	1			
	R4 THRU R10	100K	7			
	R2, R3	150K	2			
	R1	200K	1	RESISTOR		
B3						
	Q1-Q2	2N2432A	2	TRANZISTOR		
	A1 THRU A4	OP-07AJ	4	AMPLIFIER		
	C3	.1125 MFD	1	CAPACITOR		
	C2	.2251 MFD	1	CAPACITOR		
	C1	2MFD	1	CAPACITOR		
	R1	200K	1	RESISTOR		
	R4 THRU R12	100K	9	RESISTOR		
	R2, R3	150K	2	"		
B2	R11	20K	1	RESISTOR PITCH CHANNEL ONLY		
	R11	9.09K	1	RESISTOR YAW CHANNEL ONLY		
	AD1	AD436B	1	ANALOG DIVIDER		
	A1 THRU A5	OP-07AJ	5	AMPLIFIER		
	C5	.1125 MFD	1	CAPACITOR		
	C4	.2251 MFD	1			
	C3	2MFD	1			
	C1, C2	[illegible] MFD	2	CAPACITOR		
	R17 R16	[illegible]	2	RESISTOR		
	R15	20K	1			
	R14	34.8K	1			
	R12, R13	49.9K	2			
	R2	200K	1	YAW CHANNEL ONLY		
	R3 THRU R10	100K	8			
	R2	316K	1	PITCH CHANNEL ONLY		
	R1	200K	1	RESISTOR		
	C6	2400 PF	1	CAPACITOR		
B1	AD1	AD436B	1	ANALOG DIVIDER		
	C1	2MFD	1	CAPACITOR		
	DCVR	723	1	DC VOLTAGE REFERENCE 1	FAIRCHILD	
	Q1 Q2	2N2192A	2	TRANZISTOR		
	A1 THRU A6	OP-07AJ	6	AMPLIFIER		
	R20	898Ω	1	RESISTOR		
	R19	4.53K	1			
	R18	6.65K	1			
	R17	7.32K	1			
	R11 THRU R16	10K	6			
	R10	13.3K	1			
	R9	17.2K	1			
	R4 THRU R8	20K	5			
	R3	25.6K	1			
	R2	39.2K	1			
	R1	100K	1	RESISTOR		
NO.	SYMBOL SIGN	PART NO.	NO. REQD	DESCRIPTION	MATERIAL	

REV. 12-27-76

BILL OF MATERIAL

FIG. 6.1-2

UNLESS OTHERWISE SPECIFIED
DIMENSIONS ARE IN INCHES
TOLERANCES ON
FRACTIONS DECIMALS ANGLES
MATERIAL
HEAT TREATMENT
FINAL PROTECTIVE FINISH
NEXT ASSY USED ON
APPLICATION

ORIGINAL DATE OF DRAWING DEC. 7, 1976

PITCH & YAW CHANNEL
ELECTRICAL SCHEMATIC
BRASSBOARD

OAMS PHASE 2

MICHIGAN OPERATIONS

OMIGIO

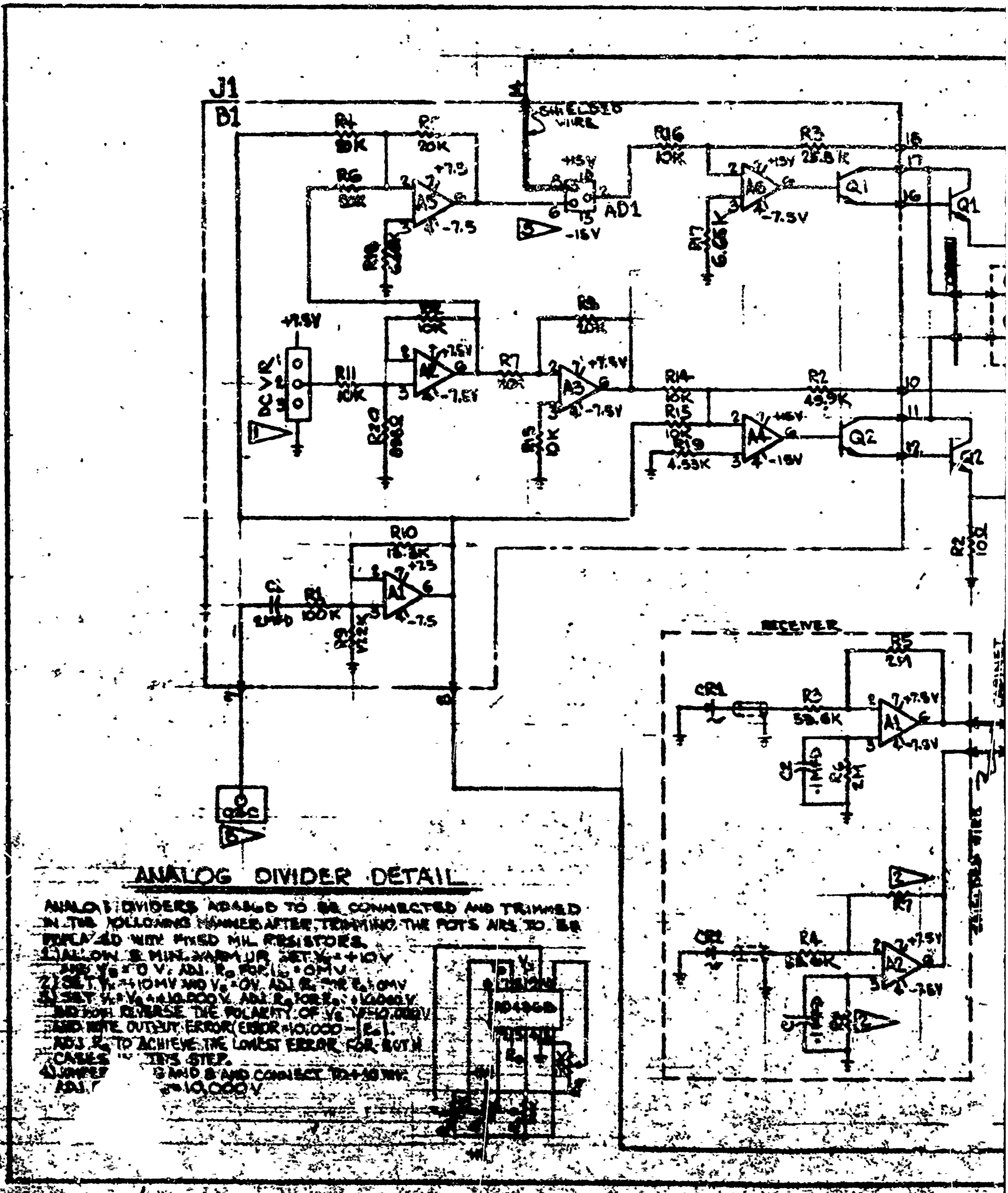
J1
B1
R4
10K
R5
20K
R6
10K
A5
+7.5
-7.5
R18
2.2K
SHIELDED WIRE
+15V
-15V
AD1
3
R16
10K
R3
25.5K
A6
+15V
-7.5V
R17
6.65K
Q1
16
17
R8
10K
R9
10K
DCVR
+7.5V
R11
10K
A2
+7.5V
-7.5V
R20
9.09K
R7
10K
A3
+7.5V
-7.5V
R13
5K
R14
10K
R2
49.9K
R15
10K
R19
4.53K
A4
+15V
-15V
Q2
10
11
1
R10
15.8K
C1
1MFD
R1
100K
A1
+7.5
-7.5
R12
100K
OSC
6
RECEIVER
CR1
R3
59.6K
R5
2M
A1
+7.5V
-7.5V
C2
R6
2M
CR2
R4
R7
A2
+7.5V
-7.5V
2
AD426B
SHIELDED WIRE
CABINET

ANALOG DIVIDER DETAIL

ANALOG DIVIDERS [illegible] TO BE CONNECTED AND TRIMMED IN THE FOLLOWING MANNER AFTER TRIMMING THE POTS ARE TO BE REPLACED WITH FIXED MIL RESISTORS.

1) ALLOW 5 MIN. WARM UP. SET V_x = +10V AND V_z = 0 V. ADJ. R_0 FOR E_0 = 0MV
2) SET V_x = +10MV AND V_z = 0V. ADJ [illegible] FOR E_0 = 0MV
3) SET V_x = V_z = +10.000V. ADJ [illegible] FOR E_0 = +10.000V AND THEN REVERSE THE POLARITY OF V_z (V_z = -10.000V) AND NOTE OUTPUT ERROR (ERROR = 10.000 − |E_0|). ADJ [illegible] TO ACHIEVE THE LOWEST ERROR FOR BOTH CASES [illegible] THIS STEP.
4) JUMPER [illegible] 8 AND 8 AND CONNECT TO +10 MV. ADJ [illegible] = 10.000V

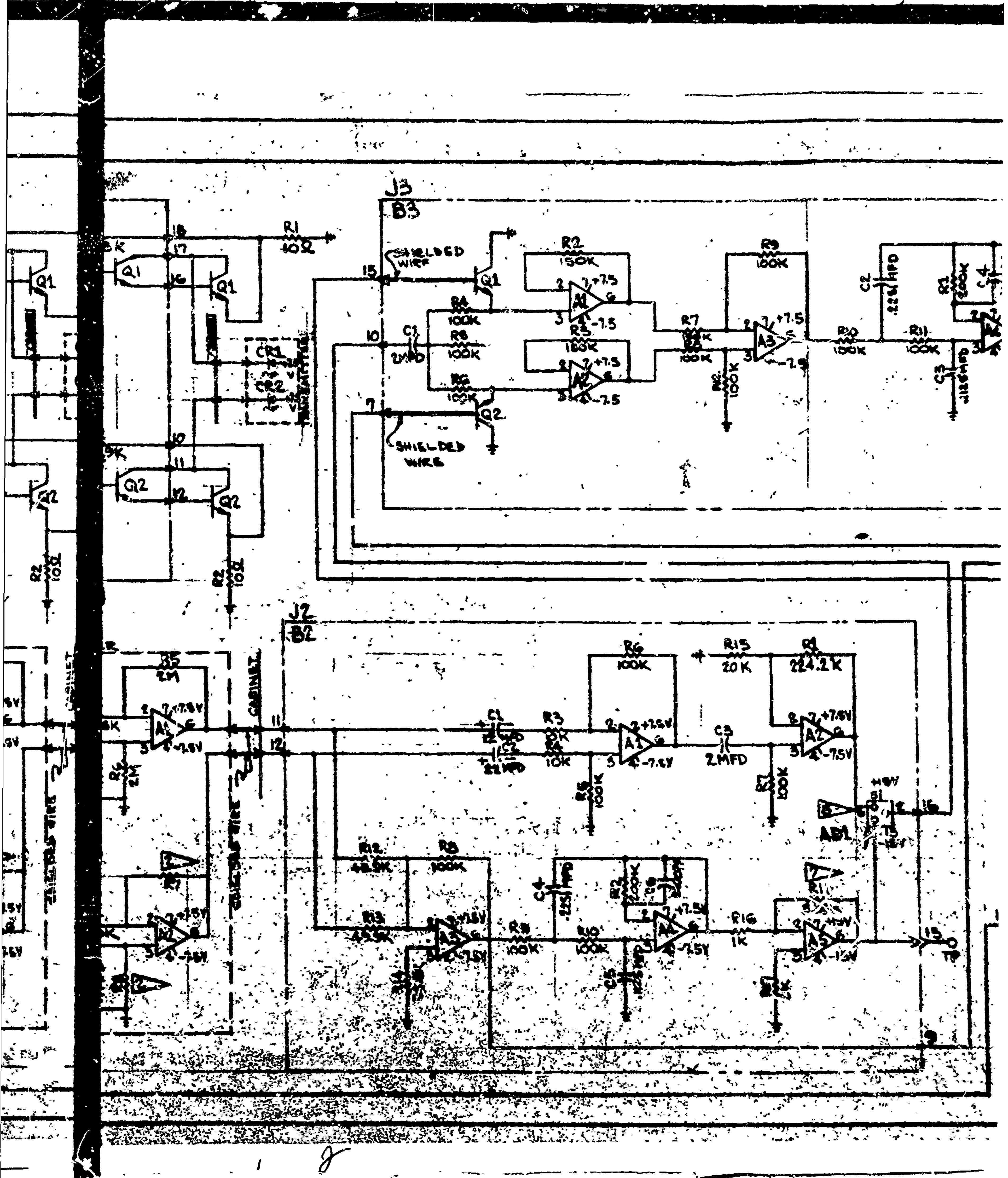
J3
B3
15
SHIELDED WIRE
Q1
R2 150K
2 7 +7.5
A1
6
3 4 -7.5
R4 100K
10
C1
2MFD
R5 100K
R3 150K
2 7 +7.5
A2
6
3 4 -7.5
R6 100K
7
Q2
SHIELDED WIRE
R9 100K
R7 100K
R8 100K
R9 10K
2 7 +7.5
A3
6
3 4 -7.5
R10 100K
R11 100K
C2 .22 MFD
C3 .112 MFD
R1 200K
C4
R1 10Ω
18
17
Q1
16
Q1
CR1
CR2
V
V
10
11
Q2
12
Q2
R2 10Ω
R2 10Ω
J2
B2
R5 2M
2 7 +7.5V
A1
6
3 4 -7.5V
R6 2M
CABINET
11
12
C1 22 MFD
C2 22 MFD
R3 10K
R4 10K
R6 100K
2 7 +7.5V
A1
6
5 4 -7.5V
R5 100K
R15 20K
R1 224.2K
C3 2MFD
R7 100K
2 7 +7.5V
A2
6
3 4 -7.5V
+15V
S1
AB1
16
-15V
R12 42.5K
R8 100K
R13 42.5K
2 7 +7.5V
A3
6
3 4 -7.5V
R9 100K
C4 .22 MFD
R2 100K
C6
R10 100K
C5 .22 MFD
2 7 +7.5V
A4
6
3 4 -7.5V
R16 1K
R11
2 7 +15V
A5
6
3 4 -15V
15
TP
9
SHIELDED WIRE
SHIELDED WIRE
R7
A2

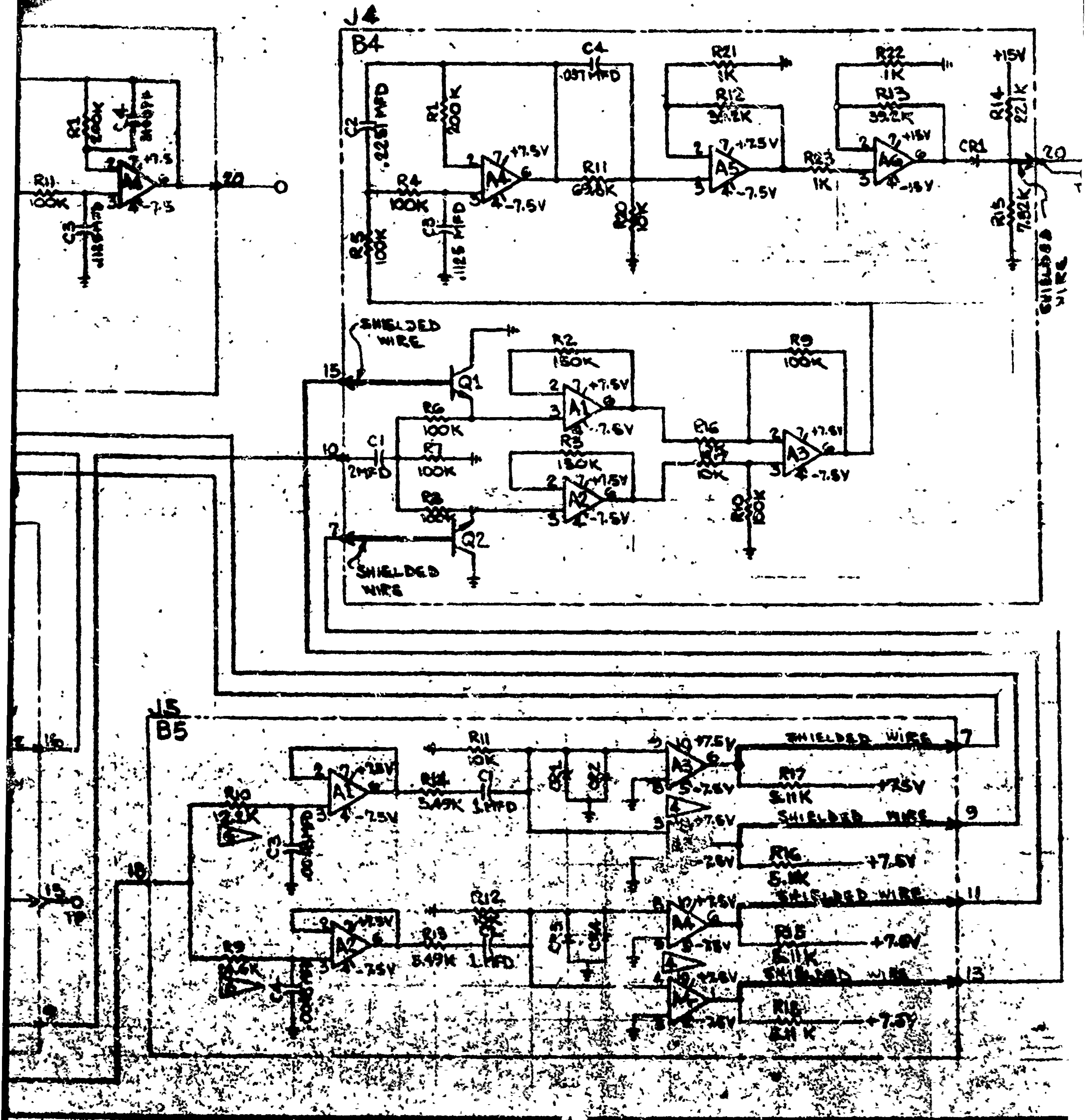
J4
B4
C4
.037 MFD
R21
1K
R12
39.2K
R22
1K
R13
39.2K
+15V
R14
22.1K
C2
.2251 MFD
R1
200K
A4
+7.5V
-7.5V
R11
69.8K
A5
+7.5V
-7.5V
R23
1K
A6
+15V
-15V
CR1
20
R4
100K
C3
.1125 MFD
R5
100K
R15
7.82K
SHIELDED WIRE
R1
200K
C4
R11
100K
C3
A4
+7.5
-7.5
20
SHIELDED WIRE
15
Q1
R2
150K
A1
+7.5V
-7.5V
R9
100K
R6
100K
R16
R17
10K
A3
+7.5V
-7.5V
10
C1
2MFD
R7
100K
R3
150K
A2
+7.5V
-7.5V
R8
100K
7
Q2
SHIELDED WIRE
J5
B5
R11
10K
A1
+7.5V
-7.5V
R14
5.49K
C1
1 MFD
A3
+7.5V
-7.5V
SHIELDED WIRE
7
R17
5.11K
+7.5V
R10
12.2K
C3
SHIELDED WIRE
9
R16
5.11K
+7.5V
18
15
TP
R12
10K
A2
+7.5V
-7.5V
R13
5.49K
1 MFD
A4
+7.5V
-7.5V
SHIELDED WIRE
11
R15
5.11K
+7.5V
R9
12.2K
SHIELDED WIRE
13
R18
5.11K
+7.5V
16

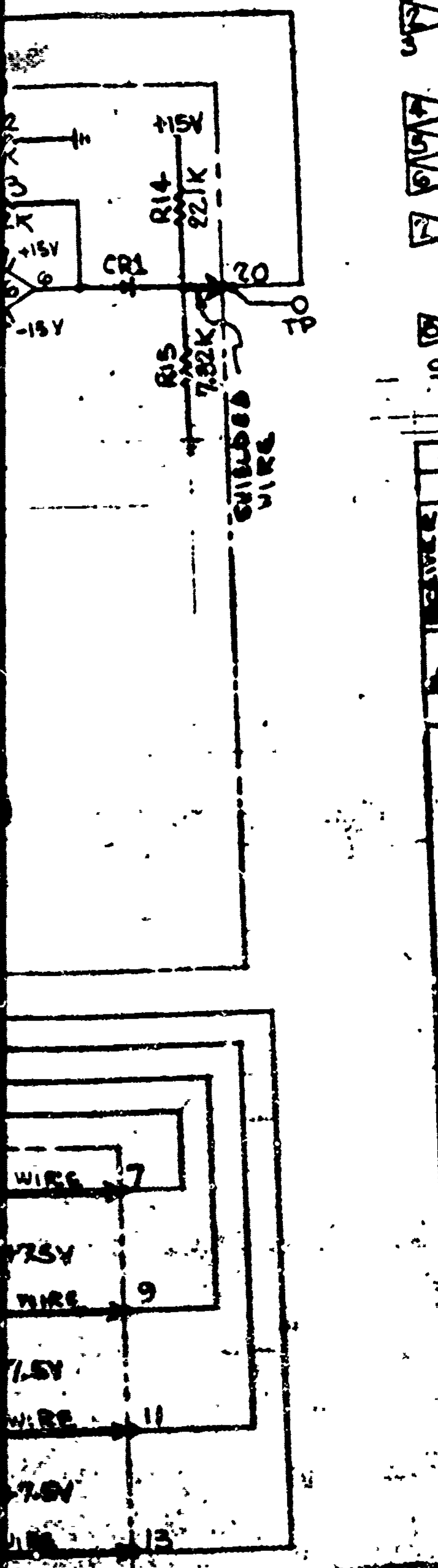

NOTES

1. VOLTAGE REF TO BE 723 FAIRCHILD WHEN AVAILABLE, AD580 SHOWN.
2. RESISTOR VALUES TO BE SELECTED AS REQD FOR DETECTOR PRE-AMP BALANCE
3. ALL RESISTORS ARE TO MEET MIL-R-55182E WITH CHARACTERISTICS EXCLUDING RESISTANCE VALUES AS FOLLOWS: RNR65E [VALUE] B1/S.
4. PINS 2 AND 7 TO BE CONNECTED TO -15V
5. SEE ANALOG DIVIDER DETAIL
6. NOMINAL RESISTANCE VALUES SHOWN. SELECT FOR CORRECT PHASE BETWEEN SIGNAL AND REFERENCE IN DEMODS.
7. AFTER WARM-UP THE CONTROL VOLTAGE AT PIN 8 OF THE AGC ANALOG DIVIDER SHOULD BE APPROX +9.5 VDC WITH MAX. OPERATING LIGHT (FUNCTION OF DISTANCE/ANGLE ETC.) ON THE DETECTORS. TRIM THIS 67.3K RESISTANCE IF REQD TO MAKE THIS VOLTAGE APPROX +9.5VDC
8. A.C. OSC VOLTAGE REQD. FOR THIS DESIGN IS 1 VRMS.
9. ALL BOARDS CONTAIN .10MFD CERAMIC CAPACITORS FOR POWER SUPPLY DECOUPLING. CARDS B2 & B3 ALSO HAVE 10MFD CAPACITORS FOR THE SAME PURPOSE.

	CIRCUIT SIGN	PART NO.	REQD	DESCRIPTION	
RECEIVER BOARD	CR1, CR2	C30852	2	DETECTOR (RCA)	RECEIVER
	C1, C2	1 MFD	2	CAPACITOR	RECEIVER
	R7, R8	2	2	RESISTOR	RECEIVER
	R5, R6	2M	2	RESISTOR	RECEIVER
	R3, R4	53.6K	2	RESISTOR	RECEIVER
	R1 & R2	10Ω	2	RESISTOR	CABINET
	Q1 & Q2	2N3766	2	TRANSISTOR	CABINET
	CR1 & CR2	SL1162-3	2	LED (TI)	TRANSMITTER
B5	A3 & A4	LM119H	2	COMPARATORS	
	A1 & A2	OP07AJ	2	AMPLIFIER	
	CR1 THRU CR4	1N4154	4	DIODE	
	C3 & C4	.0046 MFD	2	CAPACITOR	
	C1, C2	1 MFD	2	CAPACITOR	
	R15 THRU R18	5.11K	4	RESISTOR	
	R13, R14	5.49K	2		
	R11, R12	10K	2		
	R9, R10	24.6K	2	RESISTOR	
BA	A4	741HM	1	AMPLIFIER	
	R15	7.32K	1	RESISTOR	
	CR1	1N4153	1	DIODE	
	Q1, Q2	2N2432	2	TRANZISTOR	
	A5, A6	HA2-2620-2	2	AMPLIFIER	
	A1 THRU A3	OP-07AJ	3	AMPLIFIER	
	C3	.1125 MFD	1	CAPACITOR	
	C2	.2251 MFD	1	CAPACITOR	
	C1	2 MFD	1	CAPACITOR	
	R21, R22, R23	1K	3	RESISTOR	
	R16, R17, R20	10K	3	RESISTOR	
	R14	22.1K	1	RESISTOR	

	CIRCUIT SIGN	
BA	R12, R13	3
	R11	6
	R4 THRU R10	10
	R2, R3	15
	R1	2
B3	Q1-Q2	2N2
	A1 THRU A4	OP-
	C3	.11
	C2	
	C1	2
	C4	24
	R4 THRU R12	10
	R2, R3	1
	R1	2
B2	R3 & R4	
	AD1	AD
	A1 THRU A5	OP
	C5	.11
	C4	.2
	C3	
	C1, C2	2
	R17	
	R16	
	R15	
	R14	3
	R12, R13	4
	R11	
	R5 THRU R10	
	R2	
	R1	
	C6	2
B1	AD1	
	C1	
	DCVR	
	Q1, Q2	2
	A1 THRU A6	
	R20	
	R19	
	R18, R17	
	R11 THRU R16	
	R10	
	R9	
	R4 THRU R8	
	R3	
	R2	
	R1	

BILL OF MATERIAL

REV

UNLESS OTHERWISE SPECIFIED

NOTE:
WIRING NOT SHOWN ON BOARDS
REF ONLY SEE 0M1906

ILD WHEN AVALIBLE, AD580 SHOWN.
AS REQD FOR DETECTOR PRE-AMP BALANCE
WITH CHARACTERISTICS INCLUDING
RNRG5E VALUE B1/S.
TED TO -15V

OW. SELECT FOR CORRECT PHASE
CE IN DEMODS.
AGE AT PIN 8 OF THE AGC ANALOG DIVIDER
ITH MAX. OPERATING LIGHT (FUNCTION
DETECTORS. TRIM THIS 67.3K
THIS VOLTAGE APPROX +9.5VDC
THIS DESIGN IS 5 VRMS.

CERAMIC CAPACITORS FOR POWER
ALSO HAVE 10MFD CAPACITORS FOR THE

DESCRIPTION	MATERIAL		
TOR (PCA)	RECEIVER		
TOR	RECEIVER		
OR	RECEIVER		
OR	RECEIVER		
OR	RECEIVER		
OR	CABINET		
ISTOR	CABINET		
(J1)	TRANSMITTER		
ARATORS			
FIER			
TOR			
TOR			
OR			
OR			
FIER			
TOR			
E			
ISTOR			
FIER			
FIER			
ITOR			
ITOR			
ITOR			
TOR			
TOR			
TOR			

BILL OF MATERIAL

	[illegible]	PART NO.	QTY REQD	DESCRIPTION	MATERIAL	
B4	R12, R13	39.2K	2	RESISTOR		
	R11	69.8K	1			
	R4 THRU R10	100K	7			
	R2, R3	150K	2			
	R1	200K	1	RESISTOR		
B3						
	Q1-Q2	2N2432A	2	TRANZISTOR		
	A1 THRU A4	OP-07AJ	4	AMPLIFIER		
	C3	.1125 MFD	1	CAPACITOR		
	C2	.2251 MFD	1	CAPACITOR		
	C1	2MFD	1	CAPACITOR		
	C4	2400PF	1	CAPACITOR		
	R4 THRU R12	100K	9	RESISTOR		
	R2, R3	150K	2	"		
	R1	200K	1	RESISTOR		
B2	R3 & R4	10K	2	RESISTOR		
	AD1	AD436B	1	ANALOG DIVIDER		
	A1 THRU A5	OP-07AJ	5	AMPLIFIER		
	C5	.1125 MFD	1	CAPACITOR		
	C4	.2251 MFD	1			
	C3	2MFD	1			
	C1, C2	22 MFD	2	CAPACITOR		
	[illegible]	[illegible]	2	RESISTOR		
	R15	20K	1			
	R14	34.8K	1			
	R12, R13	49.9K	2			
	R11	3.83K	1			
	R5 THRU R10	100K	6			
	R2	200K	1			
	R1	224.2K	1	RESISTOR		
	C6	2400 PF	1	CAPACITOR		
B1	AD1	AD436B	1	ANALOG DIVIDER		
	C1	2MFD	1	CAPACITOR		
	DCVR	726	1	DC VOLTAGE REFERENCE IC	FAIRCHILD	
	Q1, Q2	2N2192A	2	TRANZISTOR		
	A1 THRU A6	OP-07AJ	6	AMPLIFIER		
	R20	898Ω	1	RESISTOR		
	R19	4.53K	1			
	R16, R17	6.45K	2			
	R11 THRU R16	10K	6			
	R10	13.3K	1			
	R9	17.8K	1			
	R4 THRU R8	20K	5			
	R3	28.8K	1			
	R2	49.9K	1			
	R1	100K	1	RESISTOR		

REV 12-27-76

BILL OF MATERIAL FIG. 6.1-3

DEC 7 1976

ROLL CHANNEL
ELECTRICAL SCHEMATIC
"BRASSBOARD"
DAMS PHASE I

OM1610

5

The LED drive paths are similar except that one LED is used as a reference (18) and the other controlled (16) through the action of the analog divider (14). The tuning fork oscillator supplies the sinusoidal signal used by the drive circuits A voltage reference (20) supplies the d.c. bias for summing with the sinusoidal signals to provide the composite signals for the LED drive networks. In both the reference (18) and the controlled (16) LED drive networks, the LEDs are connected between the + 7½ VDC supply and collector tie points of the darlington transistor pairs. In this configuration each LED operates about a bias current and is bounded such that the transistors neither saturate nor turn off. The a.c. signal current amplitude and the d.c. bias current amplitude for the reference LED (18) is fixed such that the controlled LED (16) can operate in power output above and below the reference output for LED balance as seen at the detector/pre amp (1) outputs.

The analog divider (14) performs the following function in controlling LED (16) signals. The analog divider controls the composite drive signal amplitude The divider output is described by the following equation where Z is the composite signal (dividend) and X is the d.c. component (divisor). The X component is the controlling parameter.

$$V_o = +10 \frac{Z}{X}$$

LED drive network (15) supplies drive current through the controlled LED (16) and LED drive network (17) supplies current through the reference LED (18).

6.1.2 Signal Processing Electronics

The function of the networks in this circuit is to operate on two electrical signals, which are proportional to the light sources seen by the two detectors (1), such that the electrical output of the snychronous demodulator/low pass filter (5) represents a relative difference in angle between the transmitter and receiver. The electronic networks required for this process are identified in figure 6.1-1 as Blocks 1 through 9 and 21 with Block 6 being the digital panel meter/indicator.

The two silicon detector diodes per channel (1) are operated in a photovoltaic mode where low noise equivalent power (NEP) is achieved. The signals from each detector are preamplified by low noise operational amplifiers and supplied to the difference amplifier (2).

Should an angular difference exist between the transmitter and receiver, two a.c. signal components (d.c. blocked by capacitors in Block 2) are applied to the difference amplifier. Since the signals have a 180 degree phase difference, the composite output signal (V_D) is effectively the sum of both input signals. This action doubles the signal level and cancels out common mode noise components. V_D is the dividend for the ACC analog divider (4). The divisor X for ACC analog divider is obtained by use of the summing amplifier (7), low pass filter (8) and inverter amplifier (9). The output signal from the analog divider (4) is applied to the snychronous demodulator/low pass filter (5). Output from the synchronous demodulator/low pass filter (5) is proportional to and represents the angular rotation between the transmitter and receiver. This analog voltage is supplied to the digital panel meter (6) where it is converted to a digital signal and supplied to its indicator for decimal read-out. Low pass filter characteristics for Blocks 5, 8 and 10 are shown in Table 6.1-1.

With V_D as the dividend and V_S as the divisor the analog divider (4) effectively normalizes the difference signal, V_D, for variations in light intensity for a given angular position. The light intensity changes may be due to 1) detector and LED responsivity degradation, 2) non-uniformity in LED light pattern and 3) change in range. This action of the divider on the difference signal is termed automatic gain control (AGC).

Because the roll channel has an optical angular sensitivity of 2 versus 60 for the lateral channels, additional gain is required in the roll channel to compensate for this condition.

Both the synchronous demodulator/low pass filter (5) in the signal processing electronics and the synchronous demodulator/low pass filter (10) in the LED control loop receive their reference signals from the phase adjust and square wave generator networks (21). There are two reference signals to each demodulator. A pair of reference signals to a demodulator has square waveforms and 180 degrees difference in phase. Their phase relative to the signal is corrected in the phase adjust section of this block (21). The input sinusoidal signal comes from the Tuning Fork Oscillator (19) isolating amplifier.

6.1.3 LED Control Loop

The purpose of the LED control loop is to drive the controlled LED (16) in a direction such that as seen by the balanced detector/preamplifiers (1), the controlled LED (16) and the reference LED (18) will have equal light output. This is accomplished in the following manner. When the intensity of both LEDs as seen by the balanced detector/preamps (1), is the same (balanced LED condition), there will be no a.c. at the signal frequency on the sum amplifier (7) output. Possible even harmonic distortion will be ignored since it will be averaged to zero in the synchronous demodulator/low pass filter (10) and will not affect LED balance. When the intensity of the LEDs, as seen by the balanced detector/preamps (1) is not the same (unbalanced LED condition), there will be an a.c. signal at the channel signal frequency on the sum amplifier (7) output. This a.c signal is used to drive the LEDs to balance.

Two cases will be described. First, at zero angle between the transmitter and the receiver, there will be equal light from each LED on either detector. With the 180 degree phase difference between the two LEDs a.c. signal components on a detector, there will be a steady d.c. light level on each detector when the LEDs are balanced. There will be no a.c. on the sum amplifier (7) output since there was none at the input. When the LEDs are not balanced this will not be true. In the extreme case of unbalance

Table 6.1-1 OAMS FILTER CHARACTERISTICS

BLOCK NO.	TRANSFER FUNCTION	CORNER FREQ W_n in rad/sec	Hz	DAMPING RATIO δ
5,8 and 10 for Pitch, Yaw and Roll	$\frac{W_n^2}{S^2 + 2\delta W_n S + W_n^2}$	20π	10	$\frac{1}{\sqrt{2}}$
11	$\frac{S + 387.2}{S + 3089.9}$	387.2	61.6	------
		and		
		3089.9	491.7	------

where one LED is extinguished for example, there will be equal light on each detector from the "ON" LED with the a.c. components on each detector in phase. When the detector/preamp (1) outputs are added under this condition by the sum amplifier (7) there will be a.c. signal at the channel signal frequency on the sum output. This a.c. signal after synchronous demodulation in synchronous demodulator/low pass filter (10) is used to drive the controlled LED (16) toward a balanced condition with reference LED (18)

When there is an angle other than zero between the transmitter and the receiver, the light from one LED is increased on one detector and reduced on the other detector. Light from the other LED is increased and reduced on opposite detectors from the first LED. Under the balanced LED condition, addition of the two detector/preamp (1) signals with the a.c. components equal in amplitude and having a 180 degree phase difference results in a d.c. output from sum amplifier (7). When the LEDs are unbalanced this is no longer the case. If under the extreme unbalanced condition where one LED is extinguished, the output from both detector/preamps (1) are in phase although not having equal amplitude on each detector. When added by sum amplifier (7) there will be an a.c. component which when demodulated by synchronous demodulator/low pass filter (10) provides a control voltage to drive the controlled LED (16) toward the referenced LED (18).

The cases described used the extreme condition of unbalanced LEDs in which one LED was extinguished. When there is any unbalance, as seen by the detector preamps (1), between the LEDs there will be an a.c. component on the sum signal which when demodulated by synchronous demodulator/low pass filter (10) will provide a correction voltage to the analog divider (14) to balance the LEDs.

The LED control loop is implemented in the following manner. Any a.c. at the channel frequency and phase is taken from the sum amplifier (7) and synchronously demodulated by synchronous demodulator/low pass filter (10). Here quadrature signals and even harmonics are rejected and the proper signal is converted to a control voltage to drive the controlled LED (16) toward the reference LED (18). This signal is supplied through a compensation network (11) for control loop stability to gain amplifiers (12), and the output from these amplifiers is supplied as the control voltage to the analog divider (14) which supplies signal to the LED drive network (15) described earlier.

6.1.4 Electronic Network/Component Description

The purpose of this subsection is to describe in more detail the individual units that are used in the OAMS electronic subsystem. The previous sections described the functional operations required in the electronic subsystem while this subsection will be less general and will focus on the specific applications and type components found in these units. Each unit may contain one or more of the networks or circuits identified in the block diagram of figure 6.1-1. These units are located either on circuit boards or housed within the main chassis or in the transmitter or receiver subassemblies as shown on the schematic drawings (Figures 6.1-2 and 6.1-3) For description purposes each unit will be categorized according to whether its function is related to: A) LED drive and control loop, B) Signal processing electronics or C) Purchased subassemblies. Refer to Table 6.1-2.

6.1.4.1 LED Drive and Control/Loop Units

6.1.4.1.1 LED Drive and Amplifier

This network contains the drive circuitry for both the controlled and reference LEDs and operates in the following manner. The oscillator output comes in to Board B1 through pin 7 to amplifier A1. This amplifier removes any d.c. from the oscillator signal, is a high impedance to the oscillator output, and provides a low impedance output to the drive networks. It has along with all other amplifiers in the OAMS system, very low offset and offset drift with temperature, low noise and high open loop gain. The output from amplifier A1 is supplied to the reference and to the controlled LED networks.

Also supplied to these networks is a stable d.c. voltage to be summed with the a.c. signal just described. The d.c. reference voltages are formed on Board B1 in the following manner. Stable and temperature compensated voltage reference labeled DCVR supplies a d.c. reference voltage which after being attenuated to the proper value by a resistor network is supplied to isolating amplifier A2. This unity gain amplifier with low output impedance supplies a positive d.c. voltage for use in the controlled LED drive network. The output of amplifier A2 is applied also to the input of unity gain inverting amplifier A3. The output of amplifier A3 is a negative d.c. voltage for use in the reference LED drive network.

The a.c. and d.c. signals are combined in the following manner in the drive networks. The positive d.c. voltage from amplifier A2 is added to the a.c. from amplifier A1 and also the polarity of both are inverted in summing amplifier A5. Amplifier A5 output is supplied through gain control analog divider AD1 with the same negative polarity to inverting amplifier driver A6 with the driver output from transistor Q1 on the chassis to resistor R1 having a positive d.c. component. The negative d.c. output from amplifier A3 is added to the a.c. from amplifier A1 and both inverted in summing amplifier driver A4 with the output from transistor Q2 on the chassis to resistor R2 on the chassis having a positive d.c. component. Although the d.c. voltage component across these resistors R1 and R2 on the chassis is positive, the a.c. component has a 180 degree phase shift between the two. This is true since the a.c. was first added to the positive reference in the controlled LED network and then the a.c. was added to the negative reference in the reference LED network.

TABLE 6.1-2 ELECTRONIC UNITS AND LOCATION ASSIGNMENT

GROUP ASSIGNMENT	UNIT NAME	LOCATION	BOARD NO.
A. LED Drive and Control Loop	1. LED Drive and Amplifier	Circuit Board (CB) and Chassis	B1
	2. Reference and Controlled LEDs	Transmitter	--
	3. Synchronous Demodulator/Low Pass Filter	CB	B4
	4. Compensation Network	CB	B4
	5. Gain Amplifiers	CB	B5
	6. Phase Adjust and Square Wave Generator Network	CB	B5
	7. Amplitude Limiting Network	CB	B[illegible]
B. Signal Processing Electronics	1. Detector and Preamplifier	Receiver	--
	2. Differntial Amplifier, AGC Analog Divider and Gain Amplifier	CB	B2
	3. Summing Amplifier, Low Pass Filter and Gain Amplifier	CB	B2
	4. Synchronous Demodulator/Low Pass Filter	CB	B3
	5. Phase Adjust and Square Wave Generator Network	CB	B5
	6. Digital Panel Meters	Chassis	-
C. Purchased Subassemblies	1. Oscillator	Chassis	--
	2. Power Supply	Chassis	--

The voltage reference is an Analog Device AD580S. This component will be replaced by a National Semiconductor LM199AH-20 883 precision voltage referenced on the flight model OAMS. This voltage reference has a temperature coefficient of better than 1 ppm °C. The AD580S has a temperature coefficient better than 40 ppm °C. All op-amps feature low offset and low noise. The analog divider is an Analog Device AD436B screened to SAMSO requirements. This divider is a module and has accuracy and electrical specifications required by the OAMS system.

6.1.4.1.2 Reference and Controlled LEDs

These LEDs are located in the transmitter. They are identified in Table 6.1-3.

6.1.4.1.3 Synchronous Demodulator Low Pass Filter

Any signal at the channel frequency from the summing amplifier B2-A3 leaves pin 9 on board B2 and enters B4 pin 10 to the synchronous demodulator/low pass filter. The circuit operates in the following manner. The signal from pin 10 on B4 passes through capacitor C1 and a resistor network to pin 3 on non-inverting and unity gain amplifiers A1 and A2. Outputs from A1 and A2 are supplied to the differential input amplifier A3. Chopper transistors Q1 and Q2 alternately and synchronously ground the inputs to amplifiers A1 and A2 at a time when the a.c signal is crossing zero. The outputs from A1 and A2 are half wave rectified signals reversed in polarity with the A1 signal output occuring on one half cycle and the A2 signal output occuring on the following half cycle. If these two signals were summed, the original sine wave representing LED unbalance would be reproduced. These two signals are supplied instead to a differential input amplifier A3, however, and the single ended output is a full wave rectified signal which is averaged to a d.c. value in the following amplifier filter network consisting of amplifier A4 and associated components. The filter characteristics are described in Table 6.1- 1.

6.1.4.1.4 Compensation Network

Following the low pass filter on board B4 is a lead compensation network for LED control loop stability. It consists of resistors R11 and R20 and capacitor C4. The closed loop output impedance of the filter amplifier A4 is very low and the closed loop input impedance to amplifier A5 to which the compensation network output supplies is very high. This impedance is such that the compensation network is affected insignificantly by its source and load.

6.1.4.1.5 Gain Amplifiers

On board 4 amplifiers A5 and A6 with associated components increase the loop gain of the LED control loop to minimize the LED unbalance to the degree required by the OAMS accuracy requirements. Two stages are required to reduce the phase shift caused by the op-amps at the required closed loop gain.

TABLE 6.1-3 LED CHARACTERISTICS

MFG.	PART NO.	CENTER WAVE LENGTH	CONTINUOUS POWER OUTPUT @ 2[illegible]	CHANNEL
Texas Inst.	SLH-19	810 n m	3.0 mw @ 100 ma	Pitch
Texas Inst.	SLH-20	850 n m	3.0 mw @ 100 ma	Yaw
Texas Inst.	SL-1162-4	935 n m	17 mw @ 100 ma	Roll

nm = 1 X 10^{-9} meter

mw = miliwatt

6.1.4.1.6 Phase Adjust Square Wave Generator Network

The square wave synchronous demodulator reference signals supplied to pins 7 and 15 on board B4 are generated on board B5 in the following manner. Oscillator isolating amplifier A1 on board B1 supplies an a.c. signal from the oscillator through pin 18 on board B5 to two phase adjust resistance-capacitance networks. One R-C network output is supplied to isolating amplifier A1 and the other to isolating amplifier A2. The output from amplifier A1 supplies an input to dual comparator A3 and amplifier A2 supplies an input to dual comparator A4, both in the following manner. The series RC networks act as loads and also prevent output offsets from amplifiers A1 and A2. The parallel diode pairs connected to the comparator inputs serve the following function. At low signal levels where the input is crossing zero voltage, a diode pair will present extremely high impedance to the input signal. This is desired since this is where the comparators switch and their input signals need to not be attenuated. After the switching has occurred and the input has increased in amplitude, however, a diode pair provides a charge-discharge path for the capacitor connected to it. Thus the non-linear characteristics of the diodes are utilized for optimum circuit operation. Square wave signal outputs leave the dual comparators A 3 and A4, one pair to the control loop demodulator on board B4 and the other pair to the channel signal demodulator on board B3. The two square wave signals in each pair have a phase difference of 180 degrees. Two pairs are required since the phase shifts of the reference square waves relative to the oscillator input, are not the same for the control loop pair and for the channel signal pair. The fast rise time square wave comparator outputs are supplied through shielded wires to their loads to prevent radiation or capacitave coupling to other networks in the system.

6.1.4.1.7 Amplitude Limiting Network

Should the output from pin 20 on board B4 be small enough representing large LED unbalance, the following events can occur. This output is the control voltage to the LED balance analog divider located on board B1. This control voltage is the divisor of the analog divider and as the divisor decreases the divider output increases. At some point the LED driver output driven by the divider will distort due to limiting or saturation. If this happens even for a short period of time it has been found that the distortion can cause the control loop to drive in the wrong direction and latch up. This could happen during turn-on of the system. To prevent this condition the resirtor network consisting of R14 and R15 and the diode CR1 were added to provide a lower limit to this output from pin 20.

6.1.4.2 Signal Processing Electronics

6.1.4.2.1 Detector and Preamplifier

The three dual detector/preamplifier pairs are located in the receiver and convert the incoming light to electrical signals for the channels. The preamplifiers are located close to the detectors to eliminate noise and pick-up. The detector signal is amplified and the pre-amplifier has low output impedance to noise and pick-up. The preamplifier is a current to voltage converter with the detector operating in the photovoltaic mode. The operational amplifiers feature low noise voltage, small output offset and low output offset drift with temperature.

6.1.4.2.2 Differential Amplifier, AGC Analog Divider and Gain Amplifier

Signal inputs to this network on board B2 are supplied by the detector/preamp through shielded cable to pins 11 and 12 on board B2. The differential amplifier consisting of amplifier A1 with associated components differences the 180 degree phase differenced a.c. signals which is the same as adding them in phase, and amplifies the result. The d.c. is blocked by capacitors C1 and C2. This signal is further amplified by the non-inverting stage consisting of amplifier A2 and associated components. Any d.c. offset coming into amplifier A2 is blocked by capacitor C3. The output from amplifier A2 is supplied as the numerator to AGC analog divider AD1. Here a filtered and amplified sum signal, next to be discussed, is applied as the denominator of the analog divider resulting in the divider having an output signal independent of changes in light intensity as seen by the detectors.

6.1.4.2.3 Summing Amplifier, Low Pass Filter and Gain Amplifier

Signals coming from the pair of channel detector/preamplifiers to board B2 are added in the sum amplifier consisting of amplifier A3 and associated components. Output from this stage is supplied to the low pass filter consisting of amplifier A4 and associated components and also out pin 9 to the LED control loop synchronous demodulator on board B4. The low pass filter just referred to has characteristics shown in Table 6.1-1. Output from the filter stage is amplified in the inverting amplifier stage consisting of amplifier A5 and associated components. The gain of this stage sets the operating point of the denominator of the analog divider to which the stage output is connected. The analog divider output, next to be discussed is supplied to the synchronous demodulator on board B3.

6.1.4.2.4 Synchronous Demodulator/Low-Pass Filter

Signal from the AGC analog divider on board B2 is supplied through pin 10 on board B3 to the synchronous demodulator on this board. This synchronous demodulator/low pass filter operates in the same manner as the one described in the section LED Drive and Control Loop Units. The filter characteristics are given in Table 6.1-1. The reference signals are supplied by the Phase Adjust and Square Wave Generator network described earlier in this section.

6.1.4.2.5 Phase Adjust and Square Wave Generator Network

The phase adjust and square wave generator network for the signal processing electronics was described earlier with the similar one under LED Drive and Control Loop.

6.1.4.2.6 Digital Panel Meters

The output signals from the filters on the three channel boards B3 are applied to terminals J4-15 on the panel meters located on the chassis. Three analog to digital panel meters (one per channel) are employed for the purpose of monitoring the angular difference between the transmitter and the receiver. The model number is AN2544, a product of Analogic. The accuracy is 0.01% at 25 degrees centegrade. The display has five digits with provisions for programmable decimal point selection. Operating temperature range is -10°C to +45°C. Supply voltage is 117 volts, 50/60 Hz.

6.1.4.3 Purchased Subassemblies

6.1.4.3.1 Oscillator

The oscillator provides three interlocked frequencies of 925 Hz, 1850 Hz, and 3700 Hz all derived from the same tuning fork source. The electrical specifications are as follows:

Output Frequency Accuracy: ± 1%
Output Frequency Stability vs Temp: ± .1% (-20°C to +60°C)
Output Frequency Stability vs Time: ± .1%/year
Operating Temperature Range: -20°C to +60°C
Output Wave Shape: Each output shall have less than 1% distortion
Output Wave Shape Stability vs Temp: Each output waveform shall remain constant in amplitude within ± 0.1% (-20°C to +60°C)
Output Wave Shape Stability vs Time: Each output waveform shall remain constant in amplitude within ± .1%/year
Oscillator Supply Voltage: ± 7½ VDC
Oscillator Power Consumption: As small as practical
MTBF = 0.5 X 10 exp + 6 hrs.
Useful life = 10,000 hrs. min.

6.1.4.3.2 Power Supply

The power supply has the following electrical specifications:

Input: + 23 to + 34 VDC with a ± 56 volt transient for 10 microseconds at a rate of five per second as defined in MIL-E-8983B, Section 328. NOTE: Chrysler is to provide the negative protection by the addition of a 10 microfarad capacitor across the input lines along with a series diode with a breakdown voltage not less than 100 VDC.

Outputs: The following voltages with the following individual circuit capability shall be provided while maintaining a maximum 30 watts at 40°C or 25 watts at 100°C case temperature from all four outputs.

+ 15V @ 7.902 Watts
- 15V @ 7.902 Watts
+ 7.5 V @ 17.184 Watts
- 7.5 V @ 3.684 Watts

Efficiency: Approximately 55% at rated load and 50% at one-third the above rated loads.

Ripple: 100 milivolts peak to peak.
MTBF = 4.35 X 10 exp + 6 hours min.
Useful life = 10,000 hrs min.

Wiring Diagram and Circuit Board Layouts

Figure 6.1-4 shows the complete wiring diagram for the electronic unit and the interconnecting cables for the transmitter and receiver units. The circuit board layouts with the major components indicated by the reference numbers from the electronic schematic diagrams are shown in Figures 6.1-2 and 6.1-3.

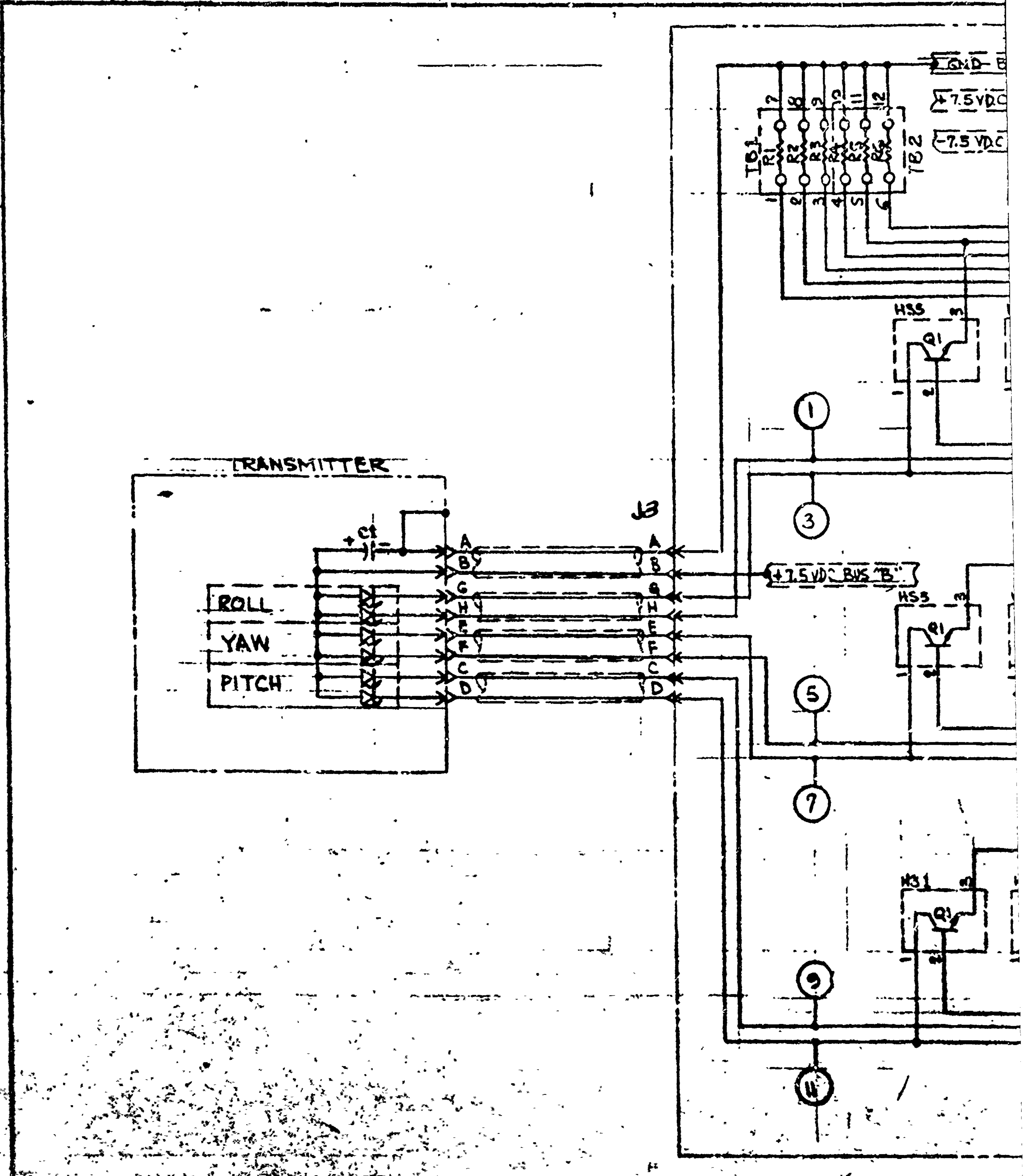

GND B
+7.5 VDC
-7.5 VDC
TB1
TB2
R1
R2
R3
R4
R5
R6
1
2
3
4
5
6
7
8
9
10
11
12
HS5
Q1
①
③
⑤
⑦
⑨
⑪
TRANSMITTER
C1
+
J3
A
B
G
H
E
F
C
D
ROLL
YAW
PITCH
+7.5 VDC BUS "B"
HS5
Q1
HS1
Q1

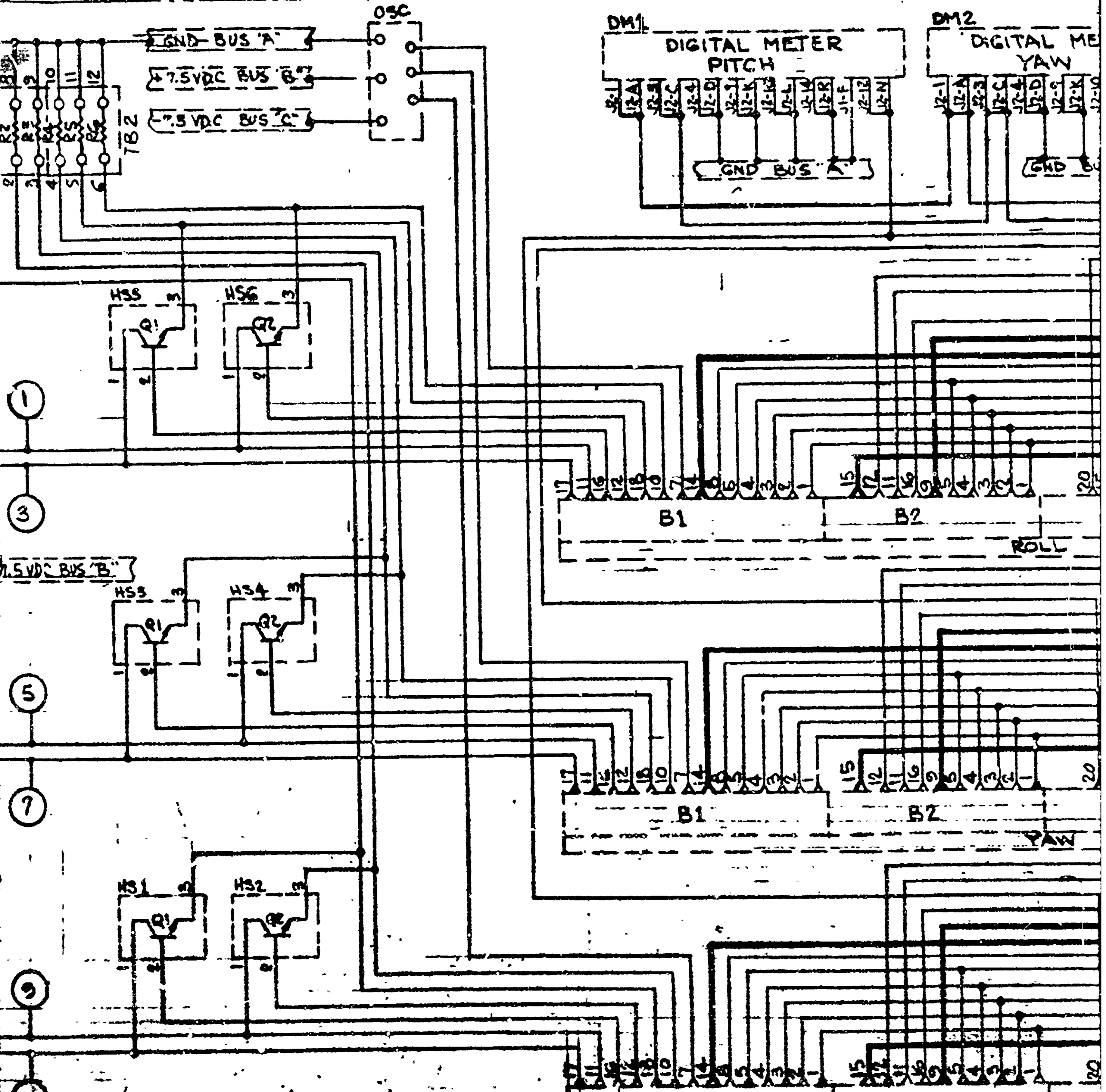
OSC
GND BUS 'A'
+7.5VDC BUS 'B'
-7.5 VDC BUS 'C'
TB2
R2
R3
R4
R5
R6
DM1
DIGITAL METER
PITCH
GND BUS 'A'
DM2
DIGITAL ME
YAW
GND BU
HS5
HS6
Q1
Q2
1
3
B1
B2
ROLL
7.5VDC BUS 'B'
HS3
HS4
Q1
Q2
5
7
B1
B2
YAW
HS1
HS2
Q1
Q2
9
11
B1
B2
PITCH

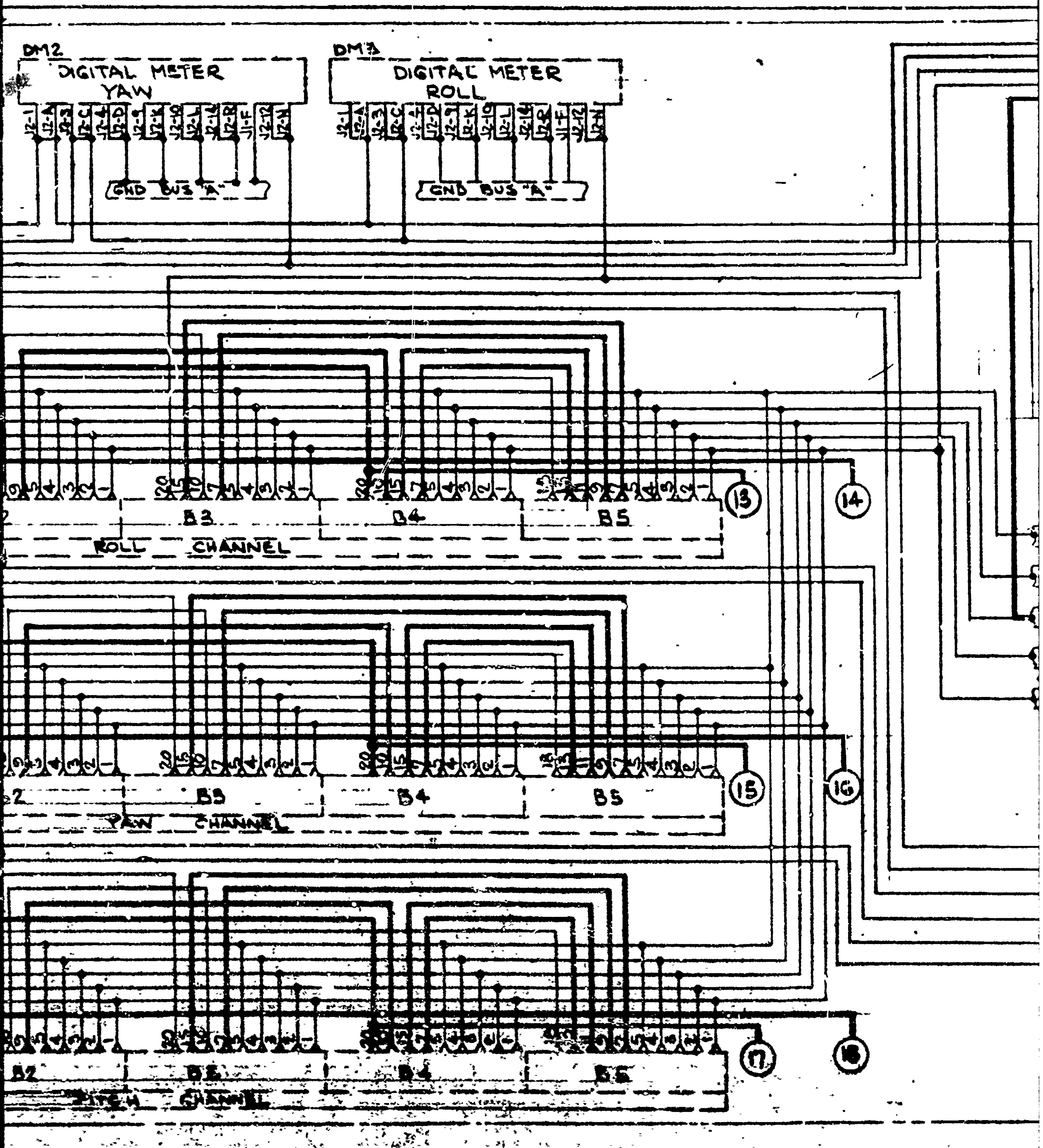
DM2
DIGITAL METER
YAW
J2-1
J2-A
J2-3
J2-C
J2-4
J2-D
J2-9
J2-K
J2-10
J2-L
J2-14
J2-R
J1-F
J2-12
J2-N
GND BUS "A"
DM3
DIGITAL METER
ROLL
J2-1
J2-A
J2-3
J2-C
J2-4
J2-D
J2-9
J2-K
J2-10
J2-L
J2-14
J2-R
J1-F
J2-12
J2-N
GND BUS "A"
B3
B4
B5
ROLL CHANNEL
13
14
B2
B3
B4
B5
YAW CHANNEL
15
16
B2
B3
B4
B5
PITCH CHANNEL
17
18

3

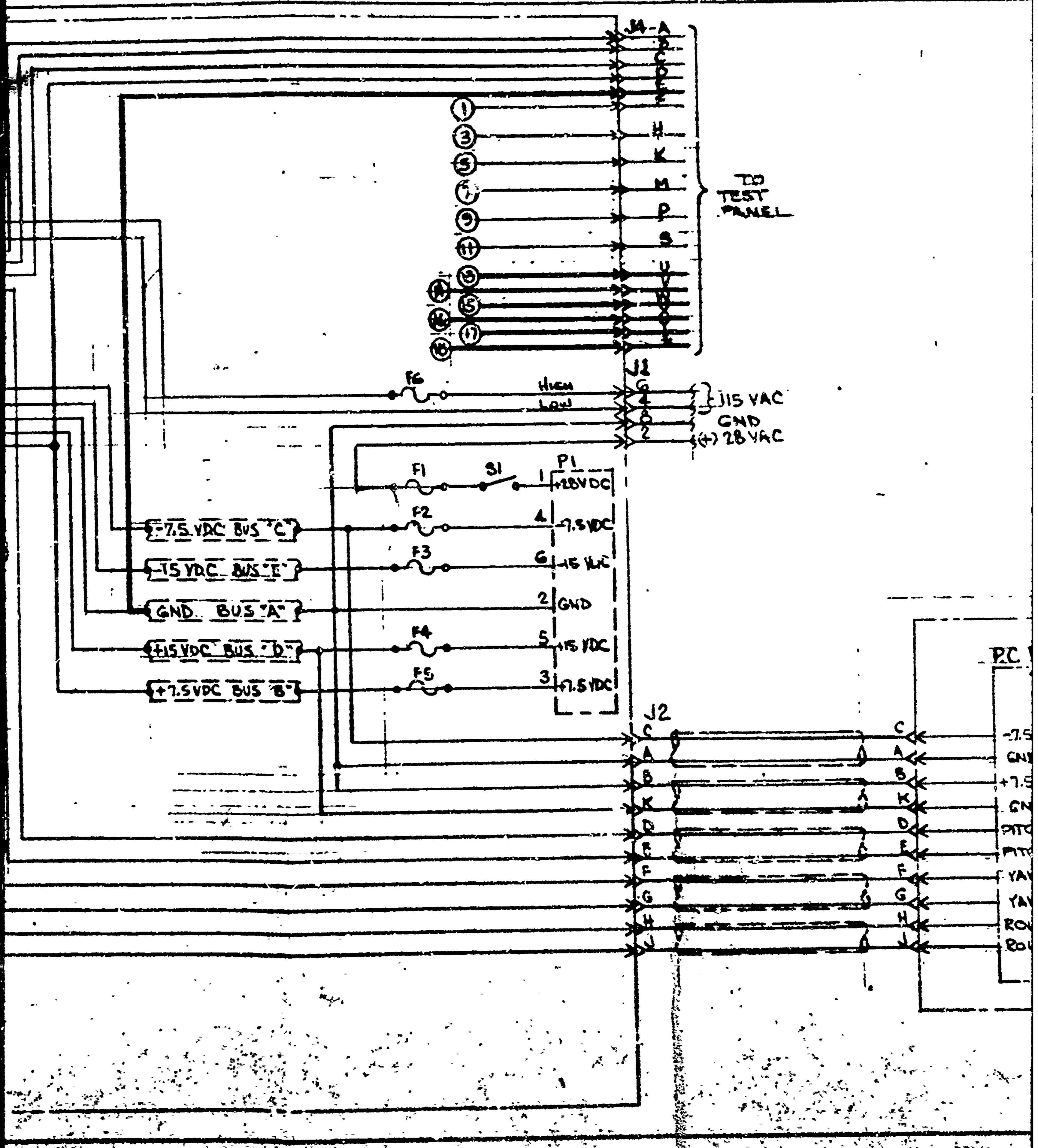
J4
A
B
C
D
E
F
H
K
M
P
S
U
V
W
X
Y
Z
1
3
5
7
9
11
13
14
15
16
17
18
TO TEST PANEL
J1
G
4
8
2
F6
HIGH
LOW
115 VAC
GND
(+) 28 VAC
F1
S1
P1
1 +28VDC
F2
4 -7.5VDC
F3
6 -15 VDC
2 GND
F4
5 +15 VDC
F5
3 +7.5VDC
-7.5 VDC BUS "C"
-15 VDC BUS "E"
GND BUS "A"
+15VDC BUS "D"
+7.5VDC BUS "B"
J2
C
A
B
K
D
E
F
G
H
J
P.C.
-7.5
GND
+7.5
GND
PITCH
PITCH
YAW
YAW
ROLL
ROLL

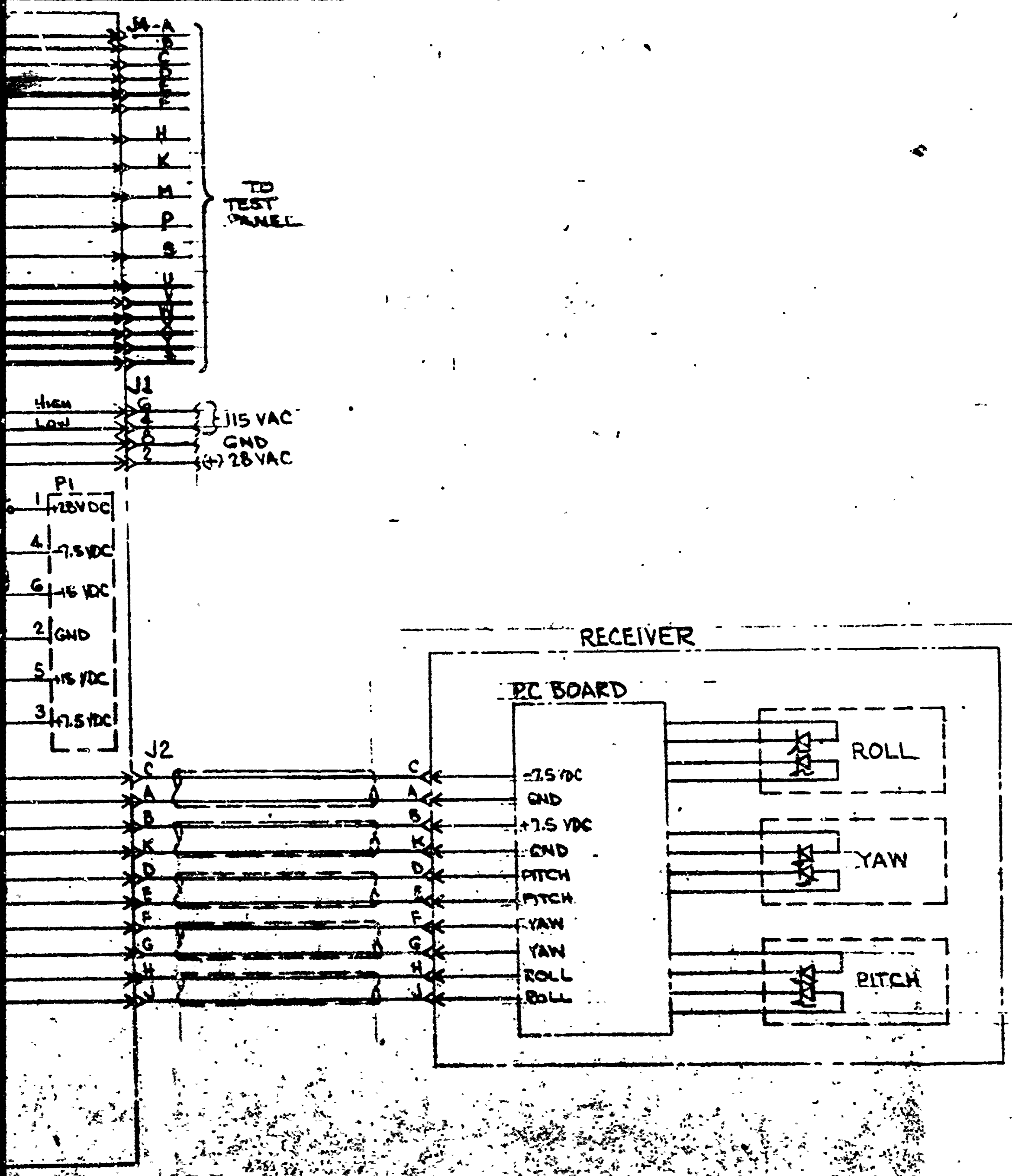

J4-A
B
C
D
E
F
H
K
M
P
S
U
TO TEST PANEL
J1
HIGH
LOW
G
4
2
115 VAC
GND
(+) 28 VAC
P1
1 +28VDC
4 -7.5 VDC
6 -15 VDC
2 GND
5 +15 VDC
3 +7.5 VDC
J2
C
A
B
K
D
E
F
G
H
J
RECEIVER
P.C BOARD
-7.5 VDC
GND
+7.5 VDC
GND
PITCH
PITCH
YAW
YAW
ROLL
ROLL
ROLL
YAW
PITCH

NOT

DARK
SHIEL

NOTE:

DARK LINE —— INDICATES
SHIELDED WIRE

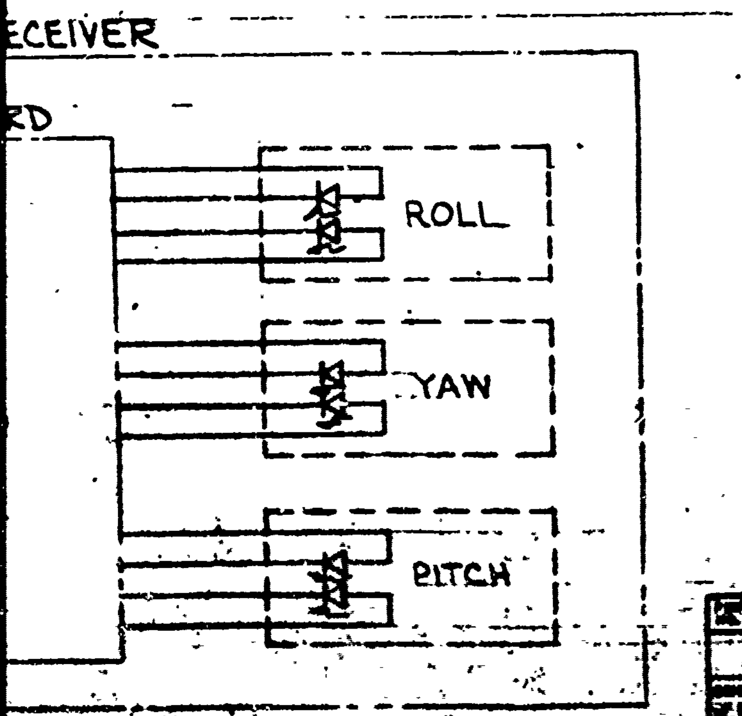
ECEIVER
RD
ROLL
YAW
PITCH

BILL OF MATERIAL

FIG. 6-1

ADVANCED ELECTRONIC
SYSTEM
BRASSBOARD SCHEMATIC
CAMS PHASE 2

OM1606

6.2 ADVANCED BREADBOARD OPTICAL DESIGN

6.2.1 Transmitter

The transmitter optical design is shown in figure 6.2-1. A simple collimator is required to image the light emitting area of the LED at infinity. The focal length of the collimator is adjusted to provide the desired field of view (FOV) or angular beam spread. The design is somewhat complicated by the fact that as a unit, the LED's are not Lambertian emitters, and the brightness or intensity as a function of angle of emission differs greatly from unit to unit. Also, it has been found that the emitting area is not of uniform brightness. Dark spots are not uncommon.

An objective lens is used to collimate the light emitted from the LED. One-half of the light from each LED is transmitted in the appropriate polarization mode, by the Wollaston Prism. This linearly polarized light is then changed to circular by the quarter wave plate. The light from one LED is right-hand circularly polarized as it leaves the quarter wave plate, while the light from the alternate LED is left-hand circularly polarized as it leaves the wave plate. These two light forms are then changed to elliptical as they pass through the angle sensing crystal (ASC).

In the previous phase a single collimating lens was used for the two LED's as shown in figure 6-2-1a. However, in the present phase three different LED's were found which have a higher output power. Consequently, after some laboratory testing, these new LED's were selected for the flight model design. The new LED's, however, have a smaller effective emitting area than the previous LED's and therefore require a shorter focal length collimating lens for the maximum beam intensity. The optimum lens as determined from laboratory measurements was a lens of approximately 12.0 millimeters focal length. The lens is aspheric plano-convex and corrected for minimum spherical aberration. This focal length is much too short to use in the configuration of 6.2-1a, because of the mechanical contraints imposed by the physical dimensions of the LED's and their holders. Therefore, a separate lens is required for each LED as shown in figure 6.2-1b. Further details of this configuration are shown in the section on the optical design of the flight model transmitter, section 7.2.1.

It was decided to incorporate this collimating lens modification into one of the present channels. The pitch channel was selected for this modification. The pitch channels conform to figure 7.2-1b and the yaw channels conform to figure 7.2-1a. The roll channel is also similar to figure 7.2-1a but with the omission of the angle sensing crystal. The improvements of the double collimating lens system over the single lens system are shown in Table 6.2-1.

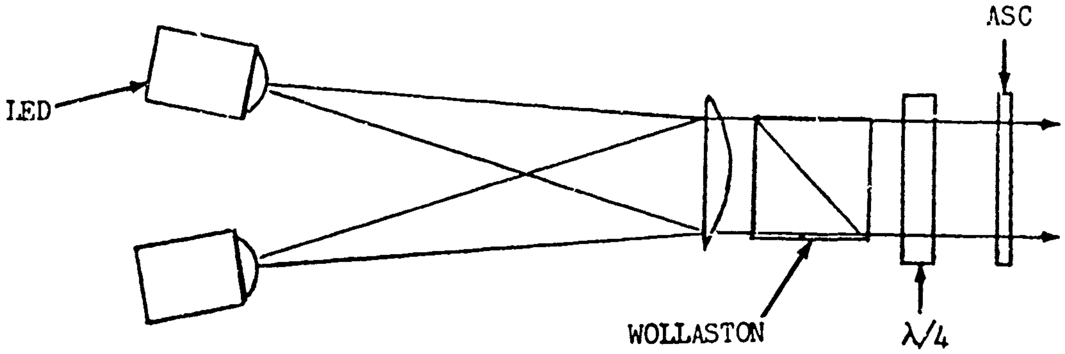
ASC
LED
WOLLASTON
λ/4

Figure 6.2-1a. Advanced Brassboard Transmitter--Yaw Channel.

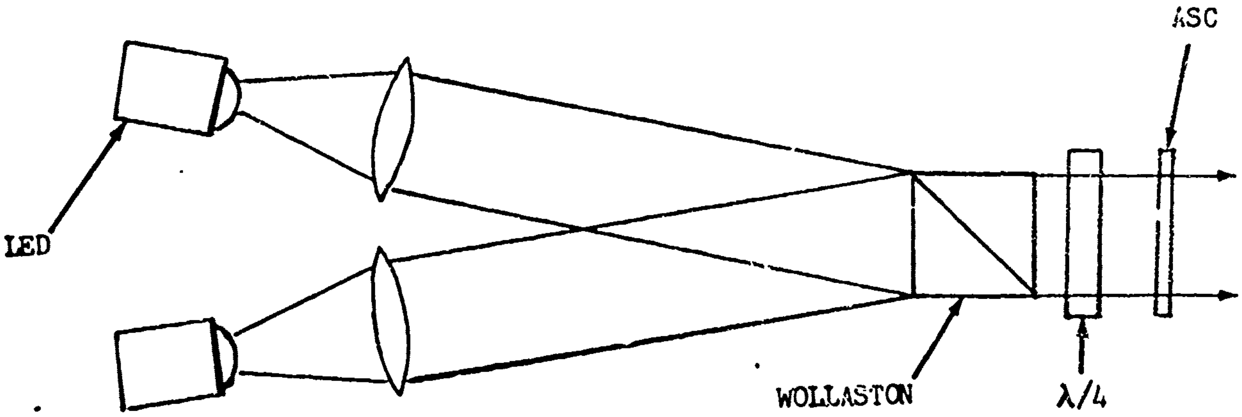
ASC
LED
WOLLASTON
λ/4

Figure 6.2-1b. Advanced Brassboard Transmitter-Pitch Channel.

TABLE 6.2-1

COLLIMATED LIGHT OUTPUT WITH VARIOUS LENS

RELATIVE PEAK OUTPUT

LED	12 mm Aspheric	15 mm	20 mm
SLH-19B(M)	419	210	269
SLH-19B(N)	529	281	349
SLH-20A(N)	319	139	170
SLH-20D(N)	659	249	322
SL-1162-3#1	659	381	495
SL-1162-3#3	517	537	709

In every case but one the maximum output was greatest using the 12 mm aspheric lens with each LED. A possible explanation is that spherical aberration of the 15 mm lens (which is f/1) is greater than that of the 20 mm lens and that the 12 mm aspheric has the best correction for sperical aberration.

The output of the SLH-19 and -20s are very nearly Lambertian while the SL1162-3 LEDs are more directional. They have a reflector placed near the emitting element which accounts for the "shoulders" in the intensity output plots (Typical plots are shown in Figure 7.1-4). The fact that the output of the #3 SL 1162-3 with the three lenses is not greatest with the 12 mm lens may be due to this LED having a narrower angular output and the faster lens is not intercepting any more light as in the case of the other LED types.

The required field-of-view of 1.1 degrees was met or exceeded in every case.

Mechanically, the eccentric mounting adjustment for the LED was removed because of: 1) the new LEDs had improved manufacturers mechanical tolerances of positioning the active area and 2) shorter focal length lens were necessary to increase collection efficiency, but would amplify the eccentricities. The new lens collimating system was incorporated in the pitch channel. The eccentric mounting is also removed from all of the channels in the flight model design.

Table 6.2-2 is a listing of the components of the transmitter and their specifications.

6.2.2 Receiver

The receiver optical design is shown in figure 6.2-2 and table 6.2-3 which gives the dimensions of the elements. The first element is the angle sensing crystal (ASC). This element is omitted in the roll channel and is replaced by a plane window. The angle sensing crystal is two millimeters thick, which provides an optical gain at the nominal system wavelength. (The gain does not vary significantly over the different channel wavelengths). The Wollaston prism is next, followed by an interference filter. Off-the-shelf filters were selected for each channel such that the

Table 6.2-2. OAMS TRANSMITTER OPTICAL COMPONENTS - PHASE II

COMPONENT	SIZE	THICKNESS	CURVATURE	COMMENTS
Plane Window	22 mm dia.	2.0 mm	-	Roll Only
ASC	22 mm dia.	1.5 mm	-	Pitch and Yaw only. Quartz
Lens:				
Pitch	15 mm dia.	5.0 mm	F.L.-12 mm	Aspheric
Yaw	20 mm dia.	6.0 mm	F.L.-40 mm	Plano-convex
Roll	20 mm dia.	6.0 mm	F.L.-40 mm	Plano-convex
$\lambda/4$ Plate:				Cemented Mica
Pitch	22 mm dia.	5.5 mm	-	810 nm
Yaw	22 mm dia.	5.5 mm	-	850 nm
Wollaston	15 x 15 mm	20 mm	-	Calcite, 20°
LED:				
Pitch	-	-	-	T.I.-SLH 19 λ= 810 nm
Yaw	-	-	-	T.I.-SLH 20 λ= 850 nm
Roll	-	-	-	T.I.-SL1162-3 λ=935 nm

Note: All optics are coated for less than 1.5% reflectivity.

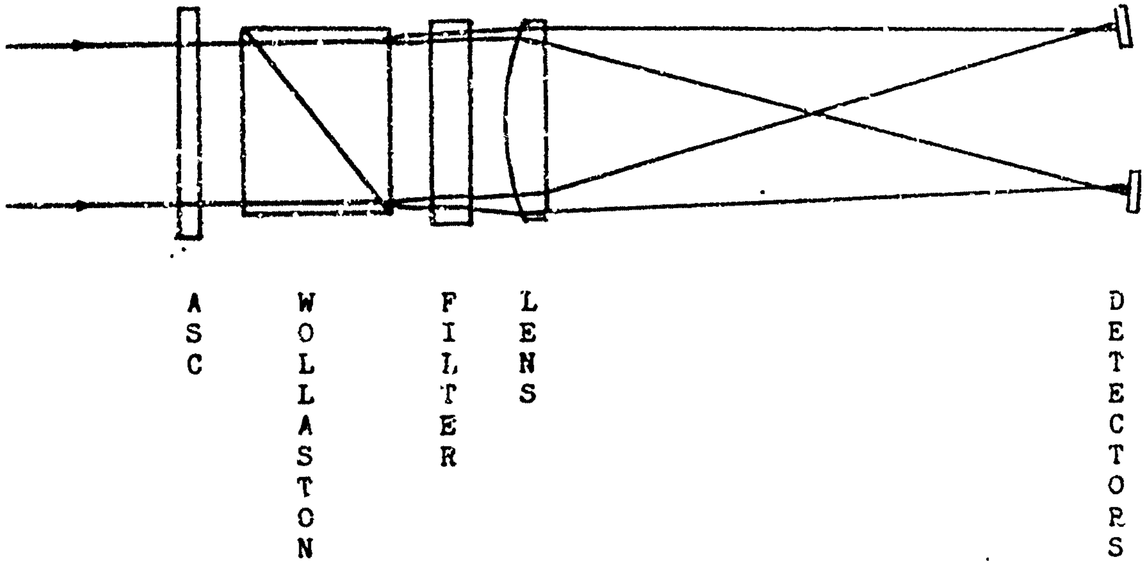
ASC
WOLLASTON
FILTER
LENS
DETECTORS

Figure 6.2-2. Advanced Brassboard Receiver—Lateral Channels. (ASC Omitted in Roll Channel).

Table 6.2-3. **OAMS RECEIVER OPTICAL COMPONENTS - PHASE II**

COMPONENT	SIZE	THICKNESS	CURVATURE	COMMENTS
Plane Window	32 mm dia.	2.0 mm	-	Roll only, BK-7
ASC	32 mm dia.	1.5 mm	-	Pitch and Yaw only, Quartz
Wolaston	25 x 25 mm	23 mm	-	Calcite, 15°
Filter	27 mm dia.	6.0 mm	-	Pitch 810 nm, Yaw 850 Roll 935 nm
Aperture Stop	25 mm dia.	-	-	13 mm before ASC
Objective Lens	25.4 mm dia.	7.0 mm	F.L. 63.5 mm	
Detector	5.0 mm dia.	-	-	RCA-C30852

Note: All optics are coated for less than 1.5% reflectivity.

transmission versus wavelength characteristics provided the least cross coupling between channels. The elements up to and including the filter are plane-parallel components having zero power and do not enter significantly into the optical design.

The system stop is located at the first surface of the instrument faceplate. It is approximately 13.0 millimeters in front of the Angle Sensing Crystal. Subsequent ray trace calculations have shown that placement of the stop at the first surface of the Wollaston Prism will significantly reduce vignetting and reduce channel cross-coupling particularly in translation. The stop has been repositioned in the flight model design.

The optical detectors are RCA C30852 single-element silicon photovoltaic photodiodes. The detectors are positioned slightly away from the objective lens focal plane. By slightly diffusing the light spot on the detector local variations of responsivity across the detector can be reduced

6.3 MECHANICAL DESIGN

6.3.1 Mechanical Design - General

Three assemblies are required for the sensor, a transmitter, a receiver and electronic unit, the units being positioned remote to each other as shown in figure 6.3-1. The transmitter and receiver mechanical assemblies are shown in figures 6.3-2 and 6.3-3. These assemblies each contain an optical package and an electronics package; the electronics package can be removed from the optical package without changing any optical component alignment.

The transmitter and receiver assemblies are hermetically sealed and the sealed containers will be purged with an inert gas prior to filling to a low pressure. Therefore, components of the transmitter and receiver assemblies would not be exposed to space vacuum conditions. This will prevent outgassing from surrounding components or from the optical components themselves from affecting the quality of the optical components. Outgassing on lens and angle sensing crystal faces would cause image blur and light transmission loss.

The reference surfaces (optical) are aligned with an autocollimator for the transmitter and receiver assemblies. The two assemblies are clamped to their respective reference platforms or positions, and autocollimated to each other to give a parallelism accuracy between the reference surfaces of ± 0.001 inch.

The required thermal stability that is necessary to obtain the accuracy of alignment is provided in the mechanical and structural configuration. This configuration has characteristics that allow a single unit construction matching capability. The multi-component mounts are positioned in cylindrical holders to ease the optical axis alignment problem. The thermal control of the sensor is accomplished by passive methods using the structural material (aluminum alloy) and, if needed, thermal coatings to give the desired amount of conduction and radiation as a means of heat transfer.

The angle sensing crystals which are the critical optical elements are so constructed that the two axes that are 90° apart have the same thermal gradient. Therefore, the temperature range requirement will have no effect on the angle sensing crystal measuring stability, provided that the elements of the angle sensing crystal are mounted together. This assures a uniform distribution of temperature

6.3.2 Transmitter Design

The main transmitter housing is bored out from a one piece block of aluminum, into which the angle sensing crystals are hard mounted for the three channels. The shoulder, to which the angle sensing crystals are butted, have been machined and lapped to 8-12 micro inches, into this shoulder is the "O" ring groove which allows the compression of the "O" to completely fill the volume of the groove when the angle sensing crystal bottoms on the housing shoulder. Behind the angle sensing crystal is the quarter wave plate, spaced between these elements is a teflon shim or washer. This subassembly is clamped together by a threaded lock ring. The complete assembly is backed up by a wave spring washer. The amount of compression

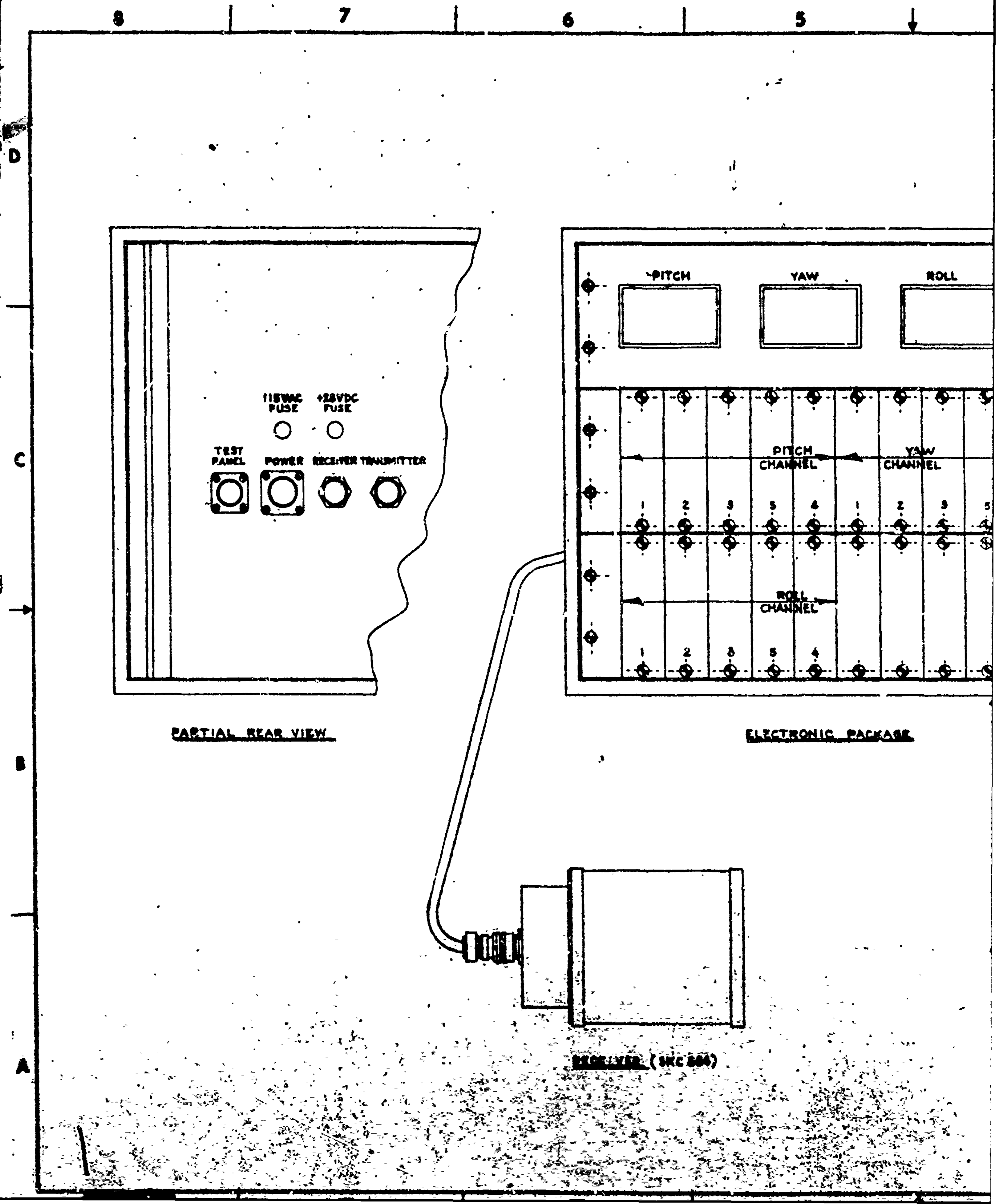
8
7
6
5
D
C
B
A
115VAC FUSE
+28VDC FUSE
TEST PANEL
POWER
RECEIVER
TRANSMITTER
PITCH
YAW
ROLL
PITCH CHANNEL
YAW CHANNEL
ROLL CHANNEL
1
2
3
5
4
1
2
3
5
1
2
3
5
4

PARTIAL REAR VIEW

ELECTRONIC PACKAGE

RECEIVER (SKC 804)

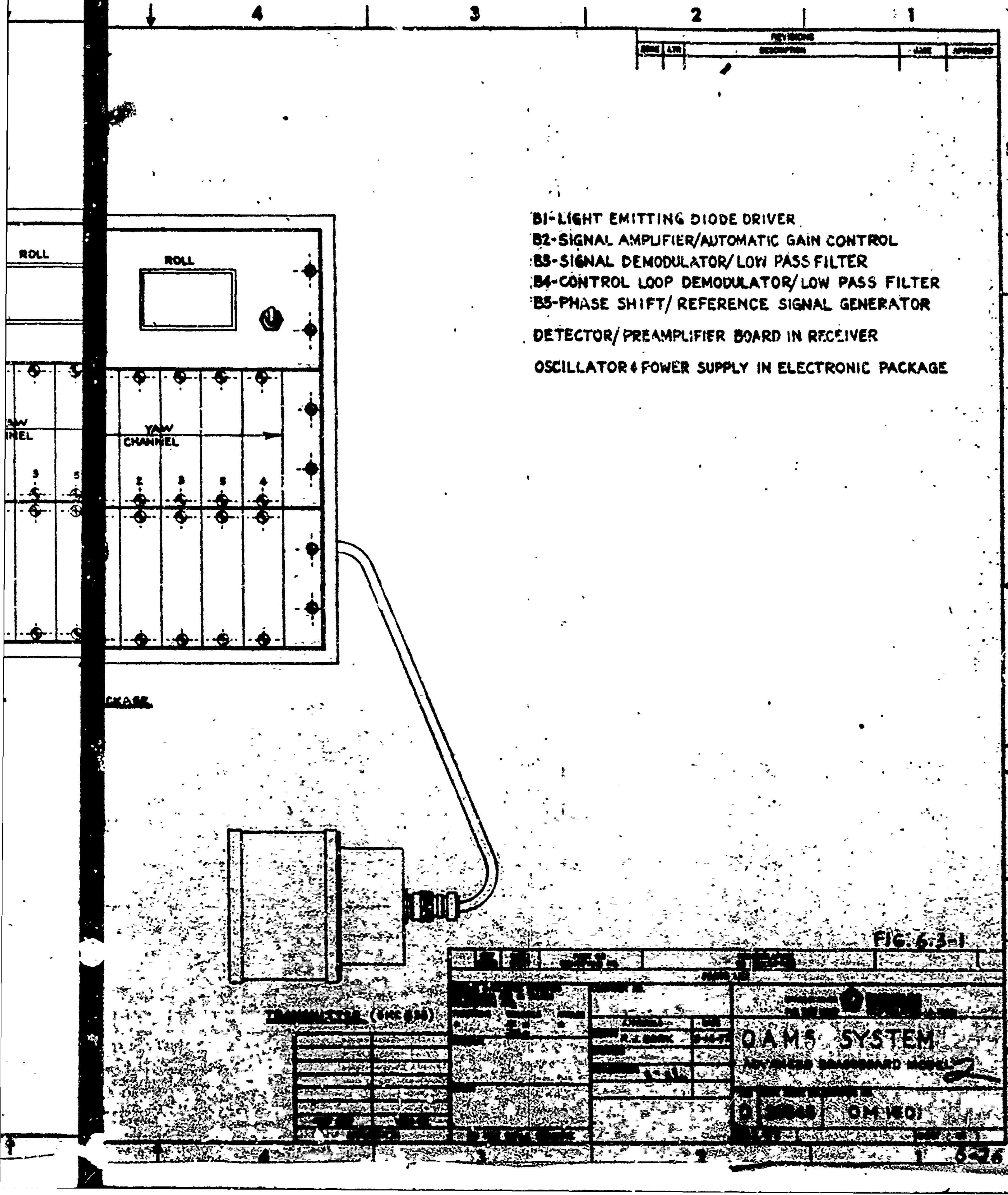
4
3
2
1
REVISIONS
ZONE
LTR
DESCRIPTION
DATE
APPROVED
D
C
B
A
ROLL
ROLL
YAW
INEL
YAW
CHANNEL
3
5
2
3
5
4
CKAGE
TRANSMITTER
OAMS SYSTEM
ADVANCED BREADBOARD MODEL 2

B1-LIGHT EMITTING DIODE DRIVER
B2-SIGNAL AMPLIFIER/AUTOMATIC GAIN CONTROL
B3-SIGNAL DEMODULATOR/LOW PASS FILTER
B4-CONTROL LOOP DEMODULATOR/LOW PASS FILTER
B5-PHASE SHIFT/REFERENCE SIGNAL GENERATOR

DETECTOR/PREAMPLIFIER BOARD IN RECEIVER

OSCILLATOR & POWER SUPPLY IN ELECTRONIC PACKAGE

FIG. 6.3-1

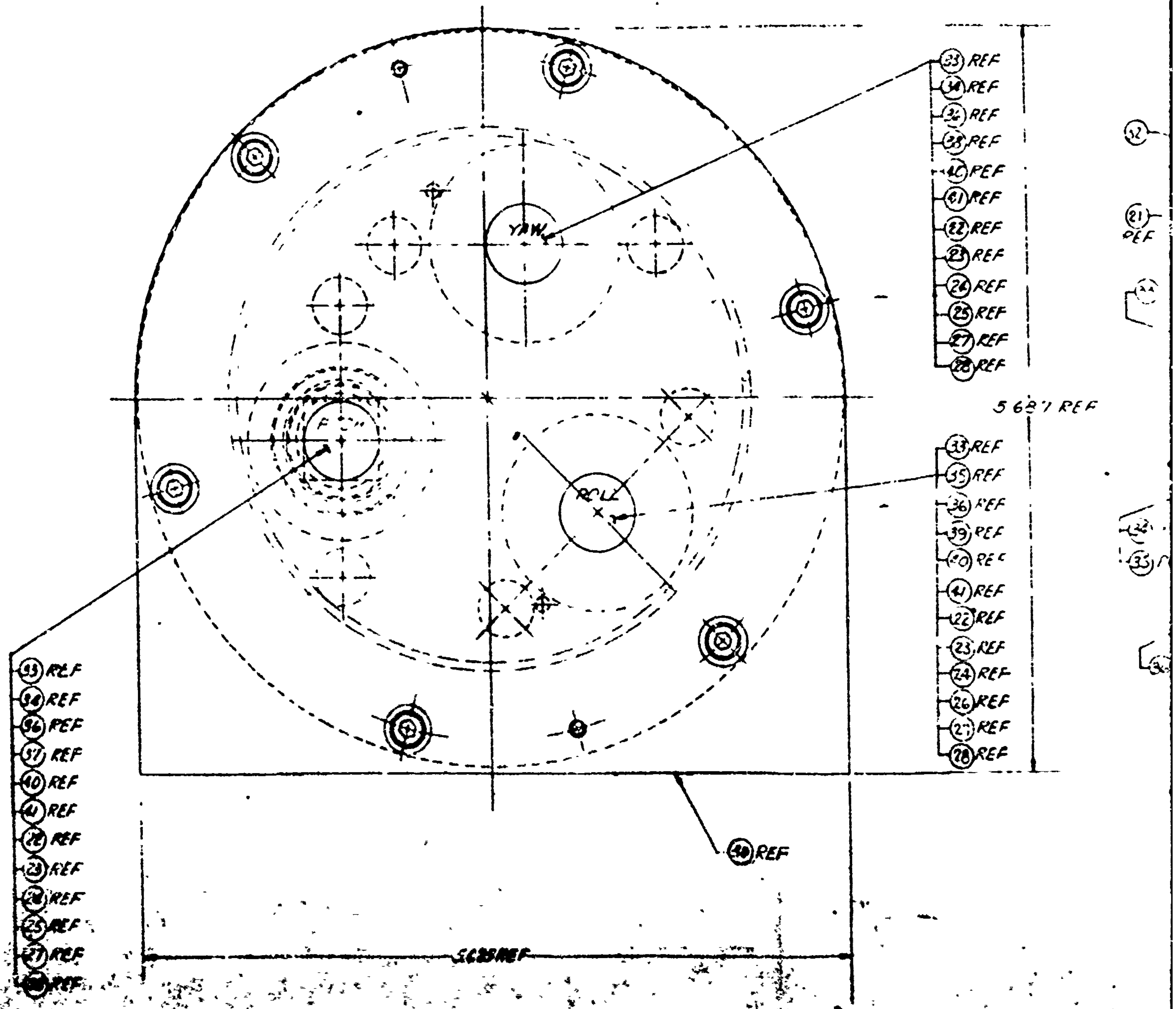
YAW
ROLL
(33) REF
(34) REF
(36) REF
(38) REF
(40) REF
(41) REF
(22) REF
(23) REF
(24) REF
(25) REF
(27) REF
(28) REF
5 687 REF
(33) REF
(35) REF
(36) REF
(39) REF
(40) REF
(41) REF
(22) REF
(23) REF
(24) REF
(26) REF
(27) REF
(28) REF
(93) REF
(94) REF
(96) REF
(97) REF
(40) REF
(41) REF
(22) REF
(23) REF
(24) REF
(25) REF
(27) REF
REF
(90) REF
5.628 REF
(32)
(21) REF

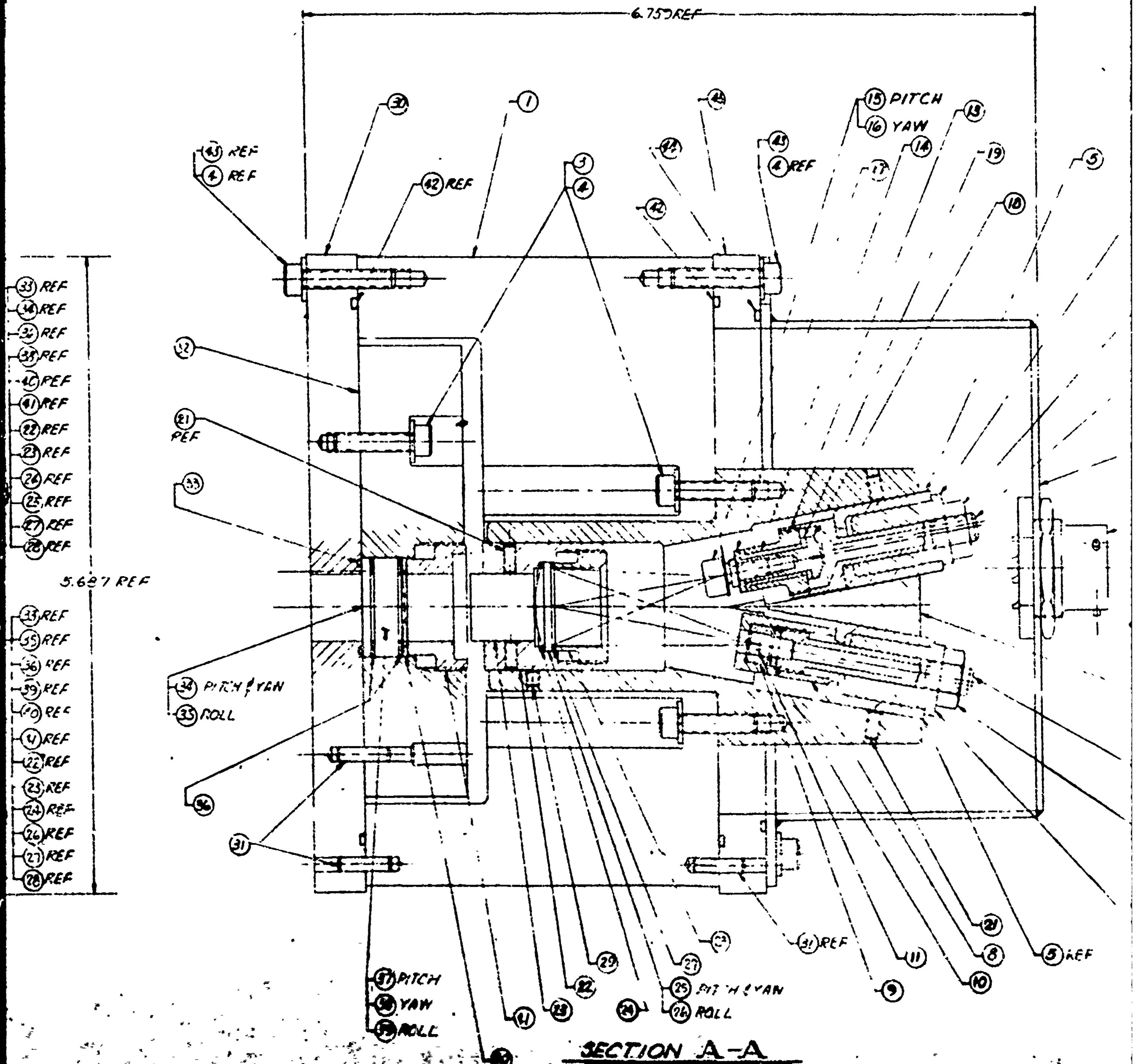
6.750 REF
5.687 REF
30
1
44
15 PITCH
16 YAW
13
43 REF
4 REF
42 REF
5
4
41
42
43
4 REF
17
14
19
18
5
33 REF
34 REF
36 REF
38 REF
40 REF
41 REF
22 REF
23 REF
24 REF
25 REF
27 REF
28 REF
32
21 REF
33
33 REF
35 REF
36 REF
39 REF
40 REF
4 REF
22 REF
23 REF
24 REF
26 REF
27 REF
28 REF
34 PITCH & YAW
35 ROLL
36
31
37 PITCH
38 YAW
39 ROLL
41
23
22
29
24
25 PITCH & YAW
26 ROLL
27
20
31 REF
9
11
10
8
21
5 REF

SECTION A-A

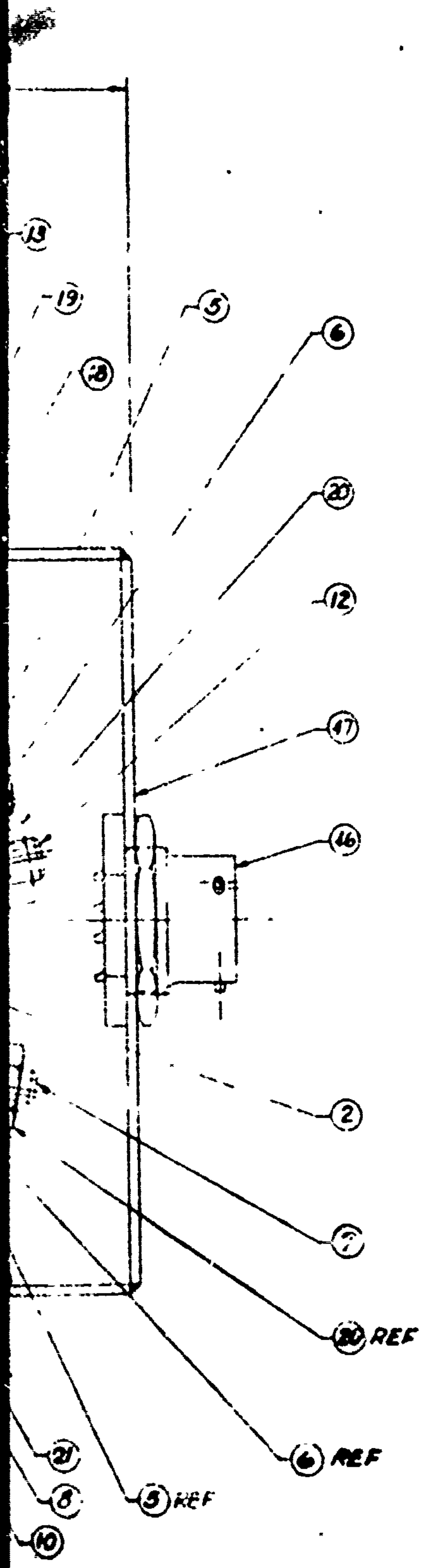

13
19
5
6
18
20
12
17
16
2
7
20 REF
6 REF
21
8
5 REF
10

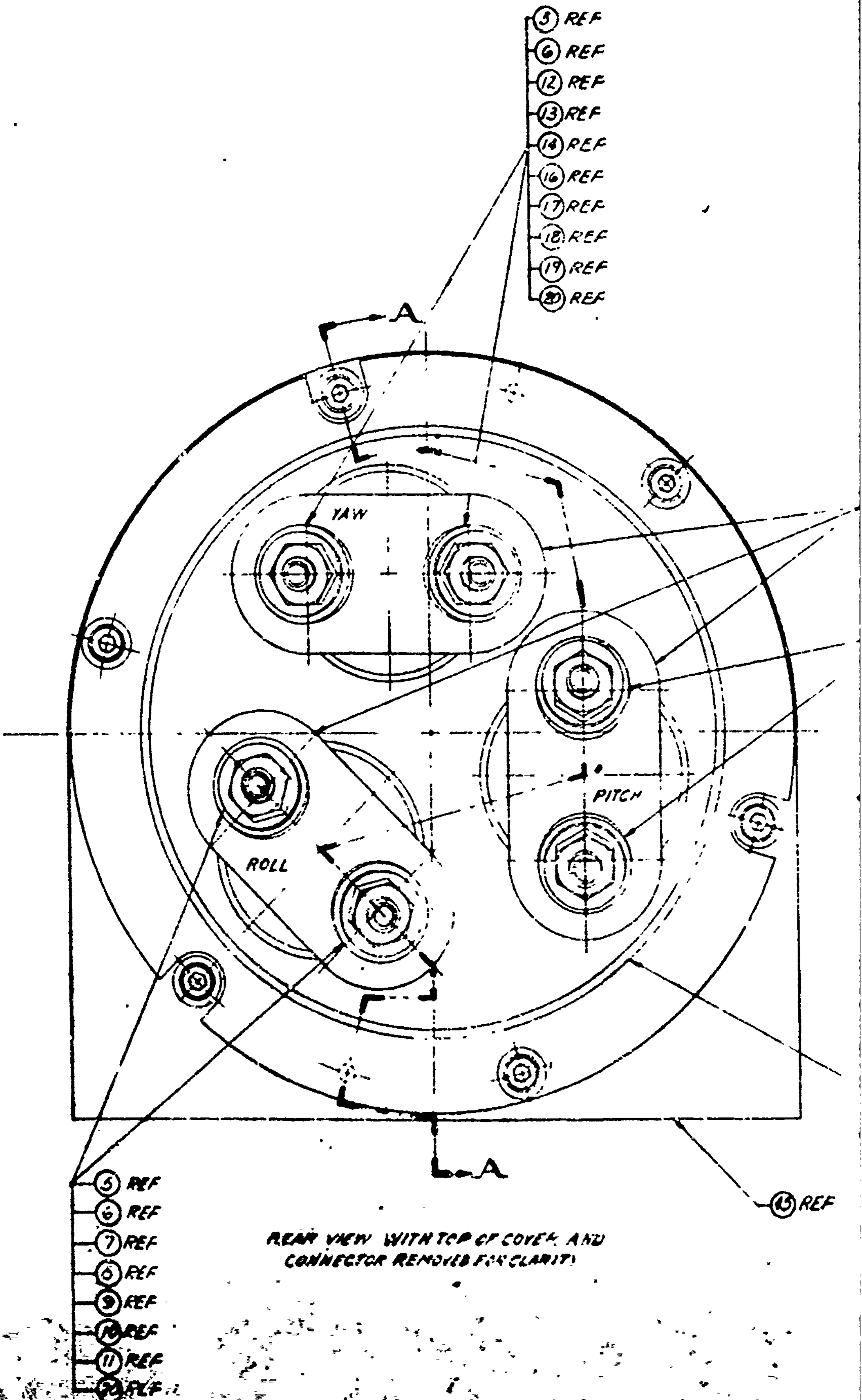

5 REF
6 REF
12 REF
13 REF
14 REF
16 REF
17 REF
18 REF
19 REF
20 REF
A
YAW
ROLL
PITCH
A
15 REF
5 REF
6 REF
7 REF
8 REF
9 REF
10 REF
11 REF
22 REF

REAR VIEW WITH TOP OF COVER AND CONNECTOR REMOVED FOR CLARITY

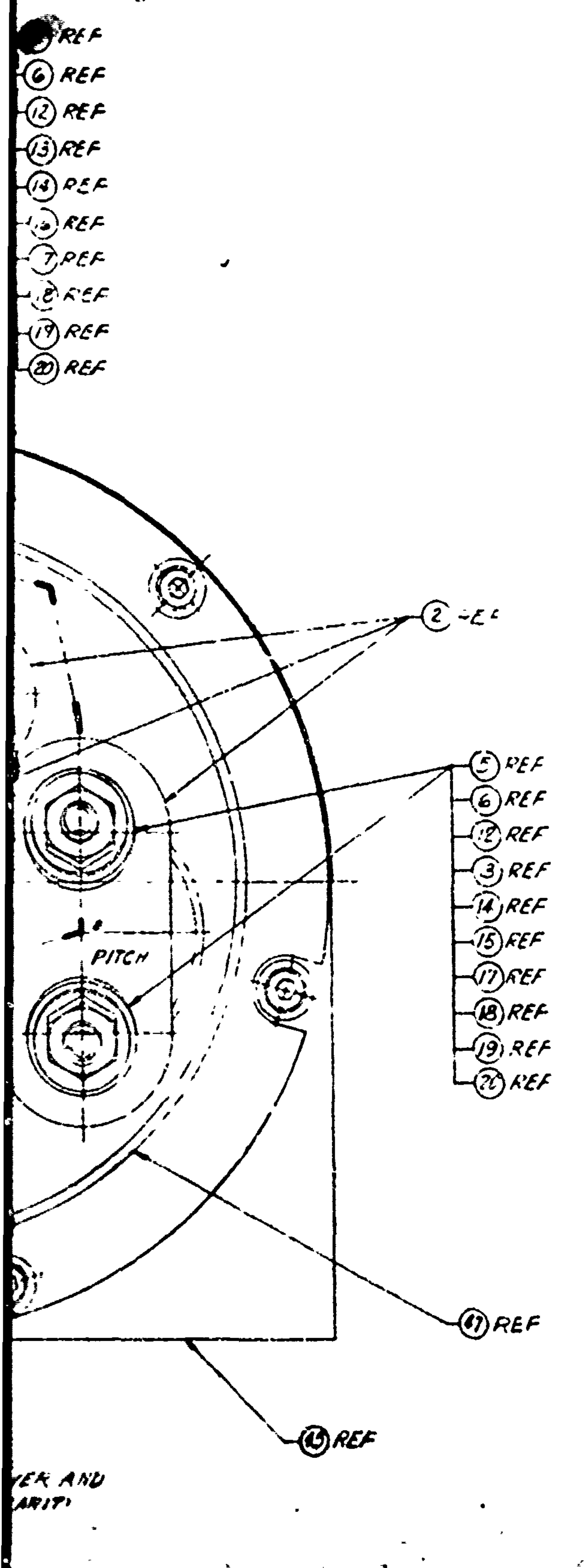

[illegible]					NEXT ASSY NUMBER SKC835
PARTS LIST					
ITEM NO.	QTY REQD	SUB ASSY	PART NUMBER	DESCRIPTION.	REMARKS
1	1	—	SKC 828	HOUSING-TRANSMITTER	
2	3	—	SKC 785	HOUSING	
3	9	—	#8-32UNC-2A×.35	SOCKET HD CAP SCREW	MATL: STAINLESS STEEL
4	21	—	#8 NARROW	WASHER-TYPE B PLAIN	
5	6	—	SKC 798	BUSHING	
6	6	—	SKC 793	ECCENTRIC	
7	2	—	SKC 794	SHAFT	
8	2	—	SKC 795	L.E.D. HOLDER	
9	2	—	SKC 797	INSULATOR-SLEEVE	
10	2	—	SKC 796	INSULATOR-WASHER	
11	2	—	SL1162-3	L.E.D.-ROLL	TEXAS INSTRUMENT
12	4	—	SKC 787	SHAFT	
13	4	—	SKC 791	L.E.D.-HOLDER	
14	4	—	SKC 789	INSULATOR-BUSHING	
15	2	—	SLH-19	L.E.D.-PITCH	TEXAS INSTRUMENT
16	2	—	SLH-20	L.E.D.-YAW	" "
17	4	—	SKC 792	WASHER	
18	4	—	SKC 788	NUT L.E.D.	
19	4	—	SKC 790	INSULATOR-WASHER	
20	6	—	250-28 UNF-2A	NUT	
21	30	—	#4-40UNC-2A×.25	HEX-SOCKET SET SCREW	MATL: STAINLESS STEEL
22	3	—	SKC 786	HOLDER-WOLLASTON LENS	
23	3	—	15MM SQ. 20°	WOLLASTON PRISM POLARIZER	K. LAMBRECHT
24	3	—	SKC 800	WASHER BEVEL	
25	2	—	01LPX081	LENS-PLANO CONVEX	OPTICAL INDUSTRIES INC.
26	1	—	01LPX107	LENS-PLANO CONVEX	" " "
27	3	—	SKC 799	WASHER PLAIN	
28	3	—	SKC 801	NUT	
29	9	—	#4-40 UNC-2A×.125	HEX-SOCKET SET SCREW	
30	1	—	SKC 819	PLATE-FRONT	
31	6	—	.25 DIA × .500	DOWEL	MATL: CRES
32	1	—	SKC 816	PLATE-ASSY ¼ WAVE PL MTG	
33	3	—	5-181	"O" RING	PARKER SEAL CO.
34	2	—	22.2 MM DIA	ANGLE SENSING CRYSTAL	K. LAMBRECHT
35	1	—	22.2 MM DIA	PLATE WINDOW	BLOOMER RESEARCH
36	6	—	SKC 812	WASHER-PLAIN	
37	1	—	22.2 MM DIA [illegible]	¼ WAVE PLATE - YAW	K. LAMBRECHT
38	1	—	22.2 MM DIA [illegible]	¼ WAVE PLATE - PITCH	K. LAMBRECHT
39	1	—	SKC 820	SPACER-ROLL	
40	3	—	3306-35-1	WAVE WASHER	SEASTORM MFG. Co. INC.
41	3	—	SKC [illegible]	NUT-ASSY ¼ WAVE PL MTG	
42	2	—	2-046	"O" RING	PARKER SEAL CO.
43	12	—	#8-32 UNC-2A×.75	SOCKET HD CAP SCREW	
44	1	—	2-247	"O" RING	PARKER SEAL CO.
45	1	—	SKC 827	PLATE-TRANSMITTER [illegible]	
46	1	—	UT07C-12-10P	CONNECTOR	BENDIX CORP.
47	1	—	SKC 822	COVER-TRANSMITTER END	

FIG. 6.3-2

TRANSMITTER,
[illegible]

21

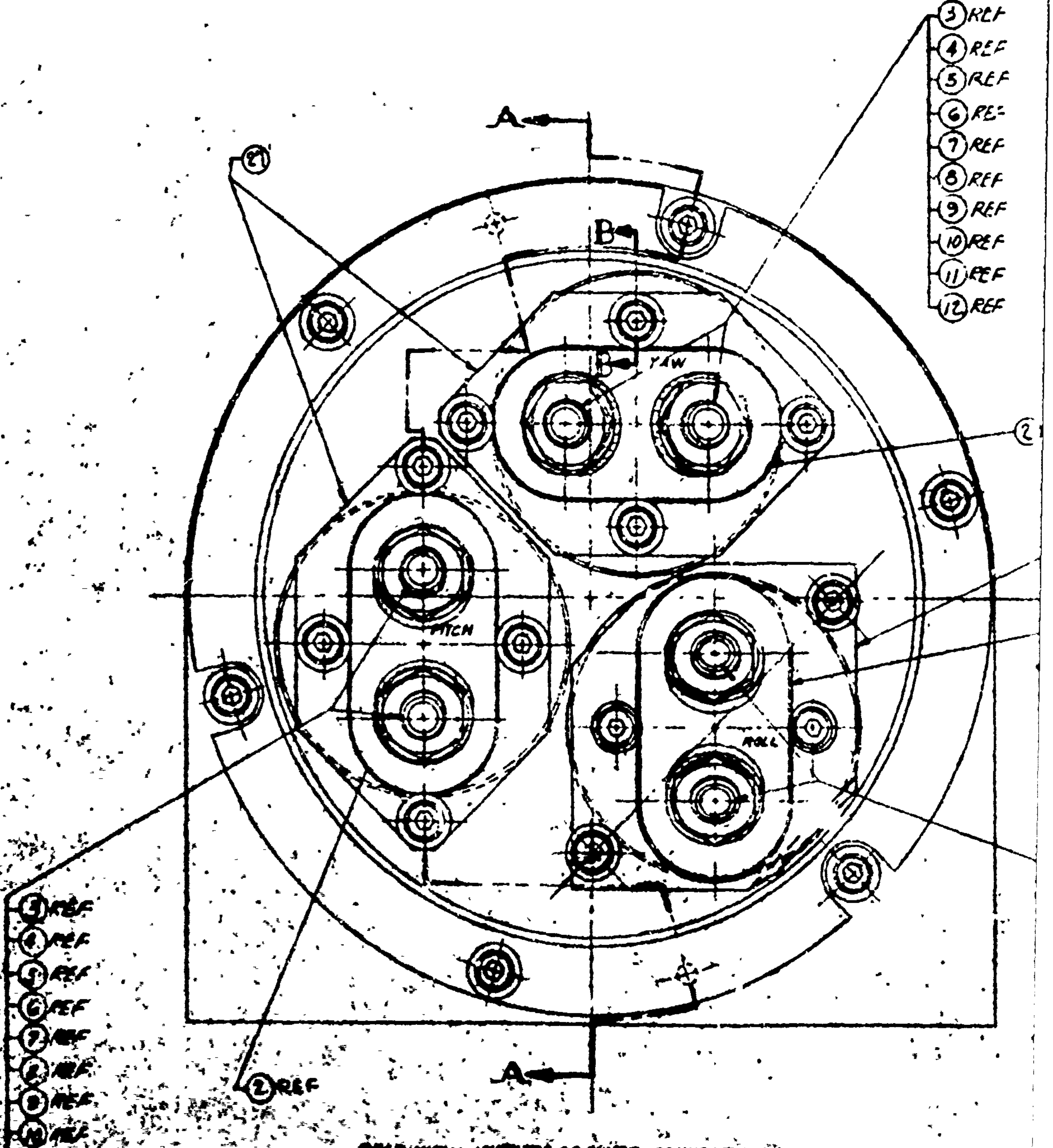
③ REF
④ REF
⑤ REF
⑥ REF
⑦ REF
⑧ REF
⑨ REF
⑩ REF
⑪ REF
⑫ REF
A
27
B
B
YAW
②
PITCH
ROLL
③ REF
④ REF
⑤ REF
⑥ REF
⑦ REF
⑧ REF
⑨ REF
⑩ REF
⑪ REF
⑫ REF
② REF
A

REAR VIEW WITH TOP OF COVER, CONNECTOR AND ELECTRONIC COMPONENT BOARD REMOVED FOR CLARITY

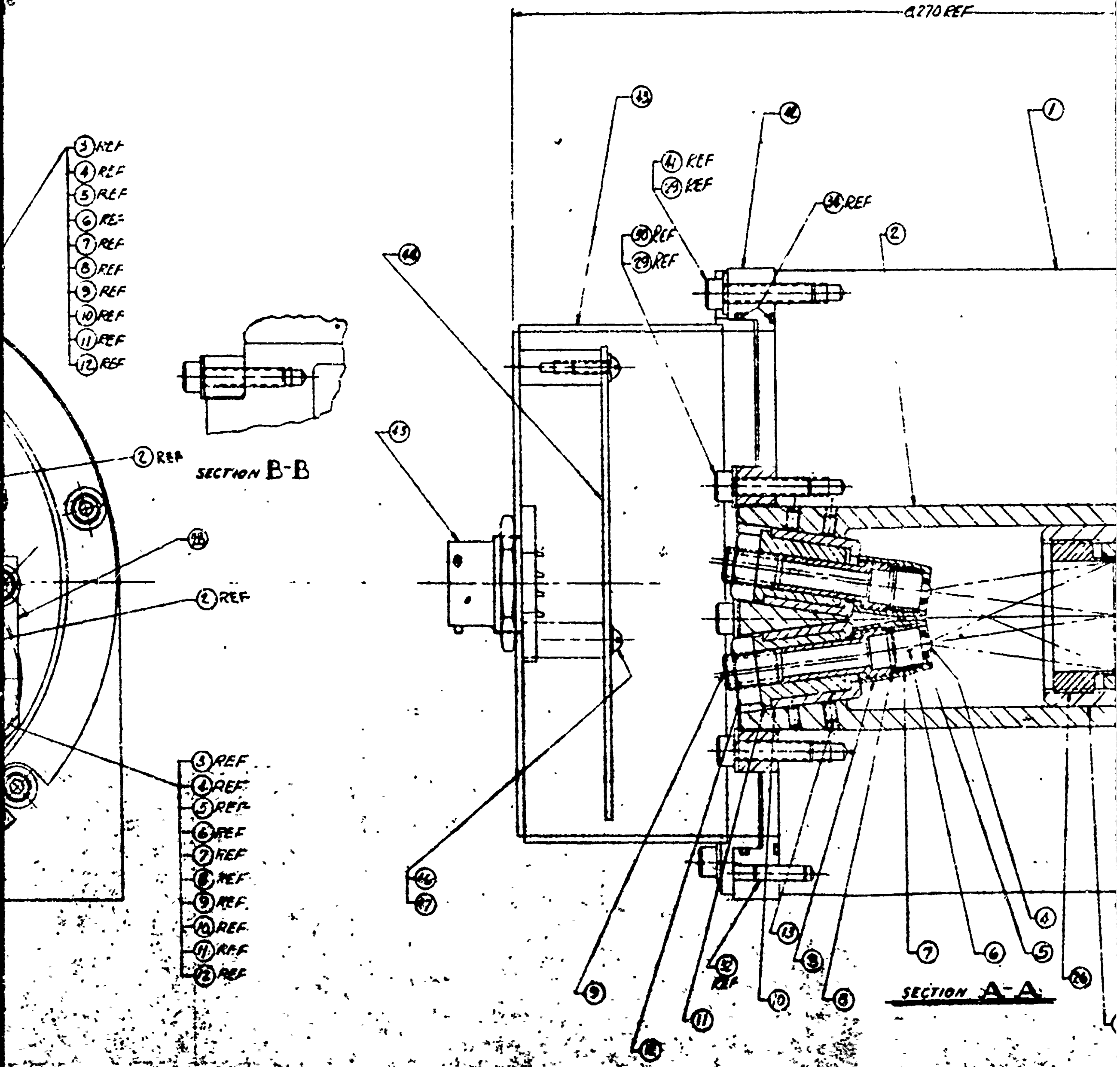2.270 REF
③ REF
④ REF
⑤ REF
⑥ REF
⑦ REF
⑧ REF
⑨ REF
⑩ REF
⑪ REF
⑫ REF
② REF
SECTION B-B
㉘
② REF
③ REF
④ REF
⑤ REF
⑥ REF
⑦ REF
⑧ REF
⑨ REF
⑩ REF
⑪ REF
⑫ REF
㊸
㊹
㊺
㊻
㊼
㊶ REF
㉙ REF
㉚ REF
㉙ REF
㉞ REF
㊷
②
①
⑨
⑱
⑪
㉜ REF
⑩
⑬
⑧
⑦
⑥
⑤
④
㉖
SECTION A-A

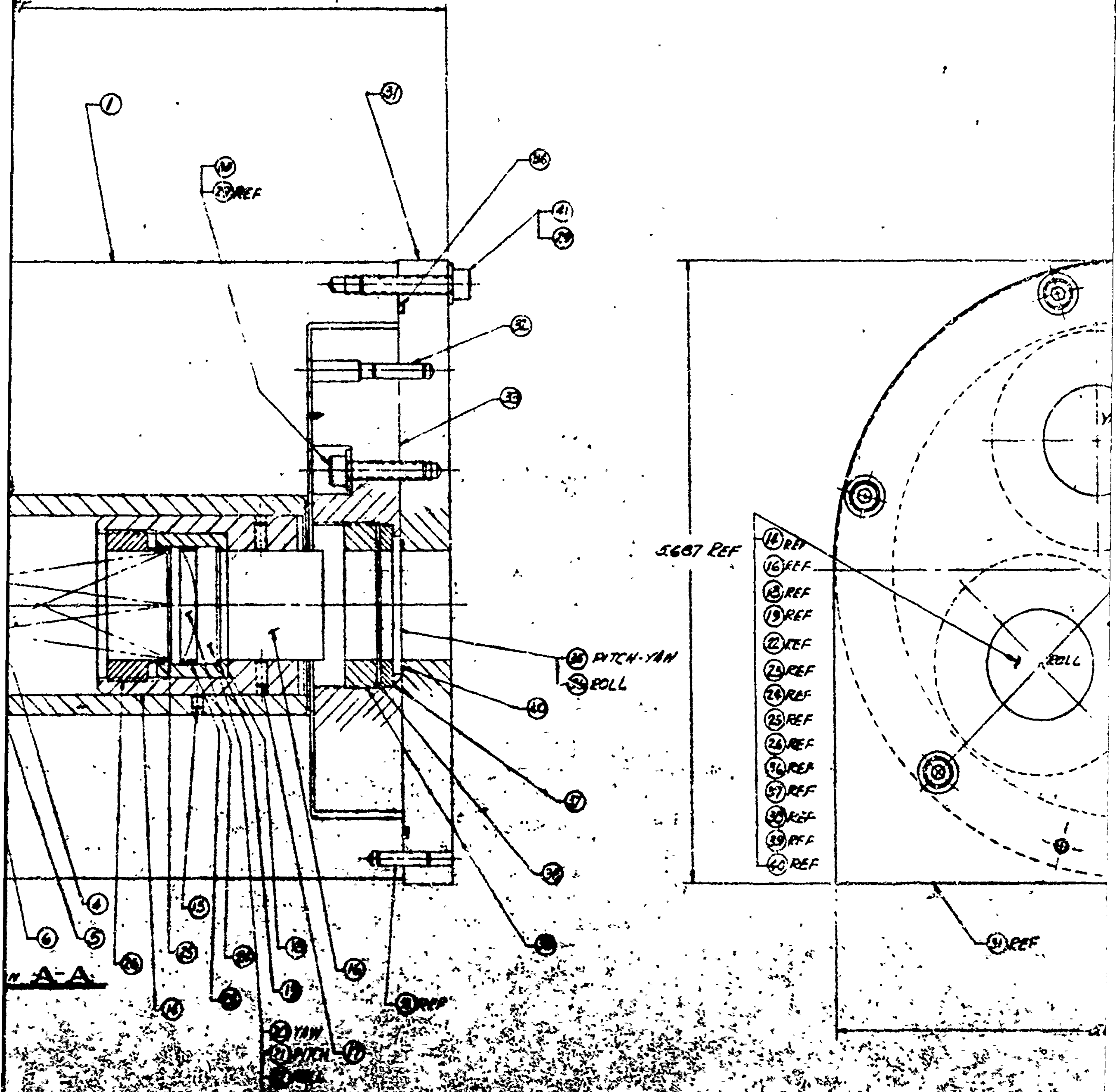
1
31
14
27 REF
36
41
29
32
33
36 PITCH-YAW
ROLL
40
17
34
5.687 REF
14 REF
16 REF
18 REF
19 REF
22 REF
23 REF
24 REF
25 REF
26 REF
36 REF
37 REF
38 REF
39 REF
40 REF
YAW
ROLL
31 REF
4
15
6
5
25
18
11
16
22 YAW
21 PITCH
ROLL
REF

N A-A

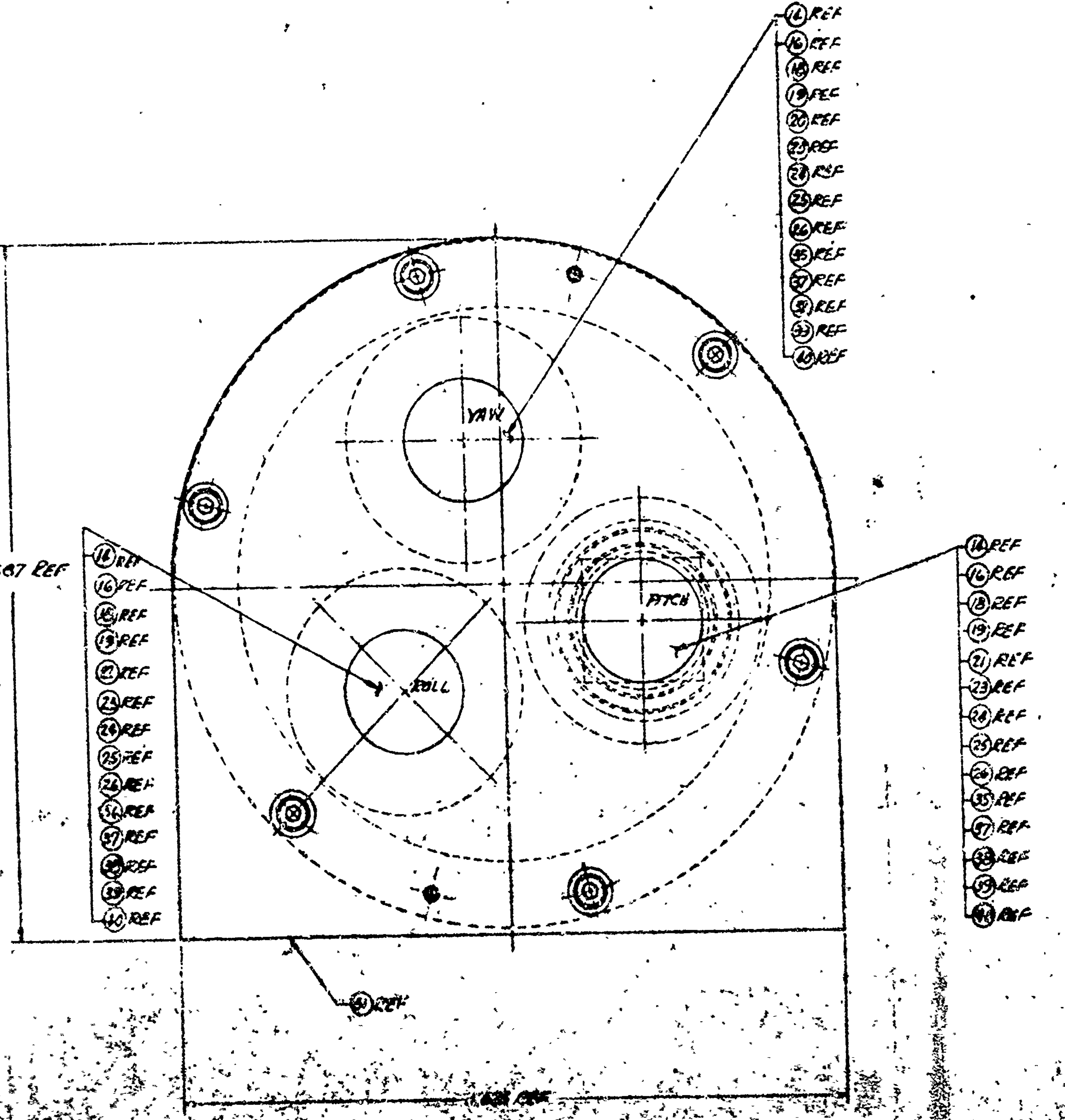

YAW
PITCH
ROLL
14 REF
16 REF
18 REF
19 REF
20 REF
23 REF
24 REF
25 REF
26 REF
35 REF
37 REF
38 REF
39 REF
40 REF
14 REF
16 REF
18 REF
19 REF
21 REF
23 REF
24 REF
25 REF
26 REF
35 REF
37 REF
38 REF
39 REF
40 REF
87 REF
14 REF
16 REF
18 REF
19 REF
22 REF
23 REF
24 REF
25 REF
26 REF
36 REF
37 REF
38 REF
39 REF
40 REF
30 REF

REVISION

ITEM NO.	QUTY REQD	S/A ASSY
1	1	—
2	3	—
3	6	—
4	6	—
5	6	—
6	6	—
7	6	—
8	6	—
9	6	—
10	6	—
11	6	—
12	6	—
13	12	—
14	3	—
15	9	—
16	3	—
17	12	—
18	3	—
19	3	—
20	1	—
21	1	—
22	1	—
23	3	—
24	3	—
25	3	—
26	3	—
27	2	—
28	1	—
29	27	—
30	15	—
31	1	—
32	6	—
33	1	—
34	2	—
35	2	—
36	1	—
37	3	—
38	3	—
39	3	—
40	3	—
41	12	—
42	1	—
43	1	—
44	1	—
45	1	—
46	3	—
47	3	—

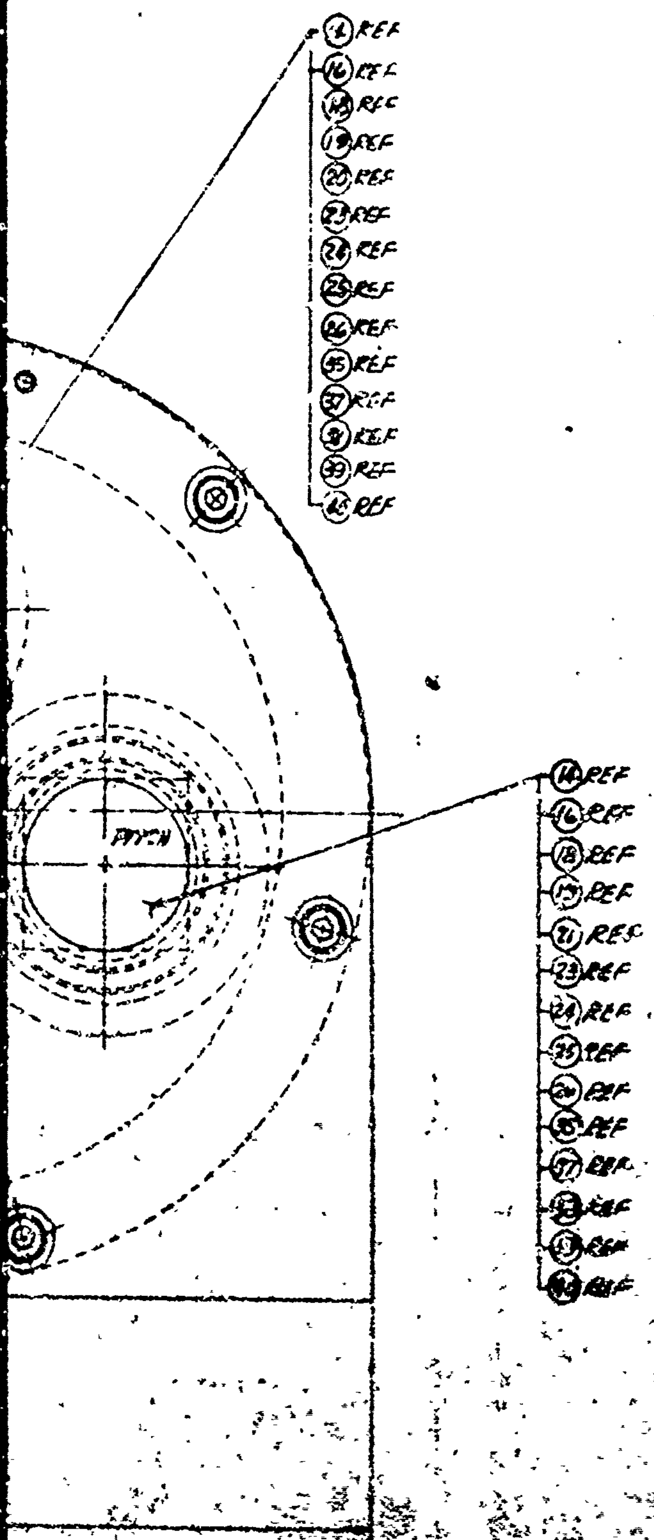

REVISION

NEXT ASSY. NUMBER SKC835

PARTS LIST

ITEM NO.	QUAN. REQD	SUB ASSY	PART NUMBER	DESCRIPTION	REMARKS
1	1	—	SKC826	HOUSING-RECEIVER	
2	1	—	SKC814	HOUSING-DETECTOR	
3	6	—	SKC802	HOLDER-DETECTOR	
4	6	—	[illegible]	IMMERSION LENS	BLOOMER RESEARCH CORP.
5	6	—	SKC832	RING-DETECTOR LENS MTG.	
6	6	—	UDT PIN/SCP	DETECTOR	(RCA)
7	6	—	SKC807	INSULATOR-BUSHING	
8	6	—	SKC806	INSULATOR-WASHER	
9	6	—	SKC803	SHAFT	
10	6	—	SKC804	BUSHING	
11	6	—	SKC805	ECCENTRIC	
12	6	—	5/16-24UNF-2A	NUT	MAT'L: STAINLESS STEEL
13	12	—	#4-40UNC-2A x .375	HEX SOCKET HD SET SCREW	MAT'L: STAINLESS STEEL
14	3	—	SKC813	HOLDER-LENS [illegible]	
15	3	—	#4-40UNC-2A x .125	HEX SOCKET HD SET SCREW	MAT'L: STAINLESS STEEL
16	3	—	25MM 5915	WOLLASTON PRISM POLARIZER	K. LAMBRECHT
17	12	—	#4-40UNC-2A x .250	HEX SOCKET HD SET SCREW	
18	3	—	SKC811	CUP-LENS & FILTER	
19	3	—	SKC808	WASHER-LOWER	
20	1	—	[illegible] 8533	FILTER-YAW CHANNEL	
21	1	—	7950	FILTER-PITCH CHANNEL	
22	1	—	7630	FILTER-ROLL CHANNEL	
23	3	—	SKC810	SPACER	
24	3	—	01LPX10A	LENS-PLANO CONVEX	OPTICAL INDUSTRIES INC.
25	3	—	SKC809	WASHER-UPPER	
26	3	—	SKC812	NUT-LENS HOLDDOWN	
27	2	—	SKC815	FLANGE-DETECTOR HOUSING	
28	1	—	SKC816	FLANGE-DETECTOR HOUSING	
29	27	—	#6 NARROW	WASHER-TYPE B FLAT	
30	15	—	#6-32UNC-2A x .750	SOC HD CAP SCREW	MAT'L: STAINLESS STEEL
31	1	—	SKC824	PLATE-RECEIVER FRONT	
32	6	—	.125 DIA x 1.500	DOWEL	MAT'L: CRES
33	1	—	SKC823	PLATE-ASS'Y WINDOW MTG.	
34	9	—	5-140	'O' RING	PARKER SEAL Co.
35	2	—	1.250 DIA	CRYSTAL [illegible]	K. LAMBRECHT
36	1	—	1.550 DIA.	PLANE WINDOW - ROLL	BLOOMER RESEARCH [illegible]
37	3	—	SKC821	SPACER	
38	3	—	3826-71-1	WAVE WASHER	[illegible] MFG. CO. INC.
39	3	—	SKC822	NUT-RING	
40	3	—	2-043	'O' RING	PARKER SEAL Co.
41	12	—	#4-40UNC-2A x .875	SOC. HD. CAP SCREW	MAT'L: STAINLESS STL.
42	1	—	SKC829	PLATE-RECEIVER REAR	
43	1	—	SKC830	COVER-RECEIVER END	
44	1	—	SKC831	COMPONENT BOARD	
45	1	—	[illegible]PC-12-10P	CONNECTOR	BENDIX CORP.
46	9	—	#4 NARROW	WASHER-TYPE B FLAT	
47	3	—	[illegible]	ROUND HD CAP SCREW	MAT'L: STAINLESS STEEL

that is applied to the complete assembly through the wave spring washer allows the angle sensing crystal to bottom onto the lapped surface of the main housing. This pre-assembled unit is positioned in the main housing and locked in position with screws, using dowel pins as guides, against the back face of the main housing. The Wollaston, collimating lens and light source are a pre-aligned assembly unit and are positioned in the main housing by pressure from a wave spring washer and a lock ring. The angle sensing crystal is also held in position by the load applied by the wave spring washer and the front mounting plate. One of the assemblies, with its angle sensing crystal and quarter wave plate, is used for each of the lateral axes (see figure 6.3-2). This assembly has provision to align the Wollaston prism, collimating lens and the light emitting diodes (LEDs). This mechanical adjustment is required to allow for tolerances in the Wollaston divergence angle (off-the-shelf Wollaston have ± 2° tolerance on divergence angles). The adjustments for the Wollaston prism are line of sight positioning and roll. The LED and its collimating lens have mechanical movement adjustments relative to each other. The collimating lens is used as the fixed reference, and the LED can be adjusted along the line of sight for focusing the collimating lens on the light emitting area in the LED. The light emitting area is not necessarily equally spaced around the mechanical center line; to adjust for this the LED is mounted in two eccentric sleeves. This allows the LED to be rotated until the light emitting area centerline is positioned on the optical axis. When the adjustments have been completed, a sleeve and jam nut lock the assembly in position. The LEDs are mounted directly in a special sleeve that will allow the heat generated to be conducted away to the main housing.

6.3.3 Receiver Design

The main receiver housing is bored out from a one piece block of aluminum, into which the angle sensing crystals are hard mounted for the three channels (figure 6.3-2). The shoulder for the angle sensing crystal is machined and lapped to 8 - 12 micro inches; into this shoulder is the "O" ring groove which allows the compression of the "O" ring to completely fill the volume of the groove when the angle sensing crystal bottoms on the housing shoulder. This sub-assembly is clamped together by a threaded lock ring. This complete assembly is backed-up by a wave spring washer. The amount of compression that is applied to the complete assembly, through the wave spring washer to allow the angle sensing crystal to bottom onto the lapped surface of the main housing, is provided by the housing of the sub-assembly holding the Wollaston prism, objectives lens, field stop, and detection and its field lens. This pre-assembled unit is positioned in the main housing. It is locked in position with screws, using dowel pins as guides, against the back face of the main housing. The wave spring washer is compressed to give the angle sensing crystal the hard mounting against the lapped surface. One of these assemblies with its angle sensing crystal is used for each of the lateral axes; see figure 6.3-3. The assembly has provision to align the prism with its objective lens to the detector and its field lens. This mechanical adjustment is required to allow for tolerances in the prism divergence angle (off-the-shelf Wollaston prisms have ± 2° tolerance on divergence angles). The adjustments for the Wollaston prism and its objective lens are axial and roll.

The detector and its field lens have mechanical adjustments for movement relative to each other. The field lens is used as the fixed reference, and the detector can be adjusted along the line of sight for focusing the field lens on the active area of the detector. The active area is not necessarily equally spaced around the mechanical center line. To adjust for this the detector is mounted in two eccentric sleeves. This allows the detector to be rotated until the active area center line is positioned on the optical axis. When the adjustments have been completed, a sleeve and jam nut lock the assembly in position.

7.0 FLIGHT MODEL DESIGN

7.1 FLIGHT MODEL ELECTRONIC DESIGN

The electronic circuits for the flight model OAMS will be the same as for the advanced brassboard. Schematics are shown in Figures 6.1-2 and 6.1-3. The circuit layout and number of printed circuit cards will of course be different than shown on the schematics for the advanced brassboard. Components, to be discussed later, will be the same type with the only difference being that flight model parts will be screened to a high reliability level. The digital panel meters used for visual readout on the advanced brassboard will not be present on the flight model OAMS. The channel outputs will be available for use in analog form.

The OAMS electronic package shown in Figure 7.1-1 will contain three similar printed circuit cards, one for each channel. Mounted toward the rear or the end containing electrical connectors will be the power supply, the oscillator and an electrolytic capacitor for the power supply. Power transistors for the LED drivers are mounted on the chassis at the rear and use the package container itself for heat dissipation. A preliminary component layout for the printed circuit cards is shown on this drawing along with preliminary package components.

An assembly showing the electronic package, transmitter and receiver and connecting cables is shown in Figure 7.1-2 for a base mount and in figure 7.1-3 for a back mount. Connector identification is shown on the package.

Located in the receiver will be the detectors and their preamplifiers. This results in a reduction in noise pickup since the preamplifiers are mounted next to the detectors and also a reduction in noise pickup on the output cables due to the low output impedance of the preamplifiers. The metal container itself is a good shield for these components where it is necessary for noise to be a minimum.

All electronic components for the flight model OAMS system are either established reliability parts or where none were available they are commercial parts tested to the appropriate military specifications. The power supply and oscillator subassemblies meet also the appropriate military specifications along with their internal individual components. Specifications for the parts are given in the following subsection.

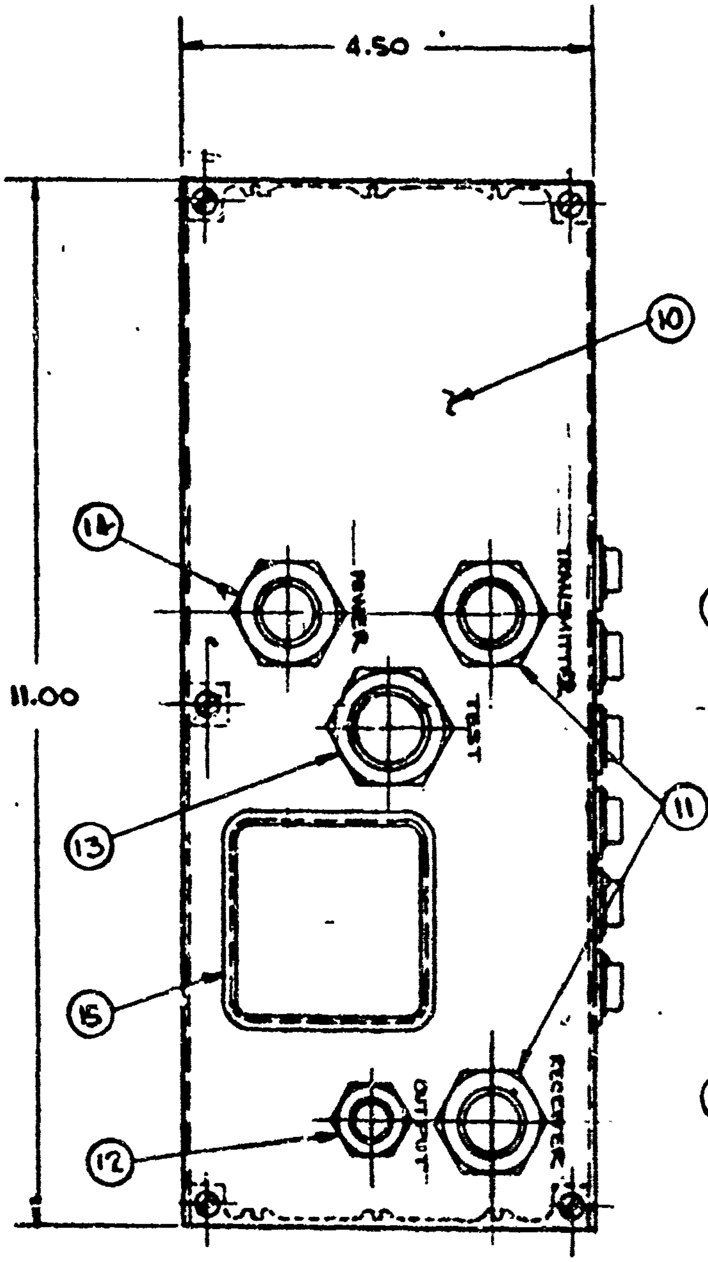
4.50
11.00
10
14
POWER
TRANSMITTER
TEST
13
15
11
OUTPUT
RECEIVER
12

VIEW A-A

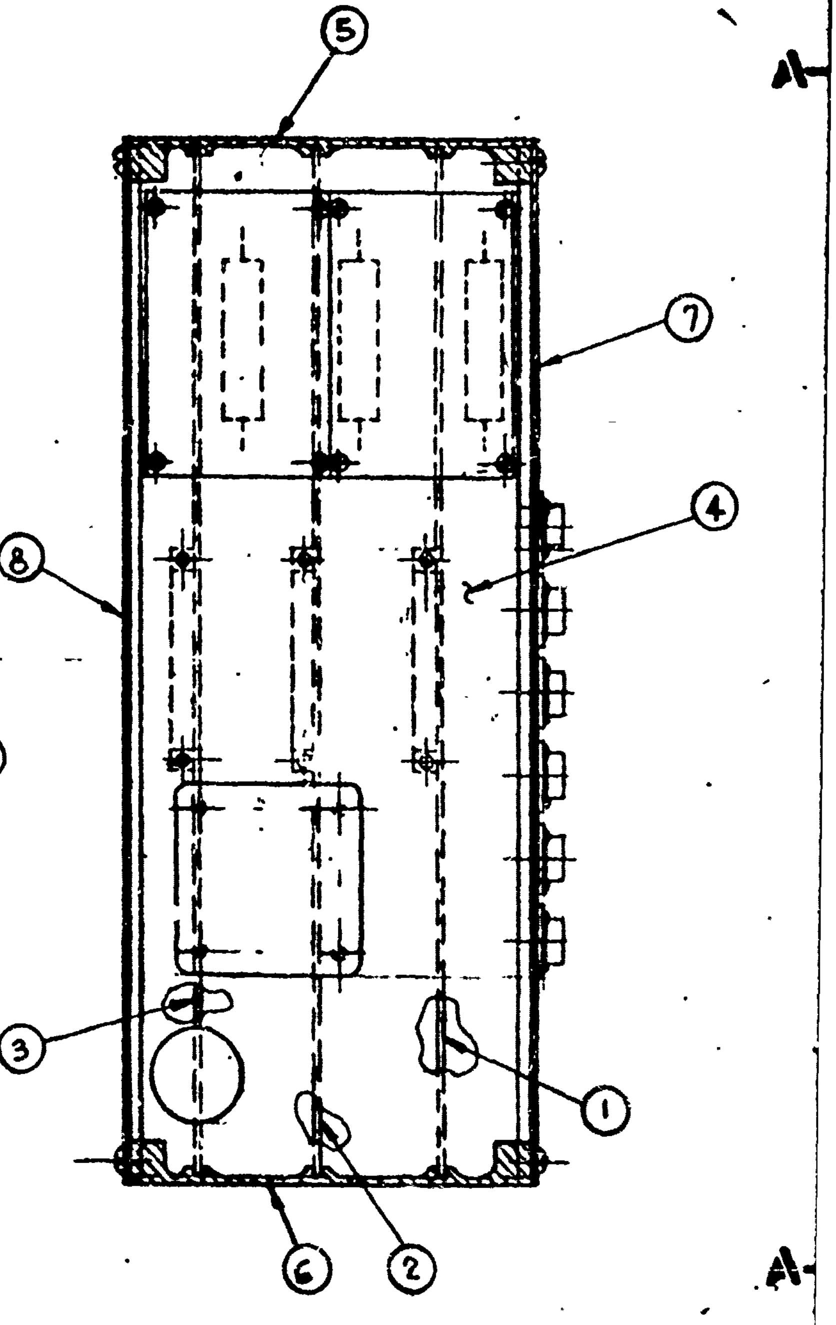
5
A-
7
4
8
3
1
6
2
A-

SECTION B-B

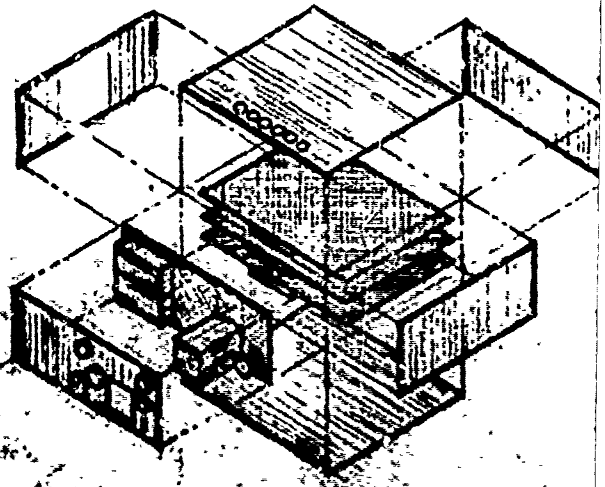

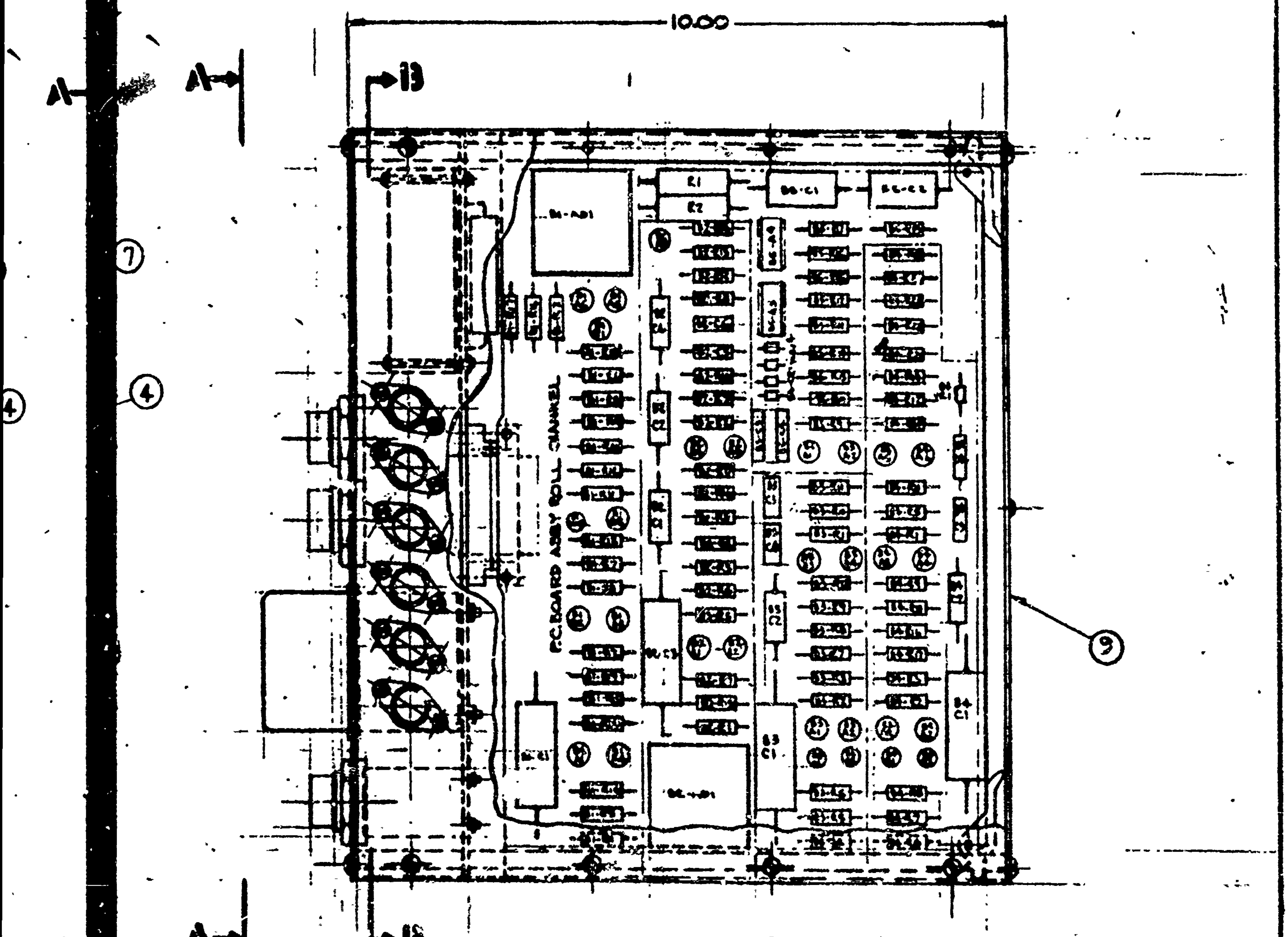

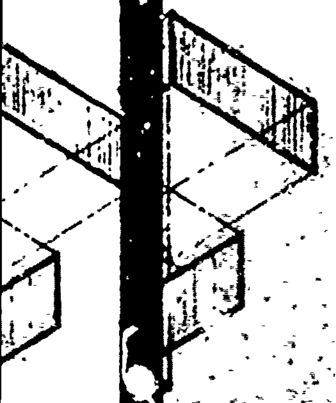

15		1	GASKET	
14	[illegible]	1	CONNECTOR - Jam Nut Receptacle	MIL-C-26482
13	[illegible]	1	CONNECTOR - " " "	MIL-C-26482
12	[illegible]	1	CONNECTOR - " " "	MIL-C-26482
11	[illegible]	2	CONNECTOR - Jam Nut Receptacle	MIL-C-26482
10		1	REAR PANEL	
9		1	FRONT PANEL	
8		1	BOTTOM PANEL	
7		1	TOP PANEL	
6		1	SIDE PANEL - LEFT	
5		1	SIDE PANEL - RIGHT	
4		1	P.C. BOARD ASSY - POWER	
3		1	P.C. BOARD ASSY - YAW CHANNEL	
2		1	P.C. BOARD ASSY - PITCH CHANNEL	
1		1	P.C. BOARD ASSY - ROLL CHANNEL	
[illegible]	PART NO.	[illegible]	DESCRIPTION	MATERIAL

BILL OF MATERIAL

FIG. 7.1-1

FLIGHT MODEL
ELELECTRONIC
PACKAGE

OMI500

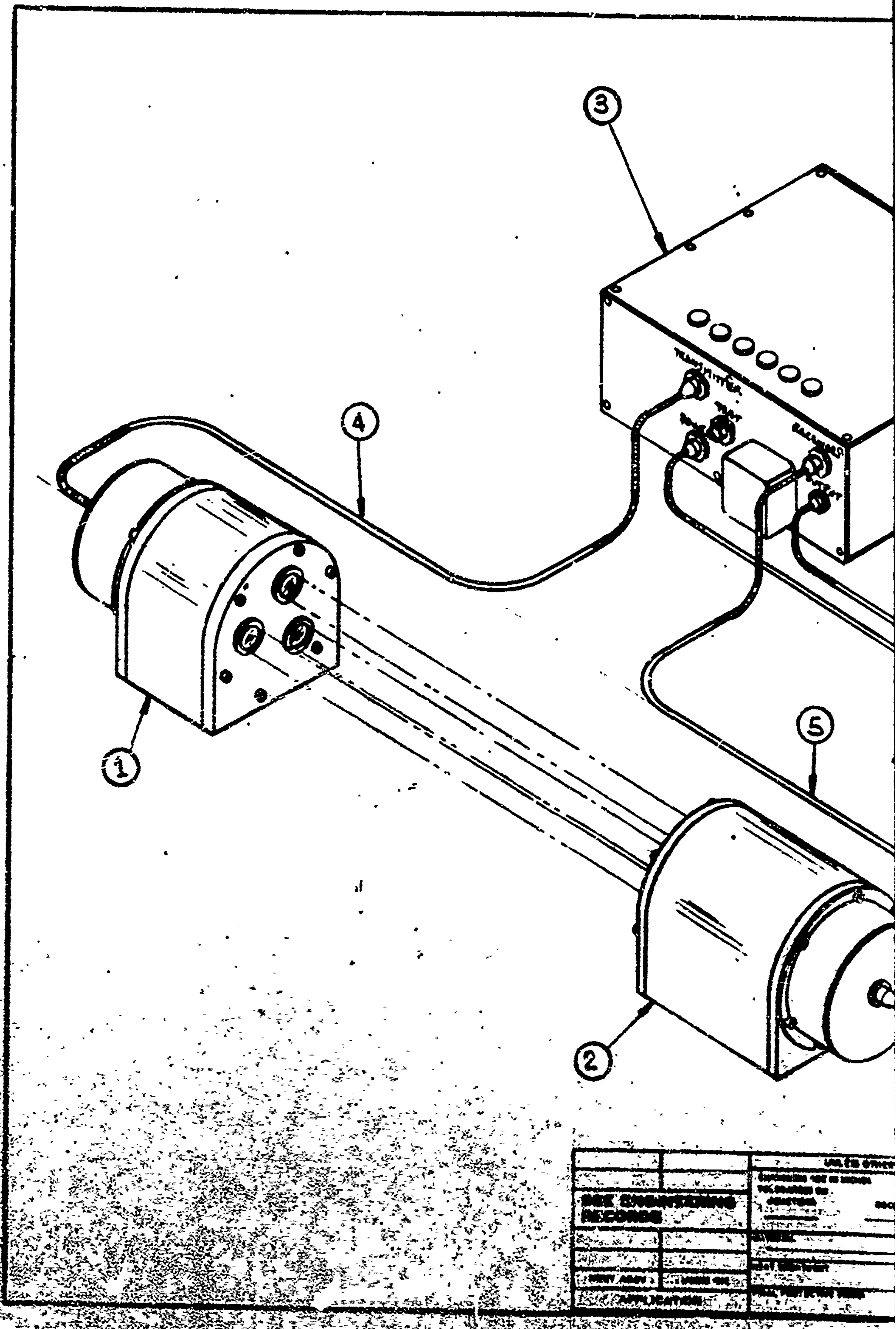
3
TRANSMITTER
TEST
4
1
5
2
SEE ENGINEERING RECORDS
NEXT ASSY
USED ON
APPLICATION

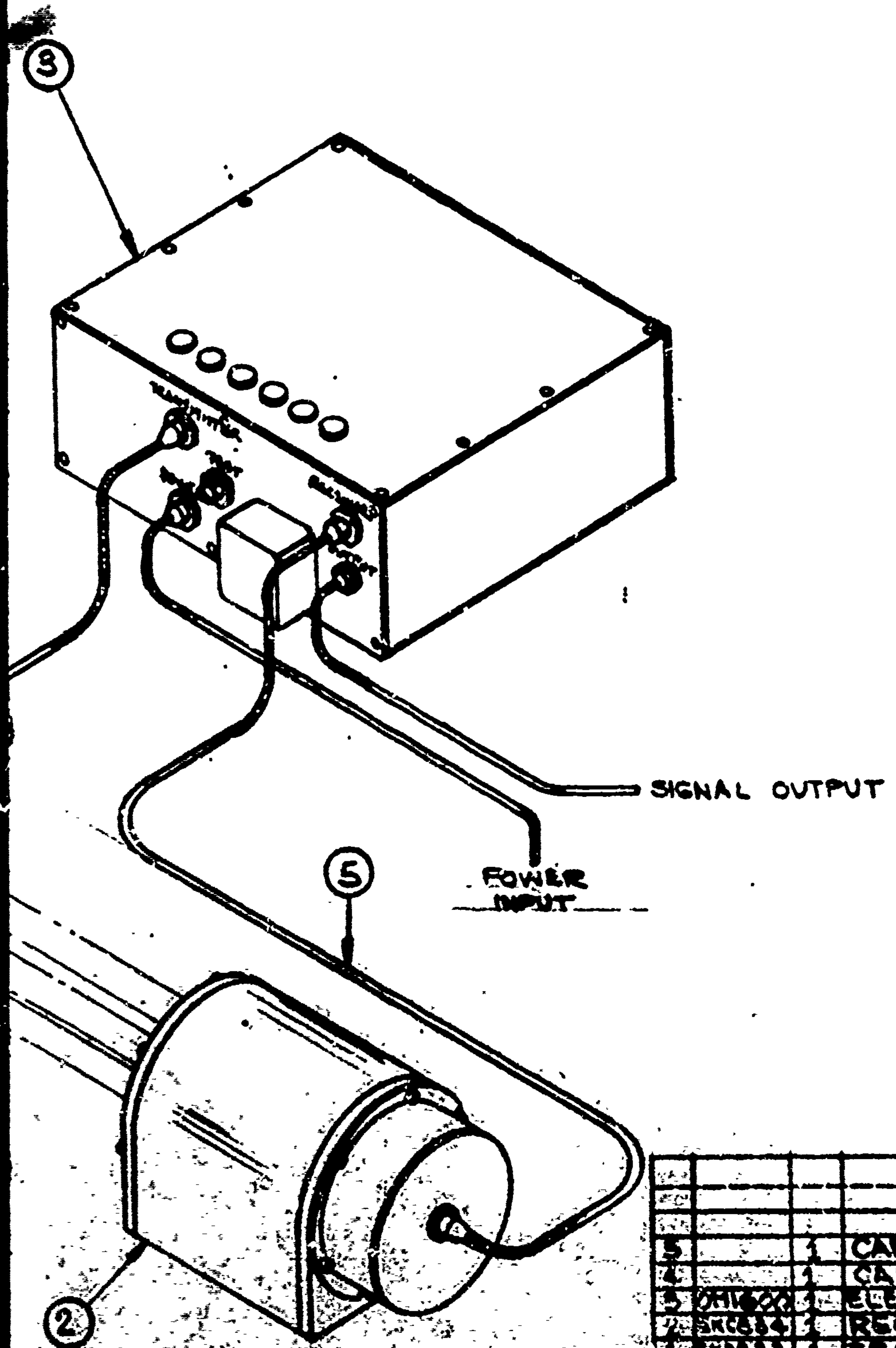
3
TRANSMITTER
TEST
RECEIVER
SIGNAL OUTPUT
POWER INPUT
5
2

	PART NO.		DESCRIPTION	MATERIAL	
5		1	CABLE - RECEIVER		
4		1	CABLE - TRANSMITTER		
3	[illegible]	1	ELECTRONICS ASSY		
2	SKC6354	1	RECEIVER ASSY		
1	SKC6353	1	TRANSMITTER ASSY		

BILL OF MATERIAL

FIG. 7.1-2

UNLESS OTHERWISE SPECIFIED

OPTICAL ANGULAR
MOTION
SENSOR
(OAMS) FLIGHT MODEL
[illegible] MOUNT

MICHOUD OPERATIONS

C 0M1001

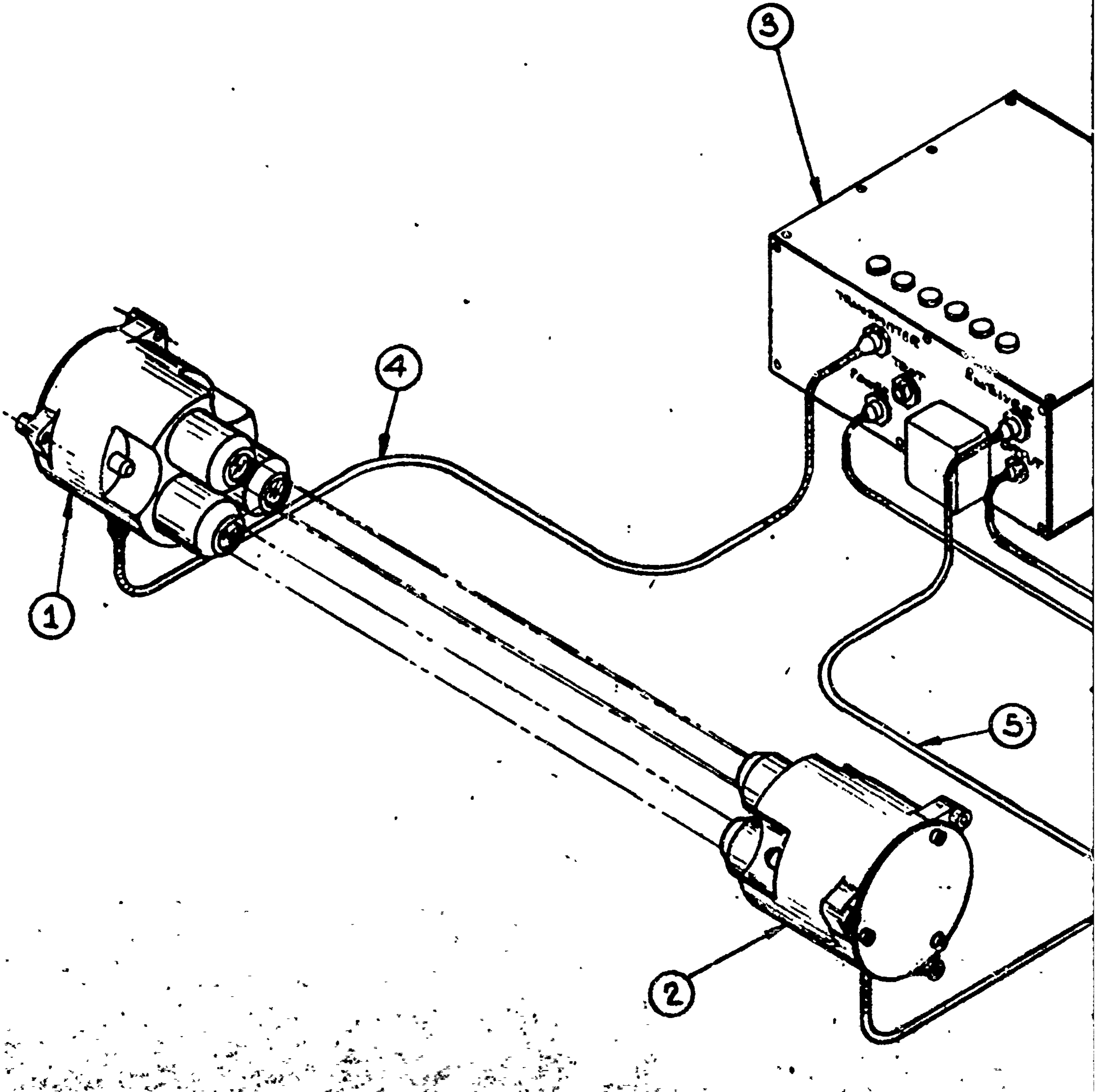
3
TRANSMITTER
TEST
RECEIVER
4
1
5
2

		[illegible]
		[illegible]
SEE ENGINEERING RECORDS		FRACTIONS DECIMALS
		[illegible]
		[illegible]
NEXT ASSY	USED ON	[illegible]
APPLICATION		[illegible]

2

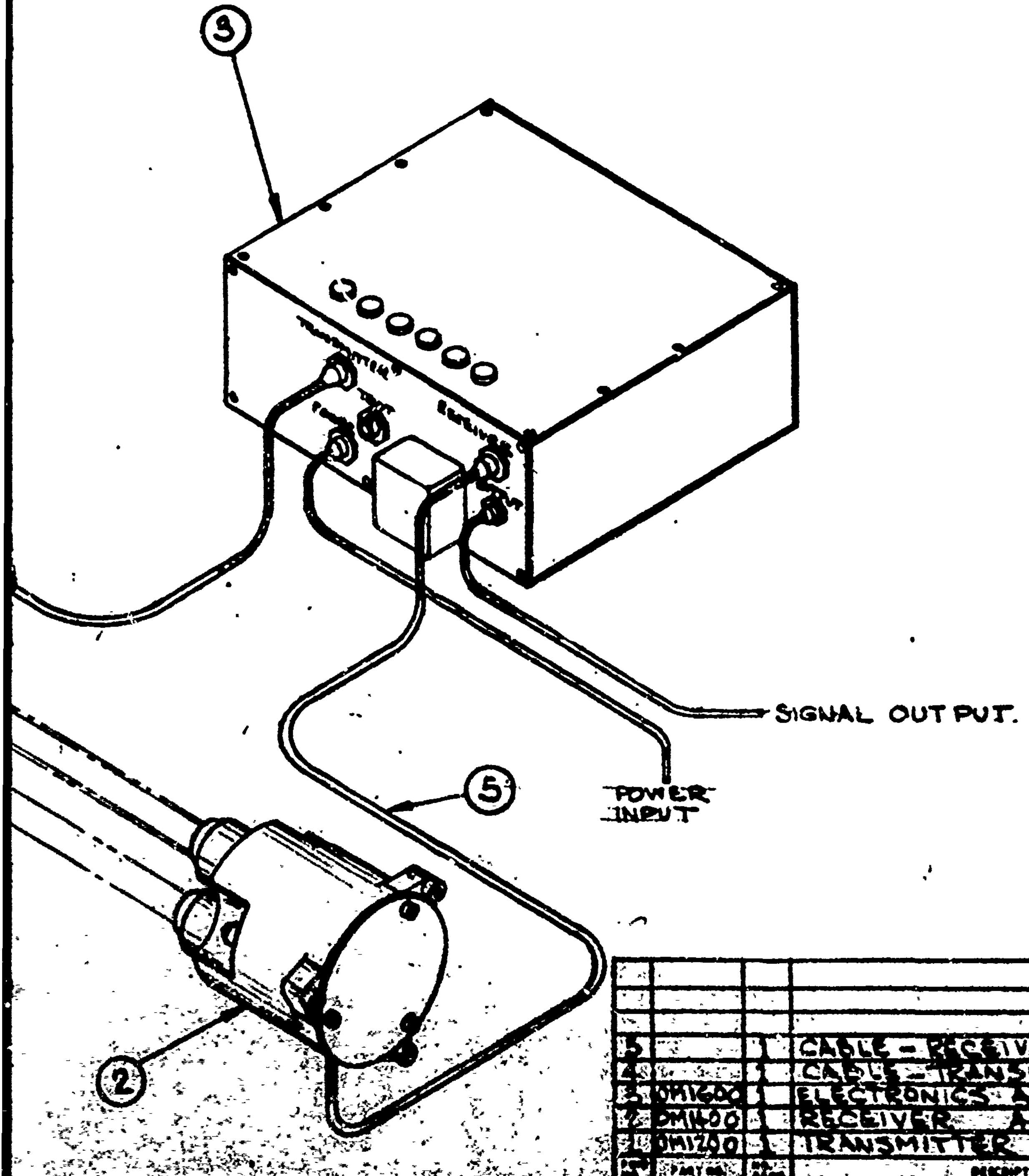
3
TRANSMITTER
RECEIVER
SIGNAL OUTPUT.
POWER INPUT
5
2

5		1	CABLE - RECEIVER		
4		1	CABLE - TRANSMITTER		
3	OM1600	1	ELECTRONICS ASSY		
2	OM1400	1	RECEIVER ASSY		
1	OM1200	1	TRANSMITTER ASSY		
ITEM NO.	PART NO.	NO. REQD	DESCRIPTION	MATERIAL	

BILL OF MATERIAL

FIG 7.1-3

1977

OPTICAL ANGULAR
MOTION
SENSOR
(OAMS) FLIGHT. MODEL
BACK MOUNT

C OM1000

7.1.1 Specifications of Components

INTEGRATED CIRCUITS, OP-AMPS, PMI OP07-068J

MIL-M-38510 Equivalent as follows:

Screened to MIL-STD-883A, Level A with the exception of "A" visual which will be to Level "B" and consequently Hong Kong assembly. SEM not included.

SAMSO-STD 73-2C SCREENING REQUIREMENTS

Internal (Precap) Visual Examination
Parameter
Acceleration
Hermetic Seal
High Temp Reverse Bias
High Temp Storage/Stab
Power Burn in/Stab
Temp cycle/thermal shock
Radiographic inspection
Radiation
Scanning electron microscope
External Visual Examination
Destructive Physical Analysis
Internal Lead Pull Test
Particle Impact Noise Detection (PIND)

Exceptions to SAMSO-STD 73-2C Screening Requirement

High Temp Reverse Bias
Radiation (Nuclear)
Scanning Electron Microscope (SEM)
Destructive Physical Analysis
Internal Lead Pull Test

DESC Approved

MODULE, ANALOG DIVIDER, COMMERCIAL DEVICE WITH SPECIAL SCREENING.

MIL-M-38510 Equivalent as follows:

Screened to MIL-STD-883A, Level "A" as follows:

1) Bake
2) Temp Cycle
3) Visual
4) Serilization
5) Electricals at 25°C
6) Burn-in

7) Electricals at 25°C, Min and Max Temps.
8) X-Ray
9) Visual

Exceptions:

Acceleration
Seal
High Temp Reverse Bias
Noise and Bandwidth will not be performed during electricals.

A waiver letter for this device was sent to SAMSO 23 November 1976.

SAMSO-STD 73-2C Screening Requirements:

Internal (Precap) Visual Examination
Parameter (Active)
Accelleration
Hermetic Seal
High Temp Storage/Stab
Power Burn in/Stab
Temp Cycle/Thermal Shock
Radiographic Inspection
Radiation
Scanning Electron Microscope
External Visual Examination
Destructive Physical Analysis
Internal Lead Pull Test
Particle Impact Noise Detection (PIND)

Exceptions to SAMSO-STD 73-2C Screening Requirements

Accel
Hermetic Seal
Radiation (Nuclear)
Scanning Electron Microscope (SEM)
Destructive Physical Analysis
Internal Lead Pull Test

DESC Approved

SUBASSEMBLY, SPECIAL OSCILLATOR, BULLOVA

MIL-M-38510 Class A as applicable Monolithic Devices

MIL-STD-883 Class A as applicable Monolithic Devices

MIL-E-8983B as applicable Electronic Equip. for Unmanned Space Vehicles

MIL-S-19500 as applicable Semiconductors

Failure rate "S" for resistors and capacitors.

Equivalen of these specification is acceptable

Screening to SAMSO-STD 73-2C for components in the oscillator will be the same as for parts used by Chrysler.

SUBASSEMBLY, POWER SUPPLY, POWER CUBE

MIL-M-38510 Class A Monolithic Devices

MIL-STD-883 Class A Monolithic Devices

Failure Rate "S" for resistors and capacitors.

JANTXV For Semiconductors.

Equivalent of these specifications is acceptable.

Screening to SAMSO-STD 73-2C for Components in this power supply will be the same as for parts used by Chrysler.

Resistors, 1 watt, RNC75EXXXXBS

MIL-R-55182E/10

Resistors, ½ watt, RNC65EXXXXBS

MIL-R-55182E/5

SAMSO-STD 73-2C SCREENING REQUIREMENTS

DC Resistance
Hermetic Seal
Temp Cycle/Thermal Shock
Power Voltage Conditioning
Overload
Radiographic Inspection
External Visual Examination

Exceptions to SAMSO-STD 73-2C

Power Voltage Conditioning
Radiographic Inspection

DESC Approved

CAPACITORS, CERAMIC DIELECTRIC

MIL-C-11015/12

SAMSO-STD 73-2C Screening Requirements

- Internal (Precap) Visual Examination
- Capacitance
- Insulation Resistance
- Power/Dissipation Factor/Q
- Temp Cycle/Therm Shock
- Power Voltage Conditioning
- De-Aging
- Radiographic Inspection
- External Visual Examination
- Destructive Physical Analysis

Exceptions to SAMSO-STD 73-2C Screening Requirements

- Internal (Precap) Visual Examination
- Thermal Shock
- Power Voltage Conditioning
- De-Aging
- Radiographic Inspection
- Destructive Physical Analysis

DESC Approved

CAPACITORS, MICA DIELECTRIC

MIL-C-?9001/5

SAMSO-STD 73-2C Screening Requirements

- Capacitance
- Dielectric Withstanding Voltage
- Insulation Resistance
- Power/Dissipation Factor/Q
- Hermetic Seal
- Temp Cycle/Therm Shock
- Power Voltage Conditioning
- External Visual Examination
- Destructive Physical Analysis

Exceptions to SAMSO-STD 73-2C Screening Requirements

- Hermetic Seal
- Power Voltage Conditioning
- Destructive Physical Analysis

DESC Approved

CAPACITORS, METALLIZED POLYCARBONATE

MIL-C-55514A/4

SAMSO-STD 73-2C Screening Requirements

Capacitance
Insulation Resistance
Power/Dissipation Factor/Q
Temp. Coefficient
Hermetic Seal
Temp Cycle/Therm Shock
Power Voltage Conditioning
Radiographic Inspection
External Visual Examination

Exceptions to SAMSO-STD 73-2C Screening Requirements

Temp Coefficient
Hermetic Seal
Power Voltage Conditioning
Radiographic inspection

DESC Approved

CAPACITORS, SOLID TANTALUM

MIL-C-39003/1

SAMSO-STD 73-2C Screening Requirements

Capacitance
DC Leakage
Power/Dissipation Factor/Q
Hermetic Seal
Temp Cycle/Therm Shock
Power Voltage Conditioning
Radiographic Inspection
External Visual Examination
Destructive Physical Analysis

Exceptions to SAMSO-STD 73-2C Screening Requirements

Hermetic Seal
Power Voltage Conditioning
Destructive Physical Analysis

DESC Approved

CAPACITOR, ALUMINUM ELECTROLYTIC

MIL-C-39018/3

Not included in SAMSO-STD 73-2C Screening Matrix

DESC Approved by Telecon but Limited Application for SAMSO.

1. Comparator, National Semiconductor LM119D/883

2. Voltage Reference, National Semiconductor LM199AH-20/883

MIL-M-38510 Class A Equiv. with exception that will not be processed to Notice 2 of MIL-STD-883 Class A

SAMSO-STD 73-2C Screening Requirements

Internal (Precap) Visual Examination
Parameter
Acceleration
Hermetic Seal
High Temp Reverse Bias
High Temp Storage/Stab
Power Burn In/Stab
Temp Cycle/Thermal Shock
Radiographic Inspection
Radiation
Scanning Electron Microscope
External Visual Examination
Destructive Physical Analysis
Internal Lead Pull Test
Particle Impact Noise Detection (PIND)

Exceptions to SAMSO-STD 73-2C Screening Requirements

High Temp Reverse Bias
Radiation (Nuclear)
Scanning Electron Microscope (SEM)
Destructive Physical Analysis
Internal Lead Pull Test

DESC Approved

Transistor, Signal: JANTXV2N3057A

MIL-S-19500/391

Transistor, Chopper: JANTXV2N2432A

MIL-S-19500/313

Transistor, Medium Power: JANTXV2N3766

MIL-S-19500/518

SAMSO-STD 73-2C Screening Requirements

Internal (Precap) Visual Examination
Parameter (Active)
Acceleration
Hermetic Seal
High Temp Reverse Bias
High Temp Storage/Stab
Power Burn-in/Stab
Temp Cycle/Therm Shock
Particle Impact Noise Detection (PIND)
Radiographic Inspection
External Visual Examination
Destructive Physical Analysis
Internal Lead Pull Test

Exceptions to SAMSO-STD 73-2C Screening Procedures

High Temp Reverse Bias
Radiographic Inspection
External Visual Examination
Destructive Physical Analysis
Internal Lead Pull Test

Exceptions to SAMSO-STD 73-2C Screening Procedures

High Temp Reverse Bias
Radiographic Inspection
Destructive Physical Analysis

DESC Approved

Diodes, Signal: JANTXVIN4153

MIL-S-19500/337

Diodes, Rectifier: JANTXVIN5618

MIL-S-19500/427

SAMSO-STD 73-2C Screening Requirements:

Internal (Precap) Visual Examination
Parameter (Active)
Acceleration
Hermetic Seal
High Temp Storage/Stab

Power Burn-in/Stab
Temp Cycle/Therm Shock
Radiographic Inspection
External Visual Examination
Destructive Physical Analysis

Exceptions to SAMSO-STD 73-2C Screening Requirements

Radiographic Inspection
Destructive Physical Analysis

ELECTRICAL CONNECTOR, PYGMY, MS3114H--and M53116F--

MIL-C-26482

To be approved by DESC

P.C. CONNECTORS

MIL-C-55302/57A

MIL-C-55302/58B

DESC Recommended by Telecon

HOOK UP WIRE, 22 AWG

MIL-W-81044/4

DESC Recommended by Telecon

SHIELDED CABLE, LOW CAPACITANCE, TWO CONDUCTOR, EC22U9-OSTX

MIL-C-55021/2

COAXIAL CABLE, MINIATURE, M27500028MBITIO

MIL-C-27500

DESC Recommended by Telecon

DETECTOR, SILICON PHOTO DIODES, RCA C30852

Screened to MIL-STD-883A as follows:

1) Method 2002.1 Cond. D
2) Method 2005 Cond. B
3) Method 1010.1 Cond. B
4) Method 2001.1, Y1 Axis only, Cond. D.
5) Method 1014.1 Cond. B, C1,C2

LED, GaAs, T.I. SL-1162-4
LED, GaAlAs T.I. SLH-19
LED, GaAlAs T.I. SLH-20

Screened to MIL-STD-750 Methods 2005 and 4011. Mechanical shock and random vibration in accordance with prime item development specification CEI No. 73-6, Release Date June 30, 1975.

7.2 FLIGHT MODEL OPTICAL DESIGN

7.2.1 Transmitter Optical Design - General

The OAMS transmitter design is shown in figures 7.2-1a and 7.2-1b. Figure 7.2-1a illustrates the optical design of the roll transmitter and figure 7.2-1b that of the pitch and yaw transmitter channels. The light from the two LED's is collimated by the two aspheric collimating lenses. The focal length of the lenses is chosen with respect to the effective LED emitting area such that the total beam spread is approximately 1.1 degrees in diameter.

The light emitted by the LED is non-polarized. One-half of the light in the appropriate polarization mode is transmitted by the Wollaston Prism. Two orthogonally polarized and coincident beams exit from the Wollaston Prism. The other polarization forms, i.e. the other half of the light from each LED, exits the Wollaston Prism 20° from the axis and is absorbed by the transmitter walls. This light is lost and does not leave the transmitter.

The axis of the Wollaston Prism and therefore the direction of polarization of the emitted light from the Roll transmitter are fixed relative to the transmitter body. This direction is the reference from which the twist or roll of the receiver is measured.

The two lateral channels, Pitch and Yaw, are similar to the Roll channels with the addition of two other components: the quarter wave plate and the Angle Sensing Crystal. These components appear in each of the lateral channels and are used to define a reference axis for each channel about which pitch or yaw is measured.

The quarter wave plate changes the linear polarized light into circularly polarized light. Since the light from each of the LED's is mutually orthogonal, the light from one LED is right-hand circularly polarized as it leaves the quarter wave plate, while the light from the alternate LED is left-hand circularly polarized. The system is modulated by sinusoidally varying the intensities of the LED's, with each LED being modulated 180 degrees out of phase with the other.

The Angle Sensing Crystal, ASC, encodes the light with respect to its direction within the 1.1 degree beam spread. The Angle Sensing Crystal behaves as a wave plate or optical retarder in which the retardation is a function of the angle of incidence on the crystal. The light within the center of the transmitter beam enters the Angle Sensing Crystal at normal incidence and is unchanged. This light leaves the transmitter circularly polarized. Elsewhere, within the 1.1 degree beam spread the light strikes the Angle Sensing Crystal at a non-normal angle of incidence, and its polarization state is altered. The light becomes more and more elliptically polarized toward the edge of the beam.

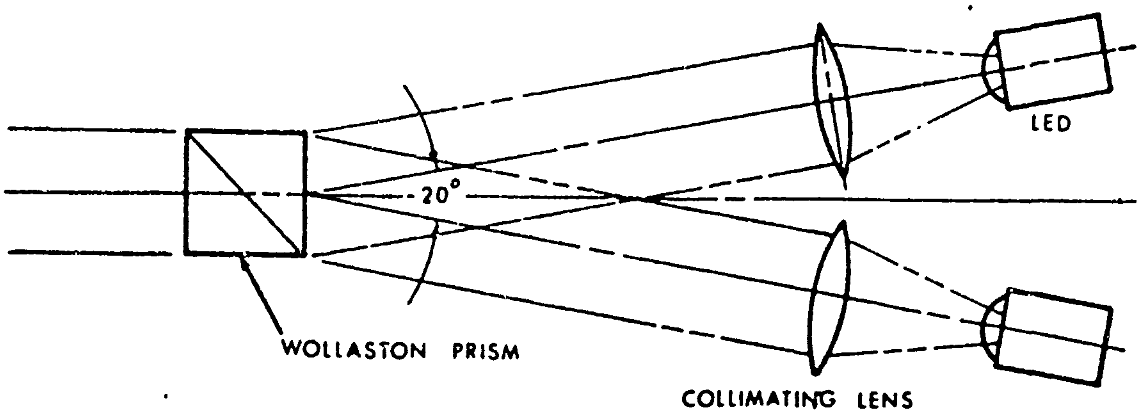
LED
20°
WOLLASTON PRISM
COLLIMATING LENS

Figure 7.2-1a. OAMS Flight Model Optical Design - Roll Channel Transmitter.

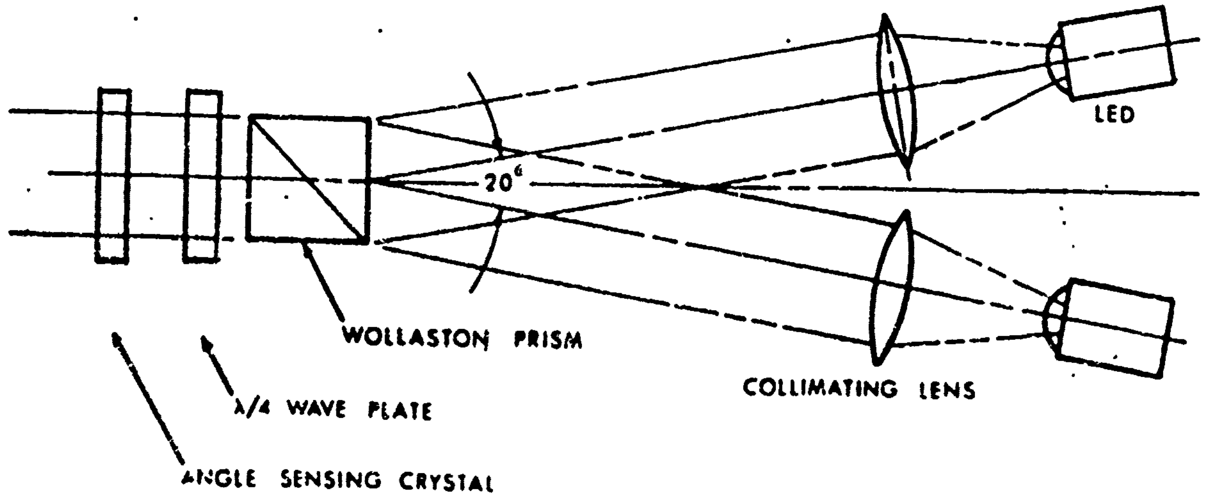
LED
20°
WOLLASTON PRISM
COLLIMATING LENS
λ/4 WAVE PLATE
ANGLE SENSING CRYSTAL

Figure 7.2-1b. OAMS Flight Model Optical Design - Lateral Channel Transmitter.

Figure 7.2-2 illustrates the results of ray trace calculations.

In the ray trace five equally spaced rays are shown coming from the LED source. At the Wollaston Prism each of these rays is split into its two polarization forms. One of the polarization forms is refracted along the line of sight of the instrument, while the other form is deviated toward the internal walls of the structure. The internal walls are black anodized aluminum, and the reflected light is reduced to a negligible intensity after two reflections A portion of this undesirable polarization form does leave the instrument through the Angle Sensing Crystal (ASC) after only one reflection. However, this light is reflected approximately twenty degrees from the line of sight between the transmitter and receiver, and cannot enter the receiver unless re-reflected from an external surface.

Table 7.2-1 lists the transmitter optical components and their specifications. A detailed description of the major components follows.

7.2.1.1 LED's and Collimating Lenses

The optical design of the Flight Model LED and collimating section differs from that of the advanced Brassboard design in that a separate collimating lens is utilized for each LED. This was necessary in order to accommodate the smaller effective emitting area of the LED's used in the Flight Model. The smaller emitting area requires a smaller focal length for the collimating lens to achieve a given beam spread.

The focal length of the LED collimating lens must be such that the lens images the LED emitting surface at infinity with the image sustending 1.1 degrees. In addition the diameter must be as large as possible, consistent with the mechanical constraints, to provide for maximum beam intensity or light collection efficiency.

The following LED's are selected for each channel; the peak emission wavelength is also shown:

Pitch	SLH - 19	810 nm
Yaw	SLH - 20	850
Roll	SL- 1162-3	935

The effective emitting area of the LED's is such that a collimating lens of focal length of approximately 12.0 mm provides an adequate beam diameter of 1.1 degrees or more. This focal length images the central emitting area of the LED. The internal reflector in the LED is not imaged within the 1.1 degree beam. If a large focal length collimating lens is used such that the reflector is imaged within the beam, very large intensity variations (greater than 50%) are usually encountered across the beam. This is caused by a dark ring between the emitting area and the reflector. This dark ring is imaged into the far field of the transmitter.

A 12.0 mm effective focal length lens, 15.0 mm in diameter is found to be optimum for the above LED's. An anti-reflection coated aspheric lens is used to reduce the effects of spherical aberration.

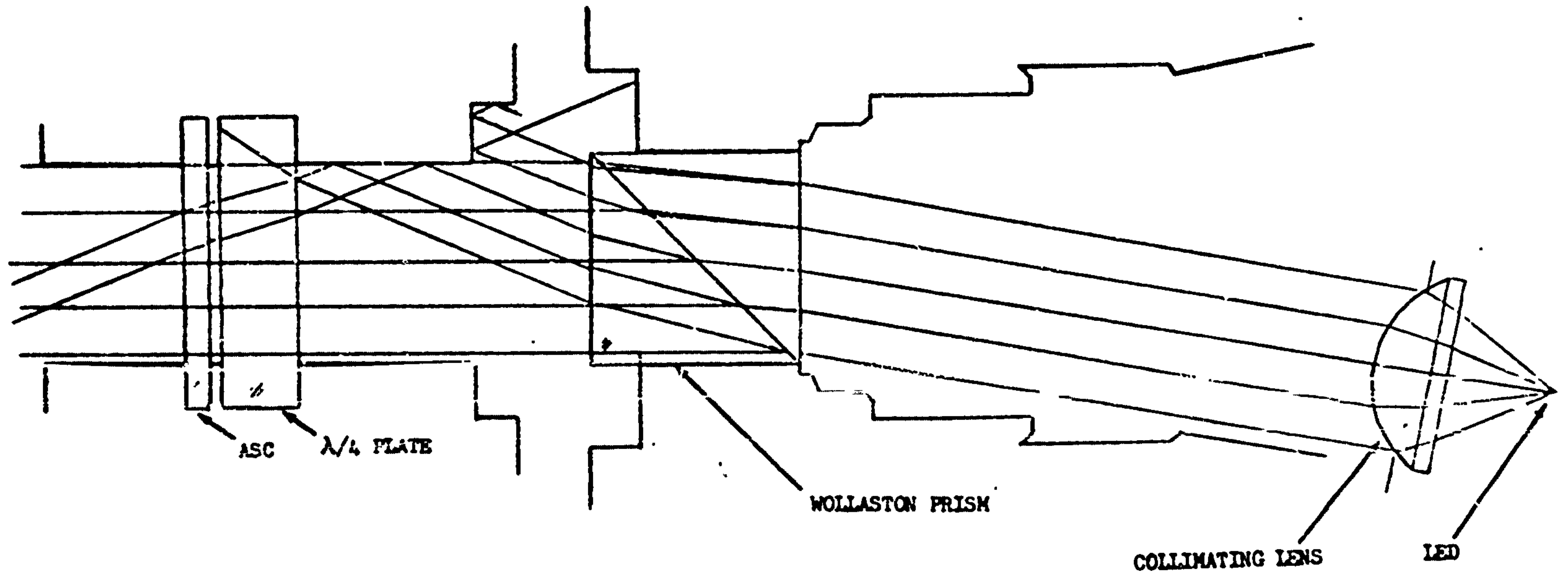
ASC
λ/4 PLATE
WOLLASTON PRISM
COLLIMATING LENS
LED

Figure 7.2-2. Ray Trace Results for OAMS Flight Model Transmitter.

Table 7.2-1 OAMS FLIGHT MODEL OPTICAL COMPONENTS

TRANSMITTER

COMPONENT	DESCRIPTION	MATERIAL	APPLICABLE MIL-SPECS	COMMENTS
Plane Window	31.7 mm diameter 5.0 mm thick	Fused Silica Grade A	MIL-G-174A MIL-G-16592A	Coated
Angle Sensing Crystal	22.0 mm diameter 3.0 mm thick	Single Crystal Quartz, Grade A	MIL-O-13830A MIL-G-16592A MIL-G-174A	Coated Cemented Construction Pitch and Yaw Channels Only
Lenses	12.0 mm F.L. 15.0 mm dia.	Optical Crown Grade A	MIL-O-13830A	Aspheric Plano-Convex Coated
λ/4 Plate	22.0 mm dia	Optical Crown Grade A	MIL-O-13630A MIL-G-16592A MIL-G-174A	Zero Order Cemented Construction Mica Coated
Pitch	810 nm			
Yaw	850 nm			
Roll	N/A			
Wollaston Prism	20° divergence 2 element 15.0 mm x 15.0 mm square aperture	Calcite Grade A	MIL-A-3920B MIL-O-13830A MIL-G-174A	Extinction Ratio less than 1×10^{-5} Coated Cement not MIL-A-3920B for temperature
LED's				
Pitch	SLH-19 (810 nm)	Gallium Aluminum Arsenide	N/A	Manufactured by Texas Instruments, Inc.
Yaw	SLH-20 (850 nm)			
Roll	SL1162-3 (935 nm)			

Figures 7.2-3 and 7.2-4 are typical beam profiles using different lenses. These figures illustrate the LED/lens combination intensity as a function of angular direction. The intensities in each profile are shown on a relative scale for a plano-convex lens and an aspheric lens of approximately the same focal length. In all cases the aspheric lens provides for a greater on-axis intensity than the simple plano-convex lens. In the lateral channel LED, figure 7.2-3, the increase is over one-hundred percent. In the roll channel, figure 7.2-4, the increase is approximately forty percent.

7.2.1.2 Wollaston Prism

The details of the behavior of a Wollaston Prism are available in almost any basic optics text. Basically, as shown in figure 7.2-5, the prism acts as a beam divider and separates an incoming beam into two beams, the intensity of each being the intensity of the two orthogonal polarization forms representing the initial beam. The two emerging beams are separated by an angle which is a function of the prism wedge angle.

The Wollaston Prism must be made from a material with the proper birefrigence, which in the present case is Calcite. The cement used to bind the two prism wedges together must be carefully selected for the required temperature range. Calcite is a brittle material when compared to glass. Most ordinary optical cements which adhere to military specification MIL-A-3920B when applied to glass are not suitable when the substrate material is calcite. The majority of the available optical cements corresponding to the above MIL-spec will cause the calcite to crack over the OAMS operational temperature range. Consequently the Wollaston Prisms are fabricated with a cement manufactured by Dow Corning, XR-6-3488. This cement, while not rated to MIL-A-3920B, has been shown to be adequate when applied to calcite. The manufacture's temperature specification for the three cemented optical components of OAMS is shown in Table 7.2-2. In all cases the manufacturer's specifications exceed the OAMS requirements.

The beam divergence of the Wollaston Prism is $20^{\circ} \pm 0.5^{\circ}$ and the entrance and exit faces are coated with a broad band anti-reflection coating providing less than 1.5% surface reflectivity between 0.78 and 0.97 microns.

7 2.1.3 Quarter Wave Plate

The quarter wave plate is oriented relative to the Wollaston Prism such that the plane polarized light emerging from the Wollaston is converted to circular polarization. Since the planes of polarization of the light from the two LED's are oriented 90° relative to each other, the wave plate converts the light from one LED into right hand circularly polarized light and other LED is converted into left-hand circularly polarized light.

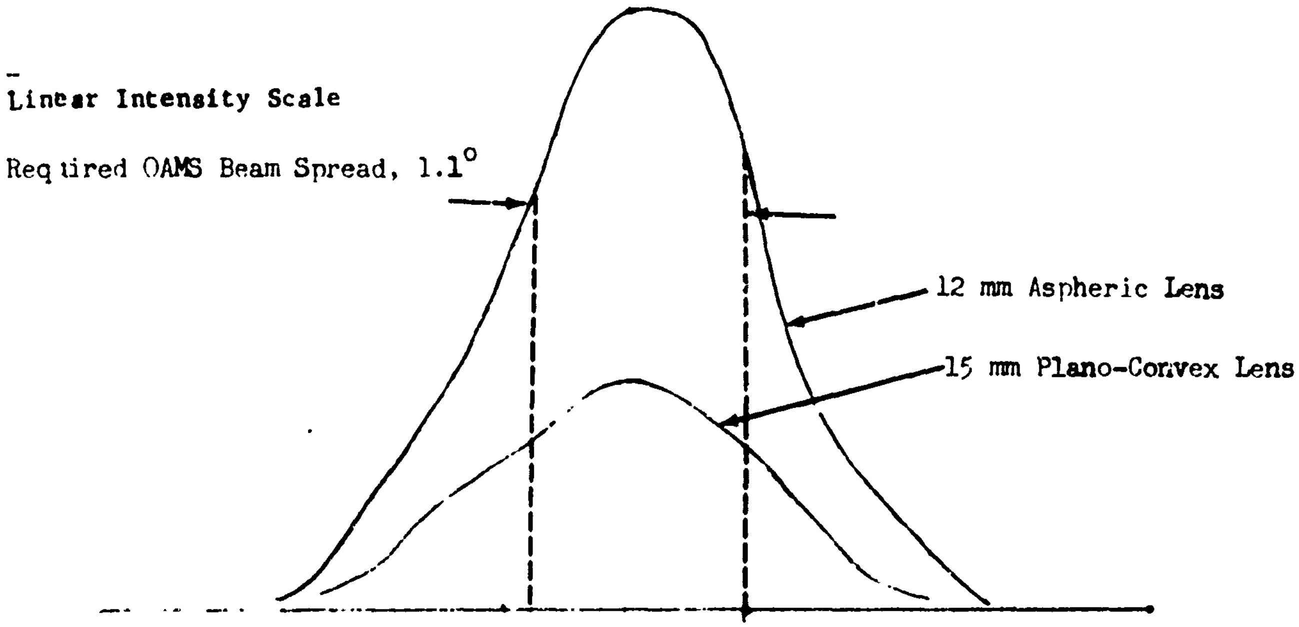

Figure 7.2-3. LED Intensity Profile, SLH-20 #D.

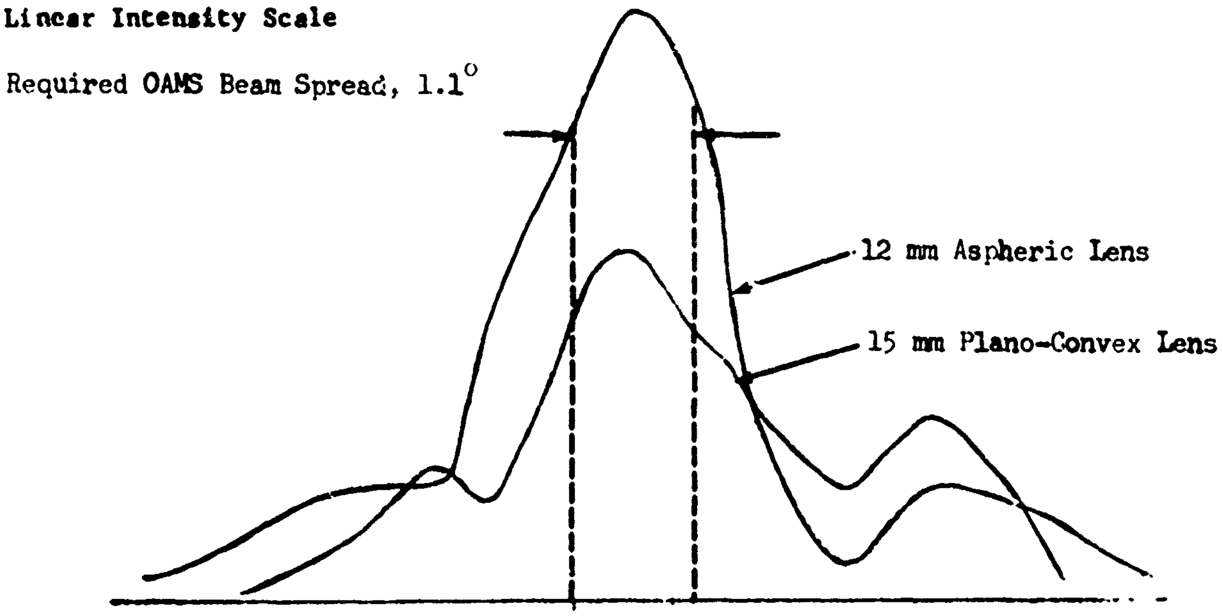

Figure 7.2-4. LED Intensity Profile, SL-1162-3 #3.

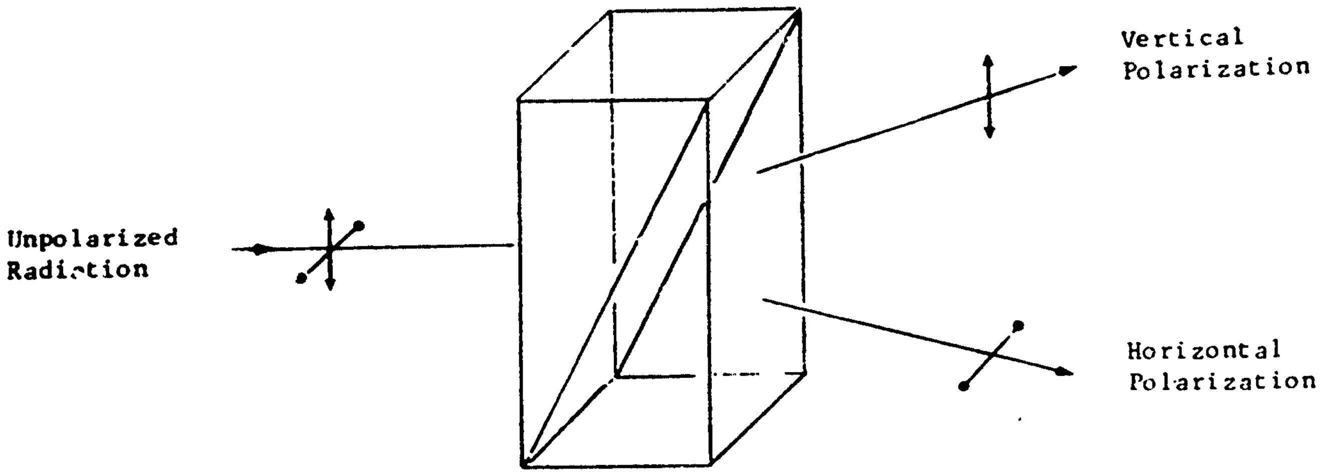
Unpolarized Radiation
Vertical Polarization
Horizontal Polarization

Figure 7.2-5. Details of a Wollaston Prism.

Table 7.2-2

TEMPERATURE RANGES OF OAMS PHASE II OPTICAL ADHESIVES

SPEC. PART (Adhesive)	REQUIRED OPERATIONAL AND STORAGE	MIL-A-3920	MANUFACTURER'S SPECIFICATION
WOLLASTON PRISM (Dow Corning XR-6-3488)	-40° to 160°F	-80° to 160°F	-70° to 300° F
ANGLE SENSING CRYSTAL (Kodak HES-1)	"	"	-65° to 160° F
QUARTER WAVE PLATE (Kodak HES-1)	"	"	"

The wave plates are made of mica cut to the required thickness to provide a zero order retardation at the proper wavelength. The mica is then cemented between two pieces of grade A optical crown for protection. See Table 7.2-2 for the cement temperature specifications. The retardation is one-quarter wave at the following wavelengths:

Pitch	810 nm
Yaw	850 nm

Both exposed surfaces are broadband, anti reflection coated for 1.5 per cent reflectivity or less.

7.2.1.4 Angle Sensing Crystal

The Angle Sensing Crystal consists of two crystalline quartz plates cemented together, with the optical axes of each plate having the proper relative orientations as described in the CEI specifications. The crystalline quartz conforms to MIL-G-174A, Grade A The total thickness of the Angle Sensing Crystal is 3.0 millimeters (± .025 m). This thickness is chosen to provide for an adequate instrument field of view.

The angular encoding is performed by the Angle Sensing Crystal, the encoding being in the form of an optical retardation which is a function of angle of incidence. The range of angles over which the encoding or retardation is unambiguous is termed the Angle Sensing Crystal Field of View. This field of view is a function of crystal thickness and wavelength. The fields of view for each channel (lateral channels only) for a 3.0 millimeter thick crystal are:

		FOV
pitch	810 nm	1.86°
yaw	850 nm	1.98°

These fields of view are chosen to be sufficiently larger than the required OAMS measurement range (± 0.25 degree). This selection provides adequate system linearity, since the encoding or retardation of the Angle Sensing Crystal with respect to angle of incidence becomes non-linear as the angle of incidence approaches the edge of the crystal field of view.

The two quartz plates which comprise an Angle Sensing Crystal are cemented together with Kodak adhesive HES-1 which is a modified methacrylate suitable over the temperature range -65° to 160°F. This is within the OAMS operation, storage and transportation temperature requirement of -40° to 160°F, see Table 7.2-2.

7.2.2 Receiver - General

The OAMS receiver design is shown in figures 7.2-6a and 7.2-6b. Figure 7.2-6a illustrates the optical design of the roll receiver and figure 7.2-6b that of the pitch and yaw receiver channels. In the pitch and yaw channels the first optical element is the Angle Sensing Crystal (ASC) which defines the axes about which the angles are measured and provides the optical angular encoding.

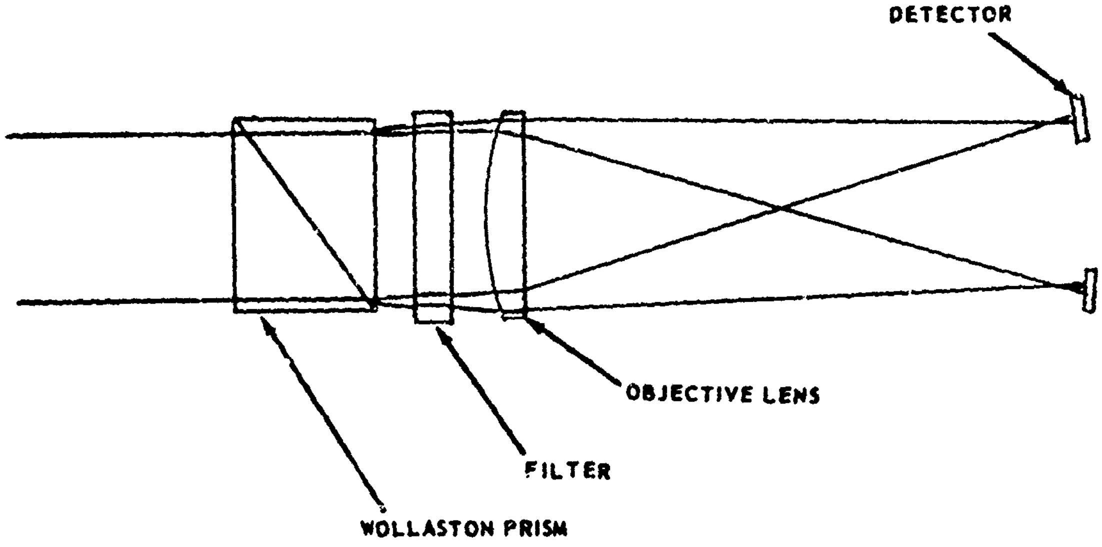
DETECTOR
OBJECTIVE LENS
FILTER
WOLLASTON PRISM

Figure 7.2-6a. OAMS Flight Model Optical Design - Roll Channel Receiver.

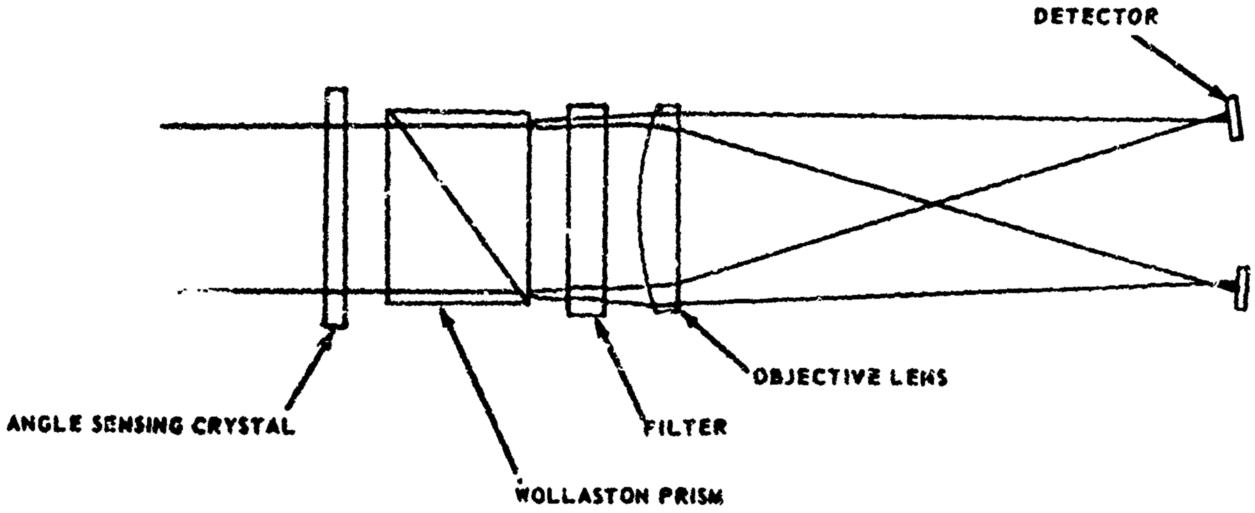
DETECTOR
OBJECTIVE LENS
ANGLE SENSING CRYSTAL
FILTER
WOLLASTON PRISM

Figure 7.2-6b. OAMS Flight Model Optical Design - Lateral Channel Receiver.

The Wollaston Prism immediately following the Angle Sensing Crystal splits the light into its two polarization components, each being directed through a filter and a lens which focuses each component onto the appropriate detector. An optical interference filter allows only light from the appropriate transmitter channel to reach the detectors.

The plano-convex lens focuses the light on each of the two detectors. The detectors, however, are placed slightly out of focus to reduce the effects of local surface irregularities on the detector.

The roll channel does not contain an Angle Sensing Crystal and the axes of the Wollaston Prism are oriented 45 degrees relative to those of the Wollaston Prism in the transmitter. Also the center wavelength of the optical filters are different for each channel. In all other respects, the roll receiver channel is identical to that of the other receiver channels.

Figure 7.2-7 shows the results of the receiver ray trace. The ray trace shows only the on-axis rays. An aperture stop is included just before the Wollaston Prism which limits the clear aperture to approximately one inch in diameter. This is required to eliminate vignetting within the prism itself. Without the stop the vignetting would cause a portion of the light in one or the other polarized beams to strike the sides of the Wollaston instead of reaching the approximate detector. This would create the same effect as a detector unbalance.

Table 7.2-3 lists the receiver optical components and their specifications. A detailed description of the components follows.

7.2.2.1 Angle Sensing Crystal

The Angle Sensing Crystais in the receiver lateral channels are identical to those in the transmitter lateral channels except for size. The receiver Angle Sensing Crystals are 31.8 mm in diameter as opposed to 25.0 mm in diameter for the transmitter angle sensing crystal. The thickness in both cases must be indentical in order to minimize cross coupling when the receiver and transmitter are translated relative to each other.

7.2.2.2 Wollaston Prism

The major differences between the receiving Wollaston Prism and the transmitter Wollaston Prism are the size and the divergence angle of the two polarized exit beams. The receiver Wollaston Prism aperture is 15.0 mm on a side which is smaller than that of the transmitter. The divergence angle is 15°. This larger divergence angle is chosen to accommodate the detector sizes and associated detector mounting components which are larger than the LED's and the LED mountings in the transmitter. The behavior of the receiver Wollaston Prism is the same as in the transmitter. The polarization state of the light received from the transmitter is changed by the Angle Sensing Crystal according to its angle of incidence. The Wollaston Prism divides the light from the Angle Sensing Crystal into two beams, the intensity of each depending of the polarization state of the incoming beam.

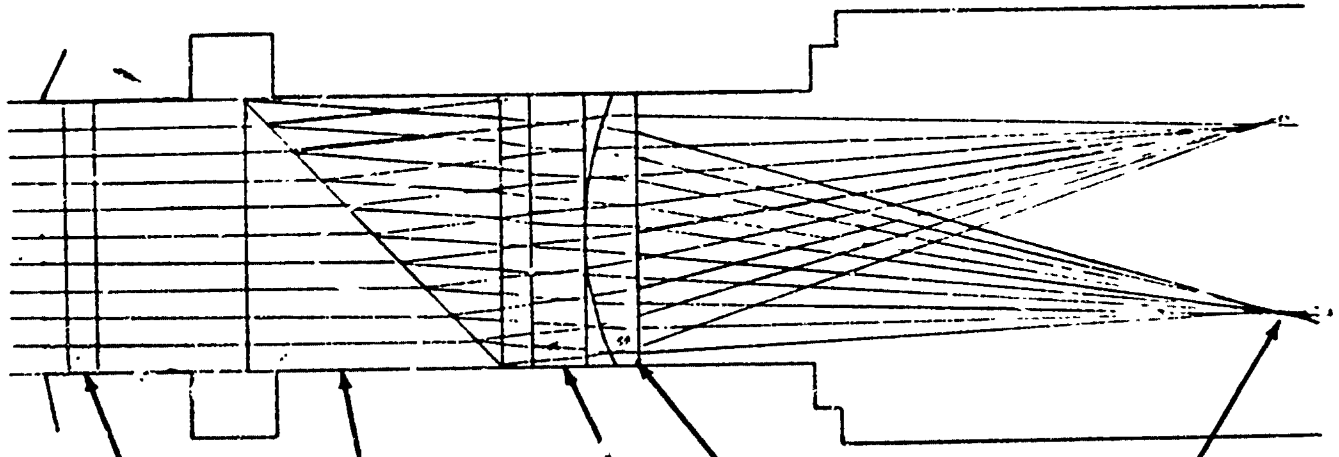
ASC
WOLLASTON PRISM
FILTER
LENS
DETECTOR

Figure 7.2-7. Ray Trace Results for OAMS Flight Model Receiver.

Table 7.2-3 OAMS FLIGHT MODEL OPTICAL COMPONENTS

RECEIVER

COMPONENT	DESCRIPTION	MATERIAL	APPLICABLE MIL-SPECS	COMMENTS
Plane Window	22.0 mm diameter 5.0 mm thick 1/10 wave	Fused Silica Grade A	MIL-G-174A MIL-G-16592A	Coated
Angle Sensing Crystal	31.7 mm diameter 3.0 mm thick	Single Crystal Quartz, Grade A	MIL-O-13830A MIL-G-16592A MIL-G-174A	Coated Cemented Construction Pitch and Yaw Channels Only
Wollaston Prism	15° divergence 2 element 25.0 mm x 25.0 mm square aperture	Calcite Grade A	MIL-A-3920B MIL-O-13830A MIL-G-174A	Extinction Ratio less than 1 x 10-5 Coated Cement not MIL-A-3920B for temperature
Filter	27.0 mm diameter	Optical Quality Glass, Grade A	MIL-O-13830A MIL-G-174A	Blocking greater than 1 X 10-4 Transmission at center wave length greater than 50%.
Pitch	810 nm, 32 nm bandwidth			
Yaw	850 nm, 30 nm bandwidth			
Roll	930 nm, 55 nm bandwidth			
Lens	64.0 mm F.L. 25.4 mm dia	Optical Crown Grade A	MIL-O-13830A	Coated Plane-Convex
Detector	RCA C30852 photovoltaic sensitive area 20 mm^2	Silicon	N/A	Supplied with a coated window.

7.2.2.3 Focusing Lens

A plano-convex lens of 64.0 mm focal length follows the Wollaston Prism in each of the receiver channels. The purpose of the lens is to focus the light from the Wollaston Prism onto the detectors. The focal length is chosen so that the focused spot falls within the detector sensitive area (5 mm in diameter) for light entering the receiver at all angles within the field of view. As shown in figure 7.2-8 the detector sensitive area is placed approximately 2.0 millimters behind the focal plane of the lens. The light spot falling on the detector is approximately 0.8 millimeters in diameter. By spreading the light over a larger area instead of maintaining a sharp focus, the effect of localized variations in detector sensitivity is reduced.

The lenses are optical crown plano-convex and are coated for less than one percent reflectivity.

7.2.2.4 Detectors

The optical detectors are RCA C30852 single-element silicon photovoltaic photodiodes. The detectors are supplied with a protective glass window. This window is coated for low relection losses over the design wavelengths. This increases the effective detector responsivity and hence the system signal to noise ratio.

The detectors are specially enhanced by the manufacturer for operation at near infrared wavelengths.

DETECTOR: RCA C30852

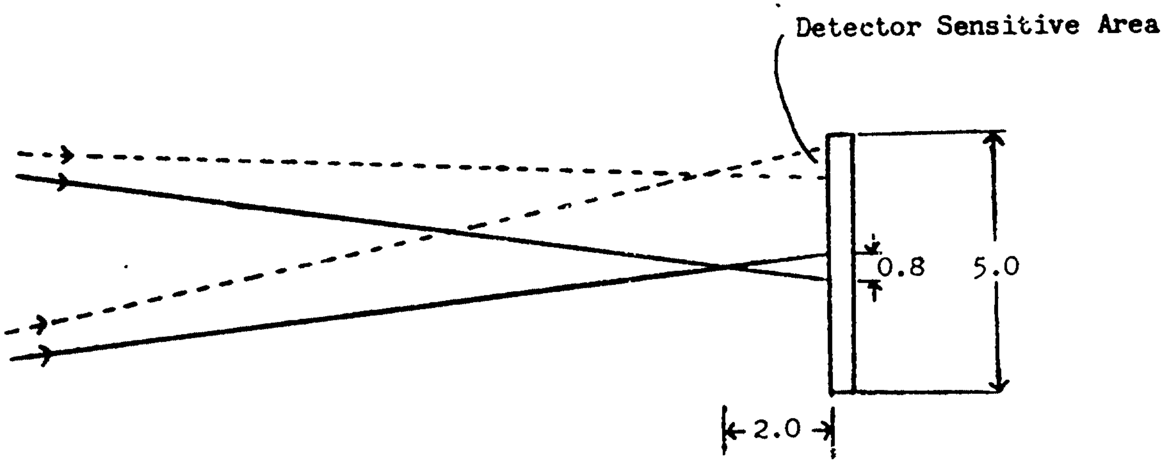
Detector Sensitive Area
0.8
5.0
2.0

ALL DIMENSIONS IN MILLIMETERS

Figure 7.2-8. Details of Detector Focal Plane.

7.3 MECHANICAL DESIGN - FLIGHT MODEL

The three assemblies that are required for the sensor are found in figures 7.1-2 and 7.1-3. Figure 7.1-2 shows the flight model design with the transmitter and receiver assemblies being base mounted. This configuration allows the transmitter and receiver head to be mounted directly to the table or surface on which the equipment being monitored is attached. The fitting of the OAMS equipment in this base mounted configuration allows for fixing either by straps around the body of the sensing heads or fixing bolts through the mounting structure directly into the end plates of the sensing heads.

Figure 7.1-3 shows the flight model design with the transmitter and receiver assemblies being back mounted. The configuration allows the transmitter and receiver heads to be mounted directly to the equipment being monitored. The fixing of the OAMS equipment in this back mounted configuration allows for fixing by hard mounting to three machined buttons at the back of the sensing heads. If required a combination of both fixing methods could be used.

Figures 7.3-1 and 7.3-2 show the details of the transmitter and receiver heads in the back mounting configuration. The basic design for the transmitter and receiver heads for the two mounting configurations is the same as in the advanced brassboard model. The outer housings are different due to the geometry of the mounting configurations. With the new optical design in the flight models the need for the mechanical eccentric mounting adjustments is not required; for this reason the flight model mechanical design does not have eccentric sleeves for mounting the LEDs. In the advanced brassboard model the pitch channel has been modified to the flight model configuration both in optical and mechanical components and hardware.

The flight electronics unit can be mounted and tailored to suit the available volume. It is shown in figure 7.1-1 as being a base mounted aluminum box with a volume of 500 cubic inches. Table 7.3-1 shows the weight and volume of the transmitter, receiver and electronics for the flight model.

	Weight	Volume
Transmitter	10 lbs	160 cubic inches
Receiver	12	200
Electronics	8	500
Total	30 lbs	860 cubic inches

Table 7.3-1 Weight and Volume - Base Mounted

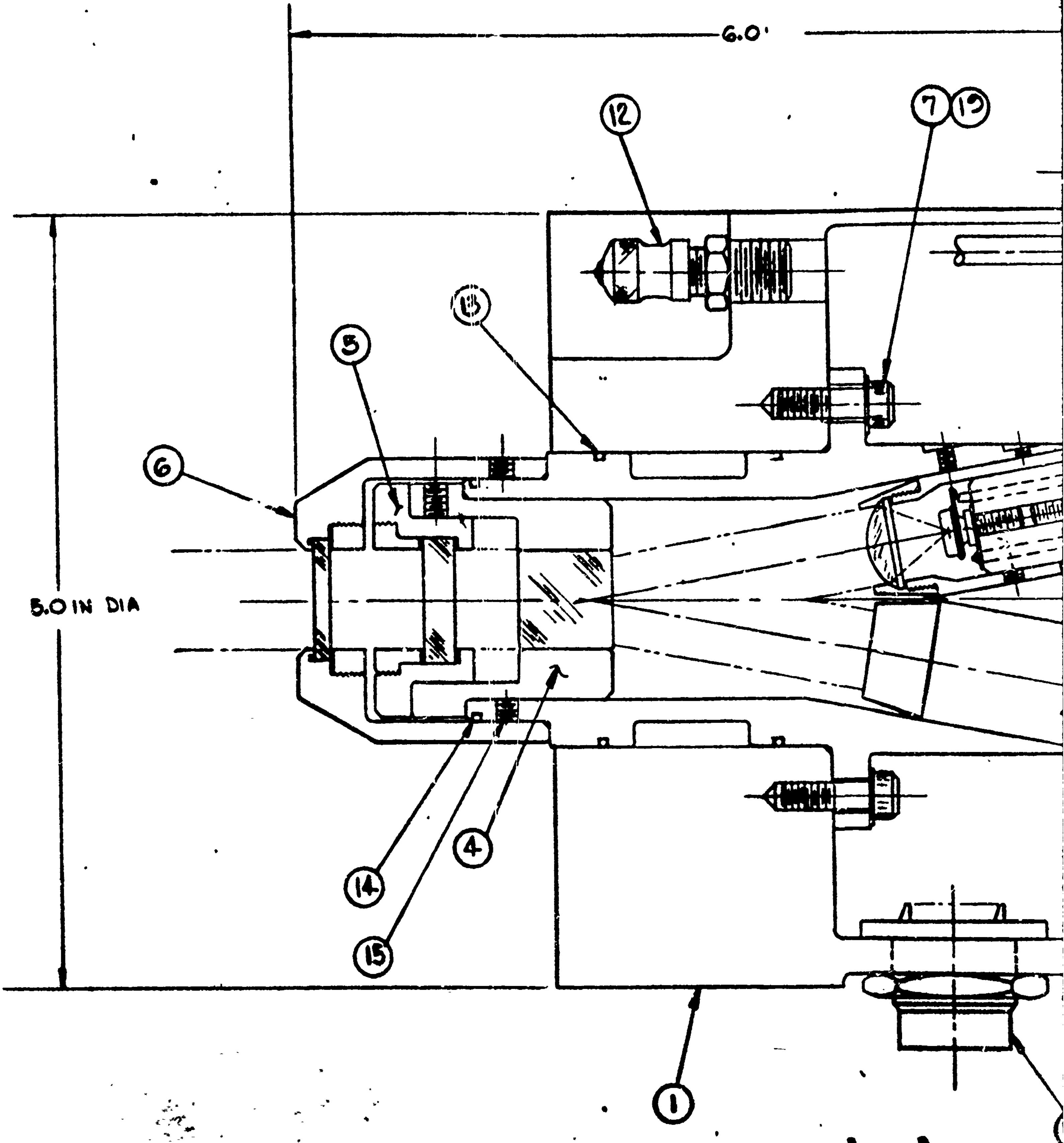
6.0'
12
7
13
13
5
6
5.0 IN DIA
14
15
4
1

SECTION A - A

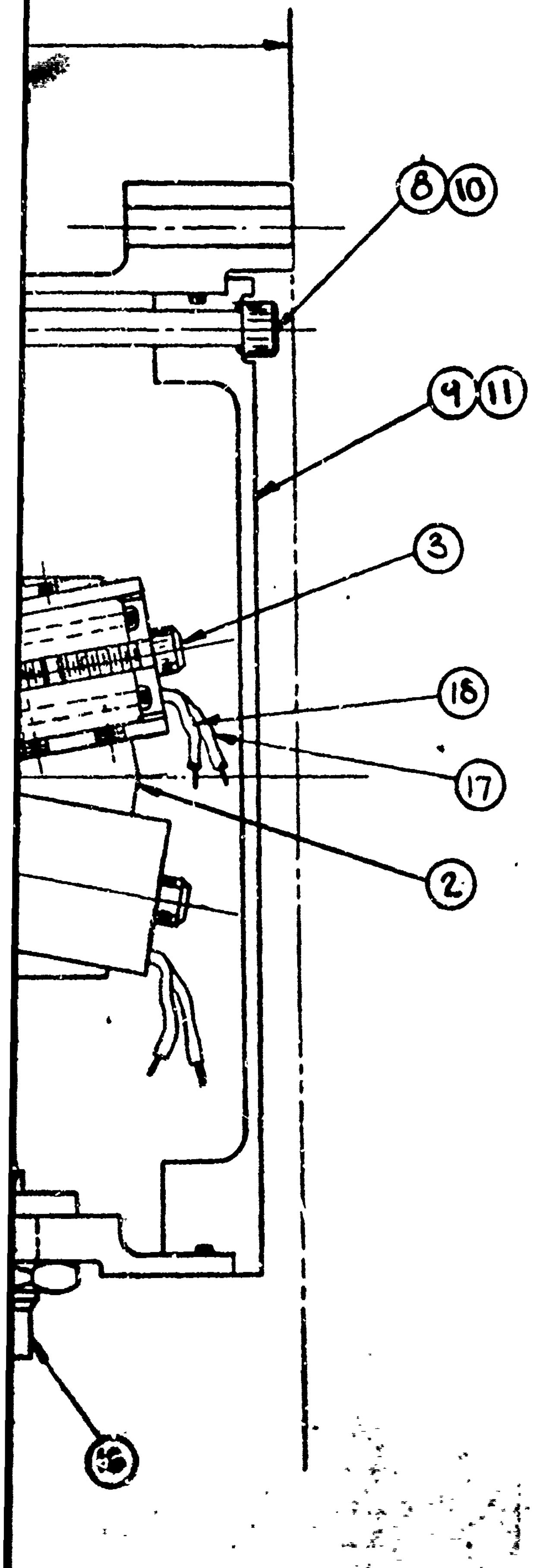
8
10
9
11
3
18
17
2
5

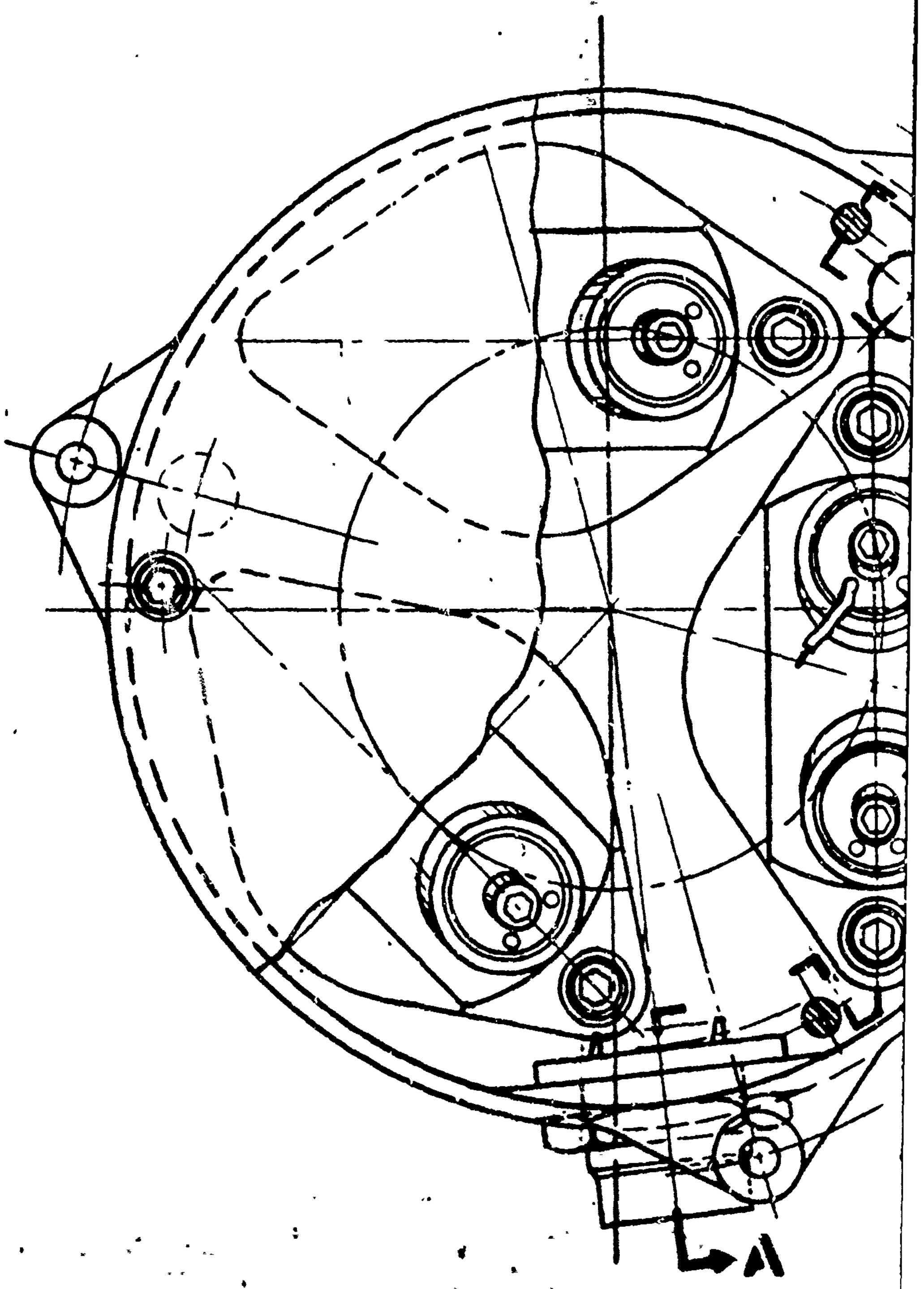

BACK VIEW
WITH COVER BROKEN AWAY

2

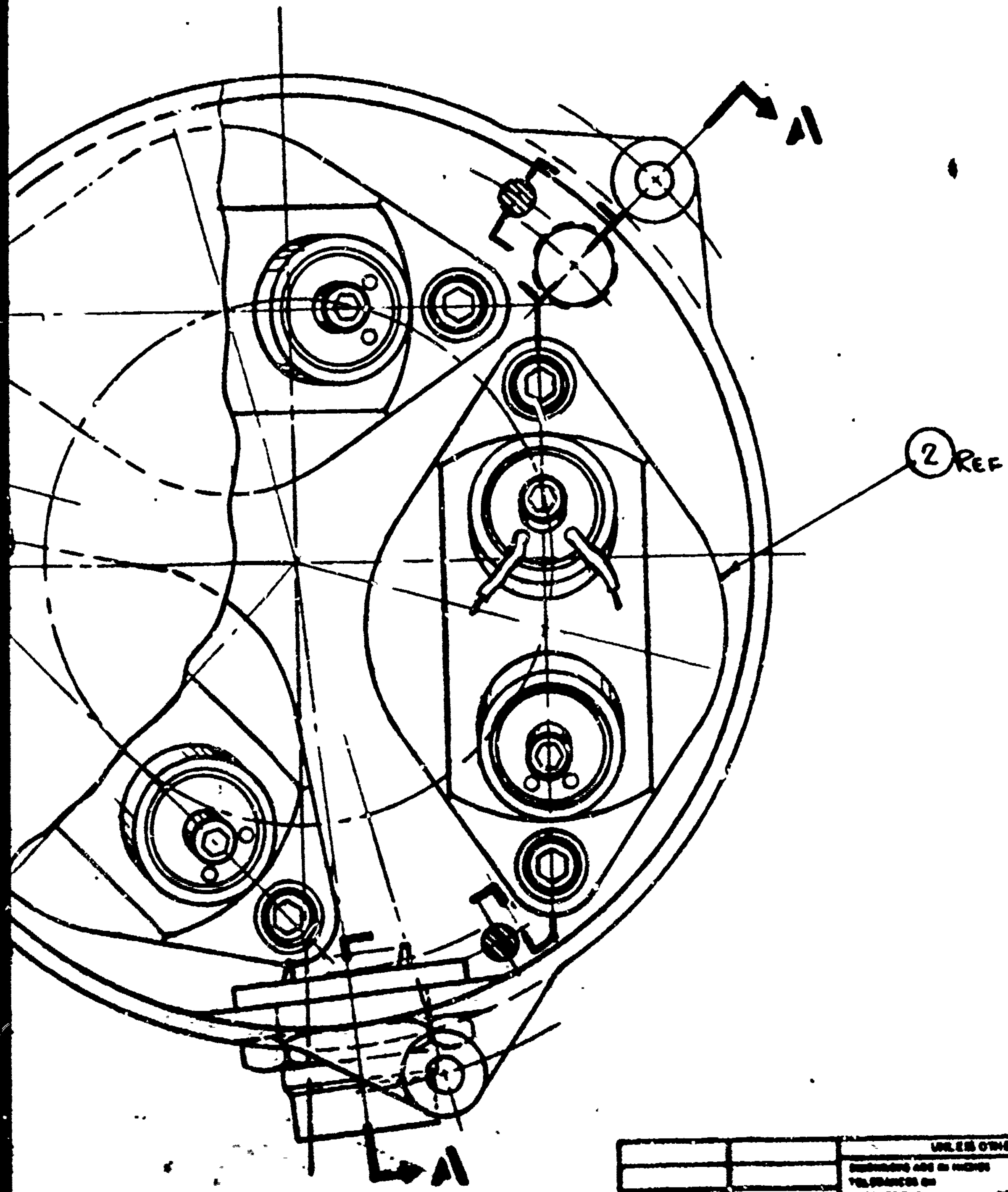

BACK VIEW
WITH COVER BROKEN AWAY

	FIND NO.	PART NO.	NO. REQD		
	19		6		WASHE
	18		A/R		WIRE
	17		A/R		WIRE
	16		1		CONN
	15		9		SCRE
	14		3		SEAL
	13		6		SEAL
	12		2		VALVE
	11		1		SEAL
	10		3		SEAL
	9		1		COVER
	8		3		SCREW
	7		6		SCRE
ANGLE SENSING CRYSTAL ASSY	6		3	1	SEAL-
				3	SET S
				1	RETAI
				1	WASH
				1	CRYST
				1	CRYST
WAVE PLATE ASSY	5		2	1	RETAIN
				2	WASH
				1	PLATE
				1	PLATE
PRISIM ASSY	4		3	7	SET S
				1	PRISM
				1	PRISI
LED LENS ASSY	3		6	2	SCREW
				1	SCREW
				1	CLAM
				1	LED H
				1	LED-S
				1	LED-T
				1	LED-G
				1	LENS W
				1	LENS M
				1	LENS
				1	LENS/LED
	2		3		HOLD
	1		1		HOUS

ENGINEERING RECORDS

UNLESS OTHERWISE SPECIFIED

NEXT ASSY
USED ON
APPLICATION

ORIGINAL DATE OF DRAWING MAR. 7, 1977

(OA

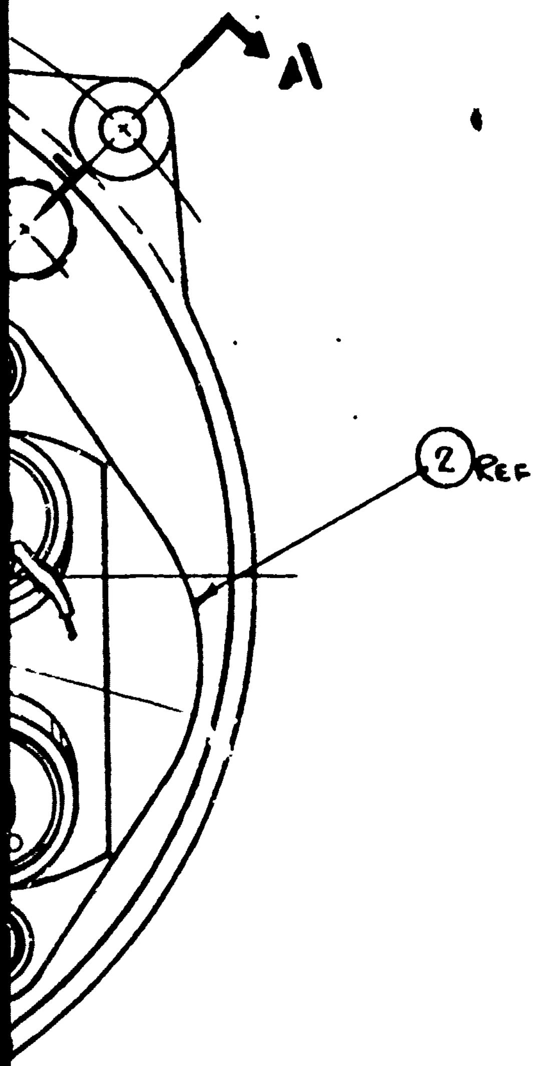

	FIND NO.	PART NO.	NO. REQD		DESCRIPTION	MIL-NO.	MATERIAL
	19		6		WASHER - FLAT	[illegible] OR EQUAL	ALLOY STEEL
	18		A/R		WIRE - BLACK	MIL-C-27500	—
	17		A/R		WIRE - RED	MIL-C-27500	—
	16		1		CONNECTOR	MIL-C-26482	—
	15		9		SCREW-SOCKET HD	MS51051 OR EQUAL	ALLOY STEEL
	14		3		SEAL-"O" RING	MIL-R-7362	NITRILE (BUNA-N)
	13		6		SEAL-"O" RING	MIL-R-7362	NITRILE (BUNA-N)
	12		2		VALVE	—	STEEL
	11		1		SEAL "O" RING	MIL-R-7362	NITRILE (BUNA-N)
	10		3		SEAL "O" RING	MIL-R-7362	NITRILE (BUNA-N)
	9		1		COVER	MIL-A-19005A	AL-ALLOY 6063
	8		3		SCREW - SOCKET HD CAP	MS51051 OR EQUAL	ALLOY STEEL
	7		6		SCREWS-SOCKET HD CAP	MS51051 OR EQUAL	ALLOY-STEEL
ANGLE-SENSING CRYSTAL ASSY	6		3	1	SEAL "O" RING	MIL-R-7362	NITRILE (BUNA-N)
				3	SET SCREW-SOCKET HD	MS51051 OR EQUAL	ALLOY STEEL
				1	RETAINER	MIL-A-19005A	AL-ALLOY 6063
				1	WASHER-(CRYSTAL)	—	TEFLON
				1	CRYSTAL MOUNT	MIL-A-19005A	AL-ALLOY 6063
				1	CRYSTAL-ANGLE SENSING	—	—
WAVE PLATE ASSY	5		2	1	RETAINER	MIL-A-19005A	AL-ALLOY 6063
				2	WASHER-(PLATE)	—	TEFLON
				1	PLATE-HOLDER	MIL-A-19005A	AL-ALLOY 6063
				1	PLATE ¼ WAVE	—	—
PRISIM ASSY	4		3	7	SET SCREW-SOCKET HD	MS51051 OR EQUAL	ALLOY-STEEL
				1	PRISIM-MOUNT	MIL-A-19005A	AL-ALLOY 6063
				1	PRISIM-WOLLASTON	—	—
LED LENS ASSY	3		6	12	SCREW SET-SOCKET HD	MS51051 OR EQUAL	ALLOY-STEEL
				1	SCREW SOCKET HD CAP	MS51051 OR EQUAL	ALLOY-STEEL
				1	CLAMP-WIRE	—	NYLON
				1	LED HOLDER	MIL-I-16923	STYCAST
				1	LED-SOLDER LUG	—	BRASS
				1	LED-T.I. FOR PITCH & YAW CHANNEL	—	—
				1	LED-GE. FOR ROLL CHANNEL	—	—
				1	LENS WASHER	—	TEFLON
				1	LENS MOUNT	—	NYLON
				1	LENS	—	—
				1	LENS/LED/HOLDER	MIL-A-19005A	AL-ALLOY 6063
	2		3		HOLDER-TRANSMITTER	MIL-A-19005A	AL-ALLOY 6063
	1		1		HOUSING-TRANSMITTER	MIL-A-19005A	AL-ALLOY 6063

BILL OF MATERIAL FIG. 7.3-1

SIZE ENGINEERING RECORDS	UNLESS OTHERWISE SPECIFIED DIMENSIONS ARE IN INCHES TOLERANCES ON FRACTIONS DECIMALS ANGLES	ORIGINAL DATE OF DRAWING MAR. 7, 1977	TRANSMITTER ASSY (OAMS) BACK MOUNTED
NEXT ASSY / USED ON			MICHOUD OPERATIONS
APPLICATION		SCALE 2:1	0M1200 SHEET 1 OF 1

3

4

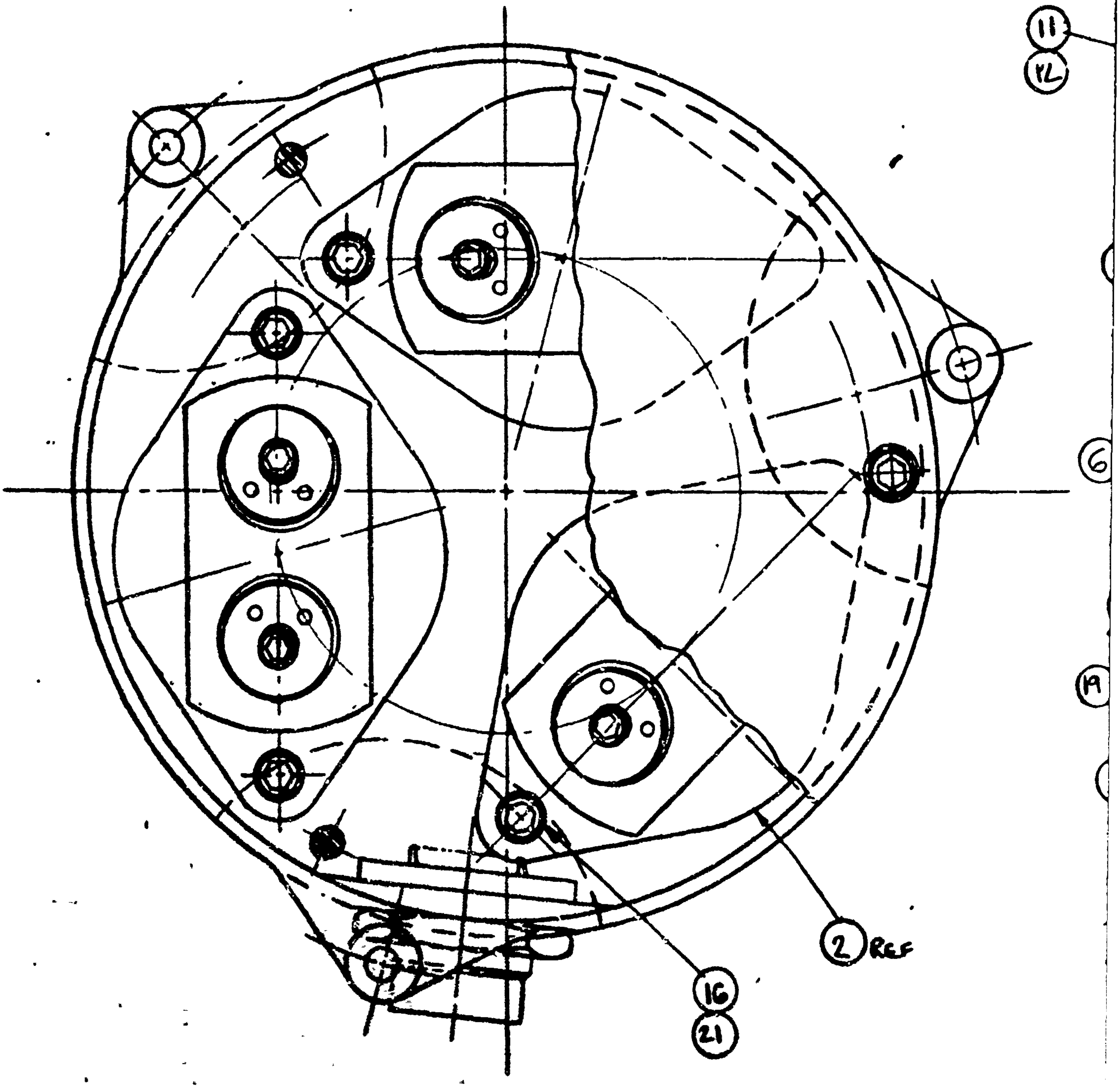
11
12
6
19
2 REF
16
21

REAR VIEW
(COVER & P.C. BOARD REMOVED)

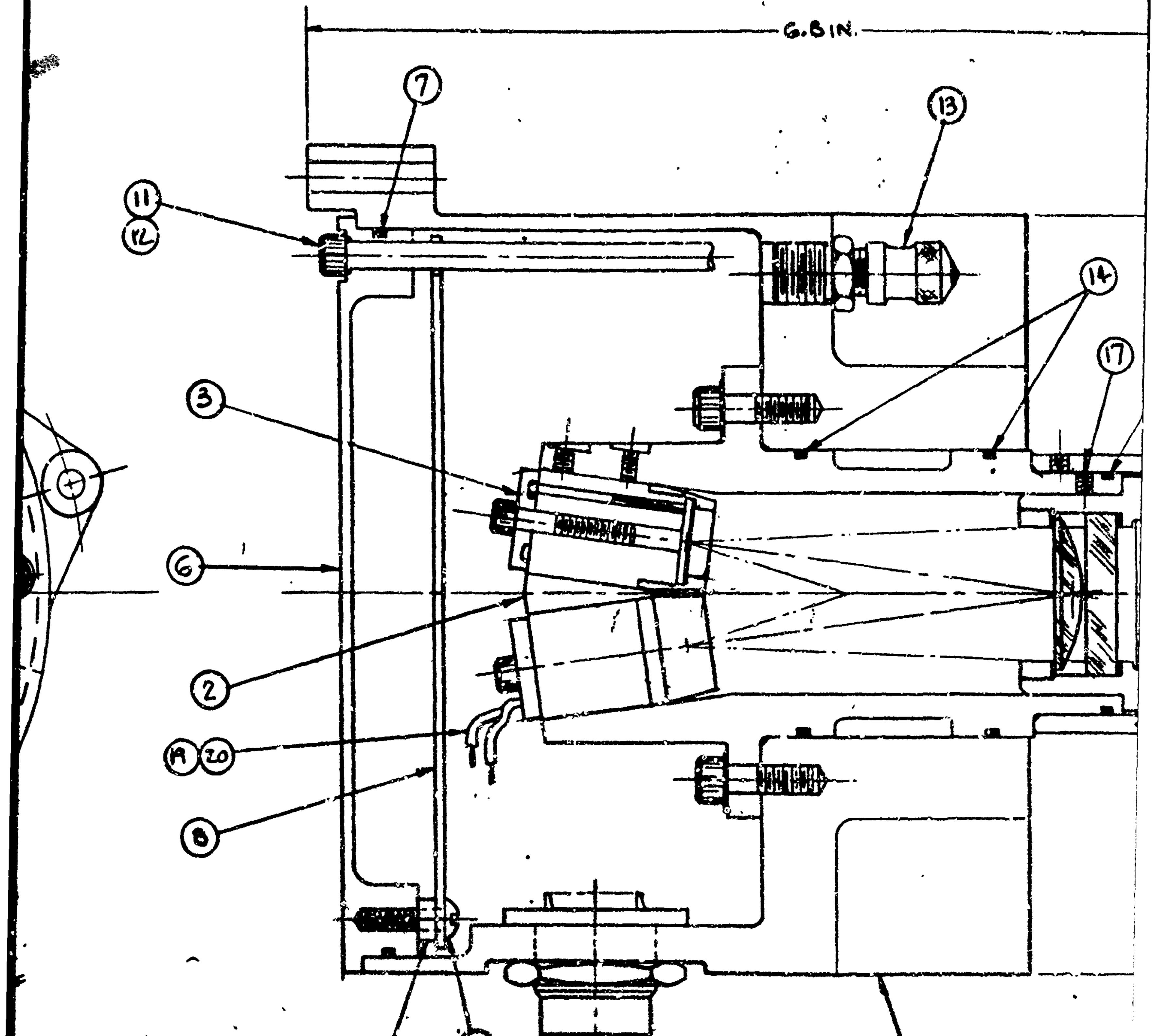
6.8 IN.
7
13
11
12
14
17
3
6
2
19
20
8
10
9
18
1

SECTION A - A

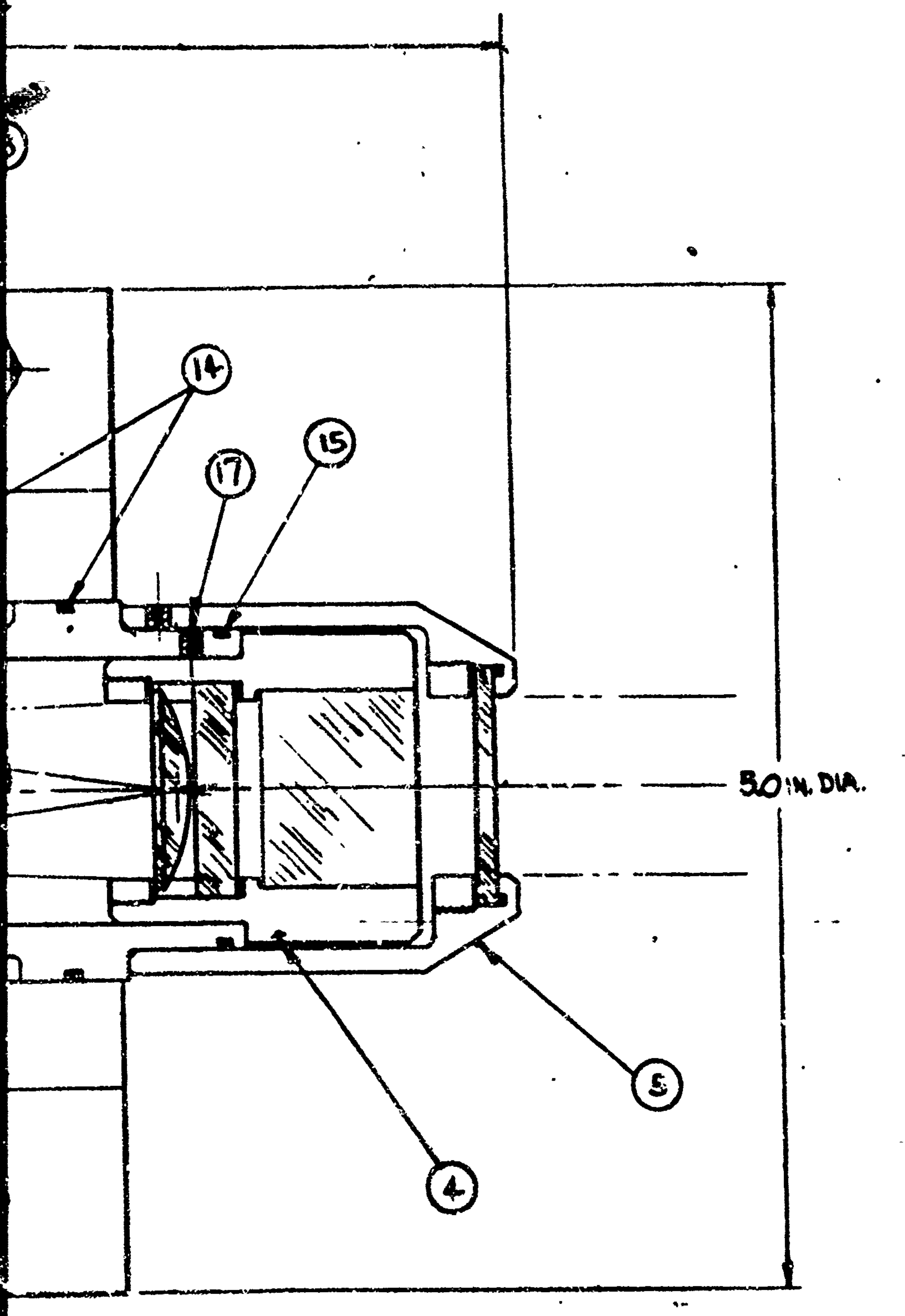

	21		9		WASHER- FLAT
	20		A/R		WIRE- BLACK
	19		A/R		WIRE - RED
	18		1		CONNECTOR
	17		45		SCREW-SET S
	16		6		SCREW-Sock HD
	15		3		SEAL - "O" RING
	14		6		SEAL-"O" RING
	13		2		VALVE
	12		3		SEAL-"O" RING
	11		3		SCREW-Sock H
	10		3		STANDOFF
	9		3		SCREW-Round HD
	8		1		P.C. BOARD
	7		1		SEAL-"O" RING
	6		1		COVER
ANGLE SENSING CRYSTAL	5		2	3	SCREW - SET Sock
				1	SEAL-"O" RING
				1	WASHER
				1	RETAINER
				1	CRYSTAL-ANGLE S
				1	CRYSTAL/MOUNT
LENS PLATE PRISM ASSY	4		3	3	SCREW-SET SO
				2	WASHER-
				1	ADAPTER
				1	RETAINER
				1	PRISM-WOLLAST
				1	PLATE
				1	LENS
				1	LENS/PLATE/PRISM HO
DETECTOR ASSY	3		6	1	SCREW - Socket HD
				1	CLAMP-WIRE
				1	DETECTOR MOUN
				1	DETECTOR
				1	DETECTOR HOL
	2		3		HOLDER- RECEI
	1		1		HOUSING- RECE
	FIND NO.	PART NO.	NO. REQD		

BILL OF MA

UNLESS OTHERWISE SPECIFIED
DIMENSIONS ARE IN INCHES
TOLERANCES ON
FRACTIONS DECIMALS ANGLES
MATERIAL
HEAT TREATMENT
FINAL PROTECTIVE FINISH

SEE ENGINEERING RECORDS

NEXT ASSY USED ON
APPLICATION

ORIGINAL DATE OF DRAWING MAR 8 1977
DRAWN
CHECKED
ENGINEER
APPROVED

RECEIV
ASSY

(OAMS) BACK

SCALE

3

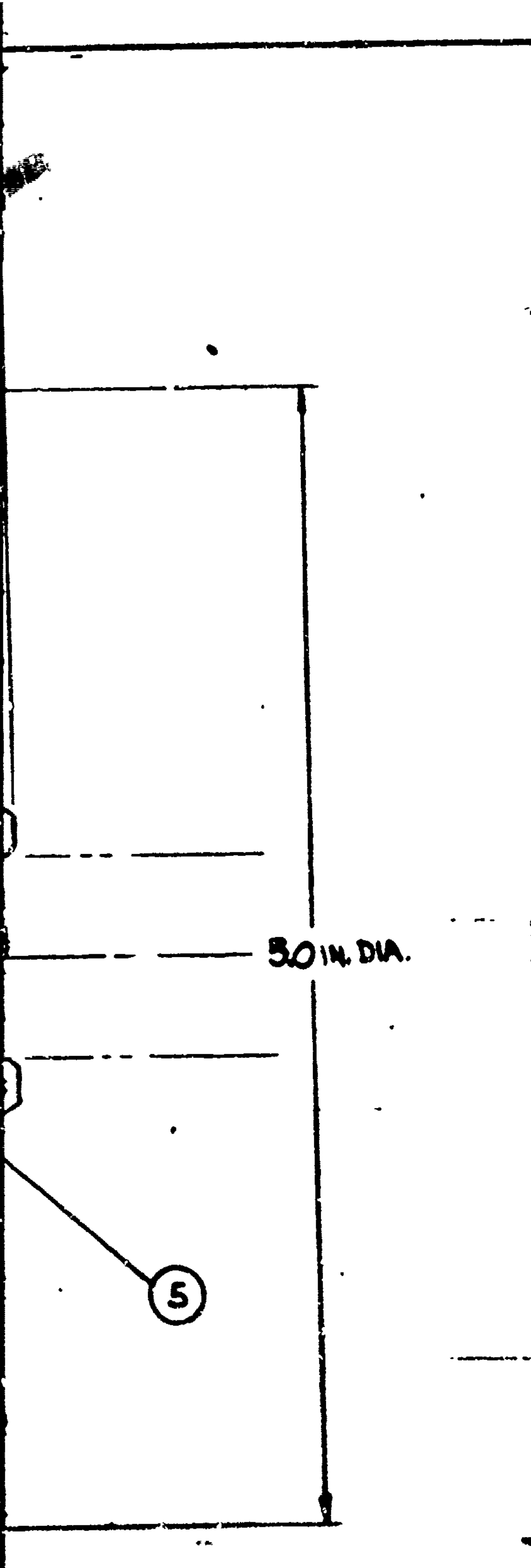

	DWG NO.	PART NO.	NO. REQD		DESCRIPTION		MATERIAL
	21		9		WASHER-FLAT	MS51031 OR EQUAL	ALLOY STEEL
	20		A/R		WIRE-BLACK	MIL-C-27500	—
	19		A/R		WIRE-RED	MIL-C-27500	—
	18		1		CONNECTOR	MIL-C-26482	—
	17		45		SCREW-SET SOCK	MS 51031 OR EQUAL	ALLOY STEEL
	16		6		SCREW-SOCK HD CAP	MS 51031 OR EQUAL	ALLOY STEEL
	15		3		SEAL-"O" RING	MIL-R-7362	NITRIL (BUNA N)
	14		6		SEAL-"O" RING	MIL-R-7362	NITRIL (BUNA N)
	13		2		VALVE	—	STEEL
	12		3		SEAL-"O" RING	MIL-R-7362	NITRIL BUNA N
	11		3		SCREW-SOCK HD CAP	MS 51031 OR EQUAL	ALLOY STEEL
	10		3		STANDOFF	—	ALLOY STEEL
	9		3		SCREW-ROUND HD MACH.	MS 51031 OR EQUAL	ALLOY STEEL
	8		1		P.C. BOARD	[illegible]	EPOXY/GLASS [illegible]
	7		1		SEAL-"O" RING	MIL-R-7362	NITRIL BUNA N
	6		1		COVER	MIL-A-11005A	AL-ALLOY 5083
ANGLE SENSING CRYSTAL	5		2	3	SCREW - SET SOCK	MS 51031 OR EQUAL	ALLOY STEEL
				1	SEAL-"O" RING	MIL-R-7362	NITRIL (BUNA N)
				1	WASHER	—	TEFLON
				1	RETAINER	MIL-A-11005A.	AL-ALLOY 5083
				1	CRYSTAL-ANGLE SENSING	—	—
				1	CRYSTAL/MOUNT	MIL-A-11005A	AL-ALLOY 5083
LENS PLATE PRISM ASSY	4		3	3	SCREW-SET SOCK	MS 51031 OR EQUAL	ALLOY STEEL
				2	WASHER-	—	TEFLON
				1	ADAPTER	—	NYLON
				1	RETAINER	MIL-A-11005A	AL-ALLOY 5083
				1	PRISM-WOLLASTON	—	—
				1	PLATE	—	—
				1	LENS	—	—
				1	LENS/PLATE/PRISM HOLDER	MIL-A-11005A	AL-ALLOY 5083
DETECTOR ASSY	3		6	1	SCREW-SOCKET HD CAP	MS51031 OR EQUAL	ALLOY STEEL
				1	CLAMP-WIRE	—	NYLON
				1	DETECTOR MOUNT	—	PLASTIC
				1	DETECTOR	—	—
				1	DETECTOR HOLDER	MIL-R-46928	STYCAST
	2		3		HOLDER-RECEIVER	-11005A	AL-ALLOY 5083
	1		1		HOUSING-RECEIVER	-11005A	AL-ALLOY 5083

BILL OF MATERIAL

FIG. 7.3-2

ORIGINAL DATE OF DRAWING MAR. 8, 1977	RECEIVER ASSY (OAMS) BACK MOUNT	CHRYSLER SPACE DIVISION
DRAWN [illegible]		MICHOUD OPERATIONS
CHECKED		0M1400
ENGINEER	SCALE	SHEET 1 of 1

UNLESS OTHERWISE SPECIFIED DIMENSIONS ARE IN INCHES TOLERANCES ON FRACTIONS DECIMALS ANGLES

MATERIAL

HEAT TREATMENT

FINAL PROTECTIVE FINISH

NEXT ASSY | USED ON

APPLICATION

ENGINEERING RECORDS

7.32
4

8.0 SYSTEM TEST AND EVALUATION

OAMS system evaluation, since Phase I final report, can be divided into three stages namely,

a. Evaluation after replacement of the detectors and the LEDs in all three channels, rebuilding of LED drive circuit, and implementation of LED control loop.

b. Complete rebuilding of the electronics in all three channels, retro-fitting of optics in the pitch channel and replacement of detectors from unsealed units to hermetically sealed units.

c. Exploratory engineering evaluation tests at Holloman AFB to determine OAMS performance envelope.

However, this report will address itself to those tests made here at the Michoud Assembly Facility. Problem areas found both at Michoud and Holloman will be discussed along with our suggested solution.

The information present here will commence with LED testing and adjustment, followed by accuracy and temperature sensitivity testing. Finally, a discussion of OAMS application and comments on OAMS performance will be presented.

8.1 LED TESTING

During Phase I OAMS testing, it was determined that the TI-SLH3 and TI -SLH4 LEDs, which are composed of GaAsP material and applied in the lateral channels, exhibited a rapid decrease in light intensity as a function of time. In the roll channel the GaAs, GE-SSL-55C, LEDs were employed and their characteristics exhibited a long life cycle. However, a need to acquire higher light output LEDs for roll channel application was genuine since a higher signal-to-noise ratio is directly correlated to an increase in light intensity. Also, the GE-SSL-55C LEDs had, by design, a less favorable heat sink dissipation property compared to others with stud mount design. Having a better understanding of LED requirements for OAMS application, a search was begun to locate LEDs that would best fit our needs for lateral and roll channel use.

As a result of this search we settled upon the Texas Instrument, Inc. LEDs. For the lateral channels we are using the GaAlAs LEDs and in roll the GaAs LEDs. Typical characteristics for these LEDs are shown in Table 8-1. All of these LEDs are stud mounted for temperature sink purposes.

Table 8-1 LED Characteristics

Channel	Part No.	Center Wave Length	Continuous Power Rating @25°C
Pitch	SLH-19	810 nm	3 mw @ 100 ma
Roll	SL1162-4	935 nm	17 mw @ 100 ma
Yaw	SLH-20	850 nm	3 mw @ 100 ma

The linearity of light output to applied drive current varies some from LED-to-LED in each type. The linearity progressively decreases for lower currents; operations below 10 ma are not recommended for OAMS application. Typical linearity for the SL-1162-4, flight qualified, at about 30 ma is -0.4% and at 21.5 ma is -1.3%. No firm linearity figures are available yet for the SLH-19 and -20 flight qualified LEDs, but from conversation with TI these LEDs should be less than 2½ per cent over the current operation range of 10 ma to 215 ma.

The operating half-life of LEDs is inversely proportional to the square of the operating current. Because of this a compromise between linearity and half-life must be made and we have chosen 100 ma as the quiescent operating point. For this current the estimated half-life for GaAlAs LEDs are about 25,000 hrs and for the GaAs LEDs are about 50,000 hrs. In connection with LED life we ran an independent 1000 hrs, but limited in quantity of LEDs, burn-in test during the summer of 1975 on the SLH-19 and -20 LEDs with a drive current of 200 ma dc. Two LEDs per type were tested and the resulting decrease in light output from zero hours is illustrated in Table 8-2. This data indicates that the most rapid drop occurs at the two hundred hour range and thereafter the drop is less abrupt. Past 1000 hrs Air Force Reports (AFAL, TR-72-159 and TR-73-251) indicate that a linear decrease somewhere around 1.8 to 3.4 per cent per 1000 hrs can be expected. The test data quoted is for two LEDs up to 6000 hrs. of testing and operated at 250 ma.

Table 8-2 LED Burn-In Test (1000 hrs)

SLH-19		SLH-20	
Device A	Device B	Device A	Device B
24% @ 260 hrs	31% @ 260 hrs	21% @ 224 hrs	31% @ 260 hrs
30% @ 458 hrs	33% @ 524 hrs	24% @ 484 hrs	33% @ 524 hrs
34% @ 740 hrs	38% @ 776 hrs	25% @ 748 hrs	41% @ 776 hrs
35% @1000 hrs	45% @1000 hrs	28% @1000 hrs	44% @1000 hrs

The SLH 19 and -20 LEDs are nonamphoterically built. Amphoterically built devices are built by growing layers of GaAs on a silicon wafer over a wide temperature range. Depending upon the temperature range it will be either an N- or P-type device. The nonamphoterically built device is made by diffusing zinc into the N-type wafer. Therefore, this means that upon heating and cooling the device does not change from a P- to N- or N- to P-type. The SL-1162-4 LEDs are amphoterically built and are more efficient and have a higher output irradiance because of this construction. The disadvantage here is that they must be protected against radiation heating to prevent changing state. The efficiency of the GaAlAs LEDs are about 1.7 per cent while that of GaAs is about 3.5 per cent.

From Table 8-2 it can be deduced that, when pairing of LEDs for CONT and REF purposes, in the OAMS it is desirable that the intensity decay rate as a function of time tracks. This will prevent the CONT voltage V_c from prematurely reaching an extreme at an early stage of OAMS operation. In addition to this matching, it is also important to test irradiance output with the actual filter used in the RCVR because some LEDs may have a high irradiance output, but are slightly mismatched, wavelength wise, with the filter.

Most important here for OAMS is the LED light pattern adjustment. By choice we have selected 100 ma dc as the quiescent current and the REF LED drive circuit has been designed to maintain this value constant. The REF LED is adjusted first; the light pattern detected at the RCVR is adjusted by a combination of focusing, defocusing, and rotation of the LED light image at the XMTR until a symmetrical d.c. light pattern is obtained. The symmetry is best determined by pitching and yawing the XMTR by ± 20 minutes and recording the data for comparison with the CONT LED. Once this condition is satisfied the REF LED is turned off and the CONT LED is turned on with the control loop opened and V_c chosen to operate the LED at 100ma d.c. The same procedure as that for the REF LED pattern is followed except that an additional constraint must be imposed. This constraint requires that the CONT LED light intensity matches that of the REF LED when pitch and yaw motions are executed at the XMTR. This match is verified by varying V_c which in turn controls the amount of current driving the CONT LED. Without this constraint LED balance is not possible for some pitch and yaw motions at the XMTR and thus offset errors will occur when the XMTR is rotated. Herein lies a major disadvantage with the Phase I geometrical optics/eccentricity configuration. With this configuration, which is now in the roll and yaw channels, it is difficult to match the REF and CONT LED light pattern and success is often dependent upon trial and error with other LEDs of the same wavelengths. The new optics now installed in the pitch channel enables easy adjustment and matching of the REF and CONT LED pattern.

8.2 SYSTEM TEST

System test for OAMS at MAF can be subdivided into two distinct phases as described in the introduction of Section 8.0. The purpose here is to present a summary of pertinent data and comments concerning the results. In this way a continuity in our rationale for various decisions during OAMS development can be better understood.

8.2.1 Brassboard No. 1 Testing

Towards the end of OAMS Phase I effort several crucial and recognizable problems emerged during testing. These problem areas were: 1) the need for a control loop that performed LED balance and maintained a constant modulation as described in Subsection 5.2.2, 2) securing three distinct wavelength LEDs that have long life and emits higher irradiance and 3) determing the source of large system output noise and finding a possible fix. The electrical noise was of such magnitude that a one hz lowpass filter had to be used during system calibration readings. After some investigation the generation of noise was attributed to the pre-amp circuit and a damping resistor R_d and circuit as described in Subsection 5.3 was implemented. Signal-to-noise ratio was further increased by replacement of the existing smaller active area and higher junction capacitance, C_j, detector by the RCA-C30852 unit which in effect increased the responsivity by about 70 per cent, lowered C_j from 500 pf to 250 pf, and increased the active area from $5mm^2$ to $20mm^2$. The new detectors were ordered without the window since the cap size was too large to fit in the RCVR barrel. However, later on during temperature testing it was found that unsealed detectors are subject to large responsivity changes due to humidity and impurities in the environment. Location and subsequent purchase of long life, high reliability LEDs and for roll higher irradiance output, lead to a further increase in signal-to-noise ratio.

In the latter part of 1975 and early 1976 Brassboard No. 1 was modified with new LEDs, detectors, pre-amp, and a control loop. In January/February 1976 the optics were aligned and on February 24 calibration curves were taken for pitch, roll and yaw with a range of 15.2 meters. The results of these curves will not be presented here since they are basically similar to that of Brassboard No. 2 and the differences will be taken up when discussing the curves of Brassboard No. 2.

Roll channel cross coupling was analyzed experimentally to establish its source. After much effort in June 1976 it was established that the effect was from the Wollaston Prisms located in the RCVR and XMTR. The polarization planes (vertical and horizontal) are nonorthogonal and this claim was substantiated from experiments and confirmed by the manufacturer. The effect of nonorthogonality is discussed in Subsection 5.1.2.2. During the process of this experiment we rotated the RCVR Wollaston and it did minimize cross coupling to some degree when the XMTR was pitched. However, the long term effect of this exercise was to transfer the larger portion of crosscoupling from the pitch axis to the yaw axis. This will be confirmed in the calibration curve analysis.

Following the crosscoupling effort, temperature testing of the three units (RCVR, XMTR and electronics box) by heating and cooling each from 4.44°C to 37.8°C (40°F to 100°F) was performed. The test results indicated that about 100 arc-sec. variations occurred over the temperature range when testing the XMTR. The RCVR unit showed variations of about 20 arc-sec. over this range. The electronic unit had about 20 arc-sec and 53 arc-sec variations for pitch and roll channels, respectively. The yaw channel sum board developed an anomaly during cooling, thus no direct comparison of the yaw electronics can be made. The purpose of this test was to identify the sources causing any variations and to get some feel of OAMS under such an environment.

By analysis of the data and through subsequent component testing and special localized testing on OA it was possible to isolate some of the contributing factors to system offset. These are:

a. LED control loop balance was not tight enough to compensate for changes in irradiance/detector/pre amp balance changes (see Equation Interpretations Subsection 5.1.1.4).

b. The GaAs and GaAlAs LED efficiency changes over the temperature range are about 63% and 90%, respectively. Since the LEDs were not paired according to similar tracking characteristics, the control voltage V_c varied and the results was a relaxation in the levels of LED balance. This problem was somewhat aggravated by the 427K divider whose phase changes were much larger than the current 436B divider (see Eqs. (5-18c) and (5-19c)).

c. The responsivity of the detectors were permanently altered due to the deposit of moisture on the active area when cooling. This was particularly true for the yaw channel since an unbalance of 50% was later confirmed. Also, a marked increase in system noise was noted thereafter.

d. Optics/mechanical effects were suspected after a simulated LED intensity change of 40 per cent was performed with little change in system output at various angular settings. This was accomplished by varying the REF LED current and allowing the CONT LED to follow. This test was particularly significant because it decoupled the electronics from the mechanical fixture (since no mechanical motion was involved). Also, it proved that LED nonlinearity is not a significant contributor to system scale factor changes.

The only significant changes recommended, other than that already planned in the new electronics, were 1) to eliminate all trim pots, especially in the pre amp circuit, 2) replace the detectors with those hermetically sealed, and 3) to increase loop gains. Because of a change in detector cap design hermetically sealed units were installed in November 1976. These sealed detectors virtually eliminated changes in detector/pre amp balance due to humidity and temperature changes.

8.2.2 Brassboard No. 2 Testing (Advanced Brassboard)

Following debugging and adjustment of the electronic circuits for proper gains, voltage levels, phases, and signal scaling, another temperature testing effort was begun. Due to lack of a cooling unit at this time only heating of the RCVR, XMTR and electronics units from 23.9°C to 37.8°C (75°F to 100°F) was accomplished. Table 8-3 lists a summary of the changes due to temperature effects.

Table 8-3 OAMS System Output at 37.8°C

Units	Pitch (arc-sec)	Yaw (arc-sec)	Roll (arc-sec)
RCVR	-30	-16	31
XMTR	37	-25	10
Electronics	0	0	0

Mechanical corrections due to movements of the RCVR and XMTR during heating where obtained by auto-collimators and the data of Table 8-3 was altered to accommodate these changes. The heating technique used here was somewhat different, than the previous temperature test, since instead of enclosing the RCVR or XMTR with an insulated heater box; we simply wrapped the rear portion of the unit with the heating coil. The Burleigh star gimbal mount now used for RCVR mount prohibited the use of the previous heater box. The electronic unit was heated by the same box used in Brassboard No. 1 testing.

Another series of tests were made to isolate the source of deviation. No unexpected changes were found in the electronics that could contribute to there changes. The pre amp circuits were individually heated and the observed effects to the system output were negligible. However, one common effect was noted when the RCVR and XMTR are heated. The irradiance/detector/pre amp unbalance changes from ambient were unusually large, as shown in Table 8-4. From Figure 5-5, K (G_dG_x/G_sG_f) is about 24 to 32 times larger in roll than that of the lateral channels. Therefore, changes in the roll channel will be amplified by 7 to 11 times that of the lateral channels, thus a larger number for unbalance is obtained. With the use of Eqs. (5-26) and (5-39) and the LED balance ratio, u, found in Table 5-5, it can be shown that, the irradiance/detector/pre-amp unbalance of Table 8-4 would yield with both LEDs on, an error of about one arc sec for all cases, except that of the RCVR roll where the error is calculated to be about -12 arc-sec.

Table 8-4 Changes In Irradiance/Detector/Pre Amp Unbalance at 37.8°C

Units	Pitch (arc-sec)	Yaw (arc-sec)	Roll (arc-sec)
RCVR	-69	-72	-1167
XMTR	127	-50	150

Since the relative responsivity, between the horizontal and vertical detectors, will change less than 0.25 per cent over such a temperature range and from the heat test on the pre amp which showed negligible changes, it can be concluded that the changes are either mechanical, optical or a combination of mechanical and optical. Possible solutions will be discussed later in this section.

On January 19, 1977, before transportation and setup of OAMS at Holloman AFB, calibration curves were taken as shown in Figure 8-1 to 8-5. Upon examination of these curves there are several key points to note:

a. The scale factors are not one arc-sec/mv since fixed resistor were used in gain adjustments and in pitch and yaw the deviations are also in accordance with the $\sin k\theta$ term of Eq. (5-26).

b. pitch and yaw crosscoupling magnitudes are directly related to LED light distribution, RCVR and XMTR ASC adjustments, and quarter-wave plate adjustments.

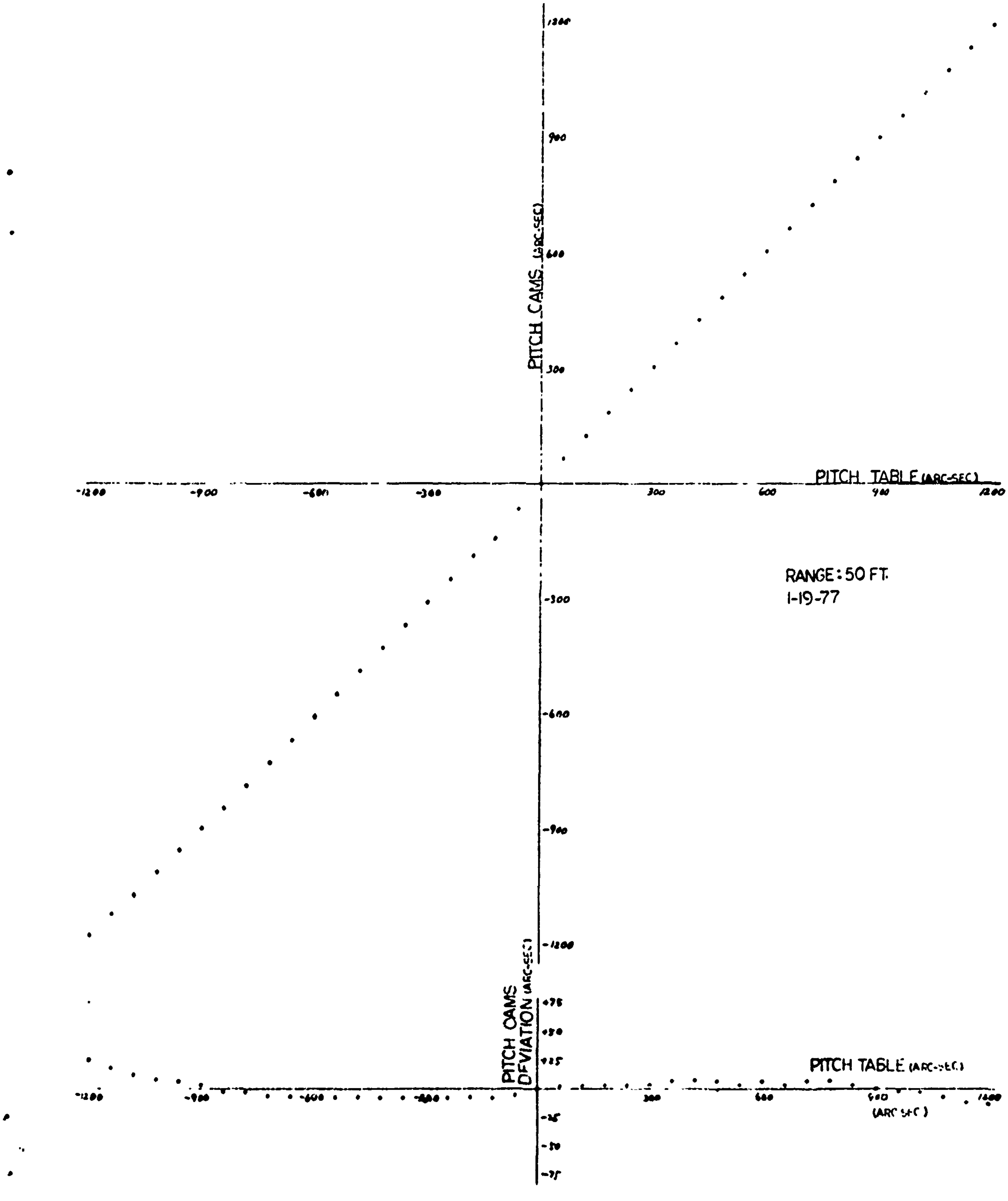

RANGE: 50 FT.
1-19-77

FIGURE 8-1 PITCH CALIBRATION CURVES

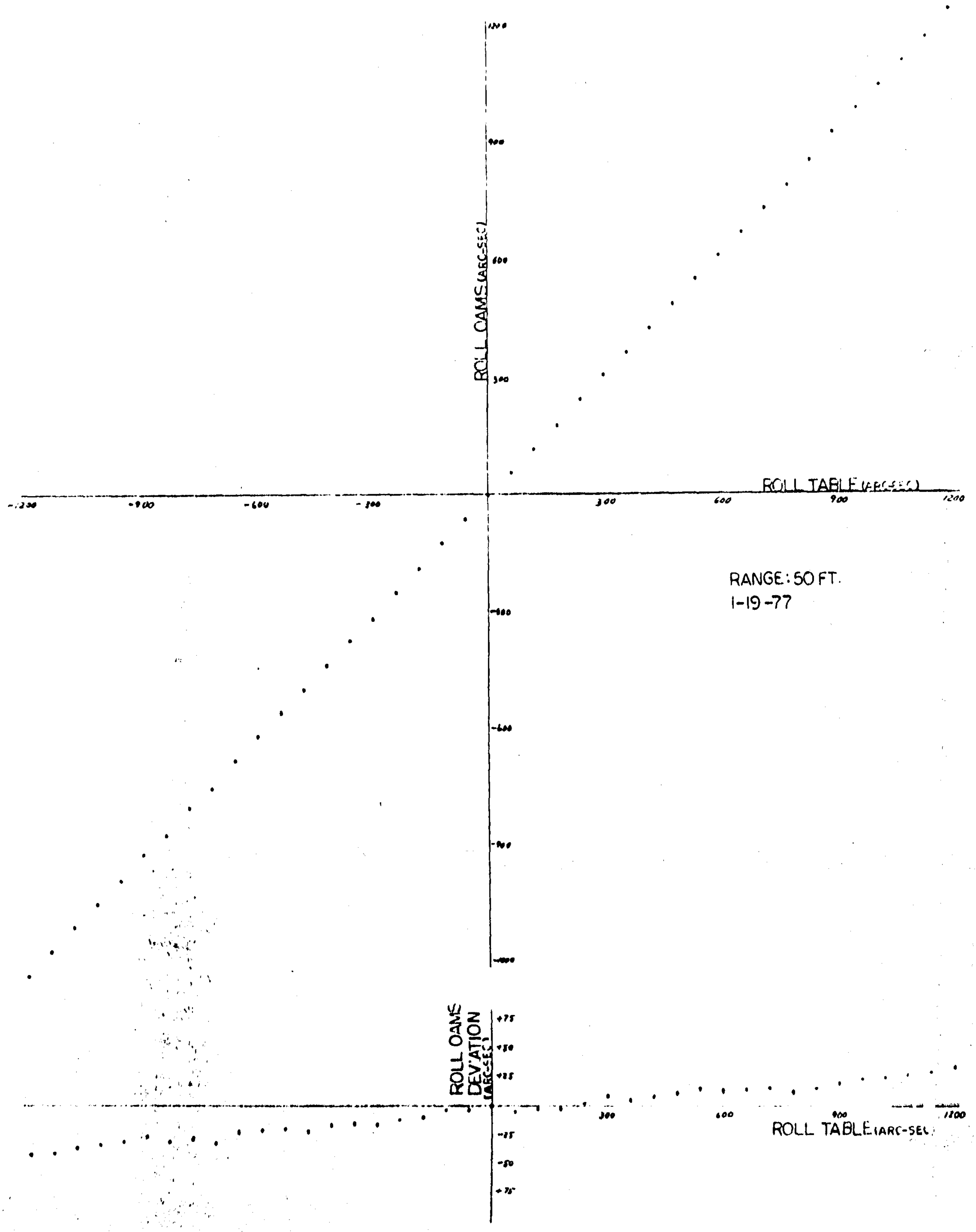

FIGURE 8-2 ROLL CALIBRATION CURVES

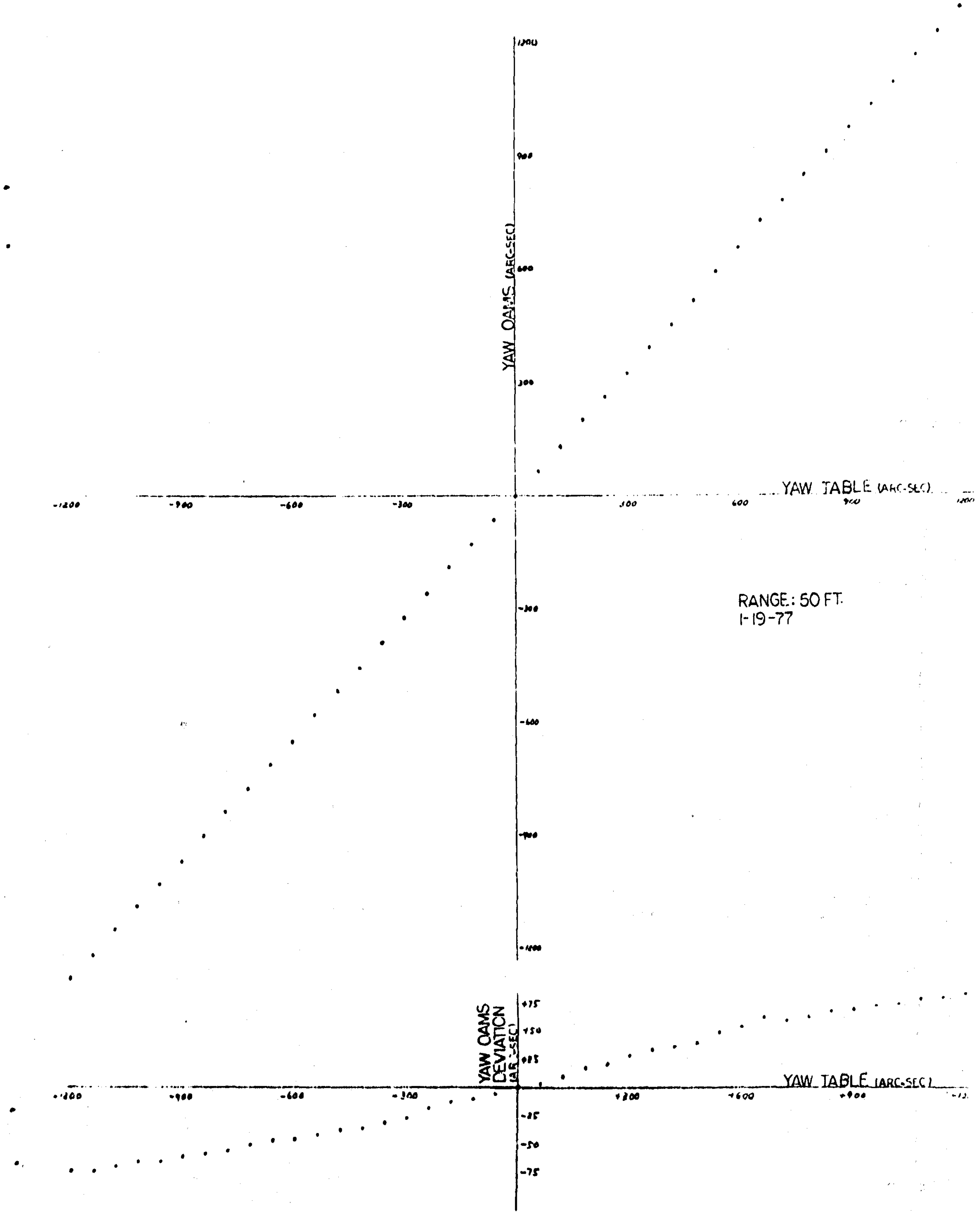

FIGURE 8-3 YAW CALIBRATION CURVES

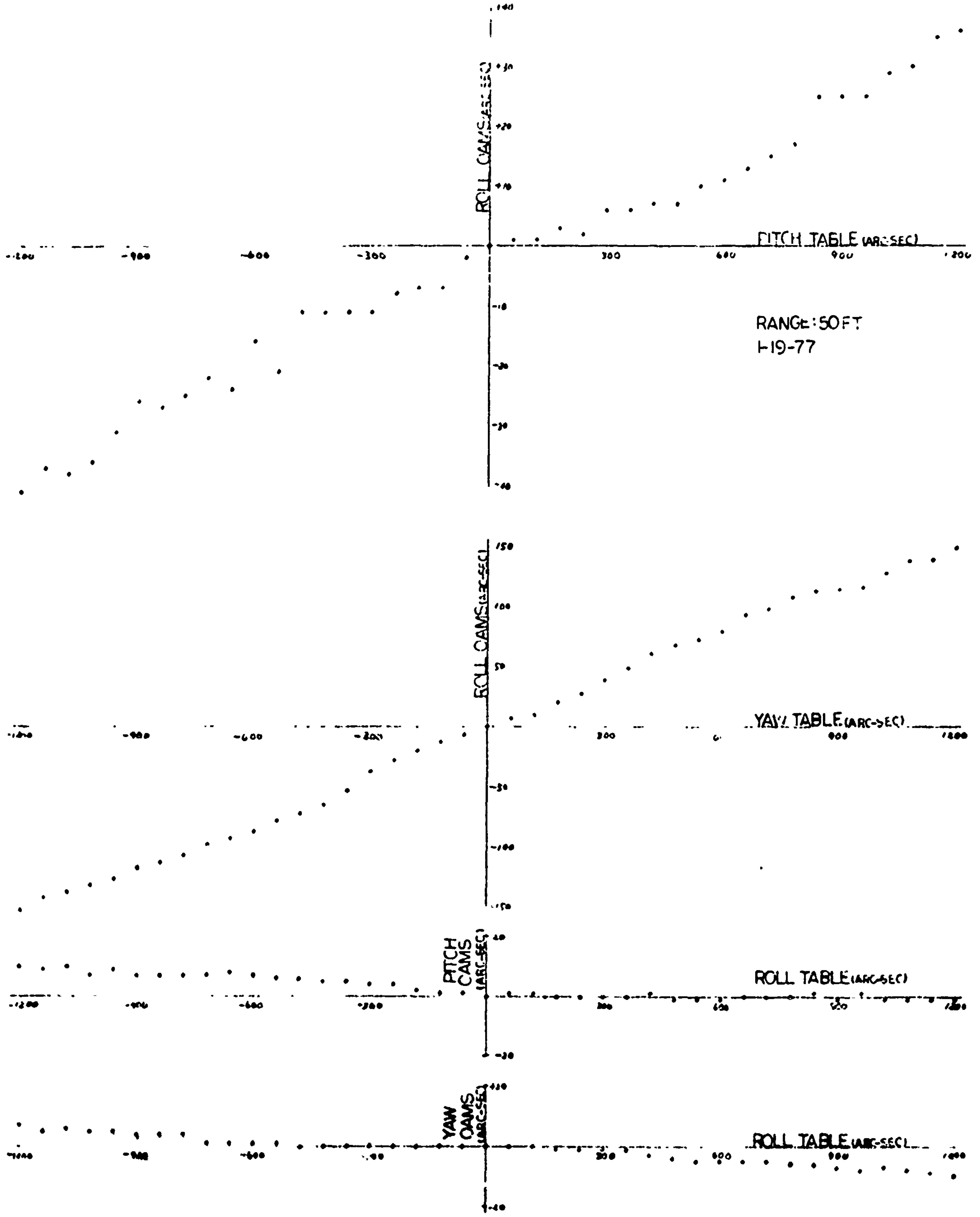

FIGURE 8-4 PITCH, ROLL AND YAW CROSS COUPLING

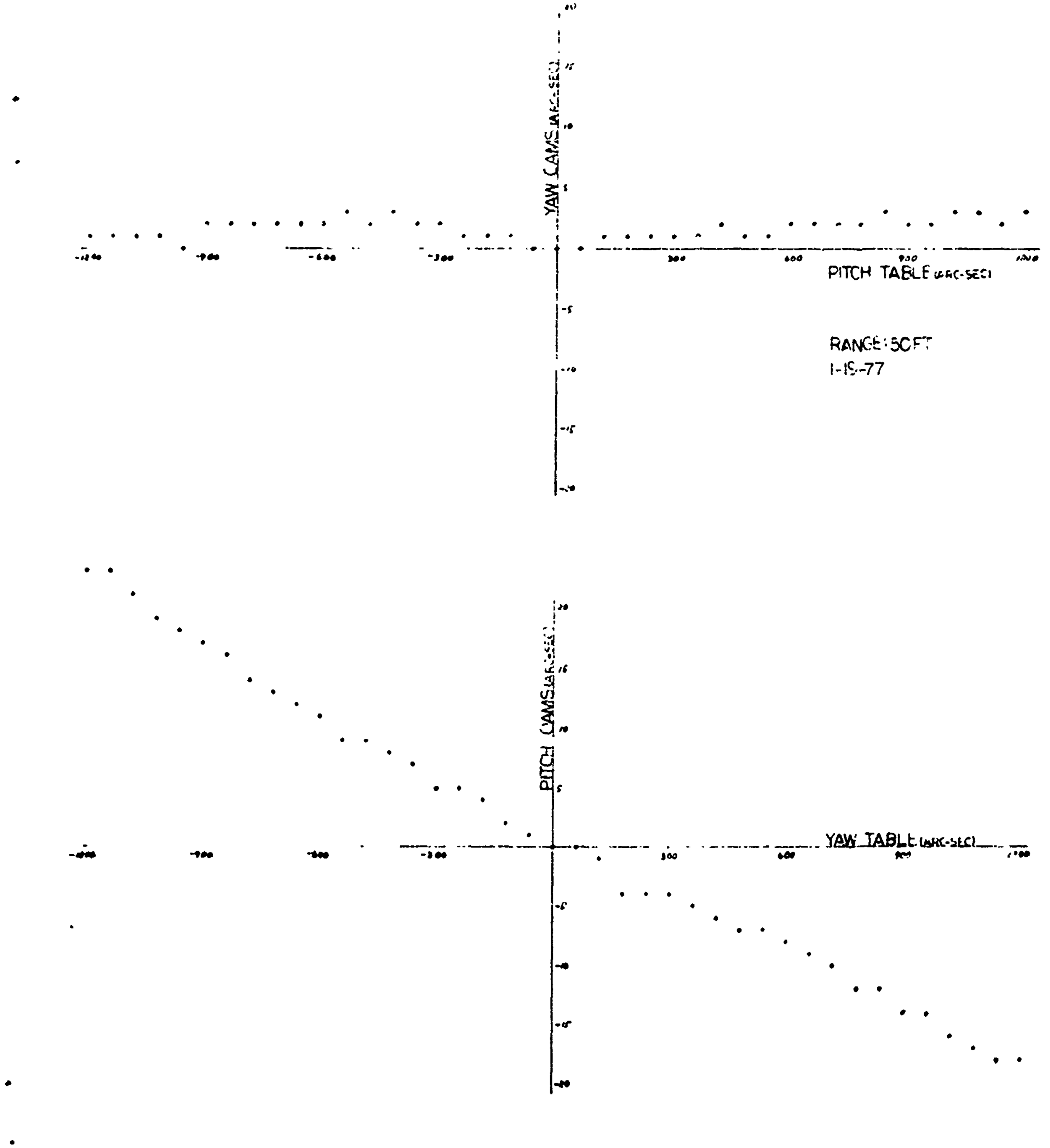

FIGURE 8-5 PITCH AND YAW CROSS COUPLING

c. crosscoupling into roll as a function of pitch and yaw table movement is directly related to RCVR and XMTR Wollaston prism adjustments, LED light distribution and degree of prism nonorthogonality (see Eq. (5-56)).

A noticeable difference between Brassboard No. 1 and Brassboard No. 2 curves is the crosscoupling into the roll channel when pitching and yawing. For Brassboard No. 1 the larger crosscoupling occurred when pitching and for Brassboard No. 2 it occurred when yawing. For this case the crosscoupling magnitude was 48 per cent larger in Brassboard No. 2 than for Brassboard No. 1. The reason for the switch in crosscoupling magnitude, as described, is because of the 90° rotation of W_R during our Wollaston nonorthogonality experiments. All other curves for Brassboard No. 2 are similar to those of Brassboard No. 1.

8.3 OAMS APPLICATION

From the data present in this section and the anticipated results from the Holloman AFB testing there are several outstanding problems remaining with OAMS. The purpose of this subsection is to define these problems and outline suggested approaches that can be taken to minimize their effects. However, a few words concerning the OAMS design/application criteria are in order before the discussion of these problems and in this way a fuller understanding of OAMS capability.

OAMS research and development effort stems from the need of the U.S. Air Force to have a device that can measure small three-axis rotational movements within a range of 15 arc-minutes; have an accuracy of 9 arc-sec; operate within a 10 hz dynamic response; withstand the transition from a missile launch environment to that of outer space (nonoperational during launch phase); operate in a radiation environment including some degree of nuclear radiation; operate at a separation range of 15.2 meters (50 feet); maintain accuracy, for RCVR traverse movements of ± 6.35 cm (± 2.5 inches), about all 3-axis; operate over a 4.44°C to 37.8°C (40°F to 100°F) temperature range; and consume about 20 watts of power from an unregulated 28 VDC source. The unique feature of OAMS is that it can measure simultaneously "roll" as well as pitch and yaw angular motions which no other system to date has been able to accomplish without extensive instrumentation, higher power consumption, and higher volume and weight. Low power consumption requirements dictated that the light source be from LEDs with a long half-life and that their operating currents be as low as possible without compromising performance. Half of the power consumption is in the electronics and the other half is lost in the DC/DC conversion process to the ±15 VDC and ±7.5 VDC sources. If power and weight constraints can be relaxed lasers can be used instead of LEDs and a corresponding increase in signal-to-noise ratio will result, thereby enabling much higher accuracy measurements with OAMS and at increased ranges.

A basic application of OAMS in a close-loop control scheme is to supply continuous angular motion measurements for a three axis position system, such as a large telescope mount, antenna, etc. From the calibration and temperature data taken, compensation for voltage scaling, crosscoupling and variation of system output due to temperature changes must be provided.

Naturally, the objective in the OAMS design is to minimize crosscoupling and variation due to temperature, however there are physical and adjustment limitations that may prevent the OAMS from operation in an ideal mode. Steps to be taken to trim unwanted behaviors in the OAMS will be outlined later in this section. If we assume for the moment that variations are present and deterministic, then it is possible to compensate for these errors by a program that calculates the necessary corrections by use of empirical formulas. These formulas can be derived to express angular movements in pitch, roll and yaw as a function of OAMS system output provided that the variations are predictable and lends itself to curve fitting in the sense of least square. Therefore, linear regression equations of angular movement θ on system output voltage (V_o) can be obtained for all three types of angular movements that influence a given channel. In addition linear regression equations as a function of temperature for both the RCVR and XMTR can be obtained if sufficient data points are taken. Equations (8-1) through (8-4) describe the methodology.

$$\theta_{ji} = b_{ji} + m_{ij}V_{oi} \tag{8-1}$$

$$\theta_{tj} = b_{tj} + m_{tj}\Delta T \tag{8-2}$$

$$\Delta T = 75^{o}F - T \tag{8-3}$$

$$\begin{aligned} \theta_j &= \Sigma\theta_{ji} + \theta_{tj} \qquad (8\text{-}4) \\ &= b_j + m_{pj}V_{op} + m_{rj}V_{or} + m_{yj}V_{oy} + \theta_{tj} \end{aligned}$$

where,

j = subscript identifying monitored axis (p - pitch, y - yaw or r - roll)

i = crosscoupling subscript p, y, and r

θ = angular rotation; arc sec.

b = intercept; arc sec.

V_{oj} = system output voltage; mv

m_{ij} = slope of linear equation; arc sec./mv

ΔT = temperature change; ^{o}F

T = temperature of RCVR or XMTR; ^{o}F

Equations (8-1) and (8-2) could take other more complex forms, depending upon the accuracy desired. In order to develop a model for θ_j, from calibration data, that will be general for all combination of movements the crosscoupling effects must be included. The procedure to follow here is to compute the curve fit equation as a function of one variable

Table 8-5 Accuracy Brassboard No. 2

Channel	θ_{ji}	b (arc-sec)	m (arc-sec/mv)	r	S (arc-sec)
Pitch	θ_{pp}	-0.293	1.002	0.99994	7.900
	θ_{pr}	2.593	-0.005	-0.92452	1.396
	θ_{py}	1.030	-0.016	-0.99674	0.979
Roll	θ_{rr}	5.548	0.972	0.99999	2.651
	θ_{rp}	2.980	0.029	0.99092	2.747
	θ_{ry}	3.463	0.118	0.99883	4.337
Yaw	θ_{yy}	-1.477	0.932	0.99998	4.176
	θ_{yr}	-2.596	-0.005	-0.96873	0.997
	θ_{yp}	0.016	0.0003	0.31298	0.750

using the calibration data, then using this equation to convert crosscoupling data to equivalent angular displacements, and finally compute the angular movement θ_j on V_{oi}. Table 8-5 summarizes the results of such a fit for ± 20 arc minutes and for Brassboard No. 2 data. The term r is the coefficient of correlation and S is the standard error of estimate V_{oi} on θ_{ji}. If $r = +1$ or -1, there is perfect correlation, that is, there is a linear relationship between the independent and dependent variable. If $r<0$ the line has a positive slope and if $r>0$ the line has a negative slope. The error estimate may be due to noise, error in instrument reading, etc. and ideally is zero. It should be noted here, that the slope for the crosscoupling in roll, when yawing, is an order of magnitude larger than the other crosscoupling terms.

Curve fitting for temperature variation were not made because of insufficient temperature data. If we average the intercept points and perform the indicated steps implied by Eqs. (8-1) and (8-4) the following approximate regression equations for pitch, roll and yaw results:

Pitch $\theta_p = 1.11 + 1.002\ V_{op} - 0.005V_{or} - 0.016V_{oy}$ (8-5)

Roll $\theta_r = 3.997 + 0.972\ V_{or} + 0.029V_{op} + 0.118V_{oy}$ (8-6)

Yaw $\theta_y = 1.352 + 0.932\ V_{oy} - 0.005V_{or} + 0.0003V_{op}$ (8-7)

Obviously a more comprehensive curve fit (for flight models) would involve more terms and would be checked for various combinations of pitch, roll and yaw movements. Also, the equations would not be the same for all OAMS units since the errors are dependent upon the individual components and upon the effort expended in alignment processes.

Should a different separation distance (range) between the RCVR and XMTR be desired several minor changes must be made. The electrical changes would involve new gain values for the CONT AMP, Sum 10 hz Filter and Differential Amp (see Figure 5-3). However, the present OAMS system can accommodate a 2:1 variation in range with no external adjustments. The limiting factor, in the reduction of range, is the increase in sum voltage V_s to such a point that the divider denominator V_x and amplifier reaches saturation and/or the control loop reaches instability (see Subsection 5.2). Also, the beam diameter will decrease, thus limiting transverse readings. For increased range the limiting factor is the decrease in irradiance at the RCVR to such a point that the system electrical noise will be dominant. For a significant change in range settings other than the present 15.2 meters refocusing of the objective lens relative to W_T is required in order to decrease or increase the diameter of the light beam at the RCVR.

The outstanding problems remaining with OAMS are:

a. Crosscoupling in all channels.

b. Temperature sensitivity of all three channels when the RCVR and XMTR are heated and cooled.

c. System offset in all three channels when relative transverse motion between transmitter and receiver occurs.

d. Light sensitivity due to background illumination that is within the optical filter spatial bandwidth and within the receiver field of view.

e. Eliminate transmitter Wollaston rejected beams.

f. Further work required on definition of error sources.

Until recently, where the electronics were rebuilt and improved methodology in alignment of LEDs, optics, and temperature testing of all three units were made, the analysis of the effects listed under Item a, b, and c was ambiguous. However, with the inherent problems of Brassboard No. 1 electronics, discussed in this section and Section 5.0, behind it is now possible to correlate these effects, to some extent, with component alignment and applications of a component or components in the OAMS mechanical/optical subsystem. The approach suggested here is systematic in the sense that affirmative steps can be taken to either eliminate or minimize certain undesirable effects and then later through experimentation identify and suggest approaches that can be used to clean up the remaining problem.

In the set-up at Holloman and at Michoud, one of the basic problems encountered is the lack of a good image quality, especially that of the CONT LED relative to the REF LED. This can be most readily understood by consideration of the initial alignment requirements for OAMS. With the receiver and transmitter mounts level and the receiver aperture within the LOS of the transmitter aperture, it is required, besides system output $V_O=0$, that the sum voltage V_S and control voltage V_C be at a mid range point. The idea here is to avoid operation of OAMS at or near extremes as far as light levels and CONT LED purposes require. Because of these basic requirements for system proper operations, the transmitter unit had to be pitched and yawed (an iterative process) until an approximate mid range point is established for V_S and V_C. Once this is satisfied the system output is zeroed (for all 3 channels) by perturbation of the receiver unit in pitch and yaw in order to offset the incident angles built in at the transmitter. Finally the transmitter mount is rolled until the roll channel system voltage $V_O=0$. The effect of this is to misalign the horizontal and vertical polarization plane of the ASC_T relative to ASC_R and for roll W_T relative to W_R. This will then, later, result in an increase in crosscoupling between channels.

Our experience with the pitch channel shows that none of the mid range adjustment problems discussed for V_S and V_C now exist. This is due to the improved optical design incorporated in Brassboard No. 2 transmitter pitch channel. Also, this new design enables easy adjustment of the REF and CONT LED light pattern such that they coalesce and are not skewed. It is recommended that implementation of this optical retro-fit be the first step in OAMS modification. The significance of this modification can not be fully assessed at this time on roll and yaw channel performances.

The crosscoupling mentioned in Item a can be reduced in the lateral channels by re-adjustment of the quarter-wave plates and ASC at the receiver and transmitter. These were last adjusted with Brassboard No. 1 configuration. Once the quarter wave plate is adjusted for circular polarized light, the ASC_R and ASC_T are successively adjusted by pitch and yaw motion until the crosscoupling effects are negligible. The roll channel adjustments are not as straightforward as that of the lateral channels and must begin by selection of a Wollaston prism (see Subsection 5.1.2.2) for the XMTR that has the least nonorthogonality. Following this, the Wollastons are aligned by use of a polaroid sheet which effectively decouples the nonorthogonality of W_T from W_R. Once the Wollastons are set the same iterative process of pitching and yawing at the RCVR and XMTR is repeated until minimum crosscoupling is attained.

Recommended approaches to the solution of RCVR and XMTR temperature sensitivity is less definite than that of crosscoupling, however, by process of elimination and previous experience with OAMS likely suspects in component behavior can be investigated. OAMS reaction, during temperature testing, is to produce an offset in V_0 as shown in Table 8-3. Along with this offset the detector/pre-amp shows an unbalance with large magnitudes in the roll channel because of the added gain (above that of lateral channels) required in scaling the system output. With LED balance values of about 1.0 per cent (see Table 5-5) the effects of this unbalance is diminished significantly as shown by the first term of Eq. (5-26). The Holloman AFB test results indicate the same behavior except that XMTR heating and cooling detector/pre-amp unbalance (for roll) are more in line with the value of that shown for the RCVR in Table 8-4. The magnitude of unbalance is directly related to temperature and returns to their initial settings when at ambient. With the RCVR at ambient and the XMTR temperature varying, the implication here is that an interaction effect between LED average wavelength changes (GaAs LED over temperature range will change by ± 10 nm) and the RCVR filter transmittance (horizontal and vertical polarization planes) will occur. The effect of this is to unbalance the two optical paths to the detectors. According to the manufacturer, the filters are sensitive to temperature, wavelength and angle of incident. Filters for use with polarized light must be designed to compensate for these effects and compromises are required. The Brassboard No. 1 and flight model filters were not ordered with this requirement. However, the flight model filters have a much sharper peak and are more compatible with the LED wavelength. Analysis of the data when the RCVR temperature is varied and during transverse movements yield similar detector/pre-amp unbalance.

According to Karl Lambrecht Corporation, the Wollaston prism manufacturer, the only change expected over the temperature range is a 600 arc sec movement in the deviation angle and no corruption of the polarized signals. Therefore, it is probable that the larger portions of angular movements during temperature variations are due to the optical mounts in the XMTR and RCVR. Examination of the mounting techniques should be made to acertain that stress and strain are not introduced on the Wollastons, ASC, and quarter wave plates.

The RCVR optics do not have an aperture stop before the W_R thus a strong possibility of vignetting at the detectors. This would naturally affect the system output during transverse movements. Also, realignment of the detectors to assure improved light receptivity is recommended.

Items d and e due to background illumination and reflection can be minimized by the use of baffles. Background illumination increases the sum voltage, V_s, and causes a change in scale factor (see Eq. 5-26). Reflected signals from the XMTR rejected beam will have a similar effect as that of background illumination, plus the introduction of an a.c. signal of like frequency in the processing electronics.

9.0 CONCLUSIONS AND RECOMMENDATIONS

During Phase II, OAMS development has undergone several modifications which significantly improved system output performance and reliability. These modifications were mostly in the electronics where higher performance LEDs, detectors, dividers, transistors, power supply and op amps where included in the new electronics (Advanced Brassboard). Improvements in the pre-amp circuit design and wire shielding were made to reduce the system electrical noise output, especially for roll. The system electrical rms noise output with a 10 hz low pass filter are 0.6mv, 0.44mv and 1.5mv for pitch, yaw and roll, respectively. The system power consumption was reduced to about 20mw. A constant modulation index and LED balance were implemented with a new LED drive amplifier circuit and a control loop; the result was a reduction in system output offsets and scale factor changes. Besides hardware changes, improvements in LED, detector and optics adjustment techniques were developed (some not fully implemented yet) to improve OAMS output during receiver and transmitter angular movements.

System testing at Michoud Assembly Facility included (not as comprehensive as that at Holloman AFB) accuracy and temperature testing. These tests were limited on the Advanced Brassboard mainly due to lack of sufficient time, equipment, a stable base, and stable ambient environment. Accuracy tests indicate that system outputs are repeatable and that the roll channel output is linear over a much wider range than that of the lateral channels. Crosscoupling was evident in all three channels with the roll exhibiting the largest values. Roll crosscoupling, depending upon receiver/transmitter orientation, could be made non-linear. Temperature testing of receiver, transmitter and electronic units between ambient and 37.8°C (100°F) indicated offsets in system output as illustrated in Table 8-3.

Modifications in the pitch channel optics/mechanical configuration were made to enable better light distribution and adjustments. Tests showed an improvement in the linearity of the crosscoupling term in pitch versus that of roll and yaw when transverse movements were made at the receiver. Offsets, during transverse movements were made at the receiver. Offsets, during transverse movements, produce the most outstanding problem in OAMS and the contributing source must be identified and a fix implemented. Crosscoupling due to receiver and transmitter rotations, accuracy calibration, and temperature sensitivity can be compensated if predictable; however, offsets and crosscoupling effects due to transverse movements can not be compensated. Because of the crosscoupling and temperature sensitivity effects, the following steps are recommended:

- Replace the roll and yaw LED, optical/mechanical configuration now present in Advanced Brassboard, with upgrading to the level of the flight model configuration.
- Perform systematic tests, where applications are questionable or information is unavailable, on the optical components to ascertain their characteristic behavior in OAMS environments.

- Replace all of Brassboard optical elements in the receiver and transmitter to conform with the improved flight components and mechanical design.

- Insert an aperture stop before the receiver Wollaston prism to prevent vignetting.

- Perform LED, optical, and detector alignment to conform with improved techniques developed during OAMS research and development period.

- Perform another calibration and temperature test after implementation of the above steps.

- Implement baffles on the receiver to ascertain its effectiveness in rejection of background illumination and beam deflection

- Further improvement on error model to account for these effects.

- Study methods of increasing dynamic range.

10.0 REFERENCES AND BIBLIOGRAPHY

REFERENCES

1. Hecht, Eugene and Zajac, Alfred, "Optics". Addison-Wesley Publishing Co., 1975

2. Shurcliff, "Polarized Lignt", 1962.

3. Strong, "Concepts of Classical Optics".

4. Schwartz, "Information Transmission, Modulation, and Noise", Mc Graw-Hill, 1959.

BIBLIOGRAPHY

Final Report - SAMSO TR-75-120

Final Report - SAMSO TR-73-6

Performance Evaluation Test Plan - CEI No. 73-6-TP

Prime Item Development Specification - CEI No. 73-6

Critical Component Specifications

Silicon Photodetector - CEI No. 73-6-A

Emitting Source - Pitch Channel - CEI No. 73-6-B

Emitting Source - Yaw Channel - CEI No. 73-6-C

Emitting Source - Roll Channel - CEI No. 73-6-D

Angle Sensing Crystal - CEI No. 73-6-E

APPENDIX A

NUCLEAR SURVIVABILITY

1.0 INTRODUCTION

This report will address the effects of Nuclear Radiation on electronic components and circuits and the selection of components and design of circuits to resist these effects for an Optical Angular Motion Sensor (OAMS).

The Optical Angular Motion Sensor (OAMS) will be used in a space environment. It will be designed by taking consideration into the radiation hazards it will face in space and possible exposure to radiation from a nuclear explosion.

The radiation effects parameters and typical values for an explosion of one megaton at a distance of 4.5 miles to be considered are listed in Table I.

TABLE I
Radiation Effects Parameters

	Parameter	Typical Value
1.	Overpressure	4 psi (peak) at wind velocity of 60 ft/sec.
2.	Thermal Pulse	15 cal/cm^2(sec) for 0.025 sec, 12.5 cal/cm^2(sec) for 1.9 sec.
3.	Neutron Density	10^{13} n/cm^2 (1 Mev equivalent)
4.	Total accumulated dose	10^4 rads
5.	Electromagnetic Pulse	$E_{max} = 10^4$ V/m, H_{max} = 30 At/m
6.	Gamma dose rate	10^{10} rads (Si)/sec
7.	Light Intensity	10^6 c/cm^2 with peak at 4000°A
8.	Fallout	1000 rads for 2 days with particle size of 1-100 microns radius

Of these parameters listed in Table 1, only neutron density, total accumulated dose, and gamma dose rate occurs in the natural space environment. In this environment, neutron density, and gamma dose rate are small and total accumulated dose is large only when the dwell time is great in those regions where the natural radiation is trapped by the earth's magnetic field.

1.1 NUCLEAR SURVIVAL IN A HOSTILE ENVIRONMENT

In a hostile space environment effects of Neutron density, Total accumulated dose, Electromagnetic pulse, gamma dose rate, and light intensity occur, usually at very high values. The rest of the effects listed can occur only in an air burst or ground explosion near the earth's surface.

A ground blast differs from an exo-atmospheric blast in that for the former, air transforms thermal energy into heat and blast shock, while the latter's thermal energy is radiated over a broad spectrum consisting primarily of X-rays.

1.2 NUCLEAR SURVIVAL IN A NATURAL ENVIRONMENT

Nuclear radiation effects upon space equipment can be due to the natural environment of space (Van Allen belts, solar flares). The most important sources of this natural radiation are trapped radiation, cosmic radiation, auroral radiation, and radiation due to solar flares.

TABLE II

PRIMARY OUTPUTS OF A ONE-MEGATON THERMONUCLEAR WEAPON BURST (EXO-ATMOSPHERIC)

OUTPUT	SOURCES	MEAN ENERGY TYPICAL	APPROX. YIELD PERCENT
Neutrons	Fission Reaction	1.3 MeV	1.0
Gamma rays	Fission Reaction Fusion Reaction Neutron Capture Inelastic Scatter Radioactive decay	1.1 MeV	2.6
X-rays	"Blackbody" radiation	--	68.9
Alpha Particles	Fusion Reaction Radioactive Decay	--	--
Beta Particles (electrons)	Radioactive Decay	1.1 MeV	2.5
Weapon Debris	Nuclear weapon and case materials	50.0 KeV	25.0
Visible Light	Fireball	--	--

The natural environment for orbital altitudes less than 500 nautical miles is not a severe one, however, the accumulated radiation dose absorbed over a long period of time can adversely affect the performance of space components such as silicon control rectifiers and optical parts. From this aspect, the effects of this natural environment must be taken into account in any long-life spacecraft system at altitudes in excess of several hundred nautical miles.

The unshielded space radiation exposure is given in TOR-0059(6311)-15 is:

Integrated ionizing dose - 10^9 roentgens/year
Integrated proton flux - 3×10^{12} protons/cm^2/year
Integrated electron flux - 10^{16} electrons/cm^2/year

The unshielded space radiation maximum dose rate is also given as:

Maximum ionizing dose rate - 10^7 roentgens/hour
Maximum proton flux (E 1 Mev) - 10^5 protons/cm^2/sec
Maximum electron flux (E 200 Kev) - 3 x 10^9 electrons/cm^2/sec

Auroral electrons are expected to be shielded out by the aluminum used in the housing since they are in the tens of Kev range of energy. The sun's spectrum outside the atmosphere contains an ultraviolet component which extends in significant quantities down to around 1000 angstroms. It will primarily affect the external windows and seal materials.

The natural environment consists of cosmic rays (high energy protons); Van-Allen belt trapped radiation consisting of electrons and protons with energies mainly in the range of 20 Kev to several Mev, this flux being a function of both latitude and altitude; auroral radiation (65° to 70° north and south latitude), consisting of relatively low energy electrons (less than 50 Kev) and a much lesser proton flux with energies ranging up to 600 Kev; solar flares which consist of intense proton flux - due to the earth's magnetic field these protons are deflected away from the equator and are most intense in the polar regions.

2.0 RADIATION EFFECTS OF ELECTRONIC COMPONENTS

The two basic interactions that describe the transfer of energy from the radiation flux to the atoms of the target are ionization and displacement. Particles may impart enough energy to a struck atom to move it to a new location in the lattice structure. In semiconductors, displacement disrupts the orderly crystal lattice structure and is equivalent to the addition of impurities. These disturbances in the lattice structure reduce current-carrier lifetime and degrade performance. Displacement is a permanent effect. The region of most interest generally will be from 0.1 to 12 MeV.

2.1 EFFECTS DUE TO FAST NEUTRONS

The role of the fast neutron is primarily the displacement of atoms from lattice sites in solids (whereas gamma rays result in the production of secondary electrons in all types of matter). The number of displacements produced by neutrons (and secondary electron effects) are primarily functions of the total exposure rather than the rate of exposure. Therefore, integration of the radiation produced by nuclear bursts is required to determine the effects. Displacements produced in solids will be permanent effects and hence are important not only during the transient radiation pulse but also following it.

2.2 IONIZATION EFFECTS PRODUCED BY TRANSIENT GAMMA RADIATION

Important transient effects due to gamma radiation include secondary electron emission, changes in gas conductivities, excess carrier effects in semiconductors, surface and volume resistivity changes in insulators, generation of E-M fields, optical effects, and changes in paramagnetic materials. Gammas react through photoelectric, Compton, and pair production.

The photo-electric effect is important for gammas below 100 Kev, the Compton process is important from 100 KeV to 3 or 4 MeVs, and pair production occurs only in excess of about 1.2 MeV and is only important in high Z materials.

Table III shows some ionizing effects in electronic parts due to gamma radiation.

For each type of electronic part used in the OAMS flight model, the dose limit given is the value that can be absorbed by the material before a measureable change occurs. The radiation doses that can be absorbed by component parts before a measurable degradation in any characteristic are tabulated in Table IV column one. The second and third colums of Table IV tabulates the amount of Neutron Fluence in neutrons per square centimeter which will cause mild and severe damage respectively.

3.0 GENERAL DESIGN GUIDELINES

General design guidelines that have been followed for the component selection and circuit design for nuclear survival hardening for OAMS are covered in the following sections.

3.1 COMPONENT SELECTION GUIDELINES

Component selection was made on the basis that the most radiation resistant component was selected that met the electronic parameter requirements and reliability criteria of the system.

3.1.1 Transistors

Transistors of each type used in the OAMS flight model were selected for their

1. High alpha cutoff frequency
2. High current gain
3. Low power
4. Low collector-to-emitter saturated voltage
5. Small geometry

3.1.2 Diodes

Diodes of each kind were selected for:

1. Fast recovery
2. Low Power
3. Small junction volume

TABLE III EFFECTS OF GAMMA RADIATION ON ELECTRONIC PARTS

COMPONENT	MAJOR EFFECTS
Resistors	Secondary Emission, Resistivity Changes Wire and In General, Metal Film Resistors Offer High Resistance To Radiation
Capacitors	
Glass Dielectric	Very Little Effect
Mica Dielectric	Small Permanent Effect - Transient Increase in Capacity
Ceramic Dielectric	No Appreciable Radiation Effect
Polycarbonic Dielectric	Very Little Effect
Paper Dielectric	Gas Evolution (in Neutron Flux), Decrease in Capacity and Severe Decrease in Insulation Resistance
Electolytic	Increase in Capacity, Decrease in Dissipation Factors
Diodes	Increase in Reverse Currents, Photocurrents, Change in Dynamic Resistance
Transistors	Photocurrents, Gain Changes, Reverse Current Increases - Transient & Permanent Damage Possibilities, Changes in Carrier Lifetimes
Insulators	
Vinyl Plastic	Severe Discoloration
Polypropylene & Silicones	Lose Tensile Strength-Become Brittle
Mica	Degradation in Dielectric Strength
Asbestos	Very Little Effect If Protected from Thermal Neutrons
Transformers	Electrical Performance Essentially Unaffected, Rupture of Hermetically Sealed Cases Can Occur
Coax Cables	Voltage Drops Along Conductor, Coax Shield Breakdown
Silicon Control Rectifiers	Very Sensitive to All Radiation Enviroments

TABLE IV RADIATION TOLERANCE LEVELS FOR OAMS ELECTRONIC COMPONENTS

COMPONENT	RDL	Neutron Tolerance Mild	Neutron Tolerance Severe
Resistors--fixed film--oxide	10^6	2×10^{12}	2×10^{16}
carbon	10^9	10^{15}	10^{17}
metal	10^{11}	3×10^{16}	5×10^{17}
Analogue Divider	10^6		
Diodes, Silicon--power	10^5		
switching	10^7		
Transistors--power	10^5	10^{14}	10^{15}
switching	10^7	10^{16}	
Comparators	10^6	10^{13}	
Precision Voltage Reference	10^6	10^{13}	
Power Supply	$2 \times 10^3 (10^6)$	10^{12}	
OP-AMPS	10^6	10^{13}	
Oscillator--Tuning Fork	10^{11}		
Capacitors--Solid Tantalum	10^7		
Metalized Polycarbonate	10^7		
Mica	10^9	10^{15}	10^{15}
Ceramic	10^{10}	10^{15}	10^{15}
LED--GaAlAs	$10^5 (10^7\text{-}10^8)$	10^{12}	
Si Photovoltaic Photodiodes	10^8	10^{15}	
Electrical Connectors	10^8	10^{15}	
Heat Sink Compound	10^9	10^{15}	
Hook Up Wire	10^9	10^{18}	
Shielded Cable	10^8		

RDL: Radiation dose limits in rads(Si) before measurable change occurs.
() 25% decrease in parameters

Neutron Fluence is given in n/cm^2

See Ricketts, FUNDAMENTALS OF NUCLEAR HARDENING OF ELECTRONIC EQUIPTMENT, Table 3.7, p130., Table 3.11, p136., Figure 10.4, p451., Figure 3.12, p161., Table 3.19, p158.

3.1.3 Silicon rectifiers

Silicon rectifiers were selected for:

1. Fast switching times
2. Large switching currents

3.1.4 Integrated Circuits

Integrated circuits were selected for:

1. Dielectrically isolated units to eliminate parasitic transistors and no latchup.
2. Those minimized for space-charged areas in the transistor and diode elements.
3. Those operated at lowest possible voltages at reverse-biased junctions.
4. Resistors or diodes are used between base and emitter to drain out photocurrent.
5. Thin-film resistors are used.

3.2 GENERAL DESIGN GUIDELINES

The following nuclear-hardening guidelines are used for OAMS circuit design:

1. Saturated logic in the oscillator circuitry is used.
2. Maximum base drive for transistors in saturation; and minimum impedance at transistor base will be employed.
3. The circuit is designed with maximum gain and maximum noise margins. The circuit is operated at high ambient temperature and high injection levels.
4. The use of direct-coupled stages, negative feedback, and current-limited designs. Protective devices to prevent burnout will be used wherever possible. Operational amplifiers have protective devices in their design.
5. Conservative fanout, maximum bias stabilization, and minimum ultrastable voltage requirement will be incorporated.
6. Cancellation of spurious currents will be insured.
7. The use of small capacitance values and low impedance levels.
8. Potting circuits with insulating materials will be considered.
9. Circuits will be designed such that electrical parameters sensitive to radiation are not extremely critical in a functional operation.
10. Adequate shielding, decoupling, bypassing, filtering, and feedback to reduce or eliminate bad effects from gamma dose rate pulses, prompt neutrons, electromagnetic pulses, or all three.
11. Impedances will be checked to eliminate possible trouble with ionization effects which may cause trouble in circuits that operate in the megohm range.

12. Interconnecting cables, wire loops, and ground paths, will be checked to certify that they are minimized for absorption of radiation energy.
13. Temperature overdesign techniques will be used to compensate for the additional heating effects due to radiation.

3.3 SHIELDING

In addition to component selection and circuit design for hardening of electronic systems to nuclear radiation, attenuation or blocking of the radiation can be effected by surrounding the electronics by solid matter or repulsive fields.

There are two types of shielding:

(a) Passive: the use of materials that will absorb part of the radiation, $I = I_0 \exp(-ux)$ for high energy gamma rays, dense materials such as lead, steel, and depleted uranium can be used. The choice of material and thickness must be traded to give the desired amount of reduction in intensity with reasonable weight and volume considerations.

For neutrons, low atomic number materials have the highest nuclear absorption cross-section. Thus lightweight materials such as beryllium and boron are potentially effective.

Most electrons and protons (with the exception of high energy electrons) can be stopped with a few tenths of an inch of aluminum. The secondary radiation emitted must be considered in such cases, however.

With the use of micro-electronic circuits and the resultant small circuit volume, passive shielding is feasible in many applications.

(b) Active: the use of electric and magnetic fields as a deflector of the charged particles (electrons and protons) has been suggested. Such methods are not recommended due to the added complexity and power, weight and size penalties.

The active method of shielding will not be considered for the reasons given. As for passive shielding; The six RCA C30852 Silicon detector/MOS-FET combinations in the receiver assembly and six Gallium-Aluminum-Arsenide light emitting diodes in the transmitter assembly are surrounded by one to two inches of solid matter, either aluminum, quartz, calcite or steel. The attenuation provided by this material compared to that of the electronics box cover which shields the rest of the components can bring the MOS-FET's survival capability up to that of the remainder of the semi-conductor parts, dependent upon the energy and type of radiation particles encountered.

4.0 ELECTROMAGNETIC PULSE DESIGN GUIDELINES

Electromagnetic Pulse design hardening is achieved by shielding, which can be prohibitively heavy for spacecraft applications or by judicious design techniques all of which are found in application in the design of OAMS:

4.1 GENERAL PRECAUTIONS

1. All cables are shielded, kept as short as possible, and all unwanted noise is kept outside the signal band.
2. All chassis openings and apertures are kept as small as possible. The same techniques as utilized in reducing rf interference are employed.
3. Filtering and decoupling are used whenever possible, particularly at inputs and outputs.
4. Component selection is used to choose components having sufficiently high voltage ratings, power ratings, current ratings, or all three.

4.2 GROUNDING

1. Incorporating where possible, a separate ground path for ac, dc, and signal currents.
2. Connecting a ground path to the most direct, lowest-impedance route possible.
3. Utilizing several arterial ground paths to the power supply common point, as opposed to using one superground bus.
4. Avoiding multiended ground buses or lateral ground loops.
5. Using as few series connection (solder joints, connectors) as possible in a ground return, and making sure that they are good electrical connections.
6. Choosing grounding points for bypass capacitors with extreme care. Never grounding a bypass capacitor near a high-flux-density chassis current.
7. A power ground should be routed with its corresponding hot wire in a twisted pair if large currents are carried.
8. Power grounds and their hot-wire complements should pass through adjacent connector pins in multiple-pin connectors.

4.3 SHIELDING

1. Use of shielded wire for external power circuits.
2. Use of twisted pair for af circuits that are grounded at a single point and for internal power circuits.
3. Use of shielded wire for multiple-ground audio circuits.

4.4 WIRING LAYOUT

1. Reference and susceptible circuits are not routed with power and interference circuits.
2. Rf-susceptible circuits may be routed with dc reference circuits, provided the rf-susceptible circuits are not a source of interference.

4.5 BONDING

1. The bond must in no way degrade the quality of the bonded structure or joint.
2. Insofar as possible, bonds should be made between the same type of metal. When different types of metal are bonded, they should be as close together in the electrochemical series as possible to prevent corrosion.
3. Bonding by means of jumpers should not be considered satisfactory unless no other practical method can be utilized.
4. Bonds should be installed in locations that are accessible for maintenance.
5. Bonds should be of sufficient cross-sectional area to carry any potential currents that may develop.
6. Bonds should not be held in place by self-tapping screws, because such connections generally produce high-resistance contacts.
7. The threads of screws or bolts should not be used to establish rf bonds.

4.6 OTHER GUIDELINES

1. OAMS has a narrow bandwidth so that interference susceptibility is reduced.
2. Impedances that vary in time cause varying currents, whereas impedances that vary with the current through them or with the voltage across them (nonlinear impedance) act as equivalent generators of varying electromotive force. Therefore, the current flowing within such circuits will contain a second and third harmonic that were not present in the original source. Any nonlinear impedance is thus a possible source of interference. All possible such sources will be reduced or eliminated in the flight model design.
3. The OAMS power supply is rfi and emi shielded.
4. Diodes are selected that will operate at the lowest current density in proportion to maximum rated current, and with the highest rated working and peak inverse voltage consistent with other design requirements.
5. The lowest possible switching rate has not been selected. Shielding will be used to compensate for radiation vulnerability. Ripple reduction and filtering requirements are foremost here.
6. Filtering of the interference signals will be made at the diodes. Actual harmonic filtering or transient current reduction is effective. Series inductors or shunt capacitors to the load may also be used.
7. Loads that are to be switched are to be kept as resistive as possible.